Hydraulic-morphological habitat assessment in rivers considering residual flow, sediment replenishment and artificial flood events

Thèse N° 9452

2019

EPFL
ÉCOLE POLYTECHNIQUE
FÉDÉRALE DE LAUSANNE

"The future will either be green
or not at all"

— Bob Brown

Meinen lieben Eltern, Grosseltern und Geschwistern in Liebe und Dankbarkeit gewidmet

Abstract

Dams store water and trap sediment in their reservoirs. Downstream river segments, hence, are affected by a limited sediment dynamics. This becomes obvious by river bed incision, limited geomorphological variability and depletion of hydraulic habitats for in-stream ecological organisms. Replenishment is a measure to counteract the lack of sediment. In segments downstream of dams such a sediment replenishment can be combined with the release of an artificial flood, by activating spillways and bottom outlets. Recent laboratory studies revealed the potential of multi-deposit replenishment configuration towards an increase of geomorphological richness in the river. However, this has not yet been tested in the field.

The hydro-morphological index of diversity (HMID), is based on the spatial variability flow depth and velocity in a river segment, allowing the quantification of the change in morphology such a measure. Its ease in computation and its objectivity makes the index a useful tool for a large variety of users. However, knowledge concerning data sufficiency and a standardized sampling procedure does not exist. Further, the HMID does not account for temporal variability.

This research aims at closing these gaps of knowledge for a sustainable management of complex floodplains downstream of dams.

Flow depth and velocity data from 19 river segments were analyzed with the HMID. Structured sub-sampling and analysis of the data revealed different data sufficiency depending on the complexity of the river geomorphology. A representative HMID value is computed from at least 100 datapoints distributed over eight cross-sections, in braided rivers more datapoints are required.

The geomorphological changes by an artificial flood event in the Sarine were analyzed with the HMID. In the impact perimeter of the multi-deposit sediment replenishment, the HMID increased by 36 % in the Sarine, in the rest of the river 18 %. A similar study was investigated at the Spöl, pointing out that sediment availability is crucial for the hydraulic habitat diversity.

With the help of 489 tracer stones, the movement of the replenished sediment was investigated in detail. The deposition pattern results in repeating sediment clusters on the riverbed,

Abstract

as it was observed in the laboratory experiments. For the two characteristic diameters, the tracers allowed the estimation of transport velocities of 19 cm/min (d_m = 57 mm) and 28 cm/min (d_{90} = 113 mm) during the flood event and consequently the erosion efficiency of the different parts of the flood hydrograph.

Macroinvertebrates were less affected by the artificial flood event in the hydropeaking river segment of the Sarine compared with the residual flow segment. The species diversity indices decreased significantly due to the artificial flood event. A direct link between flow regime and EPT richness was observed. A river with a natural flow regime hosts the highest richness of macroinvertebrates followed the residual and finally the hydropeaking flow regime. For other ecological indicators, additional physical river parameters for example the frequency duration curve or the grain size distribution need to be considered as well.

Keywords: *floodplains; hydro-morphological index of diversity; ecological indices; sampling sufficiency; river restoration; hydropower; residual flow; hydropeaking; sediment replenishment; artificial flood events; sediment particle tracking*

Kurzfassung

Talsperren stauen Wasser und halten Sedimente in ihren Stauräumen zurück. Die Sediment-dynamik von stromabwärts gelegenen Flussabschnitten ist daher limitiert. Dies wird deutlich durch Erosion der Flusssohle, begrenzte geomorphologische Variabilität und einer Verarmung der hydraulischen Lebensräume für Gewässerorganismen. Um dem Sedimentdefizit entgegenzuwirken, wird Flüssen Geschiebe beigegeben. In stromabwärts von Talsperren gelegenen Flussabschnitten kann eine solche Geschiebeschüttung mit einem künstlichen Hochwasser kombiniert werden, mittels Aktivierung von Hochwasserentlastungen und Grundablässen. Laboruntersuchungen zeigten, dass Geschiebebeigaben mit mehreren Schüttungen, die geomorphologische Vielfalt eines Fliessgewässers erhöhen können. Dies wurde jedoch noch nicht in Feldversuchen untersucht.

Der Hydrologisch-morphologische Index der Diversität (HMID), basiert auf der Variabilität von Fliesstiefe und -geschwindigkeit in einem Flussabschnitt und kann die Veränderung der geomorphologischen Vielfalt durch eine Revitalisierungsmassnahme quantifizieren. Die einfache Berechnung und die Objektivität machen den Index zu einem nützlichen Instrument. Kenntnisse über die Hinlänglichkeit der Daten und ein standardisiertes Messverfahren sowie die zeitliche Variabilität des HMIDs sind noch nicht detailliert erforscht.

Diese Forschungsarbeit beabsichtigt diese Wissenslücken für ein nachhaltiges Management komplexer Flussauen unterhalb von Talsperren zu schliessen.

Fliesstiefen- und geschwindigkeitsdaten von 19 Flussabschnitten wurden mit dem HMID analysiert. Eine strukturierte Datenanalyse ergab unterschiedliche Datehnhinlänglichkeit je nach Komplexität der Flussmorphologie. Mit 100 Messpunkten verteilt auf acht Querprofile, kann für die meisten untersuchten Flussabschnitte ein repräsentativer HMID berechnet werden.

Die geomorphologischen Veränderungen durch ein künstliches Hochwasserereignis in Saane wurden mit der HMID analysiert. Im Einflussperimeter der Geschiebebeigaben mit vier Schüttungen erhöhte sich der HMID in der Saane sogar um 36 %, im restlichen Fluss um 18 %. Eine ähnliche Studie wurde am Spöl durchgeführt und bekräftigt die Schlussfolgerung, dass die Verfügbarkeit von Sedimenten für die Vielfalt der hydraulischen Lebensräume entscheidend ist.

Mit Hilfe von 489 Tracersteinen wurde der Geschiebetransport der Schüttungen detailliert untersucht. Sich wiederholende Strukturen in den Flussbettablagerungen wurden beobachtet, was die Erkenntnisse aus den Laborexperimenten bestätigt. Für die zwei charakteristischen Korndurchmesser erlaubten die Tracersteine die Bestimmung der mittleren Transportgeschwindigkeiten von 19 cm/min (d_m = 57 mm) und 28 cm/min (d_{90} = 113 mm) während des Hochwasserereignisses und daraus folgernd die Erosionseffizienz unterschiedlicher Abschnitte der Hochwasserganglinie.

Die Auswirkungen des künstlichen Hochwasserereignisses auf Makroinvertebraten war in der Schwall- und Sunkstrecke der Saane deutlich kleiner als in der Restwasserstrecke. Die Indikatoren der Artenvielfalten von Makroinvertebraten verringerten sich signifikant nach dem künstlichen Hochwasserereignis. Eine direkte Verbindung zwischen Abflussregime und EPT Index wurde beobachtet. Im Flussabschnitt mit einem natürlichen Abflussregime wurde die höchste Artendiversität festgestellt, gefolgt von dem Restwasser und dem Flussabschnitt mit einem Schwall- und Sunk Abflussregime. Für einen ganzheitlichen Vergleich mit ökologischen Indikatoren müssen zusätzliche physikalische Flussparameter berücksichtigt werden wie zum Beispiel die Jahresganglinie oder die Korngrössenverteilung.

Schlüsselwörter: *Flussauen; Hydraulisch-morphologischer Index der Diversität; Messstrategie; Ökologische Indikatoren; Flussrevitalisierung; Wasserkraft; Restwasserabfluss; Schwall und Sunk; Geschiebeschüttungen; Künstliche Hochwasserereignisse; Tracersteine*

Résumé

Les barrages retiennent l'eau et les sédiments dans leurs réservoirs. Les cours d'eau en aval sont donc affectés par une dynamique sédimentaire limitée. Les principales conséquences sont : une incision du lit, une variabilité géomorphologique limitée et un épuisement des habitats pour les organismes aquatiques. Les rivières ont été réapprovisionnées de sédiments pour compenser leur absence. Dans une rivière avec un débit résiduel, ce réapprovisionnement peut être combiné avec une crue artificielle, produite via les évacuateurs de crue et/ou les vidanges de fond. Des études en laboratoire récentes ont révélé le potentiel du réapprovisionnement sédimentaire à plusieurs dépôts pour améliorer la richesse géomorphologique de la rivière. Cependant, cela n'a pas encore été testé en condition réelle.

L'Indice Hydro-Morphologique de Diversité (IHMD), est basé sur la variabilité de la profondeur et de la vitesse d'écoulement d'un tronçon. Il permet de quantifier le changement de richesse géomorphologique grâce à une mesure de revitalisation de cours d'eau. Sa facilité de calcul et son objectivité font de l'index un instrument utile. Cependant, il n'existe pas encore des connaissances approfondies concernant la quantité minimale de données à avoir et une procédure d'échantillonnage standardisée. De plus, le IHMD ne tient pas compte de la variabilité temporelle.

Cette recherche vise à combler ces lacunes de connaissances pour une gestion durable des plaines inondables complexes en aval des barrages.

Les données de profondeur et de vitesse d'écoulement de 19 tronçons de rivière ont été analysées avec l'IHMD. Le sous-échantillonnage structuré et l'analyse des données ont révélé différentes quantités nécessaires en fonction de la complexité de la géomorphologie de la rivière. Une valeur représentative de IHMD est calculée à partir d'au moins 100 points de données réparties sur huit sections transversales. Dans les rivières tressées, plus de données sont nécessaires.

Les changements géomorphologiques dus à une crue artificielle dans la Sarine ont été analysés avec le IHMD. Dans le périmètre d'impact du réapprovisionnement de sédiments à quatre dépôts, l'IHMD a augmenté de 36 %, dans le reste de la rivière de 18 %. Une étude similaire a été réalisée au Spöl, soulignant que la disponibilité des sédiments est cruciale pour la diversité de l'habitat hydraulique.

Résumé

À l'aide de 489 cailloux-traceurs, le mouvement des sédiments réapprovisionnés a été étudié en détail. Le modèle de la déposition montre une répétition des amas de sédiments sur le lit de la rivière, comme il a été observé dans les expériences en laboratoire. Pour les deux diamètres caractéristiques des grains, les traceurs ont permis l'estimation de vitesses de transport de 19 cm/min (d_m = 57 mm) et de 28 cm/min (d_{90} = 113 mm) pendant la crue et, par conséquent, l'efficacité de l'érosion des différentes parties de l'hydrogramme de crue.

L'impact de la crue artificielle sur les macroinvertébrés était nettement plus important dans le tronçon du débit résiduel comparé avec le tronçon de marnage. Les diversités des espèces sont diminués largement après la crue artificielle, les autres indices avaient peu changé. Un lien direct entre le régime d'écoulement et la richesse EPT est observé. Le tronçon avec un régime naturel a la plus grande richesse des macroinvertébrés suivi par le tronçon avec un régime résiduel et finalement celui avec un régime des éclusées. Les analyses ont montré qu'il convient également de prendre en compte des paramètres physiques supplémentaires, tels que la courbe des débits classés ou la granulométrie. Cela ouvre un aspect plus holistique de la rivière et de la vie qu'elle héberge.

Mots clefs : *plaines alluviales ; indice hydro-morphologique de la diversité ; Indicateurs écologiques ; stratégie de mesure ; révitalisation des cours d'eau ; l'énergie hydroélectrique ; débit résiduel ; marnage ; réapprovisionnement des sédiments ; crues artificielles ; cailloux-traceurs*

Contents

Contents

Contents

List of symbols

Notation

$b_{bankful}$	[m]	Wetted width at bankful discharge
d_{90}	[mm]	90 %-quantile of grain size distribution, based on grains' b-axis
d_m	[m]	Modal diameter, about 60%-quantile of the GSD
Δt_i	[s]	i-th time interval
$eeff$	[-]	Erosion efficiency
Fr	[-]	Froude number
g	[ms^{-2}]	Gravitational acceleration, equal to 9.81
h	[m]	Flow depth
J	[%]	Bed slope
k_{st}	[m$^{1/3}$s^{-1}]	Roughness coefficient in the Gauckler-Manning-Strickler equation
L	[m]	Deposit length
μ_i	[i]	Average value of variable i
N	[-]	Total number of macroinvertebrate individuals
n_{EPT}	[-]	Total number of EPT individuals
n_i	[-]	Number of individuals of species i
p_i	[-]	Proportion of species i relative to the total number of species
Q	[m^{3}s^{-1}]	Discharge
S	[-]	Total number of macroinvertebrate species
σ_i	[i]	Standard deviation of variable i
t	[s]	Time
t_0	[s]	Time a tagged stone is eroded
t_a	[s]	Time a tagged stone passes the fix antenna
t_d	[s]	Time a tagged stone settles
t_e	[s]	Time a tagged stone passes the downstream end of the erosion zone
v	[ms^{-1}]	Flow velocity

v_a	[ms^{-1}]	Tagged-stone transport velocity between the origin and the fix-antenna
v_d	[ms^{-1}]	Virtual velocity of a tagged-stone
v_e	[ms^{-1}]	Tagged-stone transport erosion velocity
W	[m]	Deposit width
x	[m]	Distance
x_0	[m]	Location of origin of a tagged stone
x_a	[m]	Location of the fix antenna
x_d	[m]	Location of settling of a tagged stone
x_e	[m]	Location of the downstream end of the erosion zone

Abbreviations

ADCP	Acoustic Doppler current profiler
ADV	Acoustic Doppler Velocimeter
COP 21	21st Conference of the Parties (UN Climate Conference in Paris 2015)
Eawag	Swiss Federal Institute of Aquatic Science and Technology
EKW	Engadiner Kraftwerke AG
EnG	730.0 Energiegesetz [Energy law], 30 Sep 2016, status as of 01 Jan 2018
EPFL	École Polytechnique Fédérale de Lausanne
EPT	Ephemeroptera, Plecoptera, Tricoptera
ETH	Eidgenössisch Technische Hochschule Zürich
FDC	Flow Duration Curve
FOEN	Federal Office for the Environment [in German: BAFU]
GIS	Geographic Information System
GLOF	Glacier Lake Outburst Flood
GNSS	Global Navigation Satellite System
GSD	Grain Size Distribution
HMID	Hydro-morphological Index of Diversity
HyApp	Hydro-Ecology and Floodplain Sustainability in Application
ICOLD	International Commission on Large Dams
IPCC	Intergovernmental Panel on Climate Change
KWO	Kraftwerke Oberhasli AG
LCH	Laboratoire de Constructions Hydrauliques at EPFL
LiDAR	Light Detection and Ranging
NGO	Non-Governmental Organization
NRP	National Research Programme
OCR	Occupation Ratio along the channel
PIT	Passive Integrated Transponder
PSD	Power Spectrum Density
RFID	Radio Frequency IDentification
SCCER − SoE	Swiss Competence Center for Energy Research - Supply of Electricity
SDG	Sustainable Development Goals [by the United Nations]
SFOE	Swiss Federal Office for Energy [in German: BFE]
SNSF	Swiss National Science Foundation
TVA	Topographic Variability Attributes
UN	United Nations
UNFCCC	United Nations Framework Convention on Climate Change

UZH	University of Zurich
$WGS\,84$	World Geodetic System 1984
WPA	814.20 Federal Act on the Protection of Waters, 24 Jan 1991, status as of 01 Jan 2017
WPO	814.201 Waters Protection Ordinance, 28 Oct 1998, status as of 01 Jun 2018
$WRFO$	721.101.1 Water Retaining Facilities Ordinance, 17 Oct 2012, status as of 01 Apr 2018
$WWTP$	Waste Water Treatment Plant [in French: STEP]
$ZHAW$	Zurich University of Applied Sciences

1 Introduction

1.1 Overview

This chapter introduces the reader to the topic dealt with in this research project. The situation of worldwide water infrastructure and hydropower production in different regions of the world are briefly presented briefly. Following the situation in Switzerland is explained in detail, addressing the following topics:

- After explaining the role of hydropower worldwide, the focus is directed to **Switzerland**. The lack in electricity production in winter and the surplus in summer are explained.

- Explanation of the **negative impacts of hydropower** on the environment, namely altered flow regimes and reduced sediment dynamics. Maps of dams, flow abstraction and restitution locations illustrate the extent of the impacts.

- The importance of **climate change** regarding hydropower production in Switzerland is explained. New opportunities and risks are rising with melting glaciers.

- A significant part of this chapter addresses the Swiss **environmental politics** of the past years. The effect of the Energy Strategy 2050 on hydropower and on important laws are summarized.

- The resulting National Research Program (NRP) and the **overarching research project HyApp**, which this research is part of, are briefly described.

- The last section provides the **detailed structure** of the different chapters and appendices of this research study as well as the resulting publications in peer-reviewed journals.

1.2 History of human-water interactions

Water bodies such as lakes and rivers have always been subject to anthropogenic use. Water has always been considered both as a vital and a destructive element for life. The vital part includes water supply, irrigation, hydropower and navigation. Humans used the river flow to transport goods and people (McNeill, 2000). The destructive elements were addressed with sewage treatment, drainage, protection against erosion and flood protection (Schleiss, 2000). In the 19th century river training work became popular in Europe, aiming at enhancing the sediment transport capacity and reduce inundations during flood events. Furthermore, swamps could be drained what resulted in the extinction of diseases such as Malaria and in the gain of arable land for the urgently needed food production. Sills lateral to the flow direction ensured that the river bed does not erode and the river flows controlled in its bed. The danger of flooding and death decreased and settlements could be built close to the river banks. With industrialization, the electrification came and suddenly energy and electricity were key driver of economic growth. In the beginning of the 20th century the use of hydropower became more and more popular with the electrification of urban areas. Especially in Europe and in North America, storage and run-of the river power plants were constructed to support the economic growth with the required electricity after World War II (McNeill, 2000).

1.3 Hydropower worldwide

Dams and reservoirs have always been an important driver for economic growth and welfare in every society. The World Register of Dams (WRD), by the International Commission on Large Dams (ICOLD), counts more than 59'000 dams with a height of 15 m or greater, as well as dams between 5 and 15 m height and impounding a volume larger than 3 Mio m^3 [Status: February 2019]. These dams store in total more than 16'000 km^3 water. The main purpose for dam constructions is irrigation (more than 20'000), followed by hydropower (9'700), water supply (7'600) and Recreation (7'300), see Figure 1.1. The world's highest dam is the Jinping 1 Dam in China with a total height of 305 m [Status: February 2019]. At the current state, dams are mainly constructed and planned in Asia and South America, more than 1000 of them in Brazil. In 2017, China was the world's largest producer of hydropower with 1'194 TWh annual electricity generation accounting for more than a fourth of the worldwide production (4'185 TWh/a). Second largest electricity producer in 2017 was Canada followed by Brazil (Table 1.1). In Europe, the largest hydropower producer is Norway (143 TWh/a), followed by Sweden (64 TWh/a) and Turkey with 59 TWh/a (IHA, 2018). With climate change, the role of dams and reservoirs may become even more important to supply people with environmental friendly energy as well as water in sufficient quantity and quality for human welfare (Schleiss, 2016).

Table 1.1 – Hydropower production in different world regions and countries in 2017. Installed pumped-storage capacity (p-s) is listed separately. Further contribution to the global electricity production by hydropower and the regional ranking are given. Data from IHA (2018).

|	Installed Capacity [GW]	Installed Capacity p-s [GW]	Production [TWh]	Global	Ranking
AFRICA					
Mozambique	2'191	-	13.7	0.3 %	1
Zambia	2'397	-	13.7	0.3 %	2
Egypt	2'844	-	13.4	0.3 %	3
Total	35'339	3'376	131	3.1 %	
SOUTH & CENTRAL ASIA					
Russia	48'450	1'385	178.9	4.3 %	1
India	49'382	4'786	135.5	3.2 %	2
Pakistan	7'477	-	34.1	0.8 %	3
Total	144'710	7'451	456	10.9 %	
EAST ASIA & PACIFIC					
China	341'190	28'490	1'194.5	28.5 %	1
Japan	49'052	7'637	92.55	2.2 %	2
Vietnam	16'679	-	59.9	1.4 %	3
Total	468'331	66'454	1'501	35.9 %	
EUROPE					
Norway	31'837	1'392	143	3.4 %	1
Sweden	16'466	99	63.9	1.5 %	2
Turkey	27'273	-	59.2	1.4 %	3
France	25'517	6'985	53.2	1.3 %	4
Austria	14'130	5'212	38.1	0.9 %	5
Italy	21'884	7'555	37.5	0.9 %	6
Switzerland	16'922	3'057	36.7	0.9 %	7
Total	248'564	51'769	599	14.3 %	
NORTH & CENTRAL AMERICA					
Canada	80'985	177	403.4	9.6 %	1
United States	102'867	22'809	322.4	7.7 %	2
Mexico	12'125	-	29.8	0.7 %	3
Total	203'053	22'986	783	18.7 %	
SOUTH AMERICA					
Brazil	100'273	30	401.0	9.6 %	1
Venezuela	15'393	-	72.1	1.7 %	2
Paraguay	8'810	-	59.3	1.4 %	3
Total	166'959	1'004	716	17.1 %	
WORLD	1'266'955	153'041	4'185	100 %	
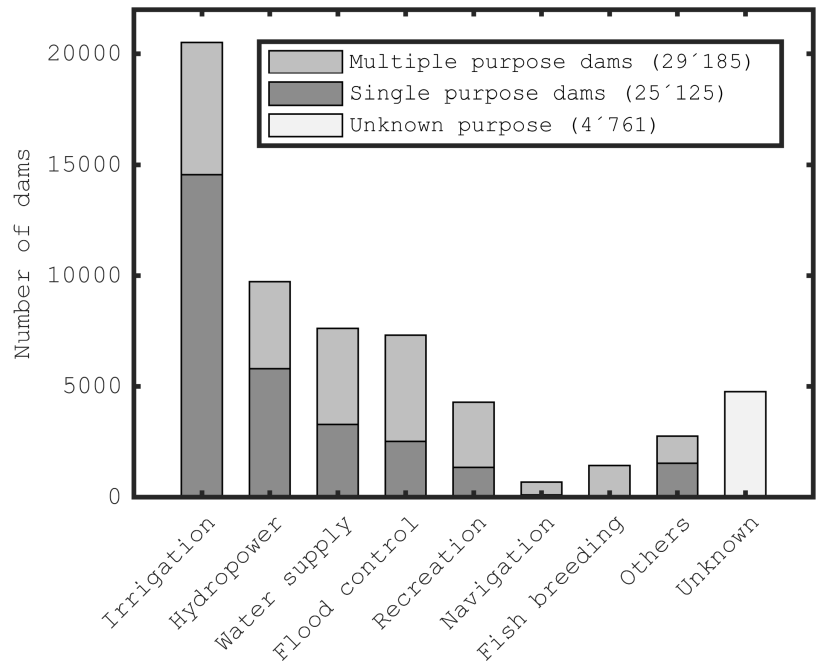
Figure 1.1 – Purposes of dams worldwide. The dams are divided into multiple purpose and single purpose dams. The data contains all 59'071 dams from the World Register of Dams (WRD) from ICOLD, accessed on 5 February 2019.

1.4 Hydropower in Switzerland

Due to a mild climate, the purpose of dam projects was rarely irrigation in Switzerland, but rather hydropower production. Nowadays, Switzerland has a dense network of hydropower plants. In 2017, 678 power plants with an installed capacity of >300 kW operated throughout the country (BFE, 2018a). Hydropower is the main electricity production technology in Switzerland with a share higher than 55 % of the national electricity production (BFE, 2018a). The evolution of the installed capacity and production of hydropower is given in Figure 1.2. The use of hydropower can be divided in different period. After the pioneer time, hydropower experienced an *upswing* driven by electrification (1910-1945), after World War II growing industry resulted in a *boom* for hydropower in Switzerland with a yearly increase of 5 % of the installed capacity and expected annual production. Until the commissioning of the first nuclear power plant in Switzerland (Beznau I, 17 July 1969), electricity in Switzerland was almost exclusively produced by hydropower (Pfammatter and Piot, 2014). At some point, the best locations for hydropower plants were occupied and the increasing use of nuclear power started a period of consolidation (since 1970). The increase in production capacity by small hydropower plants does not show in the statistics since environmental regulations such as the release of residual flow compensated for it (Pfammatter and Piot, 2014). However, with intelligent investments, the capacity could be increased significantly in the last twenty years with the commissioning of Bieudron (1998) as well as of the pumped-storage schemes Veytaux and Linth-Limmern (2016). The commissioning of the pump storage hydropower plant Vieux Emosson will further increase the installed capacity of the Swiss hydropower production. The installed capacity at the end of 2017 was 15.3 GW and the annual production for the year 2017 totalled in 36.7 TWh (BFE, 2018b). In Switzerland, hydropower plants can be divided in storage and pumped-storage power plants in the Alpine mountains, as well as run-of-the-river power plants along the large rivers in the Prealps and lowlands.

Storage and pumped-storage hydropower serve as important seasonal capacity transfer of electricity. On the one hand, snow melts in spring, whereas the glaciers melt in summer. Therefore, hydropower can produce more electricity in summer than in winter. On the other hand, electricity demand is higher in winter than in summer resulting in a net-import of electricity in most of the last ten winters (Figure 1.3). In average this corresponds to about 11 % (ca. 4 TWh) of the annual domestic production that needed to be imported every winter. In 2017, electricity was imported in January, February, March, April, September, October and December, and exported from May to August (Figure 1.4).
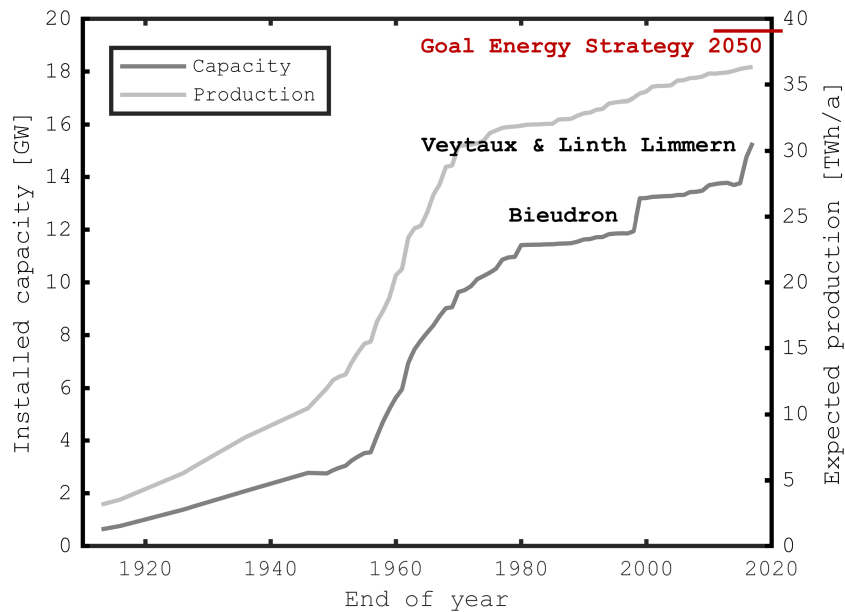
Figure 1.2 – Evolution of hydropower production in Switzerland between 1913 and 2017. The timeline can be divided in three periods: Upswing (1910-1945), boom (1945-1970) and consolidation (1970-today). The steep increases in the curve of the installed capacity are caused by the commissioning of the power plant Bieudron 1998 and Veytaux and Linth Limmern in 2016. The production goal of the Energy Strategy 2050 is 38.6 TWh/a. Data from BFE (2018b), status of 1 January 2018.

Pumped-storage hydropower schemes, with at least two reservoirs at different altitudes, work like a battery. With such a scheme, electricity can be taken from or given to the grid depending on the demand and market surplus. This function is of high importance for the stability of the electricity grid. In the recent past, more so-called new renewable electricity production techniques such as wind and solar power have been connected to a grid. These techniques produce electricity with a high degree of volatility, hence need the flexibility of storage and pumped-storage hydropower plants. Their flexibility is also a key advantage of storage and pumped-storage hydropower plants to optimize their revenue while adjusting their electricity production to the highest prices.
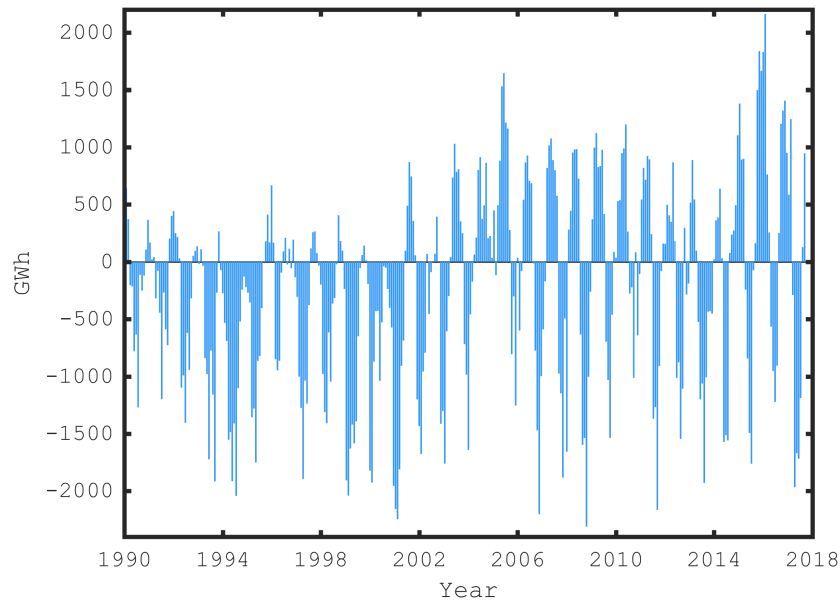
Figure 1.3 – Monthly electricity import and exports of Switzerland from January 1990 until October 2018. Peak electricity export during summer months increased significantly since 2002. Data from BFE (2018b), status of 31 January 2019.
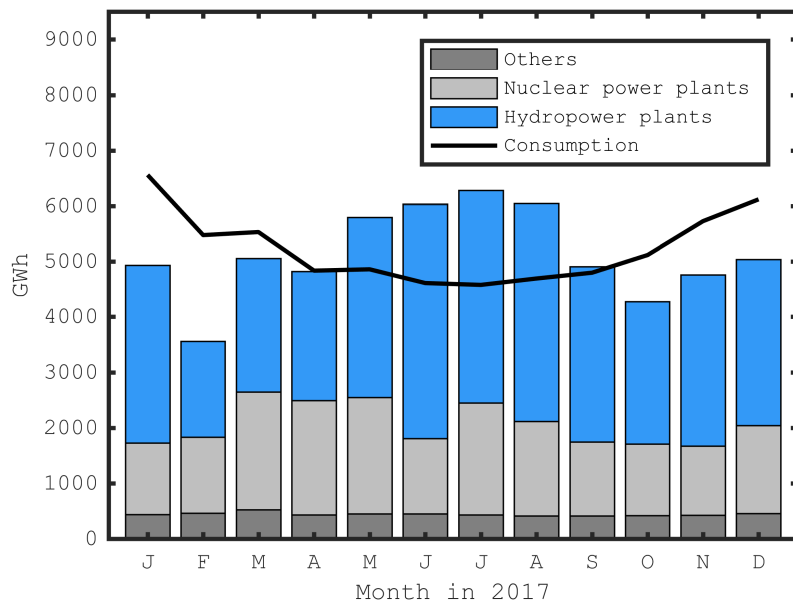
Figure 1.4 – Electricity balance and consumption of Switzerland in 2017, divided into Conventional-thermal and renewable, nuclear and hydropower plants. The maximum deficit was in February (2'161 GWh import), the maximum surplus in July (export of 1222 GWh). Data from BFE (2018b), status of 31 January 2019.

1.5   Impact of hydropower

The 678 hydropower plants and more than 200 large dams are mainly located in the Alps, Prealps and along the major rivers (see Figure 1.5). Besides the inundation of land in the reservoir, dam operation cause problems for the environment. Changes in river hydrology and sediment continuum may lead to unnatural conditions. Dams function like barriers in a river and may limit fish migration unless accurate aid- and guiding-structures are installed. The presence of artificial reservoirs also holds the risk of dam failure or impulse waves by land or rock-slides that can harm urban areas and infrastructure located downstream (Genevois and Ghirotti, 2005). However, modern design approaches reduce the probability of such events significantly. In the following, common operational problems such as residual flow, hydropeaking and sediment continuum are described in detail.
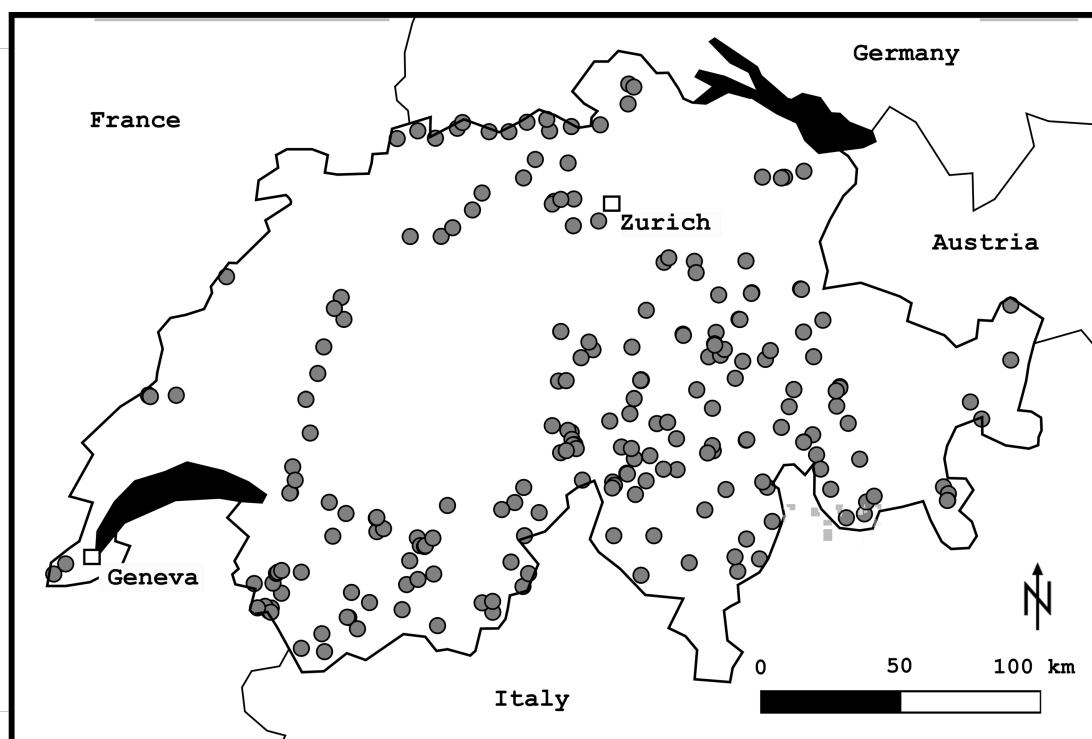
Figure 1.5 – Locations of the 222 dams in Switzerland which are subject to the Water Retaining Facilities Ordinance (WRFO). The purpose of these dams is the retention of either ice, sediment, snow or water. Data from SFOE, status of 03 July 2018.

1.5.1 Residual flow regime

The reservoir of a dam built on a river has an influence on the downstream hydrograph. To increase the energy head, water is often abstracted and released to the river a few kilometers further downstream, or transferred in another catchment. Water abstraction leads to a so-called residual flow reach starting downstream of a dam. The residual flow is defined in the Swiss Federal Act on the Protection of Waters (WPA) based on the discharge in the water course which is exceeded in at least 347 days under natural conditions (Q_{347}). The residual flow is concentrated in the main channel, and inundation of alluvial terrain and floodplains is limited or absent. Consequently, a strong armor layer is formed and relatively small shear stresses support algae colonization on the riverbed. In large reservoirs, flood events occur less frequently and with a decreased magnitude, increasing the impoverishment of the downstream morphology. The activation of spillways is a direct economic loss, wherefore companies operate their dams accordingly. Already the release of a residual flow reduces the annual domestic electricity production of Switzerland by about 2.3 GWh, corresponding to 6 % of the total annual production (Pfammatter and Wicki, 2018). Examples of different flow regimes are presented in Chapter 3. An overview map of the locations of water abstractions in Switzerland is provided in Appendix A, Figure A.1.

1.5.2 Sediment continuum

Damming causes a reservoir in which flow velocities are significantly reduced. The bed load and parts of the suspended sediments settle in the reservoir resulting in an interruption of the natural sediment continuum. Dependent on the reservoir size and management, this can lead to considerable siltation and hence a reduction in the storage capacity. The captured sediment is then missing in the downstream river causing incision and disconnection of the floodplain with the main river. By consequence of incision, a flood must be of higher magnitude to inundate the terrestrial part of the river and its floodplain.

1.5.3 River dynamics

The lack of sediment and periodical flooding hinders the morphodynamics which is a key driver for riparian and in-stream habitat diversity (Wohl et al., 2015; Moyle and Mount, 2007). Where a large flood literally turns over each stone at the surface of a floodplain and removes vegetation at a regular basis, gravel bars serve as habitat for pioneer species requiring a high light exposure and hence create conditions for species, which cannot survive in a more static environment. Exemplary are the two species *Myricaria germanica* and *Chorthippus pullus*, which have become rare in the Alps over the past decades. Prior dynamic floodplains adjunct to residual flow rivers often get disconnected from the river and hard-wood forest takes over the former dynamic river corridor. Dynamic floodplains therefore are important for conservation. More detailed information about the dynamics of a river system is given in Chapter 2.

1.5.4 Hydropeaking regime

In the case of storage hydropower plants, a sudden release of water leads to a fast increase of the water level and the flow velocities in the river, resulting in a so-called hydropeaking regime. The start and stop is a matter of minutes and depends on the electricity demand and price. Nowadays, the electricity price changes every 15 minutes due to new renewable energy technologies such as solar or wind power connected to the grid. Frequent and rapid starts of the turbines cause elevated stresses for the in-stream biota. Driven by variable market prices, a hydropower plant may launch their turbines several times each hour. This causes high stress for fish, macro-invertebrates and plants. The most visible effect is fish stranding, in case the water table decreases fast. Also amphibians, living at the interface between water and land, have difficulties with such hydropeaking flow regimes (Valentin et al., 1995). An overview map of locations of water releases in Switzerland is provided in Appendix A, Figure A.2.

1.6 Impact of river training works

The high population density in Switzerland increases human impact on rivers. According to the Federal Office for the Environment (FOEN) the morphological structure in Swiss rivers is heavily altered. Especially in the lowlands, where the large cities are located, more than 50 % of the water courses are far away from their natural state (see Figure 1.6). Mainly for agricultural land and flood protection reasons, major Swiss rivers, such as Rhône, Rhine, Aare, Reuss and Thur were subject to river training. Large-scale river training measures connected the Aare with Lake Biel, allowing the dampening of floods and hence protecting downstream cities and infrastructure from flooding. The high number of river training works reduced the space given to Swiss rivers significantly. Trained rivers transport the water faster and consequently more sediment. The lateral movement of the riverbed is limited by dykes, allowing the use of the former floodplain by humans. If then water overtops, the damage to society can be significant.

Exemplary stands the Rhône river in the Canton of Valais. During the first correction of the Rhône, the construction of dykes and groins enhanced the sediment transport in the river and gave access to arable land. Dyke heightening and the building of double trapezoidal cross-section profiles further increased sediment transport and flood protection during the Second Rhône Correction (1930-1960). Large flooding and environmental concerns initialized the third Rhone correction which is still ongoing and will last another 30 years (HLS, 2002). The Third Rhône Correction has the goal to further increase flood protection and enhance environmental conditions for in-stream organisms. Therefore, the river is widened where possible and deepened where necessary. A narrow river with an impoverished morphology dampens a wave pulse from a hydropeaking regime less compared to a larger river with well-connected floodplain and dead waters.
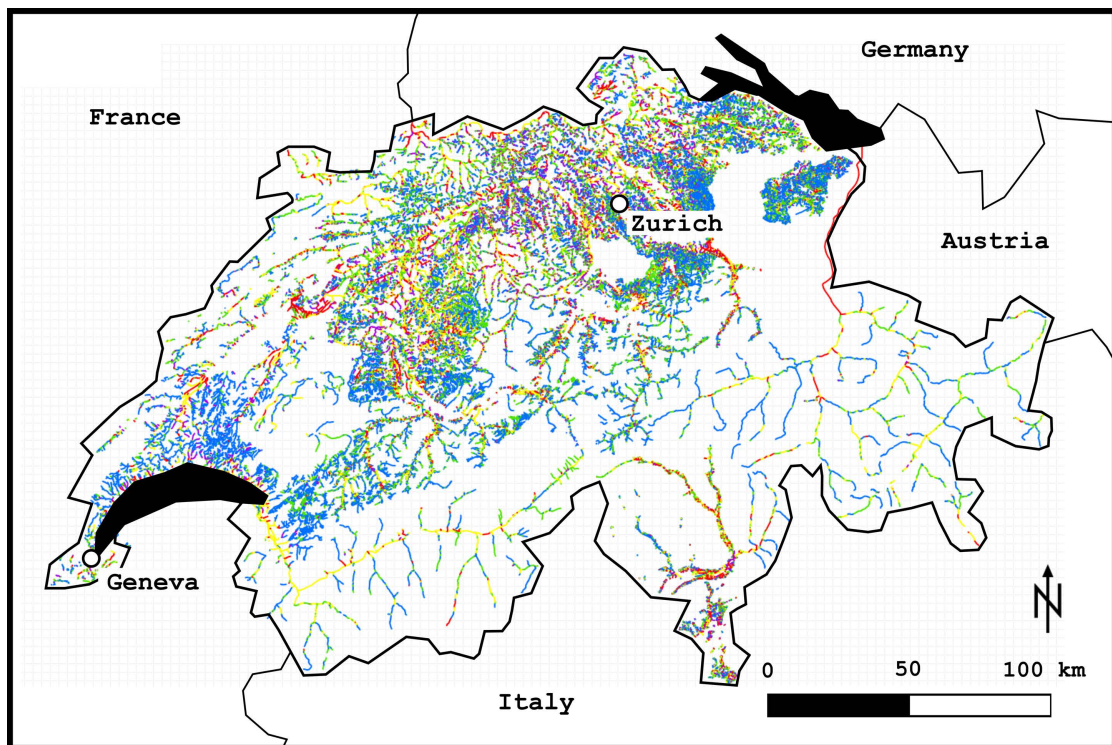
Figure 1.6 – Classification of Swiss river segments according their ecomorphological state respectively the structural variability with the method Ecomorphology level F (BAFU, 1998). Purple = culverted, red = non-natural / artificial, yellow = heavily modified, green = slightly modified, blue = natural / near natural. Data from FOEN, status of 13 September 2008.

1.7   Climate change

The Intergovernmental Panel on Climate Change (IPCC) prognoses in its latest report from 2018 that the global surface temperature is likely to exceed an increase of 2°C for almost all scenarios at the end of the 21st century compared to 1850-1950 period (United Nations, 2018). During the 2015 United Nations Climate Change Conference in Paris (UN FCCC COP21), world leaders, committed to the Paris Agreement stating that the global warming must remain well below 2°C at the end of the 21st century. This agreement is legally binding and the first of its kind. It is seen as a replacement of the Kyoto Protocol, which phases out in 2020 and interlinks several aspects of the Sustainable Development Goals (SDG) defined by the United Nations. Switzerland ratified the agreement on 6 October 2017 and agreed to reduce its greenhouse gas emissions by 50 % by 2030 compared to 1990 (UN FCCC, 2015).

Research prognoses the complete retreat of most glaciers in the alps until the end of the 21st century (Zemp et al., 2006; Schaefli et al., 2019). The loss of glaciers is connected with the creation of new lakes at high altitudes. Such lakes, however, are subject to significant danger. Rock falls, calving glaciers or landslides from the steep surrounding terrain can produce uncontrolled glacier lake outburst floods (GLOFs). Such floods can severely harm downstream

settlements and industry (Semenza and Ghirotti, 2000; Genevois and Ghirotti, 2005). In certain cases, such lakes may be secured against uncontrolled breakout by the creation of dams. These reservoirs in high elevations can also be used to store water for electricity production or for long dry periods. Such periods are expected to become more frequent with climate change (United Nations, 2018). Without glaciers, the role of reservoirs as seasonal water transfer will become more important (Haeberli et al., 2013; Schleiss, 2016). As an illustration serves the Trift project in the Grimsel area in the Canton of Bern (Figure 1.7). Due to the strict law, only at locations, where no vegetation is present, new reservoirs may be constructed. Otherwise, the focus must be directed towards improvement and upgrade of existing hydropower plants to ensure the national hydroelectric supply in the close future.

Figure 1.7 – The evolution of the Trift glacier and a visualization of the future Trift dam and reservoir. Image courtesy KWO.

1.8 Environmental politics in Switzerland

1.8.1 Legal background

Aware of problems associated with water retention and hydropower infrastructure, the Swiss Fishing Federation came up with a national initiative in 2006, which was known as the "Renaturierungsinitiative". Under this public pressure, the Parliament elaborated changes in the Swiss Federal Act on the Protection of Waters have taken effect (WPA). The main changes are the obligations for cantons to ensure the rehabilitation of waters and for the owners of hydropower plants to mitigate negative impacts resulting from water use on the indigenous flora and fauna, as well as on their habitats. This includes the problems of hydropeaking, sediment dynamics, residual flow and fish migration. The new key paragraphs are cited here:

- Art. 36a : SPACE PROVIDED FOR WATERS

  §1 "*The cantons, after hearing the parties concerned, shall stipulate the spatial require-ments for surface waters (space provided for waters) in order to guarantee the following functions: a. the natural functions of the waters; b. flood protection; c. the use of the waters.*"

- Art. 38a : REHABILITATION OF WATERS

  §1 "*The cantons shall ensure that waters are rehabilitated. In doing so, they take account of the benefits to nature and the landscape as well as the economic consequences of the rehabilitation.*"

- Art. 39a : HYDROPEAKING

  §1 "*Those responsible for hydropower plants must prevent or eliminate by means of civil engineering measures short-term artificial changes in the water flow on a body of wa-ter (hydropeaking) that cause serious harm to the indigenous flora and fauna as well as their habitats. At the request of the person responsible for a hydropower plant, the authority may order operational instead of civil engineering measures.*"

- Art. 43a : BED LOAD BUDGET

  §1 "*The bed load budget in the body of water may not be changed by installations to the extent that they cause serious harm to the indigenous flora and fauna, their habitats, the groundwater regime and flood protection. The persons responsible for the installations shall take suitable measures to this end.*"

- Art. 62c : PLANNING THE REMEDIATION OF HYDROPEAKING AND BED LOAD BUD-GET

  §1 "*The Confederation shall within the limits of the approved credits grant the cantons compensatory payments for planning in accordance with Article 83b, provided the plans are submitted to the Confederation by 31 December 2014.*"

  §2 "*The compensatory payments are up to 35 % of the attributable costs.*"

- Art 83a : REMEDIATION MEASURES

  "*The persons responsible for existing hydropower plants and of other installations on waters are obliged, within 20 years of this provision coming into force, to take the appro-priate remediation measures in accordance with Articles 39a and 43a.*"

- Art. 83b : PLANNING AND REPORTING

  §2 "*The cantons shall submit the plans to the Confederation by 31 December 2014.*"

The year 2011 has brought two main changes concerning the future of Swiss rivers and hy-dropower production. In January, the new amendments to the WPA entered into force. On 11 March 2011, an earthquake followed by a Tsunami, destroyed the cooling system of the

nuclear power plant in Fukushima, Japan. This caused three nuclear meltdowns resulting in the largest nuclear catastrophe that humankind has experienced in the late history. Consequently, anti-nuclear movements rose, followed by the decision to phase out nuclear energy production in numerous countries (e.g. Germany). In May 2011, the so-called "Fukushima Effect" arrived in Switzerland and Federal Councilor Doris Leuthard announced the willingness of the Government to phase out nuclear energy until 2034.

In the beginning of 2014, the Parliament changed the energy law to support the construction of renewable energy production technologies and granted money for energy research. Eight Swiss Competence Centers for Energy Research (SCCER) were founded to coordinate this research.

1.8.2   Energy Strategy 2050

This decision demands a fundamental change in the Swiss Energy system and the Federal Council elaborated the Energy Strategy 2050. 58.2 % of the Swiss people voted "yes" to the new energy law (EnG) on 21 March 2017. The EnG focuses on measures to increase the energy efficiency and the electricity production from renewable energy technologies. Also to ensure sufficient electricity supply in winter, power generation through wind, solar, hydro- and biomass power need to be increased (see Figure 1.8). The so-called new renewable technologies (wind, solar and biomass power) have a vanishing share in the current Swiss electricity production.

Regarding hydropower, the situation is also challenging. On the one hand there is the WPA stating that more water has to be released to respect nature while on the other hand there is the Energy Strategy 2050 demanding more hydropower. The road map foresees an increase of the mean annual hydropower production of 1.53 TWh under current and 3.16 TWh under optimized conditions compared to expected production in 2012 (SCCER, 2018). According to BFE (2012) this corresponds to an increase from 35.82 TWh/a to 37.35 TWh/a respectively 38.98 TWh/a (see Figure 1.2). The SCCER responsible for the Supply of Electricity (SCCER-SoE) states that this challenging goal can be reached focusing on two concepts:

Concept 1 : Innovative and sustainable solutions for new hydropower schemes

Exemplary stands the Trift project (see Figure 1.7). Retreating glaciers may create ecological and economically favorable locations for the construction of hydropower plants (e.g. Gorner Glacier) what is explained in detail in Section 1.7. Further, an increase of the power production from small hydropower plants with an installed capacity from 0.3 to 10 MW is expected.

Concept 2 : Extension and optimization of existing hydropower schemes

Exemplary are the construction of the Muttsee Dam and the increase of installed capacity of Veytaux for pumped-storage purpose. Dam heightening increased the storage capacity of the Lac de Mauvoisin by 30 Mio m^3 and Lago di Luzzone by 20 Mio m^3 enabling the seasonal transfer of electricity production. Similar projects are planned (e.g. heightening of the Grimsel reservoir dams).

All these modifications and new constructions of hydropower plants can only be realized if they are well thought through due to environmental regulations and potential resistance in society.
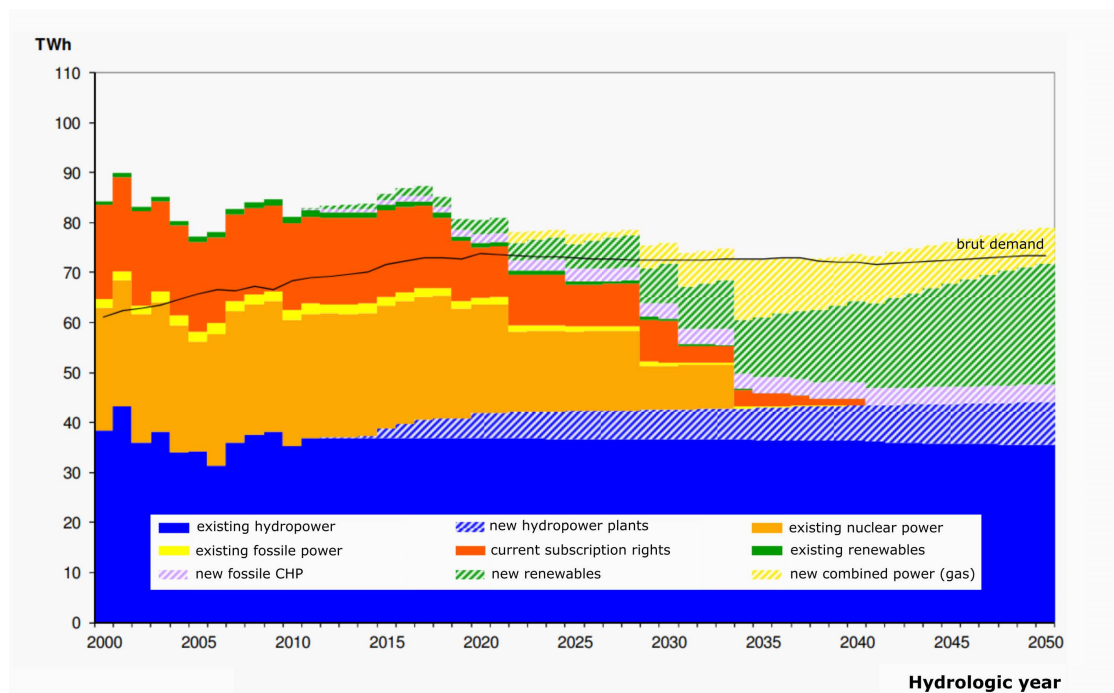
Figure 1.8 – The current and future electricity mix of Switzerland as it is foreseen in the Energy strategy 2050 (Graphic: Prognos (2012)).

1.9 Research project Hydro-Ecology and Floodplain Sustainability in Application

In order to facilitate energy transition, the Swiss government launched the National Research Program (NRP) 70 Energy Turnaround, with a budget of 37 Mio CHF over five years. It focuses on the scientific and technological aspects of the change in energy strategy to a new energy system in Switzerland. 26 projects were accepted, among them the project Hydro-Ecology and Floodplain Sustainability in Application (HyApp, see www.nrp70.ch). The HyApp is an interdisciplinary project combining hydrology, geomorphology, remote sensing, riparian and

aquatic ecology. Researchers from four different institutes, the École Polytechnique Fédérale de Lausanne (EPFL), the Swiss Federal Institute of Aquatic Science and Technology (Eawag), the Zurich University of Applied Sciences (ZHAW) and the University of Zurich (UZH), worked on this project during four years (see Figure 1.9). The overarching goal of this project was to provide tools and indicators to sustainable develop hydropower production. This includes the evaluation and optimization of restoration actions. Exemplary are adaptive management of flow and sediment regimes. Therefore, the further development and testing of indicators linking hydro-morphological structure (e.g. hydraulic diversity) and ecological function (e.g. biodiversity) applicable for the evaluation of restoration actions across floodplains. Models that allow the prediction of the ecological potential of restoration actions and remote sensing techniques for spatially explicit monitoring at the floodplain scale was integrated.

This interdisciplinary research focused on three floodplain sites, namely the Sarine (residual flow and hydropeaking flow regime) and the Sense (natural flow regime) and the Spöl River (residual flow regime). More information about them can be found in Chapter 3. The work presented in this research study mainly part of pillar two of the HyApp project: Morphodynamics of hydropower impacted floodplains. Intensive field studies allowed the definition of the data sufficiency to determine the hydro-morphological diversity in a river segment. In addition to that the dam operator and the local authorities planned an artificial flood in the Sarine floodplain during this study. By reason of this non foreseen event, the study was intensified in the Sarine, investigating a novel sediment replenishment methodology. These results could then be compared with the long-term study at the Spöl. Finally, a link between ecohydraulic conditions and in-stream biology was investigated, accentuating the need of transboundary research in sustainable floodplain management.
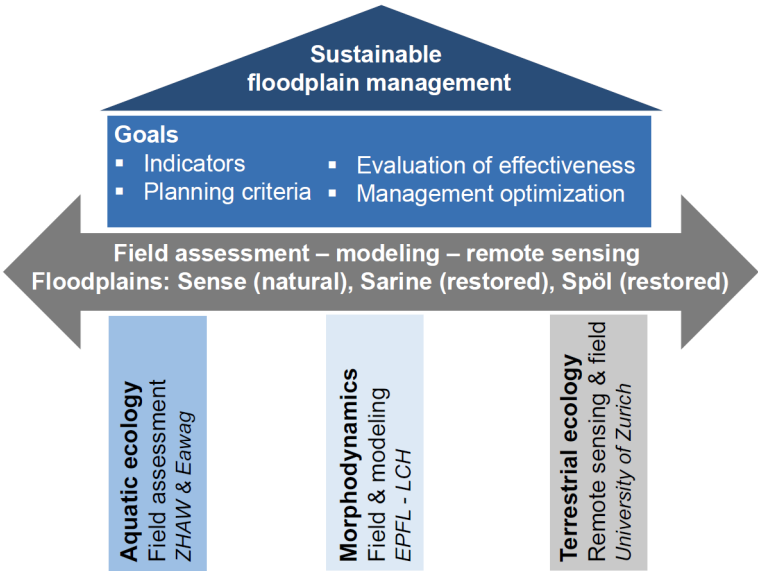

Figure 1.9 – The research project HyApp of the NRP 70 with its main three pillars and research partners.

1.10 Structure of the research report

The present document is structured into several chapters dealing with different topics. Their contents are briefly presented here:

Chapter 1 : Introduction
Problems of water infrastructure projects are presented in brief and underline that questions connected to the waterscape are not just physical problems, engineers have to solve but transboundary complex questions cross-cutting domains of water governance, economy and society. Hence, holistic sustainable solutions are needed. This leads via the current political discussion worldwide and in Switzerland to the motivation of this research study for society, engineering and politics.

Chapter 2 : State of the art
Physical and geomorphological functioning of a river as complex system is explained and the latest research presented. Some general equations used in the different chapters are presented as well. In the end of the chapter the need of research in the domain of hydropower related river restoration is highlighted underlining the scientific relevance of this research study.

Chapter 3 : Site description
The six different rivers that were analyzed in this study are described. The Sarine [german: Saane] is described most in detail and also a historical analysis of the river in the reach of interest is presented. Followed by the description of the Spöl and the Sense a bit less detailed and the Buenz, Venoge and Passer in little detail. The degree of detail corresponds to the importance of the rivers in this research study.

Chapter 4 : Sampling sufficiency for determining hydraulic habitat diversity
In order to quantify changes in the ecohydraulic parameters, such as flow depth and velocity of a reach and also changes due to restoration measures, the sufficiency and sensitivity of field data is analyzed from 19 river segments of different morphologies. The resulting figures and tables can serve as a planning help for ecohydraulic data sampling and stream assessment.
Results from this chapter are published in: Stähly S, Gostner W, Franca MJ, Robinson CT, Schleiss AJ (2019). Sampling sufficiency for determining hydraulic habitat diversity. *Journal of Ecohydraulics*. DOI: 10.1080/24705357.2019.1576021

Chapter 5 : Erosion, transport and deposition of a sediment replenishment under flood conditions
Transport processes of a four-deposit sediment replenishment configuration was applied for the first time in prototype scale. The setup was investigated by stone tracing techniques during an artificially triggered flood in the Sarine. The chapter focuses on the comparison between the experiment at the Sarine and previously conducted laboratory experiments. Further an erosion efficiency factor was defined.

Results from this chapter are under review in: Stähly S, Franca MJ, Robinson CT, Schleiss AJ (2019). Erosion, transport and deposition of a sediment replenishment under flood conditions. *Earth Surface Processes and Landforms*

Chapter 6 : Artificial floods to improve the hydraulic habitat diversity downstream of dams
The impact of artificial floods on residual flow segments at the Spöl and the Sarine were investigated. The investigation focused on the change in the HMID value by artificial flood events in different river segments. The river segments differ in geomorphology, slope and especially sediment supply.
Results from this chapter are under review in: Stähly S, Franca MJ, Robinson CT, Schleiss AJ (2019). Sediment replenishment combined with an artificial flood improves river habitats downstream of a dam. *Scientific Reports* 9(1), 5176. DOI: 10.1038/s41598-019-41575-6

Chapter 7 : The physical characteristics of the river flow and biological indices
A possible link between hydraulic habitat variability respectively the flow regime and ecological diversity is investigated in Chapter 7. Links between the hydraulic habitat diversity represented by the HMID and different indices of macroinvertebrates are investigated and discussed regarding different flow regimes and the influence of an artificial flood.

Chapter 8 : Conclusions and outlook
The overall conclusions drawn by the research presented here are given. This chapter summarizes also the limitations of the research study and the need of future research.

Appendices
Additional data and images concerning the study sites, the replenishment and the flood as well as all river segments samples for the analyses in Chapter 4 are contained in the appendices.

2 State of the art

2.1 Overview

This chapter summarizes the research previously performed in the field. First, basic aspects of river process and definitions are given. In the second part, the latest findings of how to approach problems connected with damming, river training and hydropower production are summarized. The focus is directed towards the following topics:

- The river is introduced as a complex system. Different **scales**, river **classification** and **habitat assessment methods** are presented.

- Different approaches to solve problems in rivers. Experiences with **river restoration**, **sediment replenishment** and the release of **flood pulses** to restore habitats are reviewed.

- Based on the literature research, the **gaps of knowledge**, defining the need of research crystallize and provide the **objectives** of this research study.

2.2 The river - a complex system

To restore a river, one has to understand the river behavior and its processes. Rivers differ largely in their spatial and temporal dimensions as well as their degree of dynamism (Kondolf et al., 2005). River processes and characteristics vary regionally and many attempts were taken to order rivers into groups based on their common characteristics. The slope of a river decreases starting at its origin in mountainous areas towards its mouth in a lake or sea (Schumm, 1977; Kondolf, 1994). Rivers can be split in three zones, the erosion zone, the transport zone and the deposition zone (Figure 2.1). The transported sediment changes its size and shape (Zingg, 1935). Large boulders that enter the river due to slope erosion, rockslides or glacier flow change their shape and size when being of transported. They become smaller and rounder since their edges are smoothed by every contact with other stones. Long
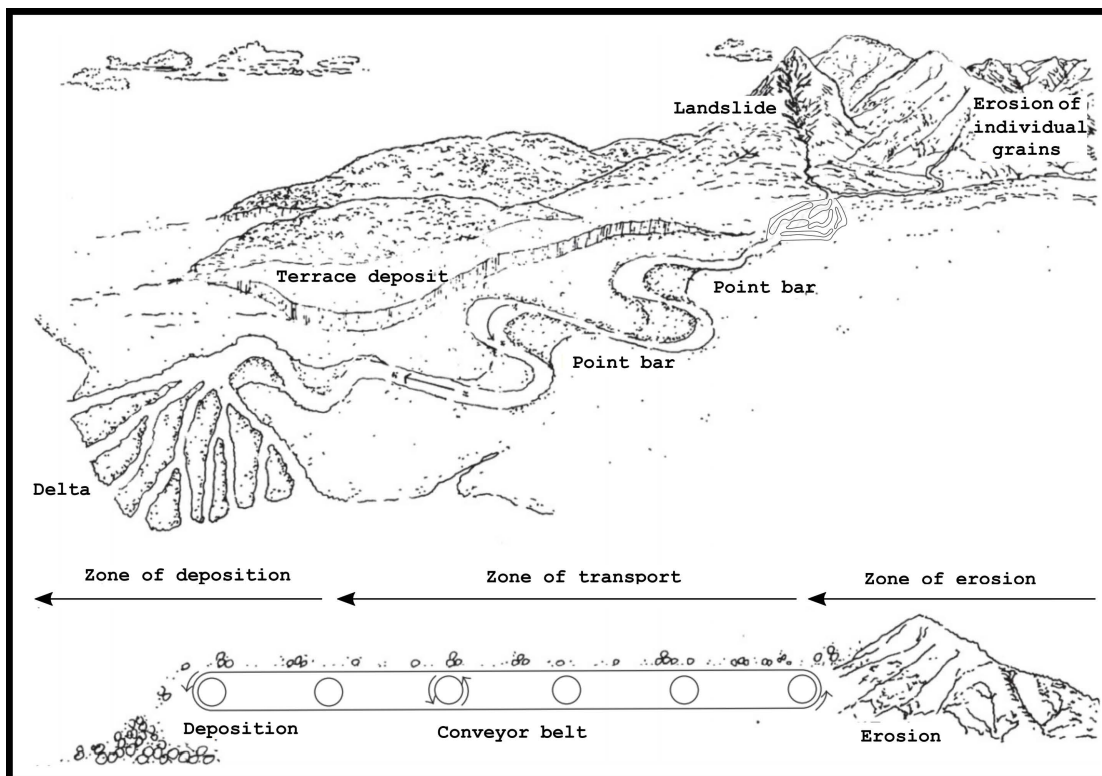
Figure 2.1 – Spatial variability of a river. Diagram of zones of sediment production, transport and deposition illustrating the conveyor beld analogy for the zone of transport (Kondolf, 1994).

rivers which end in the sea often transport only sand at its mouth and larger cobbles may not be present anymore (Krumbein, 1941; Kuenen, 1956). For example during a rain event, a river can change radically its face. A calm small river can turn into a dangerous torrent within minutes. Another example is again human activity. Depending on the land use and the change of land use (e.g. urbanization or agricultural practices) in a catchment can influence flow concentration time and sediment yield in a river to a large extend. This can change the riverine parameters like width, flood peak discharge, slope and finally channel migration (Leopold, 1973). Therefore, a river always needs to be considered as temporal and spatial variable and not as a static system. Exemplary stand river meanders, where sediment is eroded at the outer bank and deposited in the inner bank resulting in a slowly moving river pattern of time and space (Salo et al., 1986).

2.2.1 Stream classification

To better understand the complex system, researchers started to classify geological terrains in different groups based on common characteristics. Classifications were first developed for landscapes and hillslopes (Davis, 1899; Varnes, 1958). Later, rivers were classified and a commonly used classification method was defined by (Leopold and Wolman, 1957). Leopold

and Wolman (1957) classified rivers into straight, meandering, braided streams. Yalin (1992); Jäggi (1983); Da Silva (1991); Parker (1976) presented an objective classification method for different river morphologies based on physical parameters such as slope, river width, flow depth and substrate which have been widely applied for river engineering purposes. Rosgen (1994) presented one of the most detailed river classification methodologies defining 48 different river types based on physical parameters.

Today, there is a large variety of river classification methods in use. A detailed review is given in Kondolf et al. (2005) and Buffington and Montgomery (2013). Both of these reviews distinguish two main river classification concepts:

- descriptive classifications: mostly quantitative because they are based on measurements of multiple physical parameters such as slope, grain size, wetted-width;

- process-based classification: can be conceptual (qualitative) because they are based on *'mechanistic arguments and explanation of the physical processes associated with a given channel morphology'*.

Descriptive river classifications may be valuable for pattern-recognition and inventory tools that can be developed into Geographic Information System (GIS) applications despite their lack in process-based foundation (Buffington and Montgomery, 2013). However, miss-use of such classification methods have led to various discussions and controversies in the field of geomorphology and river restoration (Lave, 2012, 2016).

2.2.2 Scales

When working on rivers, it is important to look at them in different scales, in both temporal and spatial domain. Frissell et al. (1986) defined the habitats in a river in different spatial scales, ranging from the whole catchment ($10^3 m$) to the microhabitat system ($10^{-1} m$, see Figure 2.2). The geomorphic perspective of scales is of high importance when it comes to river restoration (Liébault et al., 2008). River restoration often takes place in a segment ($10^2 m$) or reach ($10^1 m$) scale. A local intervention may prevent the continuation of bank erosion. However, the geomorphic processes at basin scale do also have to be taken into account since the effects of such an intervention (e.g. dam $10^1 m$ scale) can propagate downstream and affect the river on a much larger scales (Kondolf and Piégay, 2003).

The resulting effects of an intervention in a river are not always evident. River engineering projects mostly deal in engineering time-scales (Simon et al., 2016) which are more understandable for the society. This is well reflected in the expected lifetime of hydropower dams or associated concessions of 50 to 100 years. Flood events, avalanches or landslides change rivers and occur in very short time scales. However, geomorphological times scales are mostly significantly longer than human lives wherefore riverine structures and restora-

tion measures need to be well thought through (see Table 2.1) and need to be planned accordingly (Pont et al., 2009).
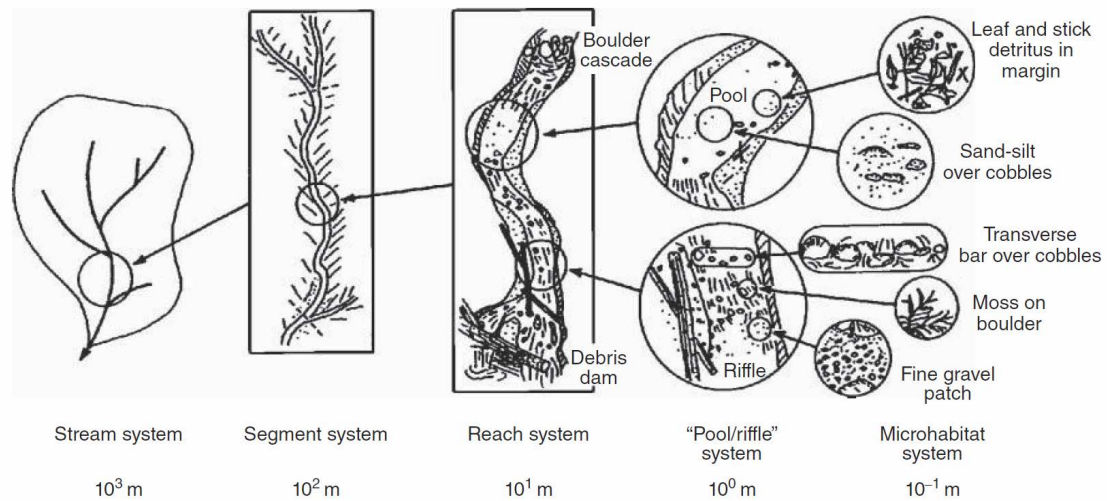
Figure 2.2 – Hierarchical organization of a stream system and its habitat subsystems. Approximate linear spatial scale, appropriate to second- or third-order mountain stream is indicated (Frissell et al., 1986).

2.3 River assessment and habitats

2.3.1 General

A river segment and its habitats can be assessed. Flow and sediment regimes (Wohl et al., 2015) can induce a large variety of habitats (Allan and Castillo, 2007). Hydro-morphological conditions are an essential factor for in-stream life. Species have preferred ecohydraulic conditions, such as flow depths, velocities and shear stresses near the streambed (Statzner et al., 1988; Heggenes, 1996). Jowett (1993) presented an objective method to classify hydraulic habitats such as pools, riffles and runs in a river reach based on flow depth and velocity. Later on, he showed that the spatial variation of flow depth, velocity and water surface depend on cross-section geometry in New Zealand rivers Jowett (1998), which allowed him to predict these flow features based on river geometry. This approach was examined in more detail by Schweizer et al. (2007). Further, Lamouroux et al. (1995); Lamouroux (1998); Gostner et al. (2013a) evaluated the statistical properties of ecohydraulic variables in rivers towards developing models for the prediction of habitat quality. The coupled interaction between ecology and hydrological conditions in rivers was the focus of follow-up research by Lamouroux et al. (1998); Parasiewicz (2001); Lamouroux and Jowett (2005); Schleiss (2005). These studies showed that hydraulic habitat diversity depends to a large extent on river geomorphology. Recently, Lane et al. (2017) pointed out the lack of topographic variability attributes (TVAs) in river classification methods Frissell et al. (1986); Rosgen (1994); Kondolf (1994); Kondolf et al. (2005) and considered TVAs in their classification. The comprising nine channel types give a high value to TVA and hence ecohydraulic variables, being of high interest in river restoration projects Gilvear et al. (2013); Schwindt et al. (2019).

Table 2.1 – Levels of channel classification in different spatial and temporal scales. From Bisson et al. (2017), after Frissell et al. (1986); Montgomery and Buffington (1997).

Classification level	*Spatial scale (magnitude)*	*Temporal Scale (years)*
Channel/habitat units	1-10 m	<1-100
Fast water		
Rough		
Smooth		
Slow water		
Scour pools		
Dammed pools		
Bars		
Channel reaches	10-1'000 m	1-1'000
Colluvial reaches		
Bedrock reaches		
Free-formed alluvial reaches		
Cascade		
Step-pool		
Plane-bed		
Pool-riffle		
Braided		
Dune-ripple		
Forced alluvial reaches		
Forces step-pool		
Forced pool-riffle		
Valley segment	100-10'000 m	1'000-10'000
Colluvial valleys		
Bedrock valleys		
Alluvial valleys		
Watershed	50-1'000 km^2	>10'000
Geomorphic province	>1000 km^2	>10'000

2.3.2 Ecohydraulic variables

The way in which the flow geometry (flow depth, velocity and wetted width) depends on changes in discharge can be referred to as at-a-station hydraulic geometry (Stewardson, 2005; Lamouroux, 2007). Leopold and Maddock (1953) fitted them to power laws (Equation 2.1 and 2.2).

$$h = a \cdot Q^b \tag{2.1}$$

$$w = c \cdot Q^d \tag{2.2}$$

These equations can be combined to calculate the flow velocity (Equation 2.3):

$$v = Q \cdot (h \cdot w)^{-1} \tag{2.3}$$

with:

h Flow depth [m]
v Flow velocity [ms^{-1}]
w Wetted river width [m]
Q Discharge [m^{3}s^{-1}]
a, c Hydraulic coefficients
b, d Exponents

In a non-rectangular channel, h and v can be referred to the mean flow depth and velocity which will be mentioned as μ_h and μ_v in the presented research. The variation of these two key ecohydraulic variables, the mean flow depth and the mean flow velocity, can be combined resulting in the hydro-morphological index of diversity (HMID). Using the sampling procedure outlined below, these variables scale up from at-a-station to segment scale hydraulic geometry.

2.3.3 The hydro-morphological index of diversity

The HMID is an easy applicable quantitative measurement and predictive tool for estimating the habitat diversity in rivers, which combines both geomorphological and hydraulic conditions (Gostner, 2012; Gostner et al., 2013a). The basic HMID of a river segment takes into account the spatial distribution of hydraulic measured values of flow depth and flow velocity

(Equation 2.4). The result is a single value that represents the habitat diversity in the river segment. In this belonging, the HMID differs substantially from other hydro-morphological river assessment methods. Most of them are based on expert judgment and are therefore less objective (BAFU, 1998; Barbour et al., 1999; Rinaldi et al., 2013; Feio et al., 2016; Rinaldi et al., 2017). Compared to these methodologies, the HMID does not give information about the water quality, turbidity or biomass found in the analyzed river segment. The HMID represents the conditions in the river at the moment of measurement and depends on the discharge. Since it measures the hydraulic habitat diversity in a river segment at a given discharge, it can be combined with numerical models. This gives the HMID predictive power to quantify the effect of river restoration measures, allowing the comparison of different restoration variants from a habitat diversity point of view. Further it can also be used as a success control of realized restoration projects.

$$HMID_{segment} = \prod_i (1 + CV_i)^2 = \left(1 + \frac{\sigma_v}{\mu_v}\right)^2 \cdot \left(1 + \frac{\sigma_h}{\mu_h}\right)^2 \tag{2.4}$$

with:

CV_i Coefficient of variation of variable i
μ_i Mean value of variable i
σ_i Standard deviation of variable i
v Flow velocity [ms^{-1}]
h Flow depth [m]

Depending on river morphology, typical HMID values between 1 and 15 are obtained representing the habitat diversity in a river segment. According to the HMID value, the current condition of a river segment in respect to habitat diversity can be classified into three categories (Gostner et al., 2013a):

- Low (HMID < 5)

  "*Channelized and morphological heavily altered sites with uniform cross sections and bed slope. An HMID close to 5 corresponds to a channelized river with minor geomorphic patches as, for example, a thalweg line continuously shifting between the two bank toes.*"

- Medium (5 < HMID < 9)

  "*Stream sites at the lower end of this range are still showing a limited variability of hydraulic units. Hydro-morphological richness typical to intact natural state are not developed yet. At the upper end of this range, sites are approaching natural morphology.*"

- High (HMID > 9)

  "*Morphologically unregulated sites, where gravel bed streams fully develop their spatial dynamics showing the complete range of hydraulic habitats. For river engineering*

projects, such sites could be classified as references."

The measurement should be done during mean flow (100 - 250 days exceedance), representing the optimum for habitat diversity and where the HMID explains the differences in physical diversity at best (Carter et al., 1998). Flow depths and velocities are measured along equally spaced cross-sections of the river segment of interest. Flow velocity is measured at 40 % of the flow depth, corresponding to the location of the mean velocity assuming a logarithmic velocity profile. Studies investigating the spacing between the cross-sections or the required data volume to compute a representative HMID have not been performed yet.

The HMID also has its limitations. The HMID values of all types of river morphologies tend to be small for extreme discharges. The difference between sites with well-developed morphological structures and sites with poor morphological diversity is therefore the rate at which this decline in HMID occurs (Gostner, 2012). Sites with higher morphological diversities tend to have constant HMID values for mean flow stages, whereas channelized river segments experience a degradation of the HMID value. This behavior is defined as the temporal stability of the HMID (Gostner, 2012). The ecohydraulics for the discharge at the day of measurement and does not take into account the yearly regime. Therefore, a river segment with residual flow, hydropeaking and a natural flow regime may result in the same HMID despite their total different characteristics over time. It has not been proofed if a high HMID represents also a high richness of macroinvertebrate or fish species. Important factors such as water temperature, organic matter, connectivity or altitude are not part of the HMID.

2.4 River restoration

Since 2011, flood protection measures must be combined with river restoration projects (see Section 1.8.1, Art. 38a, e.g. Third Rhône Correction). More space must be given to rivers to enable the sufficient transport of sediment and floods as well as ecological functionalities (the creation and connection of habitats). Therefore, reinforcement of dykes has been combined with widening of the river corridor in which the river can "freely" develop. A famous Swiss example is the Thur near Altikon (Weber et al., 2009). On an almost 2 km long river segment, the right foreland was completely removed in 2002. Sediment settled soon after this widening and a sequence of alternate bars evolved in the restored river segment (see Figure 2.3). Floods in 2010 and 2011 started an enhanced erosion process at the right bank, removing a large part of the riparian forest (Pasquale et al., 2011; Schirmer et al., 2014). The river segment has been evolving towards a meandering morphology, using more and more space, creating dynamic habitats for species, which have become rare in channelized rivers as in the Swiss lowlands (Yalin, 1992). The return of the *little-ringed plover* at the restoration site after more than 100 years of absence can be valued as a great ecological success (Schirmer et al., 2014).

Figure 2.3 – Evolution of the Thur close to Altikon since its restoration in 2002. Image courtesy Swisstopo

2.5 The role of sediment replenishment for river restoration

As mentioned above, dams trap sediment in the upstream reservoir. This interruption of the sediment continuum and can cause severe deficits in the downstream river segment (Kondolf, 1997; Brandt, 2000; Petts and Gurnell, 2005). Observations revealed an almost complete retention of sediment in large reservoirs (Williams and Wolman, 1984). Therefore, the replenishment of sediments in downstream rivers has been studied extensively, allowing a process based restoration of rivers (Wilcock et al., 1996; Gaeuman, 2012; Arnaud et al., 2017; Heckmann et al., 2017). However, the effect of sediment replenishment on the biological responses and therefore the assessment of the success or failure of a restoration project is often neglected because of inappropriately short post-restoration monitoring (Bunn and Arthington, 2002; Bernhardt et al., 2005; Kondolf et al., 2007). Staentzel et al. (2018) investigated the responses of aquatic and riparian communities in the Upper Rhine River and observed a greater richness of macrophyte species in backwaters, the recruitment of pioneer species on gravel bars as well as an increase in the taxonomic richness of macroinvertebrates.

Lately an extensive flume campaign was performed to study the erosion, transport and deposition processes of sediment replenishment in a controlled environment (Battisacco et al., 2016; Battisacco, 2016; Friedl et al., 2018; Sklar et al., 2009). Friedl et al. (2018) looked at rivers with a small slope (0.17 %) and investigated the erosion processes of different dimensions of a single deposit adjacent to the river bank. This is a common practice in sediment replenishment (Kondolf, 1997). They came up with a method to predict the erosion rate of such a single deposit replenishment. Battisacco et al. (2016) on the other hand investigated steep rivers (bed slope = 1.5 %) in her laboratory facilities. She focused also on the deposition of the sediment replenishment in the downstream river. In experiments with a single deposit adjacent to one bank a fast erosion was observed connected with a strong dispersion of the material in the channel in a first step and an almost complete discharge of the material from the experimental facilities. Therefore different multi-deposit setups were investigated to keep the sediment in the system, both with laboratory and numerical experiments Battisacco (2016); Juez et al. (2016). The results are promising for a multi-deposit replenishment configuration of alternate bars. The settling of the replenished material in the downstream segment resulted in a repetitive pattern of sediment clusters (Battisacco et al., 2016).

2.6 Artificial floods to move sediment

Dams and reservoirs may have a severe impact on flow dynamics and sediment regime causing residual flow conditions due to water storage and abstraction (Magilligan and Nislow, 2005; Moyle and Mount, 2007). The interruption of the sediment continuum results in incision and silting up of the reservoir, and thus its storage volume decreases (Warner, 2012; Schleiss et al., 2016). Therefore river dynamics need to be brought back with artificially released flood pulses (Schmidt et al., 2001; Kondolf and Wilcock, 1996). Periodically released flood pulses are supposed to mimic missing flood events in a river segment downstream of a

dam. Since flushing of a reservoir is necessary for maintenance reasons, dam operators need to flush their reservoir periodically (Kantoush and Schleiss, 2009; Kantoush and Sumi, 2010; Sumi and Kantoush, 2010; Schleiss et al., 2016). Such a reservoir flushing can be designed to restore a residual flow segment (Konrad et al., 2011; Ock et al., 2013b; Gómez et al., 2013). Long-term studies have been conducted in several rivers, well-known are the experiments at the Spöl River (Robinson et al., 2018) and the Colorado River (Pennisi, 2004). The Spöl is located in the Swiss National Park and has a special flow policy. Since the year 2000, between one to three floods have been released each year. The focus of this long-term study is directed towards the restoration ecosystem services considering biotic aspects such as the resilience and diversity of macroinvertebrates in a regime with regular artificial floods (Robinson and Uehlinger, 2008; Robinson, 2012; Robinson et al., 2018). If possible, artificial flood pulses should be combined with sediment replenishment in order to sustain the sediment equilibrium in the river (Kondolf, 1997, 1998; Gaeuman et al., 2017).

2.7 Need of research

The state of the art focused on the research and practical work previously conducted in the field of river restoration and rehabilitation of hydropower impacted rivers. Despite several decades of research and application, there is still need of research. The gaps of knowledge this research study addresses are elaborated from the state presented of the art and presented below, divided into three subtopics.

Test of flood pulses and sediment replenishment

Laboratory experiments with multi-deposit sediment replenishment pointed out the potential for habitat creation. Such a multi-deposit sediment replenishment, however, has only been tested in laboratory scale and with numerical simulations. Therefore, experiments under real conditions are needed to study the erosion, transport and deposition processes of the replenished sediment applying the multi-deposit replenishment method. Further, the influence of an artificial flood pulse and the sediment replenishment on the hydraulic habitats needs to be investigated and the erosion efficiency of the flood hydrograph analyzed. A comparison of these results with a river where long-term studies with periodic artificial floods have been performed. Furthermore, a comparison of the field with the laboratory results will provide important additional knowledge concerning the robustness and finally the practical use of the elaborated multi-deposit sediment replenishment technique and environmental flows.

Data sufficiency for HMID computation

The computation and interpretation of the HMID values are principally objective, however, the planning of the data collection in the field does underlie a wide range of uncertainties, including the definition of the river segment, the spacing between the cross-sections (CS) and the data sufficiency. To increase the application of the HMID as a tool to measure the success

of river restoration projects, a variety of river segments with different morphologies must be analyzed and the data sufficiency evaluated, defining how many data points are needed and how the data must be sampled to compute a representative HMID of a river segment.

Connection between structural and biological diversity

Despite the lack of a clear link between sediment replenishment and ecological functions in regulated rivers (Ock et al., 2013a),Staentzel et al. (2018); Robinson et al. (2018) observed that sediment replenishment and artificially released flood pulses can lead to an increase in the taxonometric richness of macroinvertebrates in their studied rivers. The HMID gives a value to the distribution of the ecohydraulic variables flow depth and flow velocity at a given discharge, hence the hydraulic habitat variability. An investigation whether river segments with a high HMID value host also a rich diversity of macroinvertebrate species or not, is still missing. Such a link could complement the information the HMID is already giving significantly. This may likely not be the case, since multiple physical factors that are important for the in-stream biology are impacted by a dam (Kondolf and Wolman, 1993). Temperature, nutrients and seasonal flow fluctuation are some of these factors and they are not captured in the HMID. The HMID may be extended with a factor that represents the temporal variability of the flow. This would allow to apply the HMID also in hydropower impacted river segments.

2.8 Research objectives

From the elaborated need of research, the following objectives for this research project are derived:

1. To characterize the **erosion, transport and deposition processes** of a multi-deposit sediment replenishment combined with an artificially released flood.

2. To analyze the **erosion efficiency** of released flood hydrograph on the replenished sediment.

3. To **compare** the effects of a multi-deposit sediment replenishment applied in a **river with the laboratory** results.

4. To **compare** the effects of an artificial flood in a **river system where such floods have been applied regularly** over years with a river system in which it is applied for the first time.

5. To highlight **limits in terms of data sufficiency** and point-out the data needed to quantify a **segment representative HMID**.

6. To investigate a **link between ecohydraulic regime variability and biodiversity** in river segments. Therefore, the **flow regime** needs to be **objectively qualified**.

3 Description of the study sites

Six different rivers were analyzed, namely the Sarine, Spöl, Sense, Venoge, Buenz in Switzerland and the Passer in Italy. The locations of the rivers are shown in Figure 3.1, detailed characteristics in Table 3.1. The main focus was given to the Sarine river, followed by the Spöl and the Sense. The Passer, Buenz and Venoge river have been used to complete the dataset and are therefore described only in brief.
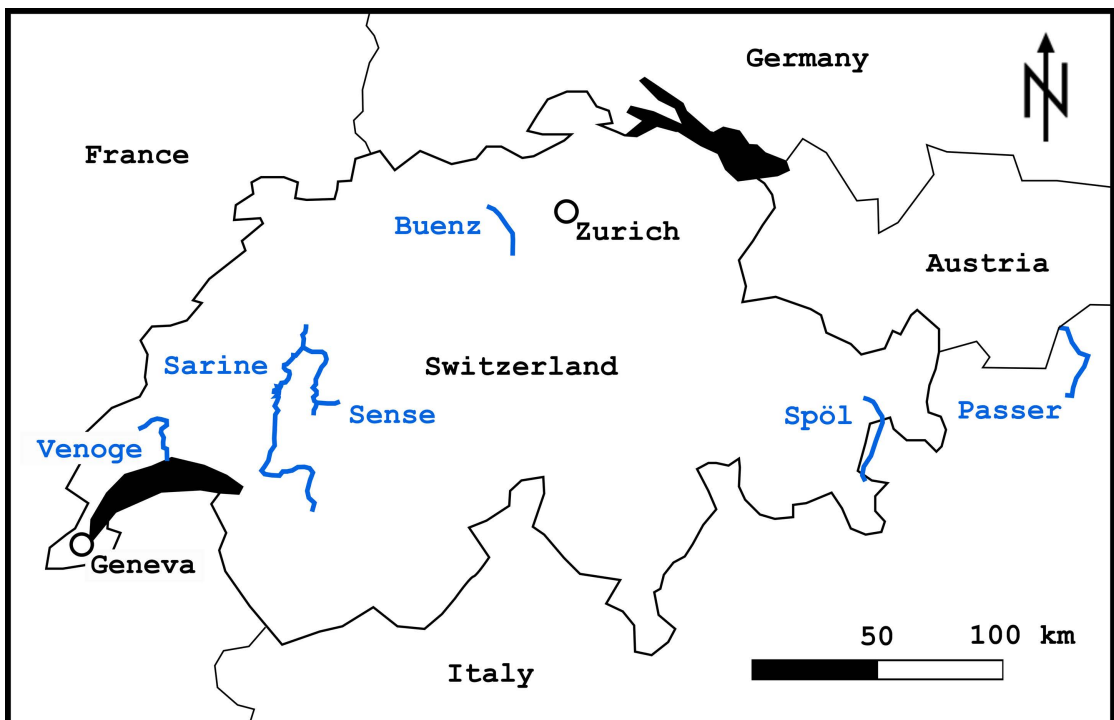

Figure 3.1 – Overview of the six river study sites from which data have been used for the analysis in the framework of this research.

Table 3.1 – Characteristics of the 22 study segments in the Sarine (3), Spöl (2), Sense (5), Buenz (4), Passer (4) and Venoge (4). b_b stands for the bankful width and J for the slope. (n) = natural, (c) = channelized, (r) = restored, (s) = sills

River name	Segment No.	Length [m]	b_b [m]	J [%]	Morphological pattern	WGS 84 NORTH	WGS 84 EAST
Venoge	I	60	5	2.2	meandering	46°37'42.54"	6°26'34.53"
Venoge	II	40	10	0.5	straight (c)	46°39'13.14"	6°30'28.99"
Venoge	III	80	7	0.4	straight (c)	46°37'38.74"	6°31'42.22"
Venoge	IV	120	14	0.4	alternate bars (n)	46°33'50.85"	6°31'43.84"
Buenz	I	140	9	1.5	straight (r)	47°22'38.57"	8°14'54.01"
Buenz	II	55	5	0.8	straight (c)	47°24'25.09"	8°12'05.68"
Buenz	III	115	10	0.3	meandering	47°24'28.72"	8°11'38.40"
Buenz	IV	150	15	0.2	braided (n)	47°24'38.79"	8°11'04.57"
Passer	I	145	50	1.3	alternate bars (r)	46°44'32.76"	11°12'21.49"
Passer	II	390	35	2.2	straight (c)	46°42'55.12"	11°11'40.42"
Passer	III	400	90	1.8	braided (r)	46°41'15.35"	11°10'38.15"
Passer	IV	405	30	0.4	straight (s)	46°40'48.86"	11°10'30.06"
Sarine	I	854	25	0.3	meandering (n)	46°45'21.61"	7°06'24.33"
Sarine	II	1880	25	0.3	meandering (n)	46°45'42.51"	7°06'41.61"
Sarine	III	500	30	0.3	meandering (n)	46°47'24.89"	7°08'54.49"
Sense	I	1850	127	1.8	braided (n)	46°44'13.15"	7°17'53.18"
Sense	II	760	66	1.3	alterante bars (n)	46°45'51.97"	7°18'07.52"
Sense	III	646	103	1.2	braided (n)	46°49'40.63"	7°19'21.81"
Sense	IV	558	41	0.5	alternate bars (n)	46°52'56.42"	7°21'13.75"
Sense	V	531	29	0.7	straight (c)	46°52'33.40"	7°20'00.55"
Spöl	I	150	12	1.1	meandering (n)	46°41'30.85"	10°07'18.69"
Spöl	II	230	25	0.9	braided (n)	46°41'41.96"	10°06'00.54"

3.1 The Sarine River

The Sarine is bed-rock alluvial river which originates at the Sanetsch at 2252 m a.s.l. It drains a catchment of about 1900 km^2 into the Aare, a tributary of the Rhine which mouths in the Northern Sea in the Netherlands. On its 126 km length, six reservoirs were built in the main stem of the Sarine, mainly for hydropower production. Close to its origin is the the Lac de Sénin on 2035 m a.s.l., the Sarine then passes by Gstaad in the Lac du Vernex in Rossinière. From there, water follows the river or through pressure pipes and turbines into the Lac de Lessoc. From there the slope of the Sarine decreases significantly. About 14 km downstream, the Lac de la Gruyère starts, with a capacity of 200 Mio m^3. This is the forth biggest artificial lake in Switzerland after the Lac de Dix (400 Mio m^3), the Lac d'Emosson (227 Mio m^3) and the Lac de Mauvoisin (212 Mio m^3, information from www.swissdams.ch). Further downstream in the city of Fribourg the Sarine crosses the Lac de Pérolle followed by the Lake Schiffenen before it mouths in the Aare at Laupen. These installations result in a regulated flow regime in the whole Sarine. Additional images of impressions of the Sarine between Rossens and Fribourg are given in Appendix B.

In the framework of this research study, the river segment between the 83 m high arch dam in Rossens (Figure 3.3) impounding the Lac de la Gruyère (667 m a.s.l. lake elevation) and the Lac de Pérolle (539 m a.s.l.) in the city of Fribourg, is investigated. Being located in a pre-alpine valley, the Lac de la Gruyère is 13 km long and the sediment continuum is completely interrupted by the dam. Currently a residual discharge of 2.5 – 3.5 m^{3}s^{-1} is released by the Rossens Dam (Table 3.3) using two small turbines at the bottom of the dam that produce 13.6 GWh electricity per year. This is the only discharge in the 13.4 km long and 25-30 m wide river segment between the Rossens Dam and the powerhouse in Hauterive. Before the dam construction, between 4'000 and 8'000 m^3 of sediment were transported through this river segment per year. Nowadays the erosion is limited to the riverbed, corresponding to 1'000 m^3 sediment (Jäggi and Hunziker, 2002; DAEC, 2014). In Hauterive, up to 75 m^{3}s^{-1} are released to the Sarine during electricity production causing downstream hydropeaking (see Figure 3.5). Downstream of the power house the tributaries La Gérine and La Glâne enter the Sarine (Figure 3.2. La Gérine supplies the Sarine with about 3'500 m^3 sediment per year (Jäggi and Hunziker, 2002). In the river segment with residual flow, two sites, referred as Sarine I and II, are of special interest (see Table 3.1 and Appendix B).

Before the construction of the Rossens Dam (Figure 3.3), there was already a water abstraction for the hydropower plant Thusy-Hauterive, built in 1902. The Thusy water intake consisted of a weir with 12 segment gates vertical to the river causing a residual flow regime in the Sarine. However, the storage volume was negligible and floods passed through the river segment without being dampened. Furthermore the gates allowed the transport of sediment downstream (see Figure 3.4). After the construction of the Rossens Dam in 1948, the Thusy weir was inundated by the reservoir Lac de la Gruyère. A situation of the intake is given in Figure B.10 in the Appendix.
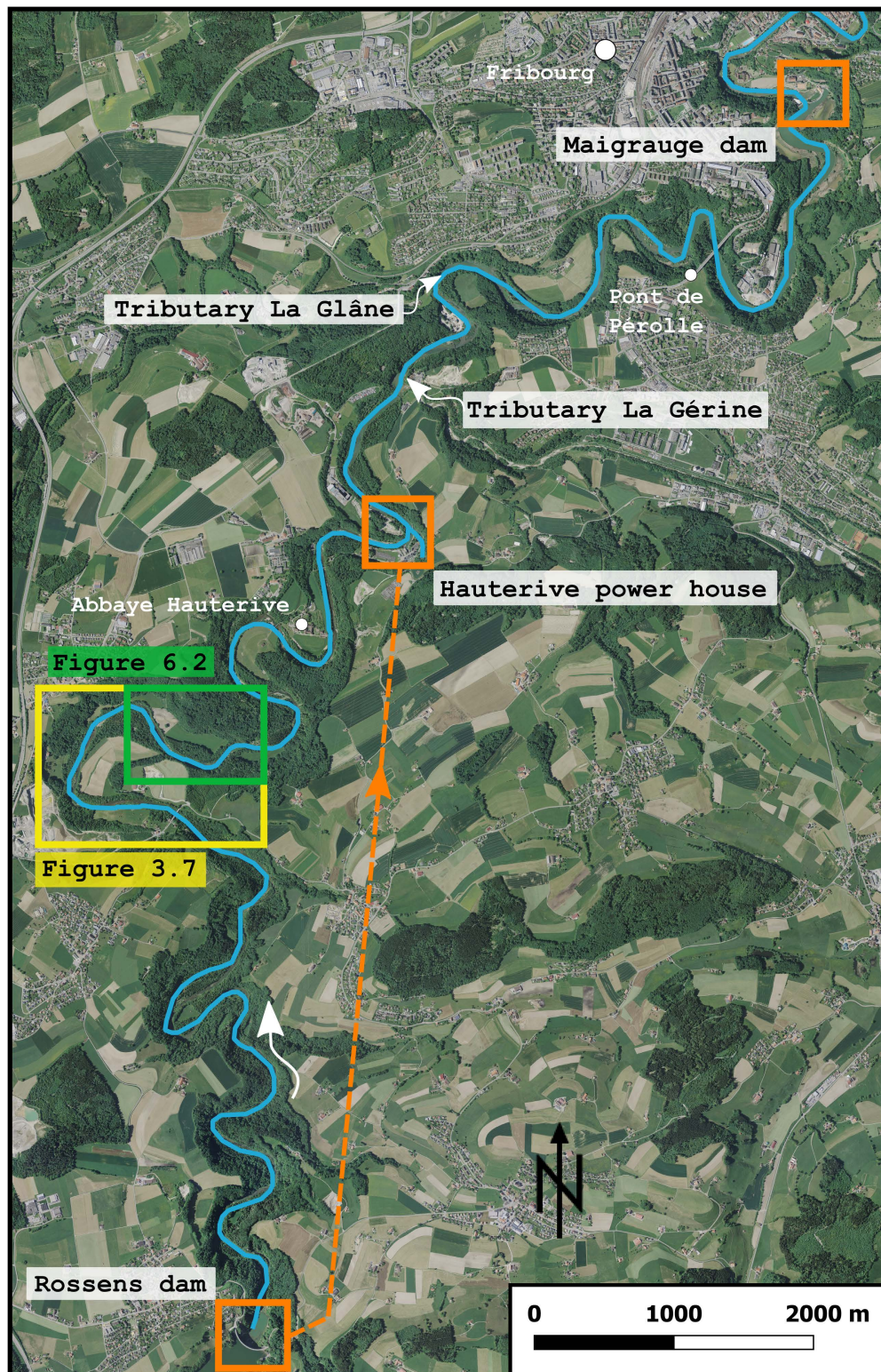
Figure 3.2 – An overview of the Sarine River segment between the dam in Rossens and the Maigrauge Dam in Fribourg. Between Rossens and the power house in Hauterive, a residual flow regime and downstream of the power house a hydropeaking flow regime is in operation (see Figure 3.5). Geodata courtesy Swisstopo

Figure 3.3 – Rossens Dam, 83 m height, built in 1948. Image taken on 14 September 2016. Image courtesy Research unit Ecohydrology, ZHAW

Figure 3.4 – Water intake of the former Thusy-Hauterive hydropower plant. The weir with 12 segment gates diverted the water from the Sarine through a tunnel to the powerplant in Hauterive from 1902. The Thusy water intake and its famous bridge in the back are inundated by the Lac de la Gruyère today. Image courtesy Bibliothèque cantonale et universitaire Fribourg. Fonds Mülhauser
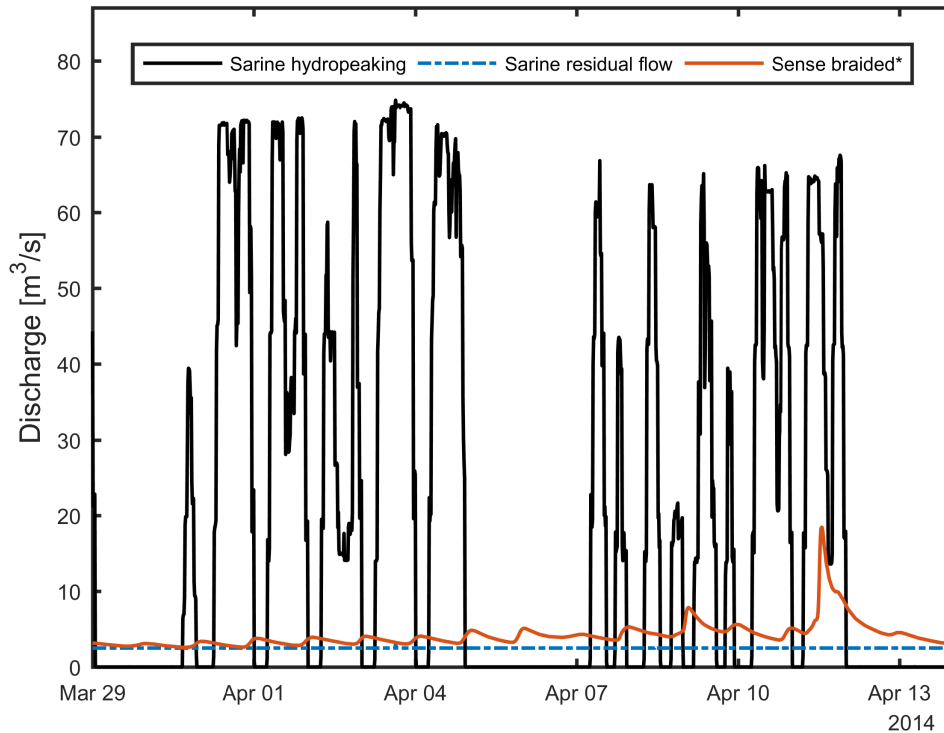
Figure 3.5 – The typical flow regime between Rossens and Fribourg, caused by the hydropower production and the Rossens Dam. As comparison serves the natural flow regime in the Sense, a downstream tributary to the Sarine. Data sources Groupe e and OFEN
*The data from the Sense were measured at the gauging station Thörishaus and corrected with the factor 0.44 based on the relevant catchment

The Sarine floodplain lies in an incised 100-m wide canyon surrounded by agricultural terrain and villages. Therefore, human-built structures in the floodplain are limited to some gravel roads, a handful of buildings and hiking paths. However, the absence of flood events and the interruption of sediment supply since the construction of the dam caused channel incision and disconnection of the floodplain. Vegetation colonized the previously wide gravel bars on the floodplain, mainly populated willows and hardwood. Exemplary the evolution of a meander bend in the Sarine between 1943 and 2004 that visualizes this scenario in the Sarine River (see Figure 3.7).

In Switzerland, the low electricity demand at weekends is generally covered by nuclear power and run-of-river hydropower plants. Storage hydropower plants generally do not produce electricity on weekends. They generate electricity at peak demands and prices, corresponding to the time when people are working between about 7:00 o'clock and 20:00 o'clock. This results in a daily and weekly flow pattern with large fluctuations, typical for storage hydropower plants (see Figure 3.5).
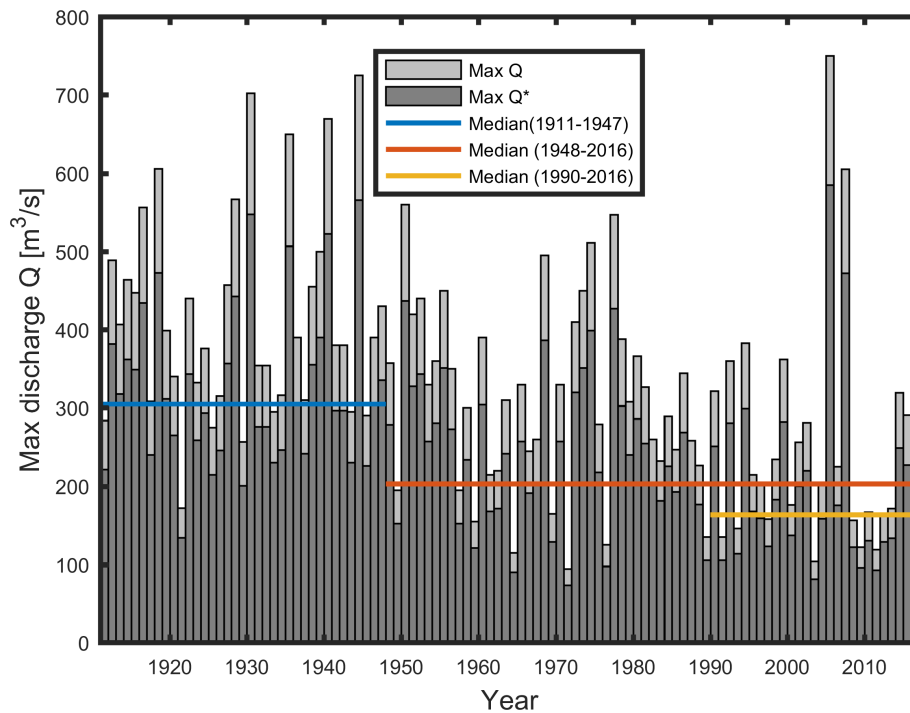
Figure 3.6 – Maximum discharge measured at the gauging station 2119 in Fribourg between 1911 and 2016. The trend indicates a decrease in the annual maximum flood magnitude since the completion of the Rossens Dam in 1948. Data source OFEN
*The data were measured at the gauging station 2119 in Fribourg and corrected with the factor 0.78 based on the relevant catchment. The medians refer to the corrected discharges

In the city of Fribourg, the gauging station 2119 of the confederation measures continuously flow depth and temperature in the river. Between the gauging station and the Rossens Dam, there is also the Maigrauge Dam which was built in 1872 and modified in 1910. Its allocated relatively small Lac de Pérolle had an initial volume of 650'000 m^3 which nowadays is largely filled with sediments, reducing the storage capacity. The hydropower operator is forced to run that power plant synchronous with Hauterive. Therefore, the measurement data from the gauging station 2119 is a good estimate concerning the flow in the river Segment of hydropeaking. The analysis of the maximum yearly discharge at the gauging station reveals a significant trend. The median of the maximal annual discharge decreased from 304 m^3s^{-1} in the pre-dam period (1911-1947) to 203 m^3s^{-1} for the post-dam period (1948-2016) what is a direct result of the construction of the Rossens Dam (Figure 3.6). This value decreased to 163 m^3s^{-1} for the recent period (1990-2016) what may be due to an optimized reservoir management system and technological advantage for hydrological forecasting, leading to less spilling of water. The yearly maximum measured discharge at station 2119 was corrected with the factor 0.78, based on the catchment size at the gauging station (1271 km^2), the Gérine (86 km^2) and the Glâne (193 km^2).

Figure 3.7 – Evolution of a river bend in the Sarine between Rossens and Hauterive (exact location is indicated in Figure 3.2). Geodata courtesy Swisstopo

3.2 The Spöl River

The Spöl River is located at the eastern end of Switzerland, in the mountainous area of the Canton of Graubünden. It lies in the Swiss National Park which was founded in 1914 and is the oldest in the Alps, covering a total area of 170 km^2. The Spöl is a main river in the National Park and originates below the Piz Ursera (3031 m a.s.l.) in the area of Poschiavo, traverses Italy and enters the Lago di Livigno at Livigno. The Lago di Livigno is an artificial reservoir with a maximum water level on 1805 m a.s.l., impounded by the 130 m high Punt dal Gall Dam, and has a capacity of 164 Mio m^3. While the lake is mainly on Italian terrain, the dam is located on the boarder to Switzerland. Most part of the water is diverted into a 7.6 km long pressure tunnel and guided to the powerhouse and the compensation basin Lai dad Ova Spin. A residual discharge of 0.55 m^{3}s^{-1} in Summer and 1.00 m^{3}s^{-1} in Winter is released to the gorge. The Lai dad Ova Spin is a compensation basin with a volume of only 6.24 Mio m^3, where two Francis turbines with a total installed capacity of 50 MW produce about 87.4 GWh per year and act as pump-storage hydropower plant with the Lago di Livigno. The Lai dad Ova Spin is impounded by the 73 m high Ova Spin dam, a strategic key structure of the hydropower complex of the Engadiner Kraftwerke AG, EKW (Schnitter, 1971). More specifications about dam and reservoir are given in table 3.2), a photo in Figure 3.8. Also galleries from other catchments divert water to the Lai dad Ova Spin and a major tributary, the Ova da Fuorn enters the Spöl at the beginning of the reservoir. From Ova Spin intake, the water is diverted through a 20.3 km pressure tunnel to the hydropower station Pradella in Scuol (1141 m a.s.l.), the power plant has four Francis turbines with total 288 MW installed capacity. At Pradella the water is released to the Inn river (Figure 3.9).

Figure 3.8 – Ova Spin Dam close to Zernez. Dam built in 1968, height 73 m. Image courtesy Gian Franco Kirchen
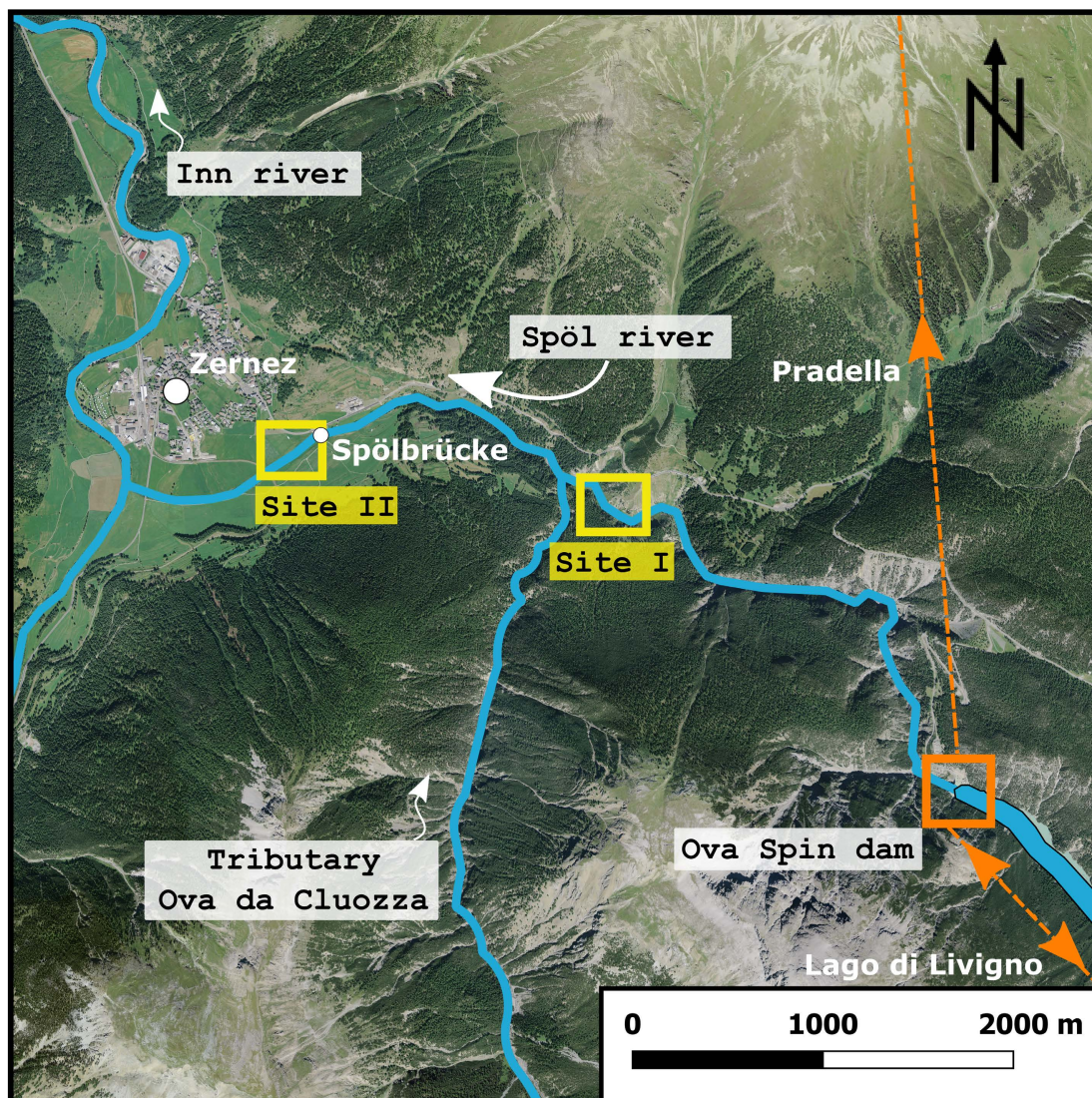
Figure 3.9 – Overview of the lower Spöl. Geodata courtesy Swisstopo

In the framework of this research study, the focus is directed on the downstream river segment of the Ova Spin dam which is also known as the lower Spöl. There, a residual flow of 0.9 m^3s^{-1} in Summer and 0.3 m^3s^{-1} in Winter is dispensed to the Spöl which still follows a meandering deep gorge with a wetted width of 10-15 m without any human influence. This steep segment has an average bed slopes of about 2 %. At the end of the gorge, the tributary Ova da Cluozza enters the Spöl and contributes a significant amount of sediment to the river (table 3.3). At this location, the Spöl widens up and becomes a braided river segment with a mean bed slope of about 1 %, that enters the Inn river in Zernez on an altitude of 1470 m a.s.l. (Figure 3.9). At the mouth of the Ova da Cluozza, gauging station 2319 of the confederation is installed, measuring continuously discharge and temperature. The flood statistics of the Ova da Cluozza as well as images of the Spöl are in Appendix B.

Table 3.2 – Specifications of the Rossens-Hauterive and Ova Spin hydropower plants. Data from SWISSCOLD, Groupe e, Engadiner Kraftwerke AG and SFOE

Characteristic	Unit	Rossens	Ova Spin
Year of construction	[year]	1948	1968
Dam type (concrete)	[-]	Arch dam	Arch dam
Dam hight	[m]	83	73
Dam crown length	[m]	320	129
Flexibility coefficient C	[-]	~ 7.8	~ 5.7
Maximum reservoir level	[m a.s.l.]	667	1630
Maximum reservoir surface	[km^2]	10	0.34
Maximum storage volume	[Mio m^3]	200	6.24
Catchment	[km^2]	908	345
Average inflow (1923-2016)	[m^3s^{-1}]	23.5	Compensation reservoir
Retention time	[years]	0.27	Compensation reservoir
Residual flow Summer*	[m^3s^{-1}]	3.5	0.9
Residual flow Winter*	[m^3s^{-1}]	2.5	0.3
Installed capacity residual	[MW]	1.7 + 0.7	0.5
Annual production residual	[GWh y^{-1}]	13.6	1.57
Length pressure tunnel	[km]	6	7.6 / 20.3
Hydraulic head	[m]	110	205 / 488
Maximal allowed discharge*	[m^3s^{-1}]	75	33 / 72
Turbines (all type Francis)	[-]	4	2 / 4
Installed capacity power house	[MW]	70	50 / 288
Annual production power house	[GWh y^{-1}]	205	87.4 / 1020

*values from concession

3.3 The Sense River

The Kalte Sense originates in the Prealps of Canton Bern as a junction of small tributaries. It flows in a 60 m wide floodplain in a canyon with a wetted-width of less than 10 m at low flow. It is a dynamic river with lots of sediment and flood events. The highest peak in the catchment is the Ochse (2188 m a.s.l.). Upstream of Plaffeien it merges with the Warme Sense, coming from the Schwarzsee a small lake (0.5 km^2) on 1045 m a.s.l. Therefore the Warme Sense is less dynamic and transports less sediment than the Kalte Sense. At the village of Plaffeien, the canyon widens to an up to 200 m wide floodplain with a braided stream. After 5 km the effluent of the wastewater treatment plant (WWTP) Guggishaus is released in the Sense and it enters a meandering gorge. Upstream of Thörishaus, the main tributary Schwarzwasser enters the Sense (Figure 3.10). While in the upper segment, the Sense is little affected by anthropogenic structures, some river training and flood protection works are present after the sharp left bend in Thörishaus. After 36 km it joins the Sarine at Laupen (length in including Kalte Sense 47.4 km).

The Sense is the longest floodplain classified of national importance by the Federal Office for Environment, FOEN. Many studies concerning geomorphology, habitat diversity and instream biota have been carried out in the river which is often mentioned as the last larger river with a natural and active flow and sediment regime in Switzerland (Alp et al., 2012; Gostner et al., 2013b). In the Sense River, the study focused on a segment in the braided segment (Sense I) and four segments further downstream (Sense II-V, details in Table 3.1 and Appendix B).

In Thörishaus the gauging station 2179 of the confederation measures continuously flow depth and temperature in the Sense. The discharge is multiplied with the factor 0.44, based on the catchment sizes of the Sense at Plaffeien (153 km^2) and the total catchment of the measurement station (351 km^2), analog the Sarine and station 2119 in Fribourg. This correction was done because the braided river segment is of importance in this study (Table 3.3).

Table 3.3 – Characteristics of the Sarine residual flow, the lower Spöl residual flow and the braided Sense natural river segments. Lengths and slopes values measured from swisstopo, flood data from FOEN, corrected with 0.78 for Sarine (1949-2016) and with 0.44 for Sense (1928-2016) based on the catchment sizes. The Spöl flood statistics correspond to the Ova da Cluozza (1962-2016). 0.77 m^3s^{-1} is the mean annual discharge for the Ova da Cluozza. Grain size values for Sense from Gostner (2012). Where two values, the Spöl represents two segments, first value upstream of the junction with the Ova da Cluozza (gorge) and the second is located downstream at the braided section (see Figure 3.9).

| Characteristic	Unit	Sarine	Spöl	Sense
Length of river	[km]	126	28	47.4
Length of study segment	[km]	13.4	5.8	5
Active channel width	[m]	30-35	13.9 / 25	127
Wetted channel width (low flow)	[m]	20-30	11.8 / 11.3	21
Mean flow	[m^3s^{-1}]	2.5-3.5	0.3-0.9 (+0.77)	3.74
2 year flood	[m^3s^{-1}]	204	63	6.6
10 year flood	[m^3s^{-1}]	358	106	10.9
30 year flood	[m^3s^{-1}]	457	137	14.4
100 year flood	[m^3s^{-1}]	568	176	19.3
300 year flood	[m^3s^{-1}]	674	218	24.9
Catchment size	[km^2]	908	394	153
Bed slope	[-]	0.3 %	1.0 % / 2.0 %	2.0 %
Dominant grain diameter d_m	[mm]	57	22 / 26	53 (d_{50})
90 %-quantile diameter d_{90}	[mm]	113	34 / 48	-
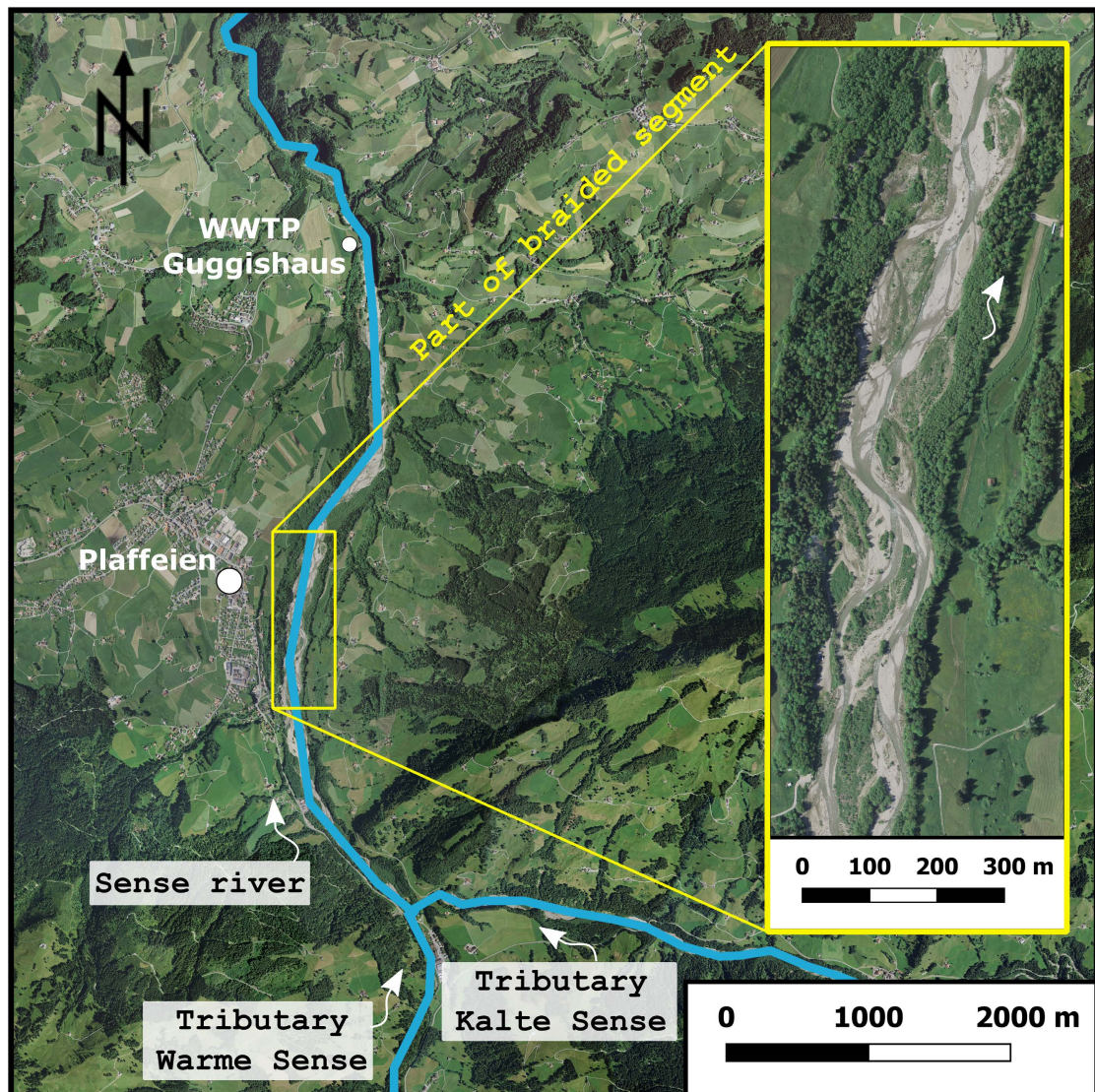
Figure 3.10 – Overview of the Sense River around Plaffeien with a zoom on Sense I. Geodata courtesy Swisstopo

In comparison to the Sarine, the Sense has a natural flow regime with no weekly pattern (see Figure 3.5). A daily pattern can be observed in the Sense caused by snow melt. The flood statistics of the Sense measured at the gauging station as well as a dataset corrected with 0.44 and images of the braided river segment are in Appendix B. Figure 3.11 shows the three different regime behaviors during a flood event, Figure 3.5 during low flow.
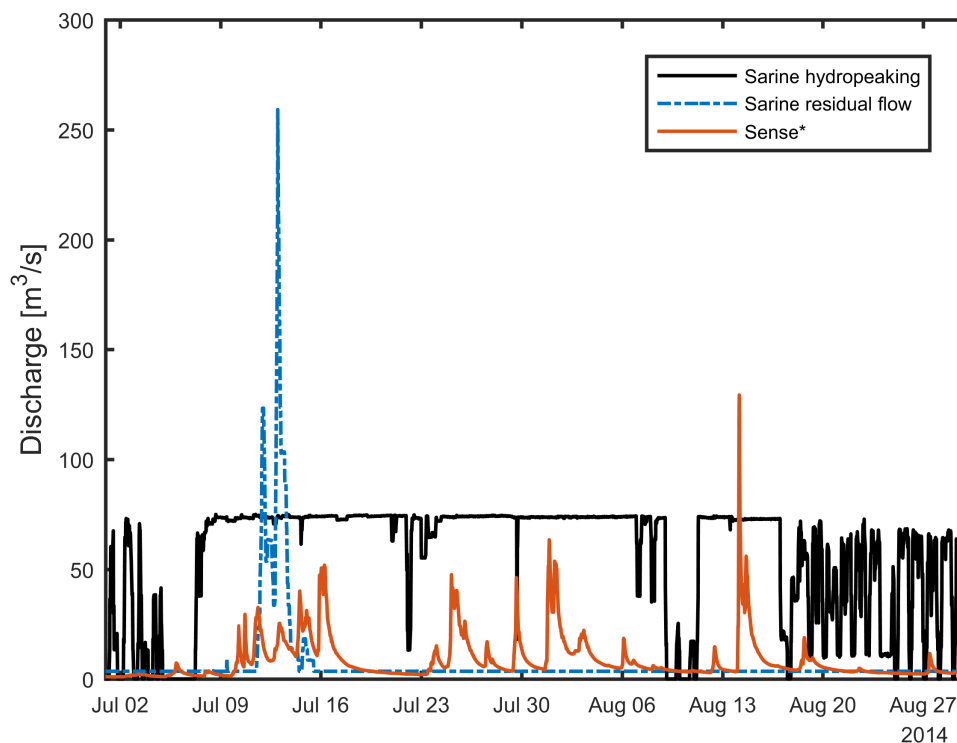
Figure 3.11 – Different regime behavior of the three studied river segments. Data sources: Groupe e and FOEN
*Data from the Sense were measured at the gauging station 2179 in Thörishaus and corrected with the factor 0.44 based on the catchment sizes

3.4 The Buenz River

The river Buenz originates at Lindenberg at 862 m a.s.l. and drains into the Aabach, Aare and eventually via the Rhine into the North Sea. The Buenz flows through intensive agricultural areas and is channelized. Segment I was restored recently. Bank protections were removed, logs and large cobbles were added, producing high hydraulic variability. Segment II is channelized and straight. Towards the confluence with the Aabach, the Buenz meanders and segment III is situated at a 90° bend in the river. Since 1999, several large floods occurred and destroyed various river training structures locally. In segment IV, the Buenz has an active floodplain with high spatial hydraulic diversity. Further information and images of the four segments at the Buenz are given in Table 3.1 and Appendix B.

3.5 The Passer River

The river Passer originates at Timmelsjoch at 2474 m a.s.l. It is a 42 km long tributary to the river Etsch which flows into the Adriatic Sea. Located in a high mountain region, the Passer is significantly steeper than the Bünz and Venoge. Its hydropower potential is mainly used by run-of-the-river powerplants without a reservoir, and thus has a natural flow regime. Nevertheless, due to urbanization and agricultural activities in the narrow valley, the river has been channelized, resulting in uniform trapezoidal cross-sections. Recent restoration measures allowed the river to gain its natural behavior locally due to widening, which created segment I as a sequence of alternate bars. The hydraulic diversity in this segment is clearly higher than in most other segments along the Passer. Segment II of the Passer is channelized. Due to a small bend, there is a large gravel bar along the inner bank of segment II. A large widening of the river was undertaken in segment III, forming a braided stream-bed. At two locations on the segment, transversal concrete sills were present that limit bed erosion. Since no other structural measures exist, the stretch has high hydraulic variability. Segment IV was channelized with a succession of transversal concrete sills that enhanced local hydraulic variability. Further information and images of the Passer River and the four studied segments are given in Table 3.1 and Appendix B.

3.6 The Venoge River

The Venoge is a lowland gravel-bed river located in southwest Switzerland. Its origin is in the Jura Mountains at 660 m a.s.l. It drains after about 40 km into Lake Geneva, then into the Rhone entering the Mediterranean Sea. Four segments, Venoge I, II, III and IV were studied in this river with a natural flow regime (see Figures B.25 and B.26). The most upstream segment (Venoge I) is surrounded by agricultural land and has high hydraulic variability due to large cobbles as well as natural river banks. A small riparian corridor is present along the water course. The study segment is meandering with a bed width of about 5 m. Segment II and III are located further downstream and close to urban areas. Both segments are channelized with a trapezoidal channel shape. No gravel bars or islands are present, and the banks are vegetated by grass. The hydraulic variability is low and characterized by a constant wetted channel width of 10 m (Venoge II) and 7 m (Venoge III). Segment IV is wider, with an average wetted width of 14 m. It has a natural river bed and there are no built structures in the river in this area. There is a natural floodplain with a riparian forest of up to 50 m on both sides of the river. It can be classified as a segment with alternate bars. This river segment is close to the river mouth at lake Geneva. Images of the Venoge and the four segments are given in Table 3.1 and Appendix B.

4 | Sampling sufficiency for determining hydraulic habitat diversity

4.1   Overview

This chapter investigates the data sufficiency of the hydro-morphological Index of diversity (HMID) as well as mean flow depth and velocity. Until this point, little is known about the sufficiency of data to produce effective and representative results. Neither is of the sampling procedure. Therefore 19 segments with differences in terms of mean annual discharge, river width, substrate, segment length, cross-section spacing and geomorphology are investigated. Measurements of flow depth and velocity were taken at multiple, equally spaced cross-sections along each segment. Data was sub-sampled using different methodologies and analyzed each time. The sets of sub-sampled data were then compared with those calculated with the full data set from a segment.

The main objectives of this chapter are the following:

1. To analyze **data** from 19 river segments concerning their **sufficiency** regarding the hydro-morphological index of diversity, HMID.

2. To derive the **minimal sample size** limits using different sub-sampling methods for the HMID and its associated variables mean flow depth and mean flow velocity.

3. To provide **recommendations** for the planning of field sampling campaigns of hydraulic and morphological variables with the purpose to reduce data uncertainties and costs.

4.2 Study sites

A total of 19 segments in five different rivers served as input data for this study. In Switzerland, these were the Venoge river in Canton Vaud (4 segments), the Sarine (2) and Sense (5) rivers in Canton Fribourg, and the Buenz (4) in Canton Aargau. In addition, the Passer (4) river in South Tyrol, Italy, was used (see Figure 3.1). Physical characteristics of the 19 river segments are given in Table 3.1. The segments were also classified according to Leopold and Wolman (1957) into straight single channel, meandering, segments with alternate bars, and braided segments. A detailed description of the sites and rivers is given in Chapter 3, on-site images and the perimeters of the different segments are provided in Appendix B.

4.3 Methodology

4.3.1 Sampling of cross-sections in a segment

In the field, a measurement tape was tightened across the river and measures of flow velocity and depth were conducted at regular distances along each transect, depending on river width. The distance between measurement points varies between 0.5 and 1 m but is constant within a segment. Usually 1 m was chosen, but the spacing distance was reduced in narrow segments (e.g., Venoge I). Flow velocities were measured as in Gostner et al. (2013a) at 60 % of the flow depth with a handheld acoustic Doppler velocimeter (handheld-ADV, Son-Tek FLOWTRACKER®). At the same location, flow depth was measured with a double meter attached to a vertical pole. After finishing the measurements along a cross-section, the procedure was repeated at each pre-defined cross-section. In total, each segment consists of a sequence of cross-sections, varying from 7 to 19 with a spacing of 5 to 313 m between cross-sections depending on the segment being assessed. Each cross-section has 7 to 25 measurement points for flow and depth. The total segment-length varies from segment to segment, in order to evaluate the influence of segment length and cross-section spacing on the HMID value. The segment lengths and locations of cross-sections were predefined based on aerial images. Segment lengths were defined either due to a previously conducted or currently planned river engineering project, or based on repetition of in-stream structures. Segment lengths vary from 40 (channelized straight segment) to 1880 m (meandering segment). The data sampling was carried out by different people wherefore the segment lengths, the distance between the cross-sections and the number of data points vary between the datasets. Especially segment lengths and cross-section distances depend on the observer leading to a heterogeneous dataset. The detailed parameters of the sampling, the resulting ecohydraulic characteristics and its relating discharge during the measurement moment are given in Table 4.1.

Table 4.1 – Sampling and ecohydraulic characteristics of the 19 study segments in the Venoge, Buenz, Sarine, Sense (Switzerland) and Passer (Italy). *CS* = cross-section, *Dist* = distance between the cross-sections, *Q* = Discharge during measurement.

River segment		Length [m]	Points [-]	CS [-]	Dist [m]	Q [m^{3}s^{-1}]	Mean h [m]	Std h [m]	Mean v [ms^{-1}]	Std v [ms^{-1}]	HMID [-]
Venoge	I	60	111	12	5	0.7	0.30	0.16	0.45	0.38	8.01
Venoge	II	40	152	8	6	2.4	0.32	0.08	0.79	0.16	2.26
Venoge	III	80	116	8	11	2.7	0.44	0.14	0.77	0.31	3.50
Venoge	IV	120	166	12	11	4.0	0.49	0.26	0.57	0.33	5.89
Buenz	I	140	157	10	16	0.7	0.46	0.22	0.23	0.18	7.18
Buenz	II	55	52	7	9	0.8	0.34	0.06	0.56	0.21	2.55
Buenz	III	115	173	12	10	0.8	0.38	0.26	0.32	0.35	12.6
Buenz	IV	150	298	15	11	1.0	0.18	0.11	0.37	0.34	9.76
Passer	I	145	149	8	21	7.6	0.27	0.19	0.36	0.36	11.7
Passer	II	390	163	11	39	8.4	0.38	0.22	0.47	0.38	8.21
Passer	III	400	224	11	40	9.9	0.32	0.23	0.34	0.33	11.5
Passer	IV	405	167	11	41	10	0.32	0.17	0.39	0.28	6.99
Sarine	I	854	237	10	95	2.5	0.51	0.30	0.30	0.33	8.19
Sarine	II	1880	150	7	313	2.5	0.46	0.32	0.35	0.24	8.00
Sense	I	1850	310	19	103	2.3	0.20	0.13	0.45	0.41	10.3
Sense	II	760	202	17	48	2.9	0.32	0.22	0.56	0.45	9.26
Sense	III	646	249	19	36	3.2	0.31	0.18	0.39	0.27	7.13
Sense	IV	558	135	14	43	5.7	0.46	0.22	0.72	0.42	5.42
Sense	V	531	216	14	41	5.8	0.31	0.15	0.71	0.29	4.41

4.3.2 Reduced sub-sampling in the number of cross-sections and measurement points for a segment

The two applied sub-sampling methods were based on the hypothesis that the computed HMID using all sampled data in a segment was representative of the segment-scale HMID value. This means that the estimated HMID was robust and did not vary significantly by adding or removing a few points to the total samples. This hypothesis was tested for the 19 river segments, by computing the HMID value cumulatively adding single measurement values. The data was analyzed using MATLAB R2016b.

Effect of cross-section number for different morphological segments

Using this longitudinal sub-sampling method, the questions of the required segment-length and how many cross-sections are needed for a good estimate of the HMID were addressed. Here, each segment was divided into sub-segments and no extension of the data by bootstrapping was done. Bootstrapping according to Davison and Hinkley (1997) could not be

applied since the data points and cross-sections were not independent of each other. A clustered bootstrap where the different numbers of consecutive cross-sections are forming independent clusters could be applied (Cameron et al., 2008). However, this method severely decreases the number of samples for larger cluster sizes because each cross-section would only be allowed to be present in one cluster (no overlapping is possible). For segments with a small amount of data, the input data are too few for analysis. Thus, an alternative procedure was applied in this study. First, the 19 segments of the five rivers were split into sub-segments of the size of one single cross-section (Figure 4.1, left).
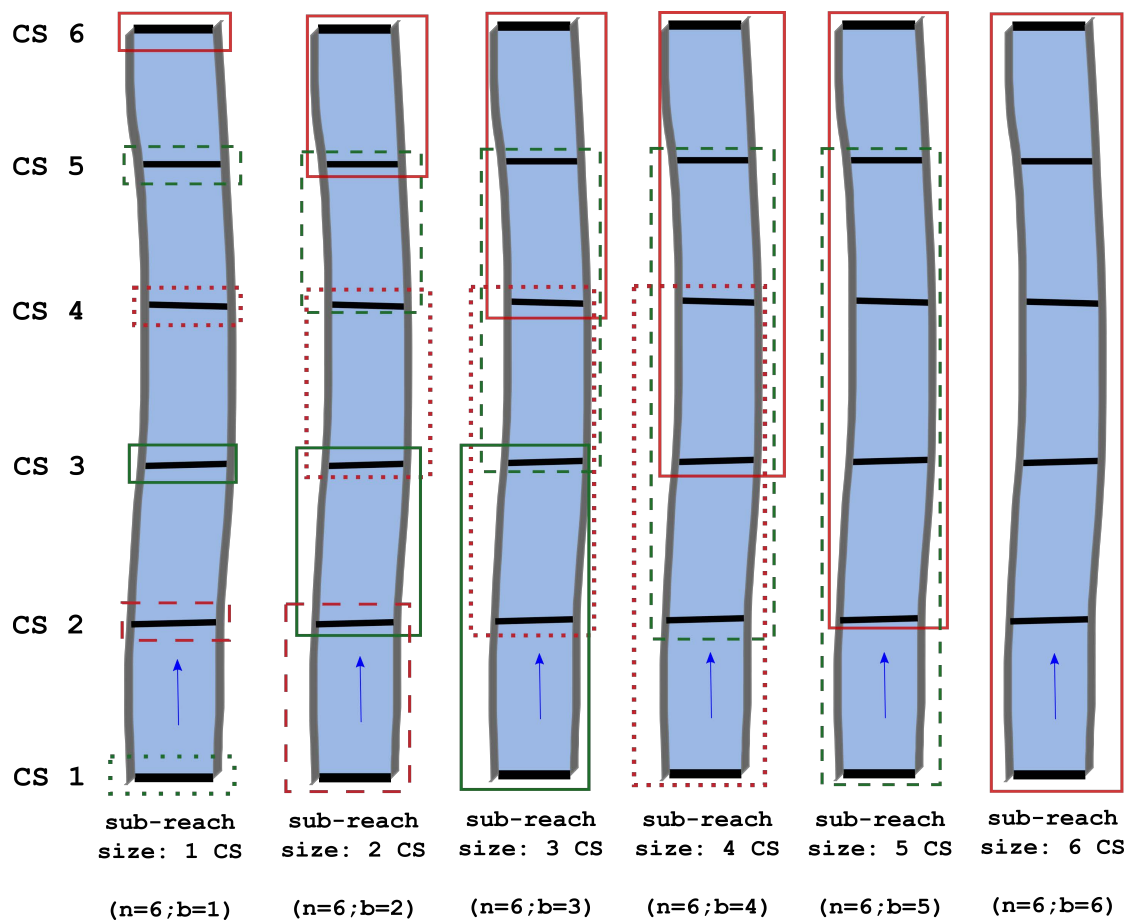
Figure 4.1 – Sampling concept for a segment with six cross-sections (CS). On the left side, six samples were taken with a sub-segment size of one CS (flat black bars). From the left to the right, the sub-segment size increases until the maximum. All possible sub-segments were simulated (rectangular shapes). Based on flow depths and velocities measured on the CSs located in each sub-segment, an HMID value was calculated. n = number of CS, b = sub-segment length

For each sub-segment, an HMID was computed. In a second step, sub-segments with the size of two spatially consecutive cross-sections were created and the HMID again calculated (details of the HMID in Chapter 2). This procedure was done for all combinations of two spa-

tially consecutive cross-sections for all segments (Figure 4.1, second from the left). Then, the sub-segment size was increased: sub-segments with three, four, five, and more cross-sections were created, until the sub-segment was equal to the original segment having a certain number n cross-sections (see Figure 4.1). For each sub-segment size, $n − b + 1$ sub-segments resulted, with n = number of cross-sections in a segment and b = sub-segment size of spatially consecutive cross-sections. Such sub-segments were systematically displaced over all 19 river segments for obtaining the corresponding HMID values.

Effect of measurement points in a cross-section

The transversal sub-sampling aimed at reducing the number of measurement points along a cross-section. In a first analysis, every second measurement point on a cross-section was kept, and thus divided the number of measurement points by two. In a further analysis, every third value was kept and in the last analysis every fourth, decreasing the measurement input for the analyses by three and four, respectively. The resulting datasets then were compared with the initial dataset.

HMID depending on sub-segment length in meandering segments

To investigate the influence of the bend and cross-section spacing, the two segments of the Sarine were analyzed more in detail. Here, the three most upstream and the most downstream cross-sections in Sarine I segment were removed from the dataset. The reduced segment Sarine Ib had six cross-sections in total, consisting of a 90° bend and was 510 m long. In segment Sarine II, only the first two cross-sections were kept and the five downstream cross-sections were removed. Between the two remaining cross-sections, three additional equally-spaced cross-sections were added. This additional sampling corresponded to a 90° bend of 340-m length with five cross-sections and a spacing of about 85 m.

Combined effect: reduction of the number of cross-section and measurement points

The key step, is the combination of the two sub-sampling methods described above. Therefore, the longitudinal sub-sampling was examined with the reduced datasets. This analysis was also exercised for the two ecohydraulic variables mean flow velocity v and depth h allowing the single analysis of the two input variables of the HMID.

4.4 Results

4.4.1 Evolution of the HMID with increasing number of measurement points in a segment

In Figure 4.2, the evolution of the HMID values based on successive additional measurement points are displayed. For the majority of segments, the HMID initially varies strongly but approaches asymptotically to a constant saturation value with increasing number of measurements, a value after which more data does not influence the HMID value. The largest difference between different river segments is observed at the beginning of the HMID evolution, when the HMIDs values are calculated with very few measurement points. In some cases, the HMID value approaches its constant value gradually starting at 1 (e.g. Venoge II), whereas the HMID value of other segments start with a rapid increase followed by a slight decrease towards its constant value (e.g. Venoge III). The flow depths and velocities achieve a stable value with less data points (see Appendix C). Looking at the pattern of HMID evolution, some segments can be grouped. Segments Venoge II, Venoge III, Buenz II, and Sense V all have a final HMID value below 5; they are straight segments and in the class with strongly limited hydraulic variability. The intermediate HMID interval (5 < HMID < 9) includes the segments Venoge I, Venoge IV, Buenz I, Passer II, Passer IV, Sarine I, Sarine II and Sense III. Here, the HMIDs of the Venoge IV, Passer II, Passer IV and Sense III evolve similarly. After an initial peak, they decrease rapidly and then increase towards a saturation HMID value. HMID development of Sense IV follows the same pattern as HMID of Venoge III. The remaining segments in this HMID interval show a unique HMID evolution. HMID-trends in the highest HMID interval (HMID > 9) are similar to what is observed in the lower classes. Their initial fluctuation is equalized later compared to the HMID evolution of segments with lower HMID values. In general, they approach a saturation HMID value after having reached an early peak. A special case is the HMID of Buenz IV that decreases after peaking without ending on a constant HMID value. The resulting HMID value of all segments are given in Table 4.2. This analysis shows that for the statistical convergence of the HMID value the sampling size taken in the present study is more than sufficient and thus be optimized as discussed below.
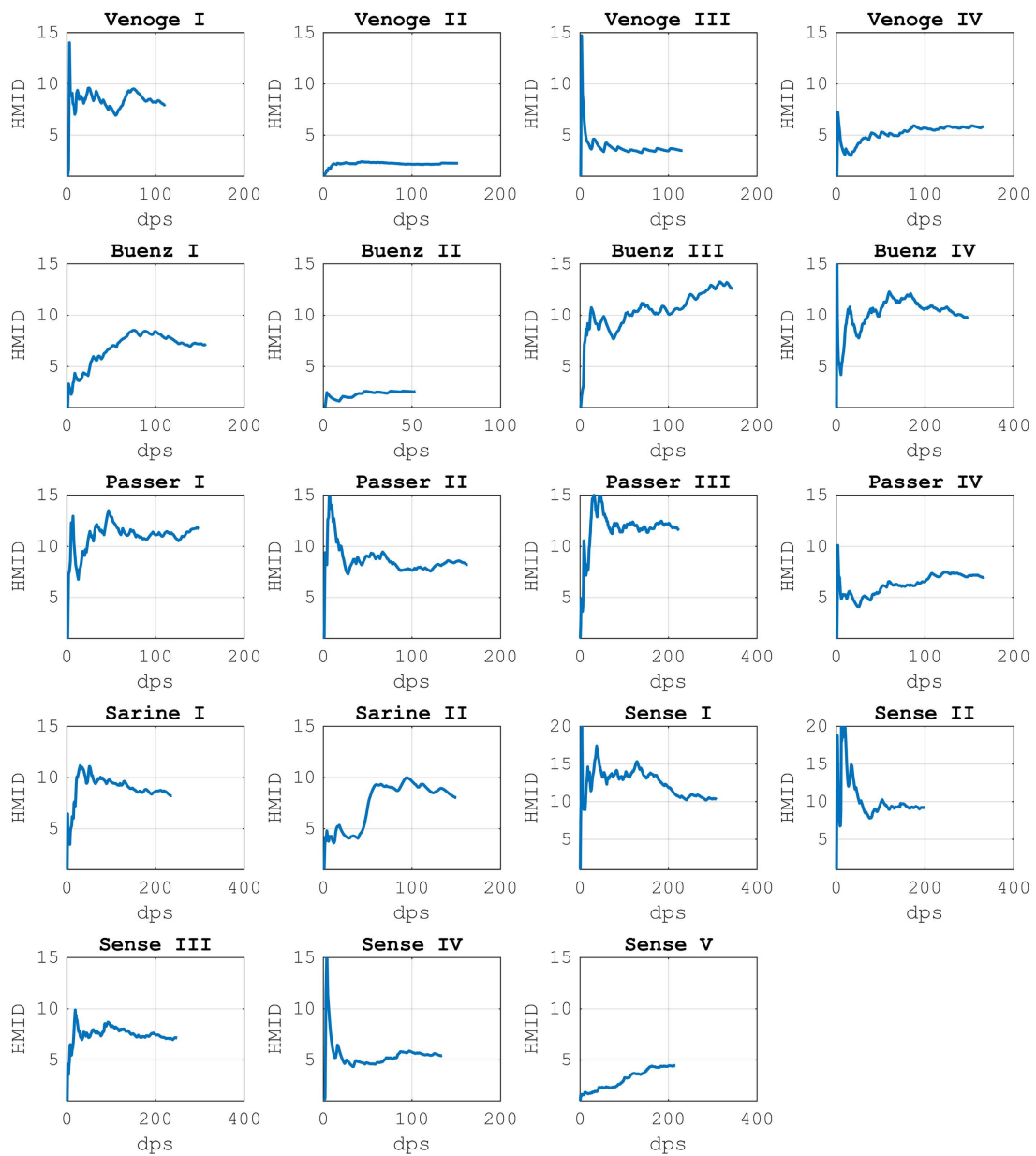
Figure 4.2 – Evolution of the HMID with increasing number of measurement points for the 19 segments of the five study rivers.

4.4.2 Effect of the number of cross-sections for different morphological segments

The 19 river segments analyzed with a longitudinal sub-sampling concerning segment length are grouped according to four different geomorphology types: straight, meandering, alternate bars and braided. As an example, one segment of each geomorphology is presented in Figure 4.4. Two straight segments are chosen, a channelized and a restored river segment, showing the differences in statistical convergence of the HMID value. The results from all 19

segments sorted by their geomorphology can be found in Appendix C. Each marker on the plots represents an HMID value calculated with the data from the corresponding segment-length. The solid line represents the mean HMID value for each sub-segment size characterized by the number of CS (*b* in Figure 4.1). The last marker in every line is the HMID calculated with the complete data set, thus the segment value of HMID. In straight segments the mean HMID value changes little with increasing sub-segment size. In channelized segments, Venoge II & III and Buenz II, the mean HMID values are low. The shaded area representing the spread of the HMID values highlights the uniform hydraulic conditions given by the channels in these segments. Buenz I, on the other hand, has a constant spread of HMID values, whereas values of Passer II & IV diverge earlier towards the mean. The HMID values of Sense V diverge gradually towards the mean HMID value with increasing sub-segment size. A different behaviour can be found in the segments of meandering rivers. While the mean HMID value for Venoge I is independent of the sub-segment length, Buenz III and Sarine I & II have different behaviors. The mean HMID value of Sarine I and Buenz III increase until a number of three to five cross-sections, respectively, is reached and then remains constant. The mean HMID value of Sarine I increase until a sub-segment size of three cross-sections, once it passes five cross-sections it decreases again. For Sarine II, the mean HMID value becomes constant if the sub-segment size is longer than three cross-sections but after five cross-sections it decreases. The spread of HMID values in Venoge I decreases up to a sub-segment length of five cross-sections, then it is nearly constant. The spread of HMID values in Buenz III decreases rapidly when enlarging the sub-segment from one to two cross-sections and then decreases gradually. A somewhat smaller but constant spread is observed in segments Sarine I & II. In segments with alternate bars the HMID evolves quite similarly as in straight rivers. Venoge IV has a constant mean HMID value independent on the sub-segment length. The spread of HMID values in all rivers with alternate bars drops significantly when enlarging the sub-segment size from one to two cross-sections. The mean HMID value of Passer I increases gradually reaching a high level (HMID > 9). Sense II has the largest spread in HMID values, remaining constant with a sub-segment size of six or more cross-sections. Its mean HMID value remains constant, similarly as the one from Sense IV. The spread of HMID values in Sense IV segment is smaller than the one observed in Sense II, it decreases with smaller sub-segment lengths than six cross-sections than with larger sub-segment lengths. Braided segments generally have the largest spread of HMID values of all geomorphology types. All braided segments have a constant mean HMID value. The spread of Buenz IV HMID decreases linearly with increasing sub-segment length. The spread of Passer III drops when the sub-segment is enlarged from two to three cross-sections and afterwards decreases until the sub-segment is seven cross-sections long, then it increases again. Sense I has by far the largest spread of all segments, decreasing slowly. At a sub-segment length of 13 cross-sections, it stabilizes. The spread of Sense III HMID is significantly less than at Sense I; its segment-scale HMID value is smaller as well. The spread of HMID values decreases rapidly until the sub-segment size reaches four cross-sections, afterwards it decreases slowly.

HMID depending on sub-segment length in meandering segments

Regarding the final value and the evolution of the mean HMID value, Sarine Ib does not significantly differ from Sarine I (see Figure 4.3). Thus, the straight sub-segment does have the same HMID as the sub-segment of the bend. The mean HMID at Sarine IIb segment, on the other hand, clearly differs from Sarine II. For small sub-segment lengths, it results in the same evolution but never reaches a mean HMID similar to the Sarine II value. After three cross-sections, the mean HMID reaches its maximum and decreases again. This is caused by a deep pool which is not present in the 90° bend of Sarine IIb and causes also the jump after about 50 measurement points the plot of Sarine II in Figure 4.2.
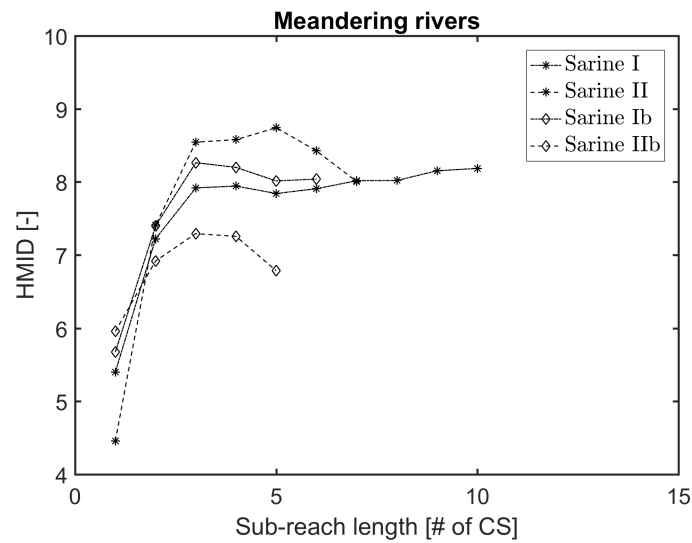
Figure 4.3 – Analysis of the mean HMID values with a shorter reach of Sarine I and Sarine II. The two sub-reaches have a similar cross-section spacing and represent both a full bend and half a meander wavelength, respectively.
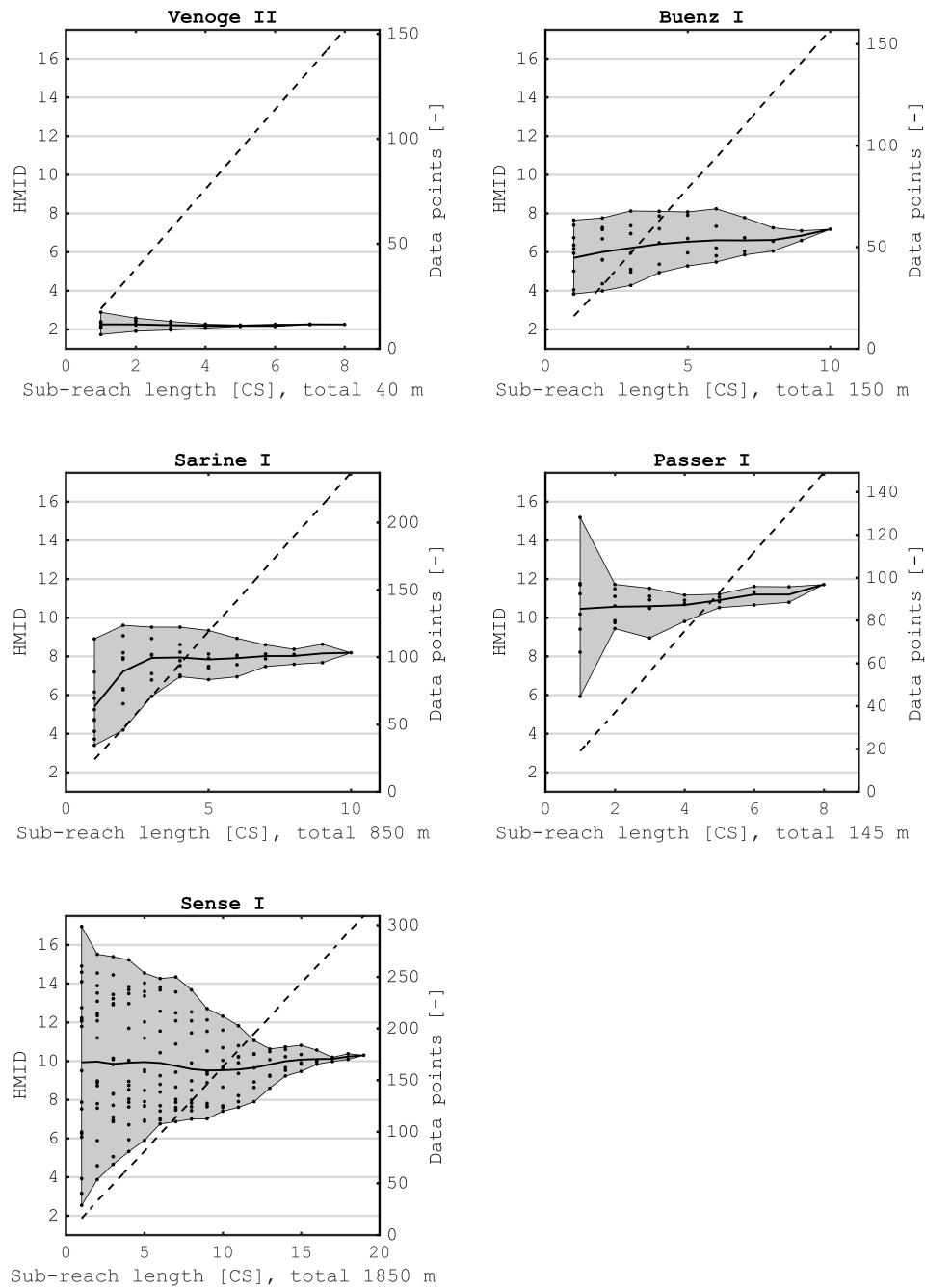
Figure 4.4 – HMID values of one segment of each analyzed geomorphology with increasing sub-segment length characterized by the number of consecutive cross-sections (CS). Venoge II (straight, channelized), Buenz I (straight, restored), Sarine I (meandering), Passer I (alternate bars), Sense I (braided). Each dot corresponds to the HMID value computed from the data of a sub-segment. The distribution of these HMID values is accentuated with the shaded area. The central solid line indicates the mean HMID. The last HMID value comprises the entire sampled data representing the segment-scale HMID value. The dashed line belongs to the second y-axis and demonstrates the average number of data points used for the computation of an HMID value for each sub-segment size. The results from all 19 segments are in Appendix C

4.4.3 Effect of the number of measurement points in a cross-section

The results of the transversal sub-sampling are displayed in Table 4.2. The value is shaded if the absolute difference between the original and sub-sampled HMID value lie within 10 %. With doubling of the distance of measurements along cross-sections, only four rivers do not fulfill the 10 % criterion. Two, Venoge III and Buenz II are straight rivers, Venoge IV have alternate bars and Passer II is a restored braided river. The 10 % criterion is fulfilled by eleven segments when the distance of measurements is tripled. The eight segments that do not fulfill the criterion are two braided, two straight, and all four Venoge segments. If the distance between measurements increases to four times the original distance, ten segments fulfill the 10 % criterion. Seven segments remain within the 10 % criterion for all three sub-samplings: restored segment Buenz I, meandering Buenz III, Passer IV with large sills, meandering Sarine I, as well as braided Sense I, Sense II with alternate bars, and channelized straight Sense V. Regarding the results in absolute values, the HMIDs differ always less than one unit from the initial HMID if the sample size is divided by two unless in the Passer III.

4.4.4 Combined sub-sampling: reduction of cross-sections and measurement points per cross-section

Considering the reduction of cross-sections with the reduced samples, one generally can obtain, that the reduced converge faster than the original datasets (see Figure 4.5 for an example of each geomorphology, all segments in Appendix C). In multiple cases, the final HMID value is slightly higher than the HMID of the total dataset. This is not observed for meandering segments, but at the Venoge III for straight, Venoge IV and Passer I for segments with alternate bars and Passer III and Sense III for braided segments. Such a change is not observed in the mean flow depth (Figure 4.7 and Appendix C) and velocity (Figure 4.6 and Appendix C), independent on the segment geomorphology. The 0.33 sample performs worse than the 0.25 sample in most of the straight segments (Figure C.7, Venoge II, Buenz II, Passer II and Passer IV). The HMID and the mean flow velocity of rivers with already few measurement points (Venoge III and Buenz II) do not tolerate the removal of data points. The mean flow depth is less sensitive in these two segments. Inversely are segments with more measurement points (Sense II and Sense IV) less sensitive to data removal regarding HMID, mean flow depth and velocity. Braided streams are generally the most sensitive to data removal regarding HMID and flow velocity (Figures 4.4 and 4.5 and Appendix C). The mean flow depth of braided segments is less sensitive to data removal than for meandering segments and segments with alternate bars. This is related to the fact that accentuated pools are not observed in the analyzed braided segments, hence they have lesser depth variation.

Table 4.2 – Results of sub-sampling with increased distances between measurement points in cross-sections. The columns indicate the percentage of the data points (dps) that are used for the analysis. In the Δ-columns, differences compared to the HMID value calculated with the full data sample (1.0) are given in percentage. In the #-columns, the number of data points for the corresponding analysis and in the last columns, the average number of data points per cross-section and segment are given. The median of the bottom row is based on the absolute values.

River segment		HMID				Δ HMID			Average dps / CS			
		1.0	*0.5*	*0.33*	*0.25*	*0.5*	*0.33*	*0.25*	*1.0*	*0.5*	*0.33*	*0.25*
Venoge	I	8.01	8.11	10.2	9.08	-1.0%	-28%	-13%	9	5	3	2
Venoge	II	2.26	2.35	2.60	2.31	-4.0%	-15%	-3.0%	19	10	6	5
Venoge	III	3.50	4.19	4.50	5.11	-20%	-29%	-46%	15	7	5	4
Venoge	IV	5.89	6.72	6.86	8.04	-14%	-16%	-37%	14	7	5	3
Buenz	I	7.18	7.74	7.86	7.82	-8.0%	-10%	-9.0%	16	8	5	4
Buenz	II	2.55	2.90	3.32	2.97	-14%	-30%	-17%	7	4	2	2
Buenz	III	12.6	13.1	13.5	13.7	-4.0%	-6.9%	-8.5%	14	7	5	4
Buenz	IV	9.76	9.65	11.6	10.9	1.1%	-19%	-12%	20	10	7	5
Passer	I	11.7	12.2	12.6	14.2	-3.9%	-7.4%	-21%	19	9	6	5
Passer	II	8.21	8.27	9.29	8.61	-0.7%	-13%	-4.9%	15	7	5	4
Passer	III	11.5	13.2	11.4	14.8	-14%	1.1%	-28%	20	10	7	5
Passer	IV	6.99	6.38	7.69	7.07	8.8%	-10%	-1.0%	15	8	5	4
Sarine	I	8.19	8.12	8.77	8.67	0.8%	-7.1%	-6.0%	24	12	8	6
Sarine	II	8.00	8.39	8.49	9.14	-4.9%	-6.0%	-14%	21	11	7	5
Sense	I	10.3	10.2	11.0	10.1	0.5%	-6.9%	2.1%	16	8	5	4
Sense	II	9.26	9.44	9.95	10.2	-1.9%	-7.5%	-9.9%	12	6	4	3
Sense	III	7.13	7.69	8.19	7.78	-7.8%	-15%	-9.1%	13	7	4	3
Sense	IV	5.42	5.63	5.95	6.35	-3.8%	-9.7%	-17%	10	5	3	2
Sense	V	4.41	4.67	4.64	4.68	-5.9%	-5.2%	-6.1%	15	8	5	4
Median						4.0%	10%	9.9%	15	8	5	4
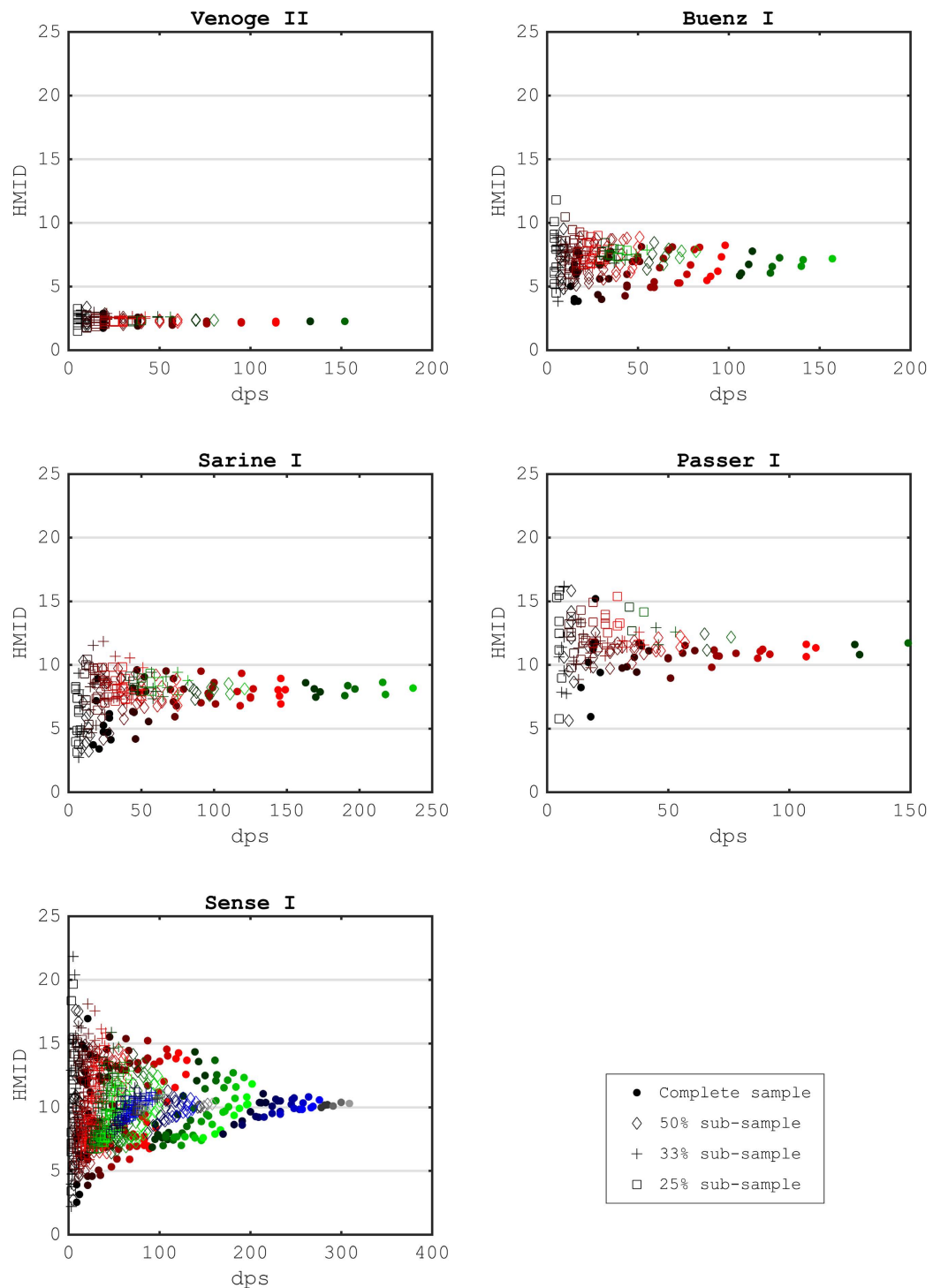
Figure 4.5 – HMID values of one segment of each analyzed geomorphology with increasing number of measurement points. Venoge II (straight channelized), Buenz I (straight restored), Sarine I (meandering), Passer I (alternate bars), Sense I (braided). The marker colors indicate the sub-segment length: reddish = 1-6 CS, green = 7-11 CS, purple = 12-16 CS, grey 17-19 CS. The results obtained for all 19 segments are presented in Appendix C.
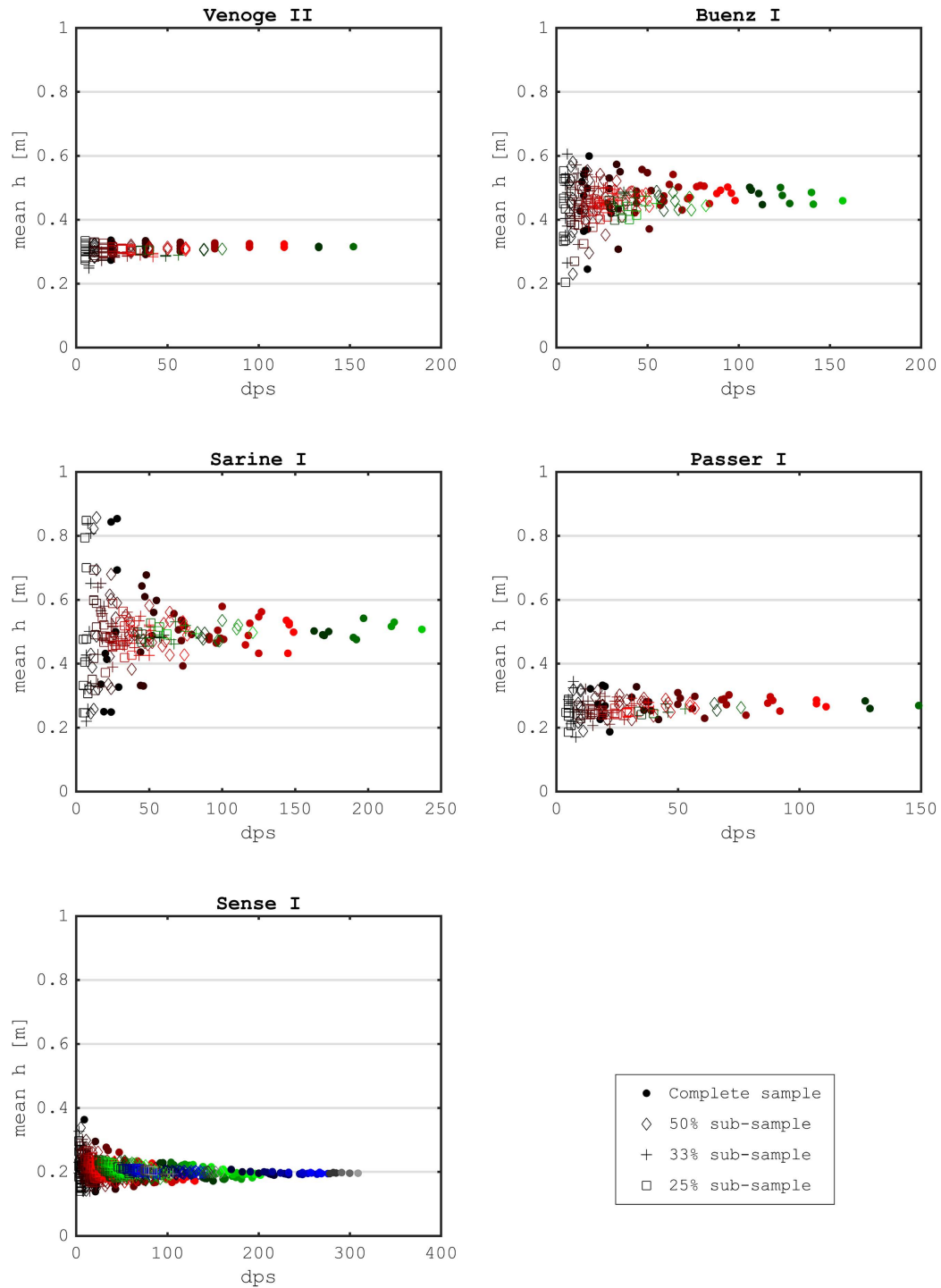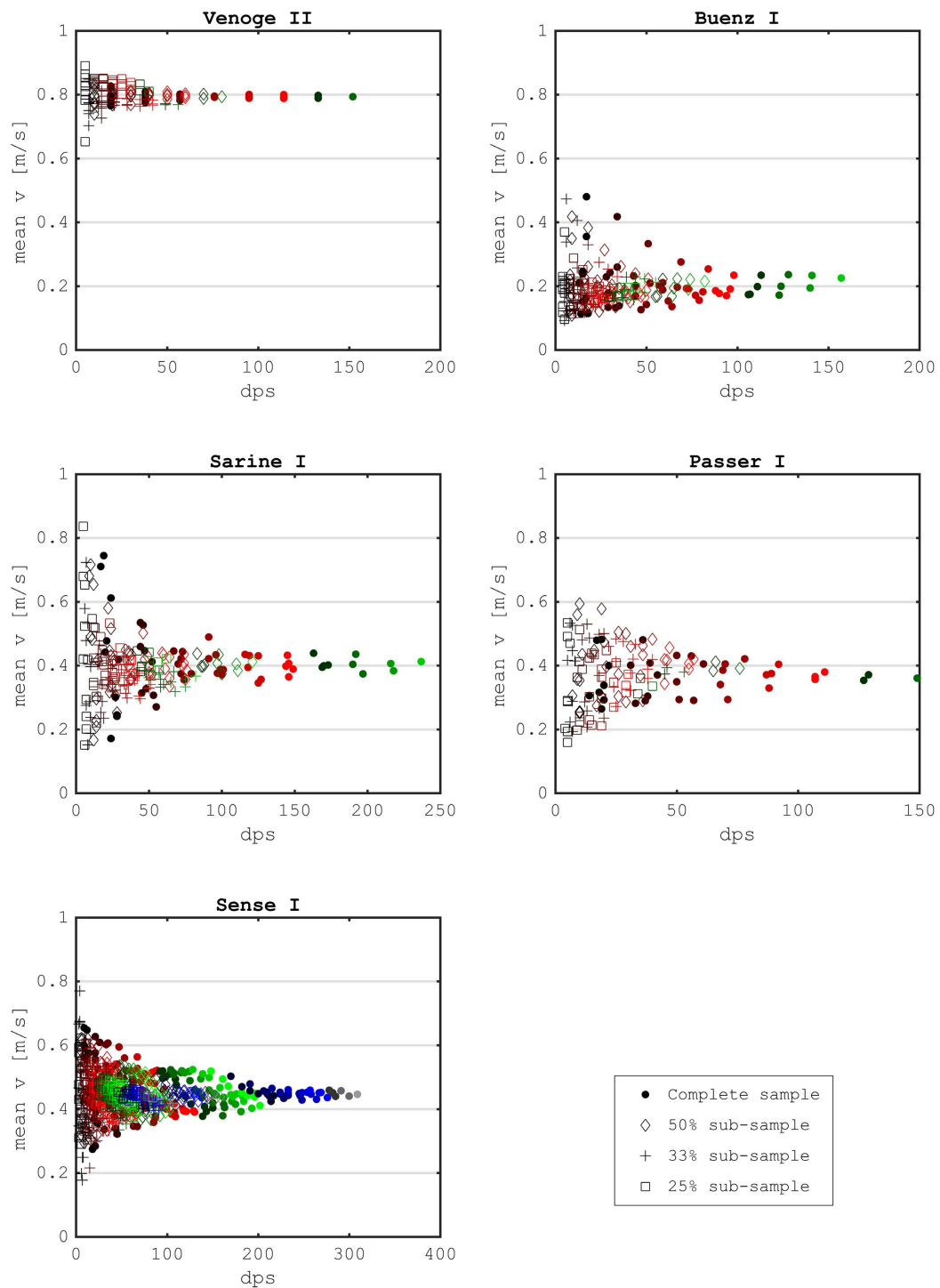
Figure 4.6 – Mean flow depth values of one segment of each analyzed geomorphology with increasing number of measurement points. Venoge II (straight channelized), Buenz I (straight restored), Sarine I (meandering), Passer I (alternate bars), Sense I (braided). The marker colors indicate the sub-segment length: reddish = 1-6 CS, green = 7-11 CS, purple = 12-16 CS, grey 17-19 CS. The results from all 19 segments are in Appendix C.

Figure 4.7 – Mean flow velocity values of one segment of each analyzed geomorphology with increasing number of measurement points. Venoge II (straight channelized), Buenz I (straight restored), Sarine I (meandering), Passer I (alternate bars), Sense I (braided). The marker colors indicate the sub-segment length: reddish = 1-6 CS, green = 7-11 CS, purple = 12-16 CS, grey 17-19 CS. The results from all 19 segments are in Appendix C.

4.5 Discussion

4.5.1 Effect of the number of cross-sections

Straight river segments rarely exist in nature and are mostly the result of river training wherefore the river channel and consequently the flows conditions become more uniform. In these cases, a short scale sub-segment is already representative of a straight river segment.

The Buenz I river segment corresponds to a case where the application of simple river restoration measures such as the addition of deadwood and large stones, increase already and significantly the heterogeneity of the flow. Before the application of the restoration measures, this river segment was similar to Buenz II. Macro-elements such as large sills or block ramps have an important influence on the flow diversity of a river segment. The Passer IV and the Sense V segments contain these elements and both correspond to situations where a late statistical convergence of HMID is observed (Tamagni et al., 2014). A slower statistical convergence of HMID is observed for steeper slopes. The Passer is a relatively steep river (1.4 %) compared to Buenz (0.68 %) and Venoge (0.85 %), and with more flow diversity and turbulence due to lower flow depths, which adding to the presence of larger river-bed cobbles leads to higher HMID values.

The statistical convergence of HMID values in meandering river segments may be associated with the sequence of pools and riffles that depend on river sinuosity. Leopold and Wolman (1957) investigated river channel patterns and discussed meanders in detail (also see Leopold and Wolman 1960). They highlight the repeating nature of riffles with shallow water and deep pools due to the meanders. Buenz III and Sarine I segments included one 90° bend each, whereas Sarine II segment included several. The mean HMID value however did not increase further once the sampling covered three cross-sections. This comes from the fact that even for the shortest distance between the cross-sections, a sampling area of three cross-sections covered a whole 90° bend. The effect of morphology singularities, such as deep pools in the case of Sarine II and IIb, are important to include in the analysis. River segments with alternate bars have a periodic structure composed of riffles and pools elements. If the HMID is calculated from two consecutive cross-sections which correspond each to one of these elements, the values will have a faster statistical convergence. The cross-section location needs to be chosen well if the sampling effort needs to be minimized. The results underline that at some sites when two consecutive cross-sections taken for the analysis corresponded to two consecutive riffles or pools, the convergence in HMID happens later. Braided segments includes more than one channel across the section. Mostly braided streams have a main channel with a strong current and side channels with low water depths or dead water arms (Leopold and Wolman, 1957). One cross-section may already contain the full heterogeneity of a braided river. However, the number of side channels can vary considerably longitudinally between cross-sections. This leads to a relatively late statistical convergence of HMID compared to single channel morphologies hence the longitudinal variation of the channel complexity (number of side channels) needs to be considered in the sampling planning.

4.5.2   Effect of the number of samples in a cross-section

Venoge III & IV segments as well as Buenz II perform poorly in this analysis. What they have in common is their relatively low HMID value and a difference regarding the segment-scale HMID value. Generally, data from Venoge is more sensitive to the removal of measurements than data from other rivers. This may come from the number of measurements in the analysis; the Venoge segments have the lowest average number of measurement points (136). For the other segments, there are 190 measurement points on average (170 Buenz, 176 Passer, 194 Sarine, 222 Sense). An extreme case is Buenz II, which only has 55 measurements, the lowest number of measurement points of all analyzed segments. A special behavior is seen in the Passer III, which final HMID value diverts more than one unit from the original HMID value, when the sample size is cut by half. This again points out the large spatial variability of hydraulic measures induced by restoration measures such as deadwood and large rocks, which does not result in a repetitive manner but is man-made and therefore can be unstructured elements.

4.5.3   Effect of the combined sub-sampling

The results of this combined analysis, provides the best support for planning a field campaign. This combined sub-sampling underlines one major point: The HMID, mean flow depth and mean flow velocity estimations are more accurate if the number of points per cross-section is reduced than the number of cross-sections in a segment. These is observed for all types of geomorphology independent of the segment length, discharge and river width.

Regarding the segment HMID, a sample number of 100 measurements results in a supportable HMID estimate for all geomorphologies. In complex braided systems (Appendix C), it is particularly important to take enough cross-sections (more than 10) to increase the accuracy of the measurement due to their high spatial variability and their change in the number of channels between the cross-sections.

Considering Table 4.2, eight measurements per cross-section lead to a good estimate (error in HMID smaller than 10 %) in all braided segments unless Passer III what result in 12 to 13 cross-sections for a braided river system. Passer III is a restored site and as for the Buenz I it is difficult to reduce the data sample.

On riffles where low water depths with high flow velocities were present, a large temporal variability of flow depths was observed. Further, the water depth varied by several centimeters within a small area especially in steeper rivers with large stones in the river bed. Therefore, a certain interval of imprecision is given by the measurement itself, independent on the observer. As mentioned, the flow depth is less sensitive than the HMID to data removal what especially is well-observed in braided segments. However, due to the mentioned random errors, the sample should be large enough, what makes a sample size of 100 measurement points a good estimate in order to compensate.

65

4.6 Summary

In this chapter data sufficiency to characterize habitat diversity of a river segment by means of the hydro-morphological index of diversity (HMID) as well as mean flow depth and mean flow velocity is investigated. It uses field data from 19 river segments with differing morphology and explicitly points out the sensitivity of the HMID to data availability. The key findings can be summarized as follows:

1. **Sampling effort**

   Analyzing the evolution of the HMID values with increasing number of sample data, revealed that in most segments too much data is sampled and the sampling effort could be substantially decreased.

2. **Minimum data sample size**

   The findings obtained with longitudinal and within-cross-section sub-sampling indicate that, generally, eight measurements per cross-section and ten cross-sections for single channel segments may lead to a robust HMID, mean flow depth and velocity estimate. For braided segments a cross-section number of 13 or more is needed. These numbers can be optimized for the different morphologies.

   For channelized and straight lowland segments without sills or groins, the tested parameters can be estimated with flow velocity and depth measurements from one single cross-section. Restored segments showed larger variability and thus more than one cross-section is needed.

   In mountainous river segments with steeper slopes where lateral structures are present, more than six cross-sections are necessary for an accurate parameter estimate.

   In meandering rivers, the segment of interest must be well defined. In the detailed analysis, one bend (half a meander-wavelength) with five cross-sections resulted in a good HMID estimate. If a larger segment needs to be classified, a full wavelength will lead to better results because they likely cover extreme conditions that may be locally present. In this case, the distance between the cross-sections should be 1/4 of a meander-wavelength. This factor should be considered during the design of experiments. Based on the Sarine data, the HMID estimate was more robust using a longer segment with larger spacing between cross-sections than using a shorter segment with shorter spacing between cross-sections. The cross-section spacing for field measurements aiming at a segment-scale estimate of the parameters HMID, mean flow depth and velocity must hence be defined depending on the local river morphology and segment length.

   As an overarching conclusion it can be said that for most segments, 100 measurement points lead to an accurate computation of the HMID, mean flow depth and velocity if the cross-sections are well spaced and if eight or more measurement points are taken per cross-section. This value can be decreased for simple geometries and following an

appropriate sampling strategy, or if one is only interested in flow velocities and flow depths.

3. **Selection of sampling locations**

It is important to choose carefully the segment of interest and include prominent geomorphological features such as pools and riffles in the data set. This counts especially for human-restored and meandering segments. The distance between the cross-sections on which the samples are taken should not be a multiplication of a repetitive structure (e.g. bend wavelength). The morphological features (pool and riffles) need to be present in the surveyed cross-sections. The distance between cross-sections as well as the distance between measurements along each cross-section should be constant within a segment. The error of an HMID, a mean flow depth or velocity value may be less with the same number of measurements if the distance between measurement points is increased but more cross-sections are measured (Table 4.2 and Appendix C). When planning a future field sampling campaign for hydraulic and morphological variables in a segment scale, the river segment of interest can be compared with the 19 segments analyzed here, finding a morphologically similar segement (use of Appendix C and Table 4.1). Combined with Table 4.2 and the figures in Appendix C the field sampling effort can be optimized.

5 Erosion, transport and deposition of a sediment replenishment under flood conditions

5.1 Overview

In this chapter, an experimental flood combined with a special configuration of multi-deposit sediment replenishment was surveyed in the Sarine river (see Figures 3.2). The sediment replenishment configuration was analogous to the tests from prior laboratory experiments by Battisacco et al. (2016) and the first time applied in the field. The aim of such a measure is to restore hydraulic habitats in a river what is analyzed in Chapter 7. Here the measure is analyzed from a holistic point of view focusing on erosion, transport and deposition processes using hundreds of tracer stones. The objectives of this chapter are:

1. To measure the **transported distance** of replenished sediment and hence, the spatial impact of such a restoration measure.

2. To identify an **average transport velocity** of tagged stones.

3. To evaluate different parts of the hydrograph and their **efficiency of erosion** on the sediment replenishment.

4. To **compare** the results from the **field experiments** with the findings from the **laboratory tests** with an analogous configuration.

This chapter is based on the scientific article "Erosion, transport and deposition of a sediment replenishment under flood conditions" by Stähly, S., Franca, MJ., Robinson, CT., Schleiss, AJ., under review in *Earth Surface Processes and Landforms.* All the analyses for the results presented here were performed by the author. During the field work the author was supported by master students and colleagues.

Chapter 5. Erosion, transport and deposition of a sediment replenishment under flood conditions

This experiment was a collaborative research effort led by the authorities of the Canton Fribourg with the participation of different institutions (École Polytechnique Fédérale de Lausanne, EPFL, Zurich University of Applied Sciences, ZHAW, Swiss Federal Institute of Aquatic Science and Technology, EAWAG and the University of Zurich, UZH), and in collaboration with the dam owners (Groupe e) and engineering offices (Hydrique, Pronat).

5.2 Field work

5.2.1 Multi-deposit replenishment configuration

The replenishment was added in four deposits of sediment and placed in the river at the coordinates 46°45'29.21"N / 7°06'11.47"E (see Figure 3.2 and 5.1a). From a river management and sustainability point of view it would be more reasonable to replenish the Sarine river with sediment directly downstream of the Rossens Dam. In the experiment studied here the results were compared with the findings from the laboratory experiments, hence, a relatively straight reach was chosen. Another criterion was the accessibility for heavy machines to the river. A detailed description of the river is given in Chapter 3. The configuration was an adaptation to field conditions of the sediment replenishment successfully tested previously in flume experiments (Battisacco et al., 2016). In total the river was replenished with 1000 m^3 sediment, divided into four deposits of about 250 m^3 each (Figure 5.1b). As comparison, before the dam construction 4'000 to 8'000 m^3 sediment was yearly transported (Jäggi and Hunziker, 2002; DAEC, 2014). Figure 5.2 shows an example of one sediment deposit. The deposit width W was about 8 m and the length L 22 m. The height of the deposits varied spatially depending on river bed elevation and was about 1.5 m in average. The main specifications of the field and laboratory experiment are given in Table 5.1. The replenished sediment was excavated from the adjacent alluvial forest on the right side of the river. Since the excavation came from the floodplain, no washing or sorting could be applied and the grain size distribution (GSD) corresponded to the material found in the river bed. While the sediment was put in place, lots of fine sediment was released to the river. Where the sediment was excavated, ponds with still water were created, serving additionally as habitats for amphibians and other species (see Appendix D).
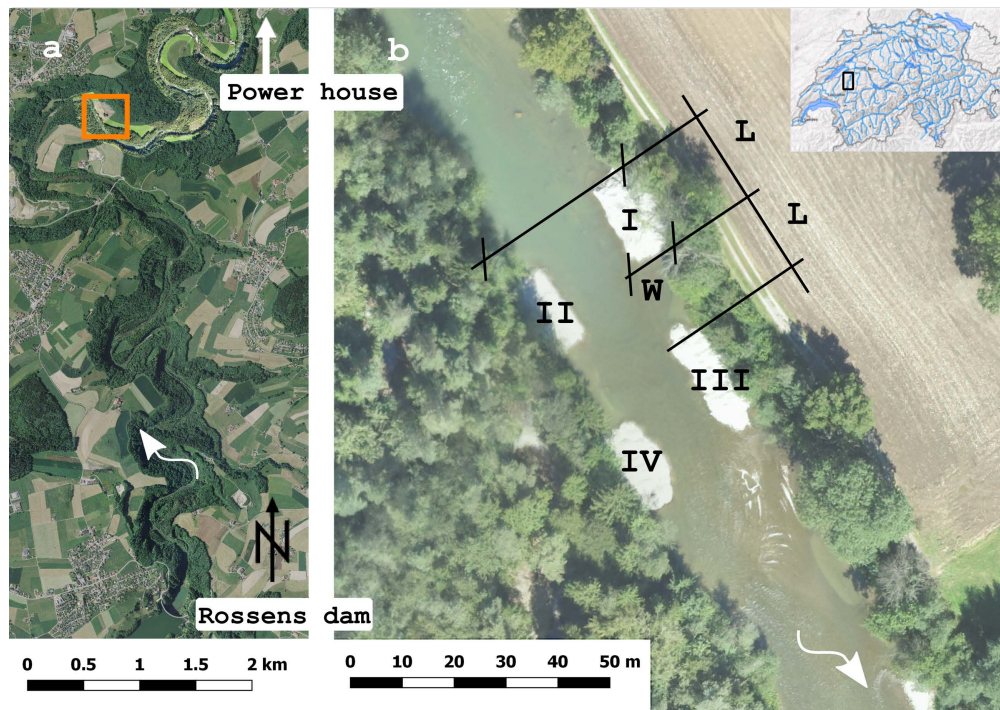
Figure 5.1 – (a) Situation of the restoration measure. (b) Configuration of the four sediment deposits in the Sarine river, indicated with the orange square in a. The distance between deposits was about a deposit length L, the shift between deposits on the left and the right bank is half a deposit length. The height of deposits was about 1.5 m above the initial river-bed. The numbering refers to the name of deposits from upstream to downstream: deposit I, II, III and IV. Geodata courtesy Swisstopo (left) and Research unit Ecohydrology, ZHAW (right).

Table 5.1 – Characteristics of the laboratory and field replenishment experiments. The deposit height in the field experiment varied from 0.5 to 2.5 m.

Parameter	Unit	Laboratory	Sarine
Mean channel slope	[%]	1.5	0.3
Hydrograph peak discharge	[$m^3 s^{-1}$]	0.031	195
Channel-bed width B	[m]	0.4	30
Channel-bed width at peak discharge	[m]	0.46	35
Mean deposit length L	[m]	0.75	22
Mean deposit width W	[m]	0.13	8
Mean deposit height H	[m]	0.07	1.5
Total replenishment volume	[m^3]	0.028	1000
90 %-quantile of the grain size distribution d_{90}	[mm]	6.95	113
Dominant diameter d_m	[mm]	4.89	57
Ratio d_{90} / d_m	[-]	1.42	1.98

Figure 5.2 – Deposit I in the river before the flood experiment. Its dimensions correspond to about 22 m x 8 m x 1.5 m (length, width, height). The material was excavated from the adjacent riparian forest. Image courtesy Elena Battisacco.

5.2.2 Hydrograph

For this study a flood pulse with a gradual increase up to a peak discharge of 195 m^3s^{-1}, corresponding to a two year flood, was released from Rossens dam on 14 September 2016 (Figure 5.3). The hydrograph was designed by engineers from the dam operator in collaboration with cantonal authorities, non-governmental organizations (NGOs) and ecological experts. The main purpose of the flood was to clean the river of excess algae, hence the threshold for incipient motion of the armor layer was not largely exceeded. Due to the presence of polluted areas near the floodplain, no larger peak discharge could be chosen. To cause sediment transport, the shape of the hydrograph was chosen accordingly. The hydrograph was designed with multiple periods of constant discharge on the increasing limb, allowing the measurement of flow depth and discharge and the peak discharge was kept for two hours with a gradual decrease. In total about 9.3 mio m^3 water was released during 28 hours. Impressions of the flood can be seen in Appendix E.
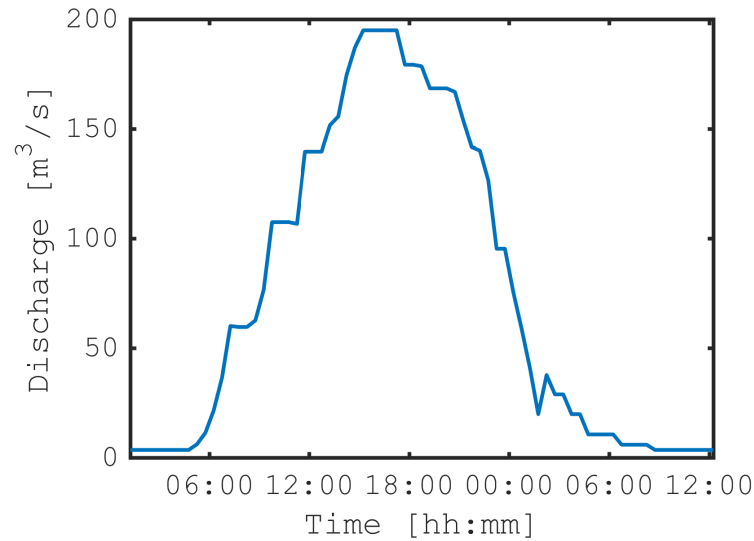
Figure 5.3 – Hydrograph of the flood pulse. The peak discharge of this two year flood was limited by restrictions in the flooding perimeter. The two year flood corresponds to post-dam conditions based on the gauging station 2119 in Fribourg (correction factor 0.78). The flood latest from 14 September 2016 at 05h00 until 15 September 08h30.

5.3 Methodology

5.3.1 Sediment tracking system

The excavated material was composed of characteristic grain sizes d_m = 57 mm and d_{90} = 113 mm. The grain size distribution was determined analyzing 21 samples of Fehr line-sampling (Fehr, 1987) and photo sieving using BASEGRAIN (Stähly et al., 2017). A total of 489 stones, divided in d_m and d_{90}, were collected in the field, drilled and the hole filled with a Radio Frequency IDentification Passive Integrated Transponder tag (RFID PIT tag) of 32 mm and 23 mm length (depending on stone size) and sealed with silicon (Arnaud et al., 2015; Cassel et al., 2017b; Brenna et al., 2019). The characteristics of the equipped stones was different between d_m and d_{90}. Despite the small variation in b-axis, the weight varies significantly especially for d_{90}. Most d_{90} stones are disc-shaped, while the shape of d_m were more diverse (Figure 5.4). Despite the small bandwidth of diameters, the weight of the tagged stones varied significantly. This come from the different shapes which were analyzed based on the ratios of the a-, b- and c-axes (Zingg, 1935; Bunte and Abt, 2001). With the software S2_Util (Texas Instruments TIRIS, Version 1.20), tags were programmed with a unique identification number. After measuring the three axes and the weight of the tagged cobbles, they were distributed equally in three layers (top, middle and bottom) in the four deposits (Figure 5.1). About 100 m downstream of deposit IV, a pass-over loop fix-antenna was mounted across the river, perpendicular to the main flow direction (Schneider et al., 2010). The antenna consisted of a single loop multiple-strand cable with a diameter of 16 mm^2, protected by a rubber hose

(Figure 5.5). The hose was fixed with cable straps close to the river bed at 1-m long armoring irons that were vertically installed into the river bed every meter. Prior to its installation, the antenna shape was optimized to a length corresponding to the local river width of about 25 m. The optimal antenna surface of 25 m x 0.3 m resulted in a detection distance of up to 1.5 m under dry conditions. Installed in the river, the detection distance below water did not exceed 0.3 m.
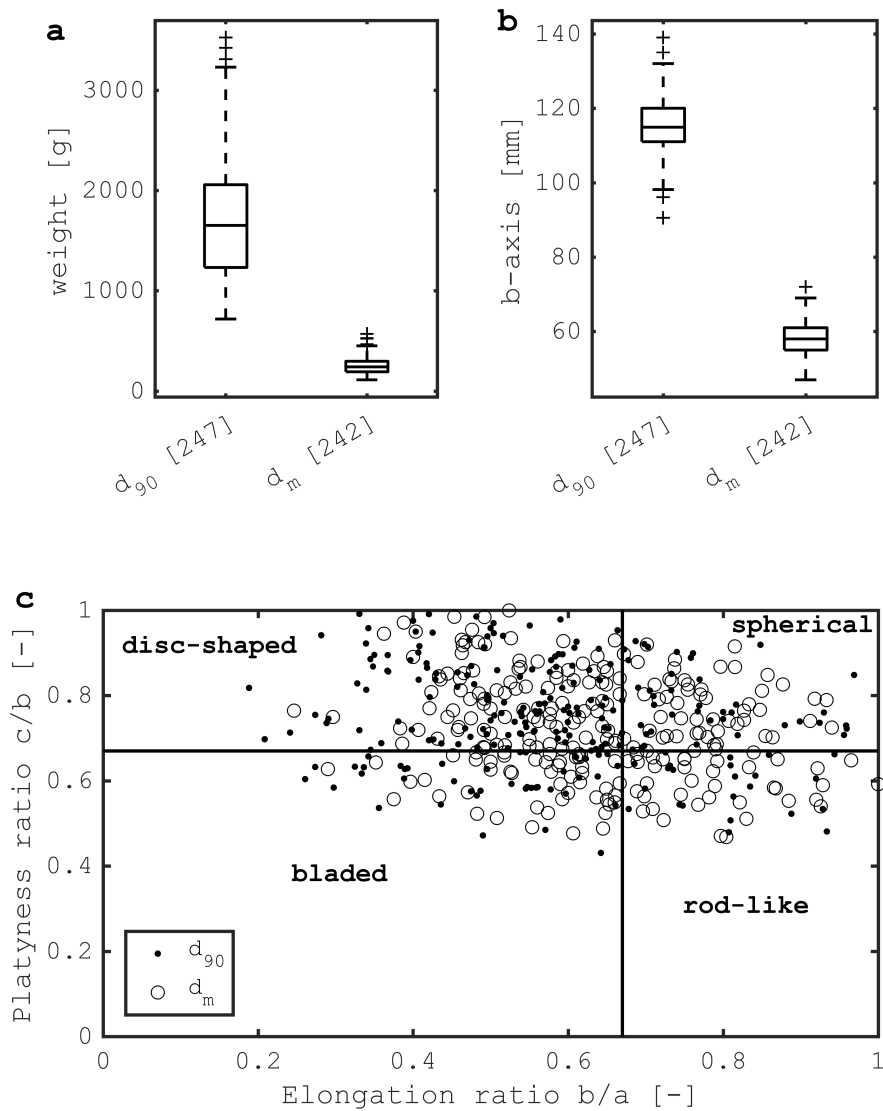
Figure 5.4 – Physical properties of the stones equipped with RFID PIT tags. (a) Weight distribution, the large variation in weight is caused by the different stone shapes; (b) *b*-axis distribution; (c) shape classification after Zingg (1935); most stones were disc-shaped.

Figure 5.5 – Installed pass-over loop fixed-antenna in the Sarine river. The single loop cable was installed for protection inside a garden hose. The hose was fixed with cable straps to 1-m long vertical armoring irons installed in the river bed every meter. The antenna had a surface of 25 x 0.3 m^2. Image courtesy Elena Battisacco

In addition to the fixed antenna, a mobile antenna was used for RFID PIT tag detection after the flood. The mobile antenna consisted of a 1.5 m long pole and 0.7 m diameter ring attached at the end, both made of plastic (Figure 5.6). Inside the ring, a double loop of 4 mm^2 multiple-strand cable formed the antenna. The electro-magnetic components are carried in a back pack. When detecting a PIT tag, the antenna made a noise and the tag ID was shown on the screen. Both antenna systems, the fixed and the mobile antenna, worked with a 12 V 7.0 Ah battery. The electromagnetic components, such as the PIT tags, Tuning Board, HDX Reader and Control board are products from OREGON RFID, Portland, USA. The PIT tags work at a low frequency of 134.2 kHz, allowing detection in submerged conditions.

With the help of the self-made mobile RFID antenna, the location of tagged stones could be detected after the flood event and their locations were recorded with a differential Global Navigation Satellite System (GNSS, model TOPCON HiPer Pro) with an accuracy of a few centimeters. The location of origin (x_0) and deposition (x_d) for tagged stones could therefore be captured with a precision of about 1 m due to the antenna-size. The location of the fix-antenna (x_a) was known. In addition, the zone of erosion was defined, covering the influence area of the deposits where flow varies highly. It reaches from the upstream end of deposit I until one river width downstream of deposit IV (x_e). The definition of this spatial division is given in Figure 5.7.

Figure 5.6 – Search of RFID PIT tags with the mobile antenna after the flood event in the Sarine river. Image courtesy Severin Stähly
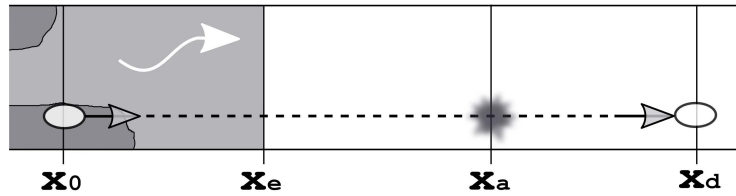
Figure 5.7 – Concept and sketch of the longitudinal scales. The erosion zone is shaded, deposit III and IV dark gray. x_0 = original position where a tagged stone was put in the sediment deposit; x_e = downstream end of the erosion zone; x_a = location of the pass-over loop fix-antenna; x_d = final position where a tagged stone was found after the flood event.

Knowing the location of deposition of a tagged stone (x_d), the time it ceased moving (t_d), the time it passed the antenna (t_a) and the location of the antenna (x_a), an average transport velocity v_d for each stone that passed the fix-antenna can be estimated for the distance between the fix-antenna and the location of final settling (Equation 5.1). This measured average transport velocity, referred to as virtual velocity v_d, is the average of a series of bouncing and stopping processes within the interval of x_a and x_d in the allocated time period (Hassan et al., 1991). On the other hand, the velocity upstream the antenna v_a can be calculated (Equation 5.2), using the time and location at the antenna (t_a, x_a) with its departing location (x_0) and earliest possible moment for erosion (t_0), which depends on the discharge. The ero-

sion time t_e indicates the time a tagged stone is transported out of the erosion zone and can be obtained by Equation 5.3 and the estimation of the erosion velocity v_e according to Equation 5.4 (see Figure 5.8). This allows then the determination of the erosion-effective periods during the flood event as well as the corresponding sedigraph representing the time-series of the erosion of the tagged stones. Based on the sedigraph and on the released volume a parameter called erosion efficiency is introduced (*eeff*, see Equation 5.5), which corresponds to the ratio between the percentage of eroded tags in a certain time period i (Δt_i) and the percentage of released water during the same time period.

$$v_d = \frac{x_d - x_a}{t_d - t_a} \tag{5.1}$$

$$v_a = \frac{x_a - x_0}{t_a - t_0} \tag{5.2}$$

$$t_e = t_d - \frac{x_d - x_e}{v_d} \tag{5.3}$$

$$v_e = \frac{x_e}{t_e} \tag{5.4}$$

$$eeff_i = \frac{Eroded\ tags\ (during\ \Delta t_i)\qquad\quad [\%]}{Released\ water\ volume\ (during\ \Delta t_i)\ [\%]} \tag{5.5}$$

with:

Δt_i	i-th time interval [s]
$eeff$	erosion efficiency [-]
t_0	time a tagged stone is eroded [s]
t_a	time a tagged stone passes the fix antenna [s]
t_d	time a tagged stone settles [s]
t_e	time a tagged stone passes the downstream end of the erosion zone [s]
v_a	tagged-stone transport velocity between the origin and the fix-antenna [ms^{-1}]
v_d	virtual velocity of a tagged-stone [ms^{-1}]
v_e	tagged-stone transport erosion velocity [ms^{-1}]

x_0 location of origin of a tagged stone [m]

x_a location of the fix antenna [m]

x_d location of settling of a tagged stone [m]

x_e location of the downstream end of the erosion zone [m]
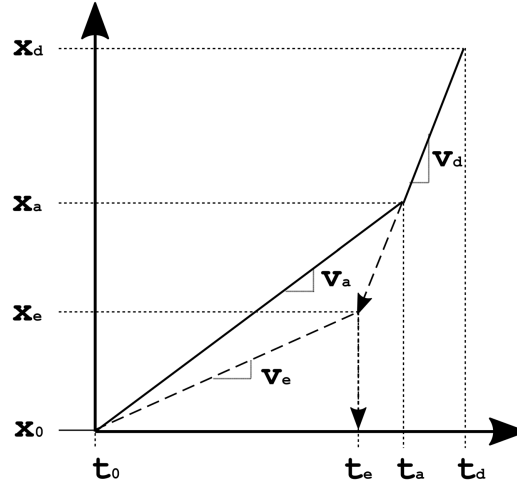
Figure 5.8 – Concept of the estimation of the average sediment transport velocity or virtual velocity (v_d) and erosion velocity (v_e). x_0 = original position where a tagged stone was put in the sediment deposit; x_e = downstream end of the erosion zone; x_a = location of the pass-over loop fixed-antenna; x_d = final position where a tagged stone was found after the flood event. t_0 = time of erosion; t_e = time of leaving the erosion zone; t_a = time of passing the pass-over loop fixed-antenna; t_d = time the stone stopped moving.

5.3.2   Critical discharge to determine t_0 and t_d

The critical discharge for the d_m and d_{90} on each deposit was determined using a numerical 2D-flow-model in BASEMENT v2.6, which is a freeware simulation tool for hydro- and mor-phodynamic modeling (for more information, see www.basement.ethz.ch). The mesh was constructed in QGIS using the plugin BASEmesh and the following data:

- Laser detection and ranging (LiDAR) data of the terrestrial surroundings from 2014 were available at a resolution of about 30 cm between points.

- River bed topography was measured prior to the placement of the deposits in the river at every meter across 10 cross-sections, using a differential GNSS (model TOPCON HiPer Pro).

- At the locations of the deposits, 1.5 m of sediment was added to the river bed.

The maximum distance between two nodes for triangulation was 2 m for the deposits and the river bed, 30 m for the embankment and 50 m for the further surroundings. This resulted in a total of 37'690 elements and 19'107 nodes. A Manning-Strickler roughness value of 30.4 $\text{m}^{1/3}\text{s}^{-1}$ for the fixed river bed and the deposits, 10 $\text{m}^{1/3}\text{s}^{-1}$ for the vegetated areas. Calibration was done with the maximum water depth observed during the flood event. The river bed was modeled as a fixed bed and the deposits with a mixed grain size, with both diameters, d_m and d_{90}. The analysis of the incipient motion of the sediment transport was analyzed based on two different sediment transport equations (Meyer-Peter and Müller, 1948; Parker, 1990). The globally smallest critical discharge was used as the deposition criterion on the decreasing limb of the hydrograph.

5.4 Comparison with the laboratory experiments

To compare the experiment with the laboratory findings, the deposition pattern of the replenishment was analyzed using two measures that were investigated by Battisacco et al. (2016): the occupation ratio along the channel (*OCR*) and the different wavelengths of the OCR longitudinal distribution, which represents a measure of the reoccurrence of sediment clusters. In the laboratory experiments, the OCR is defined as the percentage of red pixels (red pixels = replenished sediment) in an analyzed cross-section with the interval size of one pixel *x* (Equation 5.6). In the field, the OCR was calculated based on the number of tagged stones found in a certain river interval *X*. Therefore, the length of the river was fragmented into 5-m-intervals between the downstream end of deposit IV and the last tagged stone found. To normalize the data and allowing comparison with the laboratory data, the maximum number of tagged stones detected in a 5-m-interval was taken (Equation 5.7, Figure D.4 in Appendix D). The periodicity in the longitudinal direction of the river is calculated with the Fourier transformation of the OCR, the so-called power spectral density PSD (Stoica et al., 2005). The PSD represents the OCR signal in frequency domain. In this analysis the function *pwelch* in the program MATLAB version R2016b was used to calculate the PSD. The PSD and the OCR signals are of practical relevance since they indicate how the replenishment may impact the downstream segment (Battisacco, 2016). The OCR signals in the laboratory and in the field are calculated as follows:

$$OCR_{x,lab} = \frac{\Sigma\,red\,pixels\,in\,a\,cross-section}{\Sigma\,pixels\,in\,a\,cross-section} \tag{5.6}$$

$$OCR_{X,field} = \frac{\Sigma\,tagged\,stones\,in\,a\,5\,m\,interval}{Maximum\,number\,of\,tagged\,stones\,in\,a\,5\,m\,interval} \tag{5.7}$$

5.5 Results

5.5.1 Sediment tracking

From the 489 RFID tagged stones placed in the deposits, 277 were found and localized with the mobile antenna after the flood event. Out of these 277 stones corresponding to 57 %, 166 were located in the river and 111 in the remaining part of the partially eroded deposits. From these 166 stones, 84 were detected downstream of the erosion zone. The maximum transported distance observed was 286 m for d_{90} and 279 m for d_m. In average, the d_{90} was transported further than d_m, with a median transport distance 67 m (d_{90}) to 41 m (d_m) respectively. Air images revealed that deposit I, II and IV were only partially eroded (Figure 5.9). Stones from deposit I and III were transported the furthest, stones from deposit II the least (Figures 5.10). No tagged stone placed in the top layer of deposit I was recovered after the event (Figure 5.11c). In all four deposits, the tagged stones placed in the bottom were the least discovered and transported the shortest distances (Figures 5.11c-f). The pass-over loop fixed antenna detected six stones having the origin of deposit I or III (Table 5.2).
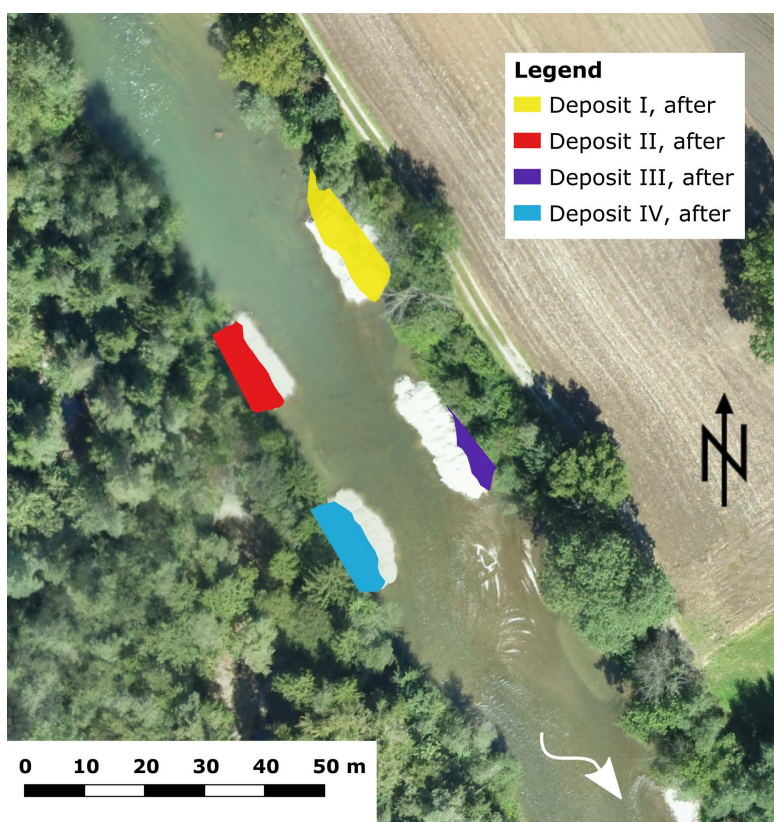
Figure 5.9 – The exposed dry surface of the four deposits before (air-image background courtesy Research unit Ecohydrology, ZHAW) and after (colored areas) the artificial flood event. The residual flow discharge was 3.5 m^{3}s^{-1} when the air-image was taken before the flood event and 2.5 m^{3}s^{-1} when the dry surface was measured after the flood event.
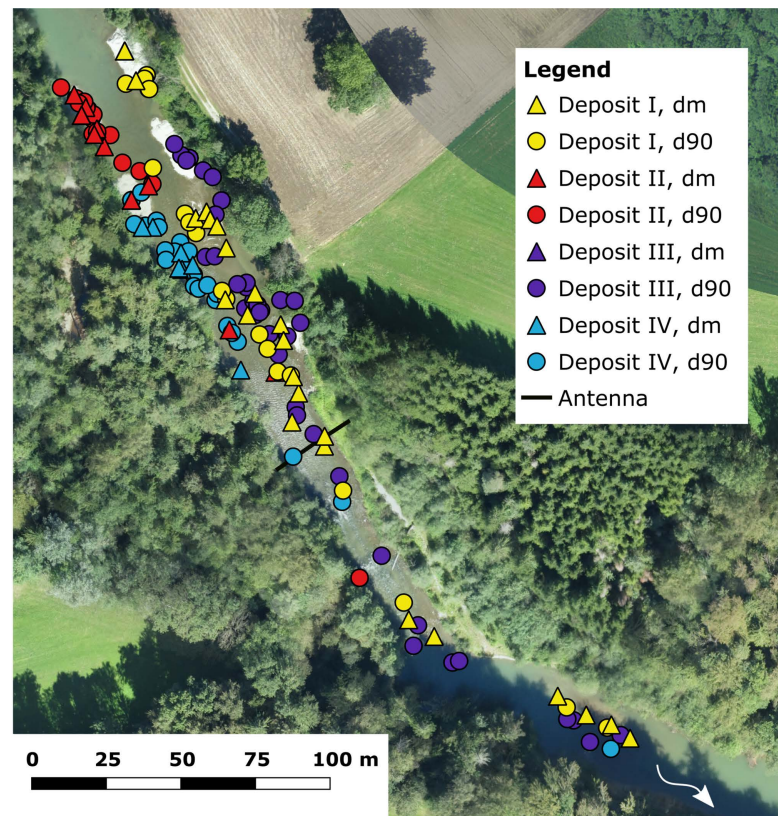
Figure 5.10 – RFID PIT tag equipped sediments detected after the flood event. Geodata courtesy Research unit Ecohydrology, ZHAW

Table 5.2 – Information about the six stones detected with the field loop antenna. bot = bottom level; mid = middle level; top = top level of initial placement in the deposit of origin. *NaN* as a result of the further travel distance (x_d-x_a) indicates that the tagged stone was not located after the flood event. The detection time refers to on-site time on 14 September 2016 except for tag ID 325 recorded on the following day.

Tag ID	Units	16	271	367	73	364	325
Deposit of origin	[-]	III	I	III	III	III	I
Level placed	[-]	mid	bot	mid	top	mid	mid
Type	[-]	d_{90}	d_m	d_m	d_{90}	d_m	d_m
Tag size	[mm]	32	32	23	32	23	23
Diameter, b-axis	[mm]	122	58	55	117	56	59
Stone shape	[-]	disc-shaped	rod-like	spherical	rod-like	disc-shaped	spherical
Weight	[g]	2251	236	328	1202	361	299
Detection time	[hh:mm]	18:25	19:37	19:39	19:44	19:53	10:11 (+1)
Detection duration	[s]	33	4	0.9	145	9.1	79
Further transport (x_d-x_a)	[m]	NaN	3	88	87	NaN	0
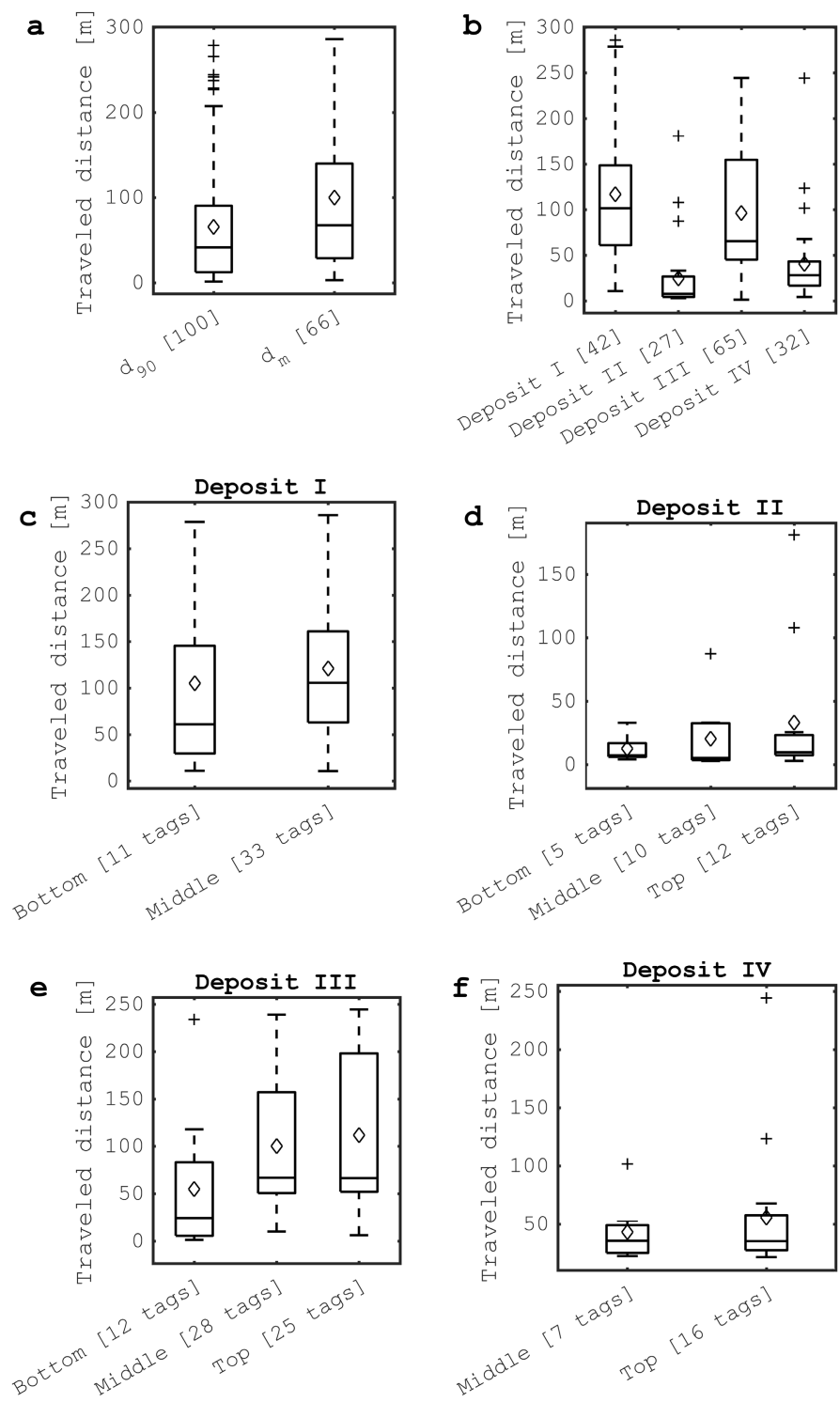
Figure 5.11 – Traveled distances of the RFID PIT tagged sediments which were detected with the mobile antenna after the flood event sorted by (a) size and by (b) deposit of origin and by (c-f) level where the tagged stones were placed in each deposit. ◇ = mean value, + = outliers

5.5.2 Erosion time and average transport velocity

From the six PIT tags equipped stones registered at the pass-over loop fixed antenna only two could be used to calculate the erosion time (Equations 5.1-5.4). Tags with the ID 16 and 364 were not located after the flood pulse (Table 5.2). ID 271 was trapped by a large rock in the river 3 m downstream of the antenna and therefore could not be considered as a representative transported stone. Once the flood passed and the discharge was low, tag ID 325 was registered. However, the stone must have arrived hours before at that location since it was registered at the residual flow of 3.5 m^3s^{-1}. It is likely that the antenna did not work properly when stone 325 arrived. Therefore, the analysis was done based on the information of stones with ID 367 (d_m) and 73 (d_{90}). For the analysis of the virtual velocities, values for critical discharge were taken based on the numerical model results (see Table 5.3). Based on field observations, it is considered as not accurate to use these results. The deposits were located after a right river bend causing an increased erosion of deposit I and III (Bathurst et al., 1977; Termini, 2004). Therefore the values between the deposits were exchanged (Table 5.3). The lowest critical discharges (29 m^3s^{-1} d_m and 84 m^3s^{-1} d_{90}) were allocated to deposit III, the second lowest (34 and 106 m^3s^{-1}) to deposit I, and the highest to deposit II (72 and 137 m^3s^{-1}). For deposit IV, the average value of the critical discharges from deposit I and II were taken (106/2 + 137/2 = 122 m^3s^{-1}). The final chosen critical discharges reflect the findings of the sediment restoration report of the Sarine, concluding that a grain with a characteristic diameter of 50 mm moves at a discharge between 70 and 100 m^3s^{-1}, the armor layer breaks at a discharge of 150 m^3s^{-1} (Jäggi and Hunziker, 2002; DAEC, 2014). The virtual velocity v_d resulted in 19 cm/min (equal to 3.1*10-3 ms^{-1}) for tag ID 367 (d_m) and 28 cm/min (equal to 4.6*10-3 ms^{-1}) for tag ID 73 (d_{90}). These two values were then assigned to all 84 tagged stones that were transported further than the lower boundary of the erosion zone, allowing the calculation of the erosion time t_e for each tag (Figure 5.12). The most effective erosion occurred after the discharge reached 175 m^3s^{-1}. Once the discharge passed its maximum and decreased, the erosion diminished quickly and equaled zero once the discharge was below 126 m^3s^{-1}. The sedigraph in Figure 5.12 indicates high erosion mainly when the discharge increased. Four periods of steep increase in discharge until 12 h, intermediated by constant discharge periods, are observed. About 40 % of the stones were transported during these periods of steep increase of the discharge, which represented only 20 % of the water released. If the whole rising limb is included (considering also the constant hydrograph periods), 51 % of the stones were eroded. During the constant peak discharge 24 % of the stones were eroded and 25 % during the decreasing limb which corresponded to 44 % of the released water. This is associated with an erosion efficiency (*eeff*) of 2.16 for the steep increase of the discharge, 1.60 for the peak discharge and 0.57 for the decreasing limb.
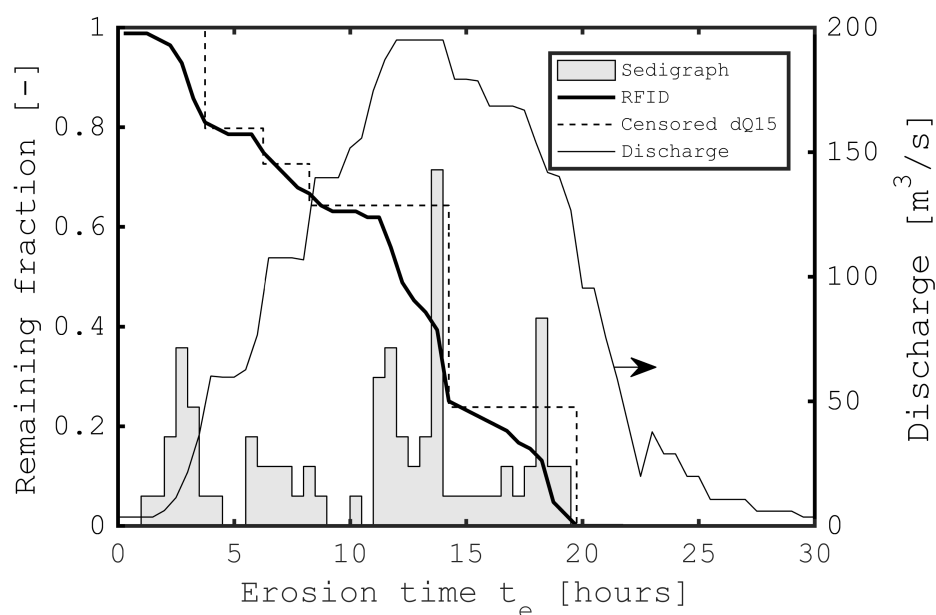
Figure 5.12 – The erosion time represents the time that the 84 stones took to leave the erosion zone. The survivor function (Davison and Hinkley, 1997) indicates the proportion of stones remaining in the erosion zone (84 stones = 100 %). To cluster the data, a censored analysis was done assembling all PIT tag-equipped stones leaving the zone within a change in discharge of 15 m^3s^{-1} or higher. The sedigraph (shaded) is for illustrative purposes and does not correspond to a y-axis, highest point at 0.14 (see Table 5.4).

Table 5.3 – Critical discharges taken for the estimation of virtual velocity and erosion time. Values used for the calculation were chosen based on the numerical model results and field observations. As a deposition criterion, the smallest discharge taken for the incipient erosion was used for each deposit.

Deposit	Incipient motion Q				Deposition Q	
	Model results		Used values			
	d_m	d_{90}	d_m	d_{90}	d_m	d_{90}
	[m^3s^{-1}]	[m^3s^{-1}]	[m^3s^{-1}]	[m^3s^{-1}]	[m^3s^{-1}]	[m^3s^{-1}]
I	72	137	34	106	84	29
II	72	106	72	137	84	29
III	34	106	29	84	84	29
IV	29	84	53	122	84	29

Table 5.4 – Erosion efficiency *eeff* and interpretation of the sedigraph and Figure 5.12.

	Eroded stones		Period	Released volume		*eeff*
	[%]	[#]	[hh:mm]	[mio m^3]	[%]	[-]
Steep increasing periods	41	34	06:30	1.79	19	2.16
Increasing limb	51	43	10:30	3.79	41	1.24
Constant peak discharge	24	20	02:00	1.40	15	1.60
Decreasing limb	25	21	15:30	4.07	44	0.57
Total	100	84	28:00	9.26	100	1.00

5.5.3 Comparison with laboratory experiments

Since the replenished sediment was not fully eroded, it was compared with an intermediate result of the laboratory tests (Figure 5.13a). Considering the evolution of the laboratory experiment, the picture taken after 60 min was analyzed for the OCR and the periodicity (one test took 180 min, more information in Appendix D, Figure D.5). The laboratory data resulted in a non-stationary periodicity at a normalized distance x/w equal to 2.5 with the strongest signal at time step 105 min (Figure 5.13b). The signal decreases with increasing experiment time. The results of the Sarine have a pronounced peak at x/w = 4.2 with small signals at shorter distances.
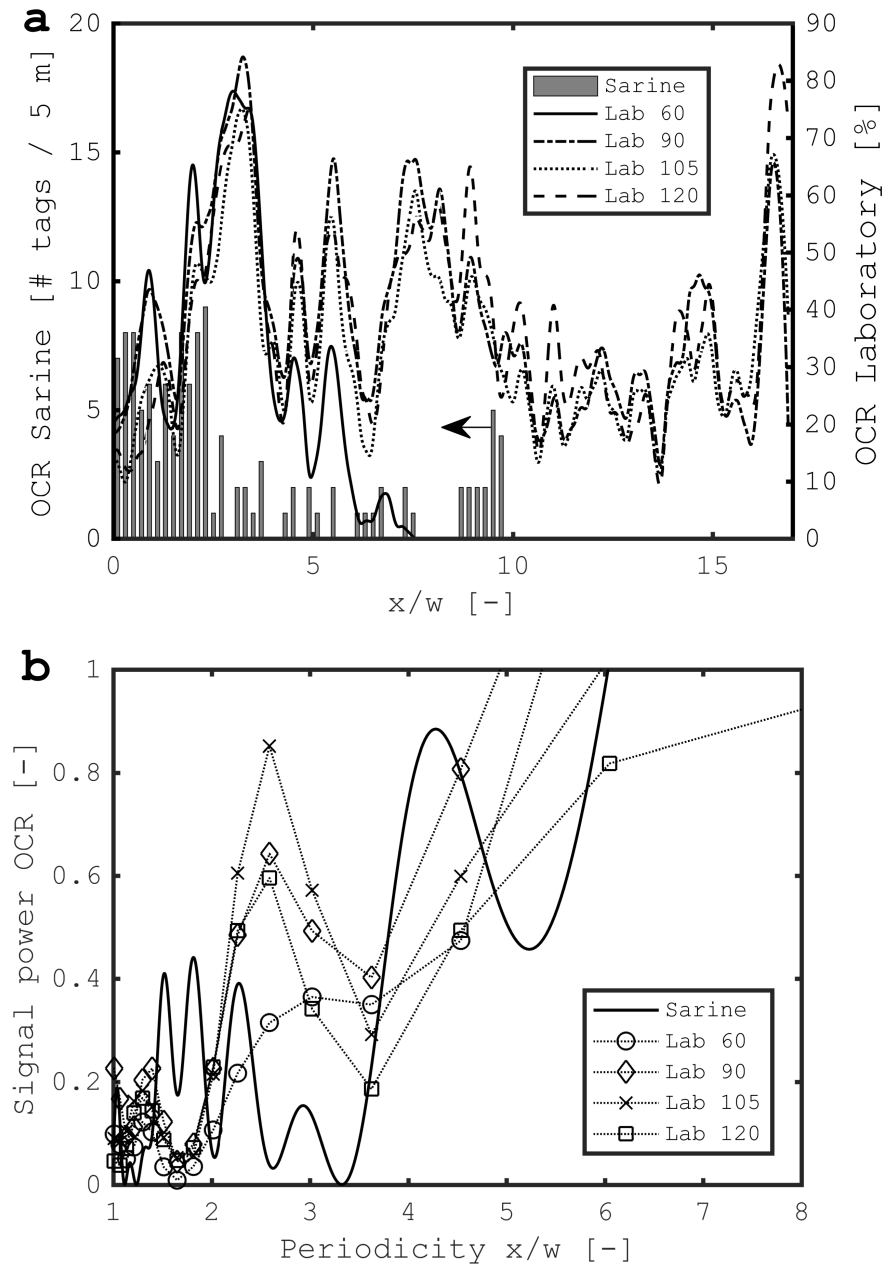
Figure 5.13 – (a) Occupation ratio density (OCR) of the field experiment in the Sarine and the evolution of the laboratory experiments. Lab 60-120 are the results from the laboratory experiment after 60 min, 90 min, etc. (b) Periodicity was calculated based on the signal power of the OCR. The two datasets were both normalized to be comparable in the same plot. The analyses are based on 125 PIT tagged stones recovered downstream of the downstream end of deposit IV.

5.6 Discussion

5.6.1 Sediment tracking technique

The fixed installed antenna did not work properly during the whole event. Post-flood investigation revealed that the system with the wire in the hose was not rigid enough. The strong forces and high shear stresses acting at the bottom of the Sarine during the flood event changed the shape of the antenna permanently and with it the electromagnetic field. An RFID detection antenna is tuned for a certain shape and the electromagnetic field around the antenna may decrease and eventually disappear if the antenna-shape changes (Schneider et al., 2010; Arnaud et al., 2015). Despite all the vertically installed metal rods staying in place, the hose was detached from some rods and the cable straps broke, resulting in a high flexibility of the antenna shape. A relatively flexible system as the one used here has the advantage that it tolerates a certain amount of impact by rolling, jumping and sliding rocks, whereas a complete rigid structure may completely break after impact and no data would be collected. Furthermore, if the bed is eroded below the antenna, a flexible system is more tolerant to such processes. The pass-over loop fixed antenna used here demonstrates that despite the high impact, the antenna worked at least partially during the flooding such that six PIT tags could be registered. In total, 36 PIT tag equipped stones were localized with the mobile antenna after the flood downstream of the antenna, but a high number remains missing. From the 489 PIT tag equipped stones, 57 % were localized with the mobile antenna. In similar studies, significantly higher recovery rates were observed (Hodge et al., 2011; Liébault et al., 2012; Nathan Bradley and Tucker, 2012). There are multiple limitations why the 57 % recovery rate was not higher:

1. The mobile antenna had a detection distance of up to 0.6 m, causing the PIT tags that remained in the mid (0.6-1.2 m) or lower (1.2-2 m) layer of the deposits to be out of the electromagnetic field of the mobile antenna. This also can occur for transported PIT tags that buried in a lower layer in the river bed (Chapuis et al., 2015).

2. PIT tag signal collision (Chapuis et al., 2014). At 134.2 kHz, PIT tags do not have an anti-collision protocol. The signal of PIT tags located about 0.3 m to each other may collide (Cassel et al., 2017a).

3. The size of the tag (32 mm and 23 mm PIT tags), and the orientation of the PIT tag influence the detection range (Arnaud et al., 2017, 2015). PIT tags oriented normal to the antenna emit a stronger signal than when it is parallel to the river bed.

4. The deep scour in the bed downstream of the fixed antenna, where the river has a slight bend. In this area, the water depth is more than 4 m and thus cannot be accessed with the mobile antenna (Figure 5.10). All tagged stones that settled in this pool could not be located after the flood event.

5. The fact that stones traveled further than the area that was searched with the mobile

antenna. After the furthest downstream stone was detected, another 100-m segment was searched with the mobile antenna without detecting any further PIT tags. The dry area on the floodplain, where water passed during the flood event, also was searched for PIT tags. It is likely that there were stones transported significantly further downstream. There are 38 PIT tagged stones from deposit I and III that were placed in the top-layer of deposit I and never found after the event. It is likely that they traveled further downstream than the searched area or stopped in the scour as mentioned above.

5.6.2 Erosion time and average transport velocity

Considering the deposition map, there is no significant transport of the tagged stones lateral to the flow direction (Figure 5.10). The PIT tagged stones from deposit I and III settled near the left bank and those from deposit II and IV near the right bank of the river. This indicates that bend-related effects (e.g. secondary currents) are of low importance downstream of the erosion zone, hence supports the choice of the erosion zone (Figure 5.7). The analysis of the erosion time underlies several uncertainties. First, there are the critical discharges. It is not exactly known when the deposits started to erode, since the field observations and the results of the numerical modeling are contradictory. However, the maximum chosen critical discharges reflect the findings of the sediment restoration report of the Sarine. The report concludes that a grain with a characteristic diameter of 50 mm moves at a discharge of 70 to 100 m^3s^{-1} and that the armor layer in the residual flow segment of the Sarine breaks at a discharge of 150 m^3s^{-1} (Jäggi and Hunziker, 2002; DAEC, 2014). Second, most of the PIT tagged stones were disc-shaped and the ratio between the different axes varied significantly in the Zingg diagram (see Figure 5.4c, Benn and Ballantyne (1993); Bunte and Abt (2001)). The stone shape has a strong influence on transport behavior. Particles with the same b-axis are transported at a significantly smaller discharge when they are disc shaped and not rod-like shaped. The different shapes result also in a large variation of volume and the weight of the tagged stones (see Figures 5.4a-b). The average weight for a d_{90} stone is 1700 g, and varied between 720 and 3500 g (d_m: 250 g, 110-570 g). The volume of a stone and therefore also its weight, have a key influence on the critical incipient motion of a particle, and a further reason why effective discharge for erosion varies from stone to stone. Since the weight of ID 367 is above average (328 g vs 250 g) and of ID 73 below average (1202 g vs 1700 g), the erosion curve in Figure 5.12 could be shifted if measured for stones with different characteristics. Despite these uncertainties, the sedigraph and survivor analysis presented in Figure 5.12 are in good agreement with observations from the laboratory experiments (Battisacco, 2016). Leopold et al. (1965) identified that bankful discharge is the effective discharge for morphological change, corresponding to a flood event with a return period of 1.5 years. Surian et al. (2009) observed a significant change in the geomorphology of side-channel by floods with a return period <1 year in the Tagliamento river in Italy. During the artificial flood, the surrounding floodplain was only inundated at limited locations and a freeboard of 1 m was observed at deposits in the Sarine (see Appendix D). Therefore, it can be concluded that the low submergence of deposits was the main reason why the deposits were only partially eroded.

Deposit submergence is a main driver of the erosion of the multi-deposit configuration as revealed in the laboratory results for different hydrographs (Battisacco, 2016). In the laboratory experiments, complete erosion of the replenishment deposits was observed shortly after the peak passed for a left-skewed hydrograph. For a right-skewed hydrograph, meaning the peak of the hydrograph arrives before 50 % of the event time, the erosion or the four deposits may be completed before the peak arrives. An armor layer was formed during the event on the residual part of all deposits (Figure 5.14). Whenever the discharge was constant for more than one hour (see rising limb), the erosion of tagged sediments from the deposits was low or even zero (at 60 m^3s^{-1}, 108 m^3s^{-1} and 140 m^3s^{-1}), as can be observed in the sedigraph and the erosion efficiency (Figure 5.12 and Table 5.4). Therefore, it may be assumed that temporary armor layers formed during the event on the deposits (Parker and Sutherland, 1990). This explains to a certain extent why sediment was not eroded from the residual part of the replenishment once peak discharge passed. In addition to this armoring, the deposits were already partially eroded after the peak passed, resulting in a reduced concentration of flow to the middle of the channel. Hence, the bed shear stress is lower for the same discharge compared to the beginning of the artificial flood event in the erosion zone.

Figure 5.14 – View from deposit I towards upstream. An armoring of the residual deposit was observed. The armoring was sorted with large stones in the bottom (left), where the submergence was higher and cobbles (right) where the submergence was smaller. Image courtesy Severin Stähly

5.6.3 Comparison with laboratory experiments

Deposit III was clearly more eroded than the other deposits (Figure 5.10). This is due to the flow concentration caused by deposit I and II towards the middle of the river. Laboratory experiments by Battisacco (2016) points out that erosion starts at deposit III (Appendix D). The final situation of experiment is comparable with the resulting state of the laboratory experiments after 60 min. Starting at deposit III in the laboratory experiments, the erosion continues with deposit IV, II and I. In the field experiment, however, deposit I was eroded similarly or even more than deposit II and IV. Nevertheless, after 60 min the two situations are quite similar, with the only difference that deposit IV was less eroded in the field (Figure 5.9).

The Sarine artificial flood mimics the laboratory conditions as good as it was possible regarding the dimensions and positioning of the gravel deposit in the river normalized to the river width (Table 5.1). Despite the differences between this prototype and the laboratory experiment, the resulting erosion and deposition patterns are similar. A periodicity was detected in both experiments underlining the robustness of the approach with the four alternate deposits. The differences in upstream conditions also may cause the difference in periodicity. The small periodicities at small distances (Figure 5.13b) are significantly smaller than the detected periodicity at a distance of 4.2 times the river width. In the laboratory results, the replenished sediment spread over a longer normalized distance than in the Sarine (Figure 5.13a). This can be explained with different boundary conditions such as the heterogeneous geomorphology found in the river, the sediment size, and the hydrograph. Important is the similar development of a distinctive periodicity and not the same location of it.

5.7 Summary

In this chapter transport processes of a multi-deposit sediment replenishment technique, applied for the first time, was investigated by stone tracing techniques during an artificially triggered flood. The key findings can be summarized as follows:

1. To measure the transported distance of the replenished sediment, 489 stones were equipped with RFID PIT tags. Thereof 57 % could be recovered after the flood. This corresponds to 277 stones, of which 166 were moved during the flood (100 d_m, 66 d_{90}). The maximum transported distance observed was 286 m for d_{90} and 279 m for d_m. In average, the d_m was transported 100 m and the d_{90} 65 m.

2. With the help of a pass-over loop fixed antenna and a numerical 2D flow model, an average stone transport velocity for both tagged grain sizes with mean diameters of 57 and 113 mm could be estimated. This virtual velocities resulted in 19 cm/min for d_m and 28 cm/min for d_{90}.

3. Knowing the average stone transport velocities as well as the initial and the final location of the stone, the erosion time of each transported stone and a sedigraph were

estimated. Based on the sedigraph and the released volume, erosion efficiencies *eeff* for the different parts of the hydrograph were calculated. The *eeff*s resulted in 1.24 on the increasing limb, 1.60 for the constant peak discharge and 0.57 for the decreasing limb. Erosion was most effective during periods with steep increasing discharge. In these periods, the average *eeff* was 2.16. The low *eeff* of the decreasing limb is mainly due to the formation of temporary armor layers on the deposit surface during the event leading to a complete absence of erosion after the decreasing limb of the hydrograph drops below $126\,\mathrm{m^3s^{-1}}$.

4. A similar configuration of the replenishment with four deposits as alternate bars adjacent to the river banks was investigated in laboratory experiments prior to this event, which allowed comparison. In the laboratory experiments, the most upstream deposit functions as obstacle that concentrates the flow in the center of the river, resulting in erosion of the downstream deposits first. A sharp river bend upstream of the sediment replenishment led to an increased erosion of the deposits positioned at the left river bank of the Sarine. Otherwise the deposition pattern of the Sarine experiment covers with the laboratory situation after 60 min (a third of the total erosion time). The normalized power spectral density (PSD) based on the occupation ratio (OCR) resulted in a clear peak at a distance corresponding to 2.5 times the channel width in the laboratory and 4.2 times the river width in the field experiment. Hence this indicates the robustness of the investigated sediment replenishment methodology.

6 Artificial floods to improve the hydraulic habitat diversity downstream of dams

6.1 Overview

In this chapter, the effect experimental floods was tested at two rivers: In the Sarine River downstream of Rossens Dam and at the Spöl River downstream of Ova Spin (see Figures 3.2 and 3.9 in Chapter 3). In the Sarine such an experiment was conducted for the first time and a special configuration of multi-deposit sediment replenishment, analogous with one tested in laboratory by Battisacco (2016), was applied in the river (detailed description in Chapter 5). In the Spöl River, such flood events have been periodically released since the year 2000, allowing the determination of the long-term effects of such a modified residual flow regime. The release of artificial floods from dams is of special interest, since such flood pulses must be released by dam operators for maintenance reasons. Therefore can a well-planned release of such a flushing serve as a river restoration measure. The objectives of this chapter are:

1. To evaluate quantitatively the effect of **one single artificial flood** in the residual flow segment of the Sarine concerning habitat diversity.

2. To evaluate quantitatively the effect of a **combination of one single artificial flood and a multi-deposit sediment replenishment** in the Sarine concerning habitat diversity.

3. To evaluate quantitatively the effect of a **regime with periodical artificial floods** in a segment with **sediment scarcity and a steep slope** in the lower Spöl concerning habitat diversity.

---

4. To evaluate quantitatively the effect of a **regime with periodical artificial floods** in a segment with **sediment supply** (downstream of the Ova da Cluozza) in the lower Spöl concerning habitat diversity.

6.2 Case study

A brief description of the two study rivers is given in the following. More detailed information can be found in Chapter 3.

6.2.1 Sarine

To restore the Sarine residual flow segment, an experimental flood, combined with sediment replenishment was tested downstream of Rossens Dam on the Sarine (exact location see figure 3.2). A detailed description of the sediment replenishment is given in Chapter 5.

In short, a flood pulse with a peak discharge of 195 $\mathrm{m^3s^{-1}}$, corresponding to a return period of two years, was released from Rossens Dam in September 2016. At one location the river was replenished with 1000 $\mathrm{m^3}$ or sediment. In total about 9.3 Mio $\mathrm{m^3}$ water was released during 28 hours (Figure 5.3). Impressions of the flood can be seen in Figure 6.1 and in Appendix E.

6.2.2 Spöl

The flood in the Spöl took place on 4 September 2018 with a peak discharge of 25.9 $\mathrm{m^3s^{-1}}$ and a duration of about 7.5 hours (Figure 6.2). The largest flood released since the first of this adapted management method was 50 $\mathrm{m^3s^{-1}}$ on 17 June 2013. A comparison of some key numbers of the two flood events is given in Table 6.1.

Table 6.1 – Comparison of the artificial floods in the Sarine and the Spöl River.

	Units	Sarine	Spöl
Maximal flood discharge	[$\mathrm{m^3s^{-1}}$]	195	25.9
Maximal residual flow discharge	[$\mathrm{m^3s^{-1}}$]	3.5	0.9
Ratio	[-]	56	29
Released volume	[mio $\mathrm{m^3}$]	9.26	0.46
Duration	[hh:mm]	28:00	07:30

Figure 6.1 – Top view of the Rossens Dam during the artificial flood in the Sarine on 14 September 2016. Image courtesy Research unit Ecohydrology, ZHAW
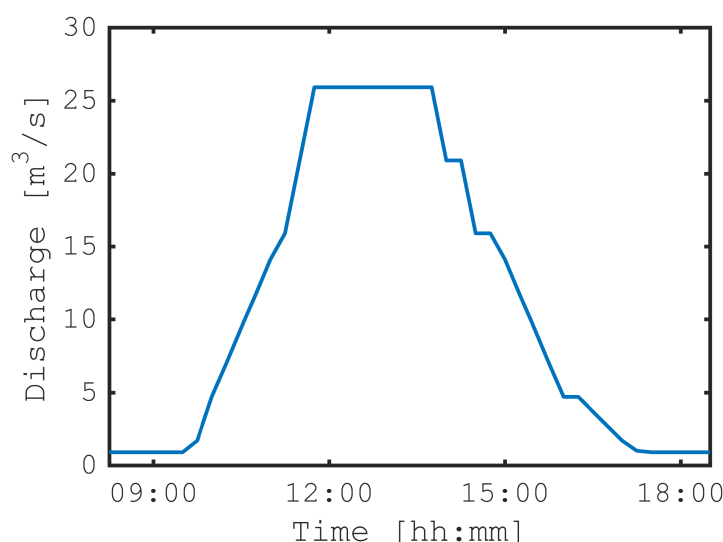
Figure 6.2 – Hydrograph of the flood pulse at the Spöl, released from the Ova Spin Dam. The peak discharge corresponded to 25.9 m^{3}s^{-1}. The whole flood lasted 7.5 hours from 09h45 to 17h15 on 04 September 2018.

6.3 Methodology

The hydraulic habitat diversity was analyzed with the HMID which is explained in detail in Chapter 2. To enable an accurate comparison of the HMID from before and after the flood events, the cross-sections were documented with GPS data and photography.

Sarine

A 850 m segment was analyzed. Measurements of flow depth and flow velocity were made at the exact same locations before and after the flood event, across the river at nine different equally-spaced cross-sections with a distance of about 95 m (Figure 6.3). A total of 207 velocity and water depth measurements were taken in the segment before, and 192 after the flood event. The cross-sections that lied within the influence of the sediment replenishment was determined based on the transported RFID PIT tags (see Chapter 5 for more information) and defined as the *impact zone*. The residual cross-sections were defined as the *rest zone* allowing the separation of the change induced by the flood only (rest zone) and the combination of the flood with the sediment replenishment (impact zone).
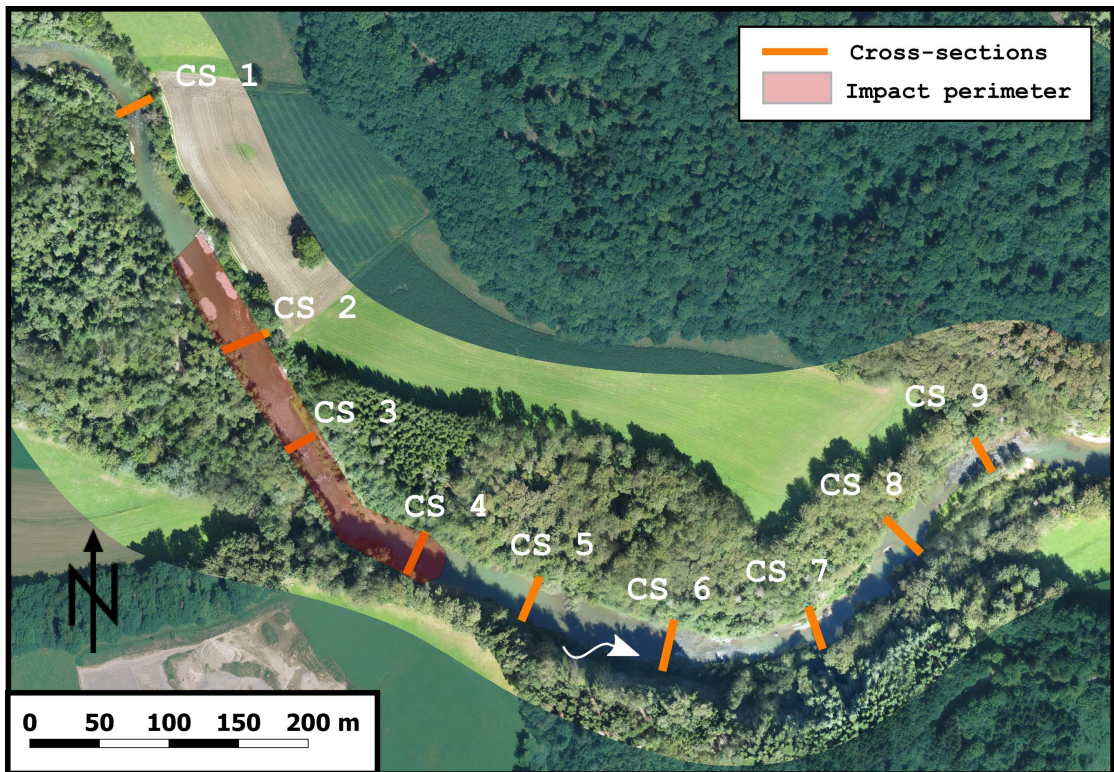
Figure 6.3 – Nine cross-sections (CS) in the Sarine, along which flow depths and velocities were measured. CS 2-4 correspond to the impact perimeter of the sediment replenishment, CS 1 and 5-9 are located outside the perimeter. Geodata courtesy Research unit Ecohydrology, ZHAW

Spöl

At the Spöl, two segments were analyzed. One upstream of the junction with the Ova da Cluozza and one downstream (more information in Chapter 3 and Figure 3.9). In the upstream segment Spöl I, 90 measurements were surveyed in an about 150 m long split on ten equally-spaced cross-sections, after the flood, 107 data points were surveyed on identical cross-section locations. The downstream segment Spöl II is about 230 m long and 90 (prior) respectively 104 (past the flood event) measurements distributed on ten cross-sections with constant spacing were used to calculate the HMID. The spacing between the cross-sections corresponded to the average river width in the segment and was either 16 m (upstream) or 25 m (downstream), the spacing between the measurements on the same cross-section was about 1 m where possible. In the lower segment, at some cross-sections the first measurement was up to 2 m away from the bank because of willows and other vegetation in the river.
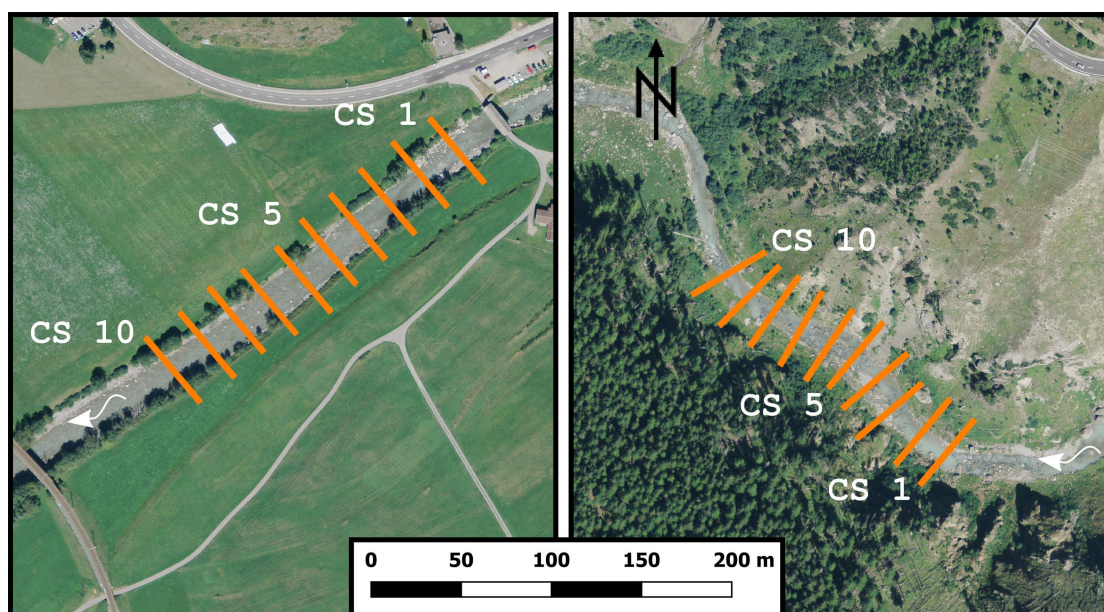
Figure 6.4 – The ten cross-sections (CS) in the Spöl river, along which the data for the HMID computation was sampled. Upstream (right) and downstream of the junction with the Ova da Cluozza. Geodata courtesy Swisstopo

6.4 Results

Change in hydraulic habitat diversity With the RFID PIT tagged stones (see Chapter 5), the perimeter of influence of the sediment replenishment could be determined. Cross-sections 2,3 and 4 lie within the replenishment impact zone, resulting in the calculation of two HMID values, one with the data of the cross-sections mentioned, and a second one with the data of the cross-sections 1 and 5-9 (see Figure 6.3).

Table 6.2 provides the resulting changes in hydraulic habitat diversity using the HMID. The HMID is calculated prior and post the artificial flood events. The Sarine, the HMID within the impact perimeter of the sediment replenishment increased by 36 %. HMID computed with the values sampled outside this impact zone increased by 18 %. Generally, the HMID outside is higher than inside impact perimeter. In the Spöl I, the HMID decreases by -11 % while in Spöl II, where the river has a braided geomorphology, increases slightly (9 %).

In both river segments of the Sarine, the mean flow velocity and depth decreased during the flood event. In the segment that lies within the perimeter of the sediment replenishment, the standard deviation of both measures increases as well, while the segment outside of the replenishment impact perimeter, the standard deviation of the flow depth increases minimally, while the standard deviation of the flow velocity decreases.

Looking at the Spöl, the standard deviation and mean value of the flow depth decrease in both segments. The mean flow velocity on the other hand increases in both segments, while

the standard deviation of the flow velocity decreases at the Spöl I and increases at Spöl II.

Table 6.2 – HMID values before and after the flood events in the Sarine I, the Spöl I and II. The Sarine segment is divided into the impact perimeter of the replenishment (3 CS) and outside impact perimeter of the replenishment (6 CS).

		HMID$_{impact}$		HMID$_{outside}$	
		PRIOR	POST	PRIOR	POST
SARINE I					
Data points	[-]	71	58	136	134
μ_h	[m]	0.40	0.38	0.55	0.49
σ_h	[m]	0.18	0.23	0.33	0.34
μ_v	[ms^{-1}]	0.45	0.42	0.42	0.38
σ_v	[ms^{-1}]	0.28	0.31	0.37	0.35
HMID	[-]	5.6	7.7	9.0	10.6
Variation			**+36 %**		**+18 %**
SPÖL I					
Data points	[-]			90	107
μ_h	[m]			0.25	0.21
σ_h	[m]			0.15	0.13
μ_v	[ms^{-1}]			0.50	0.52
σ_v	[ms^{-1}]			0.34	0.30
HMID	[-]			7.2	6.4
Variation					**-11 %**
SPÖL II					
Data points	[-]			90	104
μ_h	[m]			0.25	0.20
σ_h	[m]			0.12	0.11
μ_v	[ms^{-1}]			0.74	0.78
σ_v	[ms^{-1}]			0.40	0.43
HMID	[-]			5.3	5.7
Variation					**+9 %**

6.5   Discussion

The change in HMID varies significantly between the analyzed segments. While in the Sarine the HMID increases both, in- and outside the sediment replenishment impact zone, it decreases in both segments of the Spöl. As already indicated in different results of the Sarine, it may be associated with the sediment availability in a river segment, how the HMID is changing through a flood event. The Spöl II has a significantly shallower bed slope and hence a different geomorphology than the Spöl I. Another large difference, it lies downstream of the junction of the Ova da Cluozza, which supplies the lower part of the Spöl with sediment (Chapter 3). Further, Spöl II experiences frequent flooding through the Ova da Cluozza tributary. The increase of 9 % in HMID value in this segment is quite small, considering an HMID at the lower boundary of a site with medium hydraulic variability. The increase of HMID value by 0.4 may also correspond to an accumulation of uncertainties related to the measurement of flow depth and velocities (see Chapter 4). Further the field sampling took place roughly two weeks after the flood event took place. The river may not have incised the same way in its channels as prior to the flood. Observations during the post-flood measurement campaign support this statement.

While the availability of sediment may explain the differences in HMID change between the Sarine impact zone and rest zone as well as between the lower and upper Spöl segments, the difference between positive and negative change of the HMID cannot be holistically explained by this fact.

The flood frequency may be more important for this fact. Both segments in the Spöl are subject to periodical artificial flooding since the year 2000. In the Sarine downstream of Rossens Dam on the other hand, an artificial flood has been released for the first time. There have always been natural flood events in both rivers, when spillways need to be activated. However, such a hydrograph does have a rather natural shape and the increase in discharge may not happen as fast as during an artificial flood event. The analysis in Chapter 5 pointed out that the increase in discharge caused high erosion of the replenished sediment in the Sarine. A large lake surface as it is the case in the Sarine fills slowly wherefore a natural activation of the spillways would in most cases not result in a hydrograph with a steep increasing limb.

6.6   Summary

In this chapter the impact of artificial floods on residual flow river segments at the Spöl and the Sarine were investigated. The Sarine I was replenished with 1000 m^3 sediment at one segment, another segment, where the sediment replenishment has no effect, was analyzed for comparison (more information concerning the sediment replenishment in Chapter 5). The Spöl I and II segments with a different slope and river morphology were investigated. One segment was upstream and one downstream of a tributary that supplies the Spöl with sediment and natural flood events. The knowledge gained from these investigations are:

1. The HMID in the Sarine increased by 18 % after one single artificial flood.

2. In the impact perimeter of the sediment replenishment, the HMID in the Sarine increased by 36 %.

3. In the Spöl, where artificial floods have been applied regularly for many years, an additional flood may cause river incision if a segment has a sediment scarcity and hence, can cause a decrease in HMID. The HMID decreased by -11 % in the Spöl I.

4. In the Spöl II, downstream of the junction with the Ova da Cluozza, which contributes additional flood events and significant amount of sediment, the HMID increases (+9 %) with an additional flood event but significantly less than in the Sarine. The Spöl is in a dynamic sediment equilibrium.

7 The physical characteristics of the river flow and ecological indices

7.1 Overview

In this chapter, the HMID values of three different river segments are put in relation with their hydrology and ecological indices which have been calculated based on macroinvertebrate data, on species and family level. The ecological data was sampled by collaborating ecologists. Beside two species diversity indicators, the species richness and the EPT richness are analyzed (E = Ephemeroptera,P = Plecoptera, T =Tricoptera). The three studied river segments were the braided segment Sense I, serving as natural reference site, the meandering Sarine II and Sarine III, with a residual respectively hydropeaking flow regime. At the Sarine river, the data was also collected before and after the flood event to compare the changes. The objectives of this chapter are:

1. To **compare** the river segments based on the **ecohydraulic and ecological data** using different macroinvertebrate indices.

2. To **investigate** the changes in HMID and the different macroinvertebrate indices **caused by an artificial flood** in the Sarine.

3. To characterize the flow regimes in a quantitative manner, allowing **the comparison of natural and hydropower impacted regimes**.

7.2 Data

7.2.1 Ecohydraulic data

The river segment representing natural conditions was the Sense I. Sarine II represented a river segment with a residual flow regime without an active management of artificially released floods (see Chapter 3). The Sarine data was sampled before the flood event on 14 September 2016 (see Chapter 6).
The HMID base data, the sampling methodology and description for the Sense I and the Sarine II are provided in Chapter 4, Table 3.1 and 4.1.

Additionally, ecohydraulic data from the hydropeaking segment Sarine III was sampled before the artificial flood event. The sampling took place during a weekend, when the turbines were turned off and residual flow conditions ($2.5 \ \mathrm{m^3 s^{-1}}$ + tributaries, see Figure 3.2 and Table 3.1).

7.2.2 Ecological data

The ecological data from the Sarine and the Sense segments were sampled by project partners from the Research unit Ecohydrology from ZHAW and EAWAG. More details concerning the sampling procedure and information about the macroinvertebrate data is given in Döring et al. (2018). The ecological data was sampled in four seasons, October 2015, January and June and August 2016 (see Table 7.1).

7.2.3 Hydrological data

The discharge data for the Sense I was measured at the gauging station No. 2179 in Thörishaus and corrected with the factor 0.44 to account for the sub-catchment size (for more detailed explanation see Chapter 3). The data series comprised of 39 years (1978-2016) of 15-min intervals, where each datapoint corresponds to the mean discharge value of a 15-min time interval. The Sarine II is based on the concession residual flow with a constant discharge of $2.5 \ \mathrm{m^3 s^{-1}}$ from October-May and $3.5 \ \mathrm{m^3 s^{-1}}$ from June-September. For the hydropeaking discharge for Sarine III, the powerhouse outflow in Hauterive was available (data source Groupe e). The data series consists of the average discharge of 15-min time intervals for the years 2014-2016. Eventual spilling of the Lac de Gruyère reservoir is not accounted for in the Sarine discharge data, allowing the use of data from year 2016. Detailed information is listed in Table 7.1, the resulting Flow Duration Curves (FDC) in Figure 7.1. The FDCs were normalized with the one year flood HQ_1. As the one year flood, the smallest yearly maxima from the mentioned gauging station in Thörishaus and the gauging station No. 2119 in Fribourg were taken and corrected with the sub-catchment size factor. For the Sense, the minimum yearly maxima measured in Thörishaus was $64.8 \ \mathrm{m^3 s^{-1}}$ in 1933 (measurement period 1928-2015) and for Sarine in Fribourg $94 \ \mathrm{m^3 s^{-1}}$ in 1971 (measurement period 1911-2015).
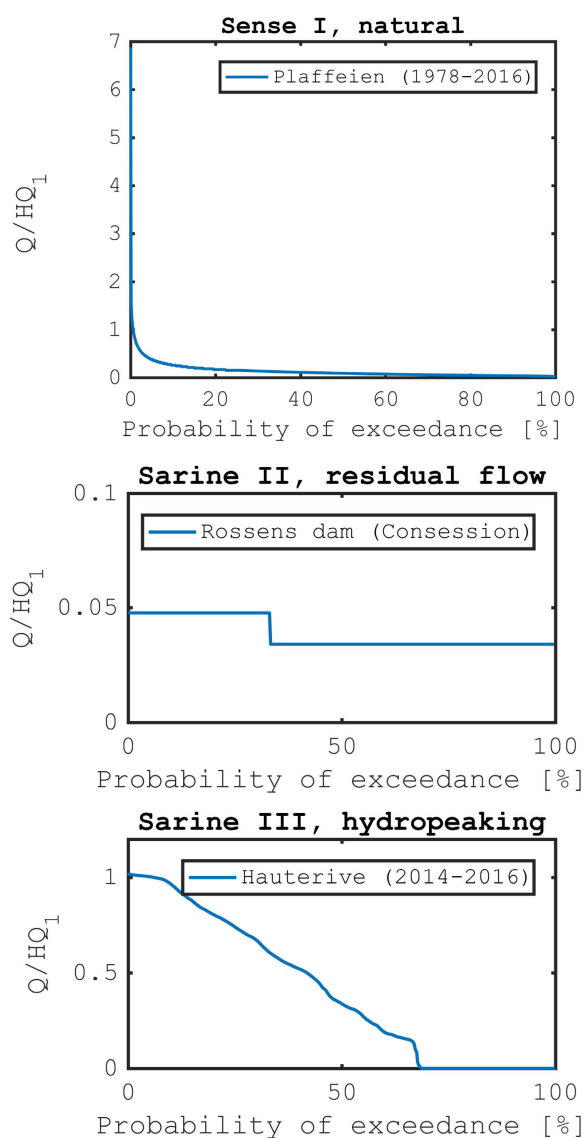
Figure 7.1 – Flow duration curves for the three different river segments obtained from data with a resolution of 15 min. The discharge is normalized with the one year flood. The discharge of the one year floods are derived from gauging station No. 2119 in Fribourg for the Sarine II and III ($HQ_1 = 0.78*94$ m^{3}s^{-1}) and from gauging station No. 2179 in Thörishaus for the Sense I ($HQ_1 = 0.44*64.8$ m^{3}s^{-1}). More detailed information is given in Table 7.1.

Table 7.1 – Available data of the three different domains of the three studied river segments.

River segment Flow regime		Sense I natural	Sarine II residual flow	Sarine III hydropeaking
ECOHYDRAULIC DATA				
Reach length	[m]	1850	1880	500
# of CS	[-]	19	7	6
# of dps	[-]	390	150	93
Median h	[m]	0.17	0.35	0.55
Median v	[ms^{-1}]	0.36	0.33	0.34
Max h	[m]	0.7	1.24	1.34
Max v	[ms^{-1}]	1.56	0.95	0.89
Sigma h	[m]	0.13	0.32	0.32
Sigma v	[ms^{-1}]	0.41	0.24	0.22
ECOLOGICAL DATA before flood				
Source		ZHAW	ZHAW	ZHAW
Date I	[dd.mm.yy]	30.10.15	02.11.15	07.11.15
Date II	[dd.mm.yy]	14.01.16	15.01.16	30.01.16
Date III	[dd.mm.yy]	22.06.16	29.06.16	03.07.16
Date IV	[dd.mm.yy]	11.08.16	12.08.16	03.08.16
# Species S	[-]	50	61	46
# Individuals N	[-]	15'138	49'337	20'912
# EPT individuals	[-]	10'234	9'657	2'494
ECOLOGICAL DATA after flood				
Source		ZHAW	ZHAW	ZHAW
Date I	[dd.mm.yy]	19.09.16	16.09.16	18.09.16
Date II	[dd.mm.yy]	04.11.16	11.11.16	12.11.16
# Species S	[-]	42	43	39
# Individuals N	[-]	16'481	22'353	31'053
# EPT individuals	[-]	12'994	3'561	3'462
HYDROLOGICAL DATA				
Source		OFEN	Concession	Groupe e
Period	[yy-yy]	78-16	any year	14-16
Duration	[years]	39	1	3
Resolution		15 min	1 day	15 min
# of dps	[-]	1'367'520	366	105'216
Q$_{max}$	[m^{3}s^{-1}]	196.2	3.5	78.5
HQ$_1$	[m^{3}s^{-1}]	28.5	73.3	73.3

7.3 Methodology

7.3.1 Ecohydraulic index

The hydro-morphological index of diversity (HMID) is used here as the ecohydraulic indicator. A detailed description about the methodology of the HMID is given in Chapter 2.

7.3.2 Ecological indices

Four different ecological indices are used in this analyses. The Shannon (also known as Shannon-Wiener or Shannon Weaver Index) and the Simpson diversity are the most used indices to determine the species diversity (Shannon and Weaver, 1949; Spellerberg and Fedor, 2003; Simpson, 1949). They are mathematical measures of the species diversity in a community. Unlike the species richness, the third index used here, they account also for abundance and evenness of a present species in a community. The Simpson diversity index has its minimum at 0, corresponding to the case that all individuals belong to a different species and the higher the diversity, the more the value moves towards its maximum value of 1. The maximum value of the Shannon diversity index has no fixed interval but the higher the value is, the more equal the individuals are distributed between the species. Another indicator is the species richness. It represents the number of species in relation to the sampled individuals, another commonly used ecological index (Maurer and McGill, 2011). The forth index used for the analysis is the EPT richness. EPT stands for Ephemeroptera (mayflies), Plecoptera (stoneflies) and Tricoptera (caddisflies). The EPT taxa are three orders that, unlike Diptera, are highly sensitive to many pollutants in their aquatic environment, wherefore they are a good indicator for water quality (Hilsenhoff, 1982). An EPT value of 0 means that there is no individual of a species of EPT, a value of 1 means that all analyzed individuals are EPT species. The indices are defined in Equations 7.1-7.4.

Shannon diversity index:

$$ShD = -\left(\sum_{i=1}^{S} p_i \ln p_i \right) \tag{7.1}$$

$$p_i = \frac{n_i}{N}$$

Simpson diversity index:

$$SiD = 1 - \frac{\sum_{i=1}^{S} n_i(n_i - 1)}{N(N-1)} \tag{7.2}$$

Species richness:

$$SR = \frac{S}{\sqrt{N}}$$ (7.3)

EPT richness:

$$EPT = \frac{n_{EPT}}{N}$$ (7.4)

with:

N	Total number of individuals
n_{EPT}	Number of EPT individuals
n_i	Number of individuals of species i
p_i	Proportion of species i relative to the total number of species
S	Total species number

7.3.3 Hydrology

The combination of natural and hydropower impacted flow regimes in this study does not allow the use of classical flow regime characterization methods. Natural river regimes can be characterized by monthly (Weingartner and Aschwanden, 1992) or seasonality (Cooper-smith et al., 2012) variations. For hydropeaking flow, sub-daily fluctuations are of importance (Meile et al., 2011). To characterize the different flow regimes, the shapes of these three typical FDCs (Figure 7.1) were analyzed with the following two methods. Once the data was analyzed based on the effective discharges and once with the normalized data. The discharge was normalized with the one-year flood.

Classification by area

The area between the x-axis and the FDC was integrated, resulting in the normalized yearly flow surface (matlab function: trapz). This procedure was also done for the non-normalized FDCs (Equation 7.5).

$$FDC_{area} = \frac{1}{2} \sum_{i=1}^{N} (Q_i + Q_{i+1}) \cdot \Delta t$$ (7.5)

Classification by slope

The slope of the FDCs between two discharge measurement was calculated for all measurement points (matlab function: gradient). Then, the absolute values of the slopes were summed up (Equation 7.6). This measure indicates the total changes and hence the variability of flow

regime on a yearly scale.

$$FDC_{cum\ slope} = \sum_{i=1}^{N-1} abs\ \left(\frac{Q_{i+1} - Q_i}{\Delta t}\right) \tag{7.6}$$

Δt Time interval
i Index i
N Total number of measurements
Q_i Discharge at moment i

7.4 Results

7.4.1 Hydraulics

In the Sense I, 390 datapoints were sampled to calculate the HMID, in the residual flow segment of the Sarine 150 and in the hydropeaking 93 (see Table 7.1). The 390 datapoints of the Sense I were distributed over 19 cross-sections, in the Sarine II, data was sampled across seven and in the Sarine III across six cross-sections. The HMID in the natural reference river segment Sense I has the highest HMID value, followed by the Sarine II and Sarine III, which have a medium HMID value of eight and six respectively (Table 7.2). The HMID of the braided Sense is mainly dominated by the diversity of flow velocity, while in the Sarine, flow depth and velocity variations are of similar importance.

The largest FDC area results from the hydropeaking, followed by the natural and the residual flow regime. This is the case for both, the measured discharge and the normalized discharge data. The area under the FDC of the residual flow segment of the Sarine is the lowest for all hydrological analyses. Considering the cumulative absolute slope of the FDC, the natural regime results in a two magnitudes higher value than the hydropeaking and the residual flow regime results in 0 (see Table 7.2). The same observation is done for the normalized discharge. This large difference is caused by the absence of flood events in the studied Sarine segments.

7.4.2 Ecological indices

The number of macroinvertebrate species and the total number of individuals sampled before the flood event was by far the highest in the Sarine residual flow segment. The sampled individuals counted in the residual flow segment were more than double the amount found in the hydropeaking segment and more than three times compared to the natural reference, the Sense I. However, most EPT individuals were counted in the Sense, resulting in a EPT value of 0.68 before the flood event. The least amount of EPT individuals and species was

counted in the hydropeaking segment (see Table 7.1).

The relation between the four ecological indices and the HMID differs. The Sarine II results in a higher Shannon diversity index then the Sense I where the HMID is inverse. The Simpson Index values of the two segments on the other hand is about the same (Figure 7.2). Following the arrows, it can be observed that the river segments with the natural and residual flow regimes a significantly higher values for the tow diversity indices compared to the hydropeaking flow regime. Considering the Species and EPT richness, the natural flow regime results in distinct higher values. The Sarine III with the lowest HMID does also result in the lowest value for the diversity indices and the EPT richness. It however, it hosts a larger species richness than the Sarine II. The clearest trend between HMID and ecological indicators is observed for the EPT richness.

Table 7.2 – Results for the ecohydraulic, hydrological and ecological analyses (* = The discharge used for the FDC was normalized with the one year flood). The magnitudes of the one year floods came from gauging station 2119 for the Sarine II and III (HQ$_1$ = 0.78*94 m^{3}s^{-1}) and from gauging station 2179 for the Sense I (HQ$_1$ = 0.44*64.8 m^{3}s^{-1}).

| River segment | | Sense I | Sarine II | Sarine III |
Flow regime		natural	residual flow	hydropeaking
ECOHYDRAULIC RESULTS				
HMID		10.3	8.00	6.11
ECOLOGICAL RESULTS before flood				
Shannon diversity index		2.10	2.18	1.80
Simpson diversity index		0.82	0.82	0.75
Species richness		0.41	0.27	0.32
EPT richness		0.68	0.20	0.12
ECOLOGICAL RESULTS after flood				
Shannon diversity index		2.18	1.44	1.30
Simpson diversity index		0.81	0.54	0.56
Species richness		0.33	0.29	0.22
EPT richness		0.79	0.16	0.11
HYDROLOGICAL RESULTS				
FDC area	*10^2	3.8	2.8	29.5
FDC area*		13.5	3.9	40.2
FDC cum slope	*10^5	28.0	0.0	0.8
FDC cum slope*	*10^3	98.1	0.0	1.1
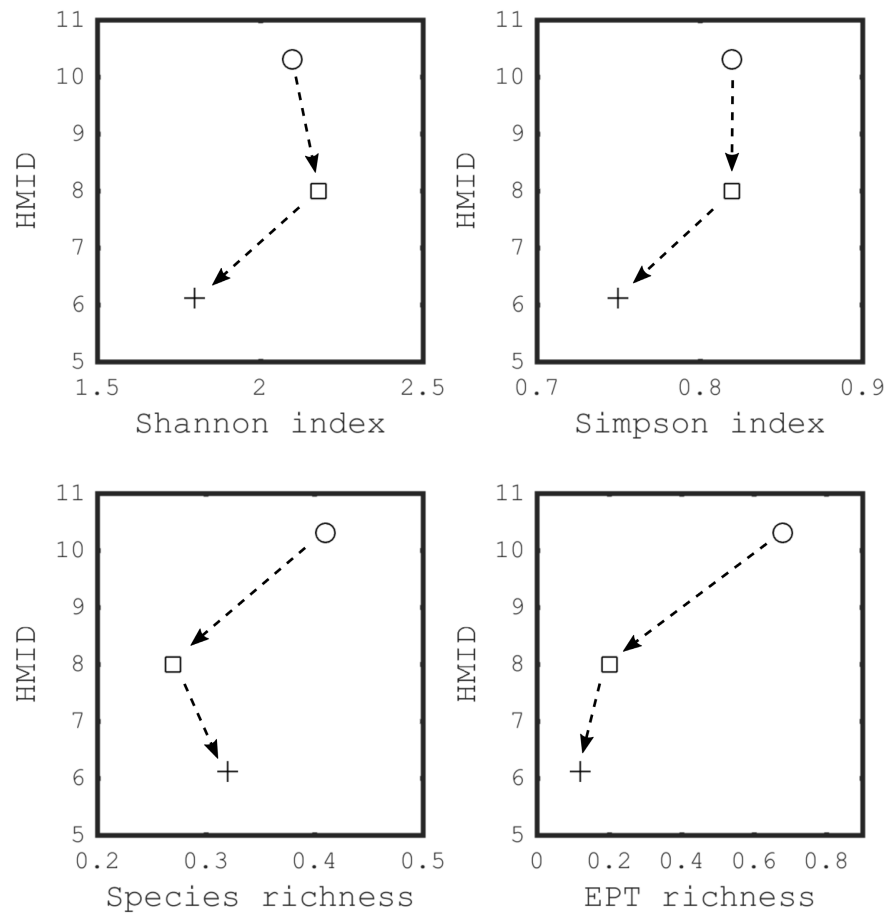
Figure 7.2 – Relation between ecohydraulic (HMID) and the four chosen ecological indicators. ◯ = Sense I natural flow regime, □ = Sarine II residual flow regime, + = Sarine III hydropeaking flow regime.

7.4.3 Changes by the flood event

Considering the ecological indicators before and after the flood the change differs between the indicators in both Sarine segments. Both species diversity indices, the Shnnnon and Simpson Index, decreased significantly in both studied segments directly after the flood (see grey arrows in Figure 7.3). The Species richness decreased significantly for the hydropeaking segment of the Sarine while it remained constant for the residual flow segment. The EPT richness increased by 16 % in the Sense with a natural flow regime. In the regimes with an artificial flow regime, the change in EPT is negligible. This was observed while the HMID increased by about 18 % in the Sarine. In the Sense, which represents a natural river system, the diversity indices remained constant. A decrease in the Species richness and a slight increase in EPT richness were observed over the same time period. This represents the natural

seasonal variability, between the samples from four seasons and from the fall season, based on differences in nutrients and temperature.
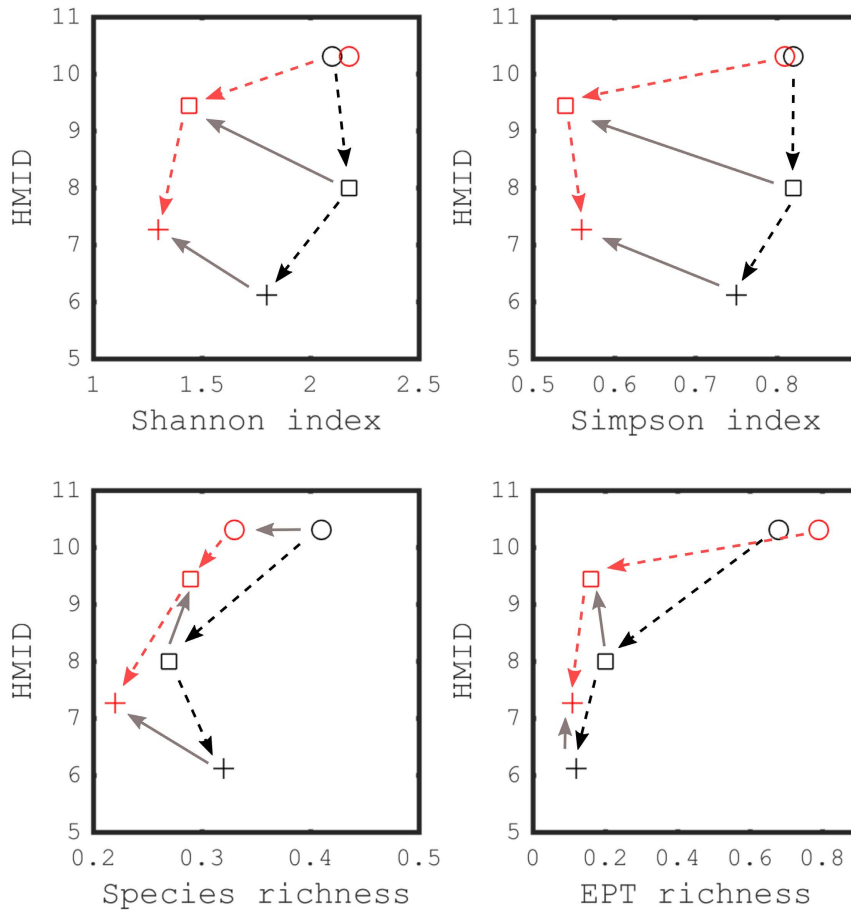
Figure 7.3 – HMID and ecological indicator values before (black) and after (red) the flood. ◯ = Sense I natural flow regime, □ = Sarine II residual flow regime, + = Sarine III hydropeaking flow regime. The HMID values were increased by 18 % in the Sarine based on the results from Chapter 6.

7.5 Discussion

The Sense is a tributary of the Sarine draining a neighboring catchment. The fact that they are located in the same region, is important for the comparison with ecological data since the different seasons in a catchment depend on geographical location and altitude. The most promising link with the HMID is observed with the EPT richness, an indicator for water quality. The species diversity indices as well as the species richness do not convey information about the analyzed species composition of a community. Hence, the uniqueness or potential

ecological importance of individual species is not taken into account. A community with a large diversity may comprise of common and undesirable species. In the case of the Sarine II, 34.4 % of the sampled species were Amphipoda, almost exclusively from the family Gammaridae. In the Sarine II their share exceeded 40 %. Gammaridae are well adapted to stable environmental conditions. Stoneflies (Plecoptera) however, represented only for 0.2 % of the found species in the Sarine II and 1.3 % in the Sarine III (Döring et al., 2018). Therefore, the total number of species, which was the highest in Sarine II, and the diversity on species level have to be considered in context to the desired species.

The Gammaridae were mainly flushed from the residual flow segment in the Sarine what, besides the seasonal differences, is the major cause of the decrease of the total number of individuals by more than 50 % from 49'337 to 22'353. In addition, the number of different macroinvertebrate species decreased significantly in the segment with residual flow in the Sarine. The macroinvertebrate populations in the downstream segment were more resistant to the flood. Macroinvertebrates in this part of the Sarine are exposed to a hydropeaking flow regime and natural floods coming from the Gérine and the Glâne (see Chapter 3). Therefore, the macroinvertebrates are more resistant to the artificial flood. Experiences at the Spöl measured a decrease of macroinvertebrate individuals right after the artificial flood event and an increase between floods (Robinson et al., 2018). This may also be the case in the Sarine. Overall it can be stated that analyzed macroinvertebrate indices result in the highest values in the natural flow regime, followed by the residual flow regime. The hydropeaking regime has the poorest results in all indicators unless the species richness. It must be stated that the species richness is only a measure of the heterogeneity of the sample. Since lots of Gammaridae were observed in the residual flow segment, the better performance of the hydropeaking regime regarding species richness is biased.

Despite a promising trend between the HMID and the EPT richness it must be mentioned that the analyzed data represents only three river segments. Important factors for in-stream organisms such as nutrients, temperature or habitat disturbance are not taken into account in the HMID. Therefore, it may need to be corrected based on the FDC of the river segment. The three segments in this study do have all a characteristic FDC for their regime. The methodology of the FDC slope may help to add another factor to the HMID to include disturbance. A single artificial flood in a residual flow reach will already change the FDC slope significantly compared to the Sarine II segment. The FDC area may overestimate the hydropeaking regime.

7.6 Summary

In this chapter three different river segments were investigated based on their ecohydraulic, biological and hydrological data. The presented results reveal a potential link between flow regime and in-stream ecology, based on objective measures. These promising results will have to be validated by data from additional rivers to allow a representative conclusion. Fur-

ther parameters such as the disturbance or grain size distribution to account for the flow regime respectively temperature to account for river altitude and exposure may complement this link. The chapter can be summarized as follows:

1. In river segments with a high HMID value, an elevated EPT richness was determined. This is not the case for the Shannon and Simpson diversity indices, neither for the species richness. The EPT richness represents percentage of species that are sensitive to water quality.

2. A drastic decrease in macroinvertebrate diversity indices is observed in both river segments with an artificial flow regime after the flood event. The observations are comparable with the knowledge gained from the research at the Spöl. The EPT proofed to be the most constant ecological indicator with minor changes due to the artificial flood event.

3. Concluding can be said, that the natural flow regime attains the highest macroinvertebrate index values followed by the residual flow and finally the hydropeaking regimes.

4. To further complete the analysis, the different hydrographs were characterized based on their FDC slope and area. The analysis indicates that the slope of the FDC may be a useful objective measure to add in river habitat assessment.

8 Conclusions and outlook

8.1 Overview

Hydropower was introduced in the framework of the food, water, energy nexus, its associated problems and the future perspectives for hydropower concerning the Energy Strategy 2050. This was followed by a summary of the state of the art. In this research, ecohydraulic and biological data of natural and hydropower impacted rivers were collected and analyzed. A major case study took place at the Sarine River, where an artificial flood was released in a residual flow river, combined with sediment replenishment. The findings of this research study reveal an interesting approach how to restore and quantify the habitat diversity in residual flow rivers. These results contribute directly to flood safety, the achievement of the Energy Strategy 2050 in Switzerland and the Sustainable Development Goals (SDG) from the United Nations six "Clean Water and Sanitation", seven "Affordable and Clean Energy" and fourteen "Life Below Water". The main topics of the research were:

- In Chapter 4, investigations upon the data sufficiency and sensitivity of the hydromorphological index of diversity (HMID) were presented.

- In Chapter 5, a novel multi-deposit sediment replenishment method was tested for the first time in a river combined with an artificial flood.

- The effect on the HMID of this measure and the comparison with a river system where artificial floods are released for about 20 years were presented in Chapter 6.

- Chapter 7 completes the study, answering the question of the link between the change in habitat diversity, flow regime and in-stream biology.

This chapter highlights the main results and conclusions of Chapter 4-7, also considering limitations. From there, an outlook of the future need research is derived.

8.2 Sampling sufficiency for determining hydraulic habitat diversity

In Chapter 4, data sufficiency to characterize habitat diversity of a river segment by means of the hydro-morphological index of diversity (HMID) as well as mean flow depth and mean flow velocity was investigated. Field data from 19 river segments with differing morphology was analyzed. The resulting figures and tables point out the sensitivity of the HMID to data availability. Summarizing, the figures point out a clear **correlation between necessary data points and river complexity**. In addition, the general river dynamics, and the stream power have a large influence on the data required to compute a representative HMID value. In all segments of the Sense River, independent of their geomorphological classification, more data points than the segments from the Passer River are needed. Grouping the segments according to their geomorphology, the following suggestions can be given concerning data sufficiency:

- **Straight river segments**
  The lowest complexity has a **straight rectangular or trapezoidal channel**. Exemplary for such a segment are the Venoge II, Venoge III and Buenz II. In all of these river segments, 30 data points give a solid HMID estimate if they are at least distributed on two cross-sections.

  A **straight channel** with gravel banks and therefore some additional complexity needs more data points. If the data is distributed on at least seven cross-sections, 50 data points give a representative HMID estimate for rivers like the Passer II and IV.

  Special cases that fall out of these rules are **restored straight channels** such as the Buenz I, where elements such as large logs and rocks influence the flow to a large extent, and **natural straight** river segments in a highly dynamic river system such as the Sense V. In these segments, the longitudinal extent should be chosen as long as feasible and the measurements distributed over at least ten cross-sections. With this procedure a representative HMID estimate can be obtained.

- **Meandering river segments**
  The HMID in meandering river segments evolve in a distinct way. A minimum 50 data points distributed on at least four cross-sections need to be taken to compute a reasonable HMID. Deepened analysis in the Sarine pointed out, that an increased spacing between the cross-sections, analyzing a longer segment leads to a better HMID estimate. Hence it is important to include **at least half a wavelength of a meander, corresponding to a 90° river bend** to capture geomorphological variability.

- **River segments with alternate bars**
  River segments with an of alternate bars geomorphology need at least 50 data points distributed over six cross-sections, in order to result in a solid HMID estimate. In segments with a limited geomorphological complexity (e.g. Passer I), less data points lead

to an acceptable result.

- **Braided segments**
  Braided river segments have the **highest geomorphological complexity**. Since the number of channels differs between the cross-sections, the highest importance herein is to distribute the data on at least 12 cross-sections in order to minimize the uncertainty. For all braided segments except for Sense I, 100 data points are enough for an accurate HMID estimation.

8.3 Erosion, transport and deposition of a sediment replenishment under flood conditions

The multi-deposit sediment replenishment was applied for the first time outside of the laboratory. The study took place at the residual flow segment of the Sarine downstream of the Rossens Dam. 489 stones replenished sediment, with a characteristic diameter of 57 or 113 mm, were equipped with tracers. The tracer stones allowed the analysis of the impact perimeter of the replenishment, the transport velocities of the tagged stones and the erosion efficiency of the hydrograph. From the 489 tagged stones, 277 were recovered after the flood event with a maximum transported distance of 286 m.

Comparison between field and laboratory results

The released hydrograph, having a peak discharge with a **return period of two years, was not powerful enough** to erode all the replenished sediment. Compared with the laboratory experiment of 180 min, the final situation in the field corresponded to 105 min of the laboratory experiment. The erosion, sediment transport and deposition processes of the field experiment follow a **similar behavior as expected from the laboratory experiments**. Replenished sediment settled in local sediment-clusters downstream of the replenishment location. This was seen in an explicit peak of the power spectral density (PSD). The PSD of the laboratory experiment resulted in a maxima at 2.5, the PSD of the field experiment at 4.2 times the channel width.

Sediment transport velocity

With the help of a fixed installed pass-over loop antenna, radio frequency identification passive integrated transponder (RFID PIT) tag equipped tracer stones could be detected while passing the antenna. Despite the elaborated installation, the system with garden hose was too flexible and not rigid enough. During the flood, **the antenna could not keep its shape and could not resist the forces of the river**. Therefore, only six stones were detected. Combined with numerical modeling, the transport velocities of $3.1*10^{-3}\mathrm{ms}^{-1}$ (diameter = 57 mm) and $4.6*10^{-3}\mathrm{ms}^{-1}$ (diameter = 113 mm) could be estimated.

Erosion efficiency and sedigraph

The **erosion efficiency** (eeff), defining the percentage of sediment eroded divided by the percentage of the released water volume in a certain interval, **was defined**:

$$eeff_i = \frac{Eroded\ tags\ (during\ \Delta t_i)\ \ \ \ \ \ \ [\%]}{Released\ water\ volume\ (during\ \Delta t_i)\ [\%]} \qquad (8.1)$$

with:

Δt_i i-th time interval [s]

$eeff$ erosion efficiency [-]

The analysis pointed out that **75 % of the tagged stones were eroded during (rapid) increasing and constant high discharge** (eeff = 1.24-2.16). Decreasing discharge, even if the discharge is above the critical value for incipient motion of the armor layer of the riverbed, had a minor effect on the erosion of the replenishment (eeff <= 0.57). This comes from the fact that armor layers formed on the deposits during the flood event. Consequently, entrainment of sediment was limited at decreasing discharge.

8.4 Artificial floods to improve the hydraulic habitat diversity downstream of dams

At the Sarine, an artificial flood event was released and locally combined with sediment replenishment. Such a flood has been released for the first time in this river. In the Spöl, a regime with periodical flood releases has been introduced in 2000. In both rivers, a segment was investigated with the HMID prior and post the release of an artificial flood. The gained knowledge can be summarized as following.

- **Sarine**
  A single release of an artificial flood could increase the HMID in the Sarine by +18 %. Where the released flood was combined with **sediment replenishment**, the HMID **increased significantly by +36 %**.

- **Spöl**
  In the Spöl, where a regime of **periodical flood releases** has been **applied for multiple years, the HMID remains about constant** by an additional flood (slight increase from 5.3 to 5.7), as long as there is no lack in sediment supply. If there is a **lack in sediment supply, the HMID may decrease significantly** with each additional flood release as it was observed in the upper segment of the Spöl.

8.5 The physical characteristics of the river flow and biological indices

The HMID values of three different river segments with a different flow regime were put in relation with biological indices. Beside the commonly used Shannon and Simpson diversity indices, Species richness and EPT richness were analyzed (EPT = percentage of Ephemeroptera, Plecoptera and Tricoptera). The three segments Sense I (natural flow regime), Sarine II (residual flow regime) and Sarine III (hydropeaking flow regime) were also characterized by their Flow Duration Curves (FDC).

HMID vs Biological indicators

The Sense I with a **natural flow regime** resulted in the **highest macroinvertebrate indices, followed by the residual and hydropeaking flow regimes**. Segments with a large HMID and a natural flow regime host a large EPT richness, which is an estimate for water quality, the opposite is observed for segments with an altered flow regime. This trend is not observed for the other three investigated indices. The most macroinvertebrate species and individuals were found in the Sarine II segment. However more than a third of them belonged to the family of the Gammaridae which live best in a more static environment and consequently were washed away by the artificial flood event.

The value of the two diversity indices decreased significantly by the flood event for the residual and hydropeaking flow segments. The Species and EPT richness changed minimally in both segments with an altered flow regime.

Combining HMID with other parameters

To complete the analysis of the physical characteristics of the river flow and the biological indices, additional parameters need to be considered. Based on the slope of the flow duration curve, the disturbance in the three river segments could be described.

8.6 Outlook

The present study highlights that sediment availability is key for hydraulic habitat creation. In the case of the Thur near Altikon with a moderate bed-slope, sediment was eroded from the river banks. In river segments with steep bed-slopes this is not possible and sediment needs to be replenished to create bedforms. The gained knowledge of the novel multi-deposit sediment replenishment technique will support the ecological and economical management of floodplains downstream of dams, in the nexus of food, water and energy. Considering the bigger framework, this research contributes directly to the success of the Energy Strategy 2050

and to several SDGs defined by the UN.

Despite the relevant contribution in the domain of hydropower related river restoration and hydraulic habitats, the presented data are case studies and limited to the observed rivers. In this context, the following points may require further investigations to expand the knowledge in applied sediment replenishment. The following research questions concerning a wide application of the method still need to be answered:

- What frequency **differences in costs** of a multi-deposit compared to a single-deposit sediment replenishment configuration and are they justifiable?

- What would be an optimal **design of a flood hydrograph**, both for sediment movement and for in-stream organisms?

- What is the **long-term** evolution of the experiment with the four-deposit sediment replenishment configuration in the Sarine?

To draw conclusions from the study regarding the physical characteristics of a river and biological indices, the principle current question is: How do trends between HMID values and biological indices look like if **additional data from other rivers** is added to the analysis?

A Appendix: Introduction
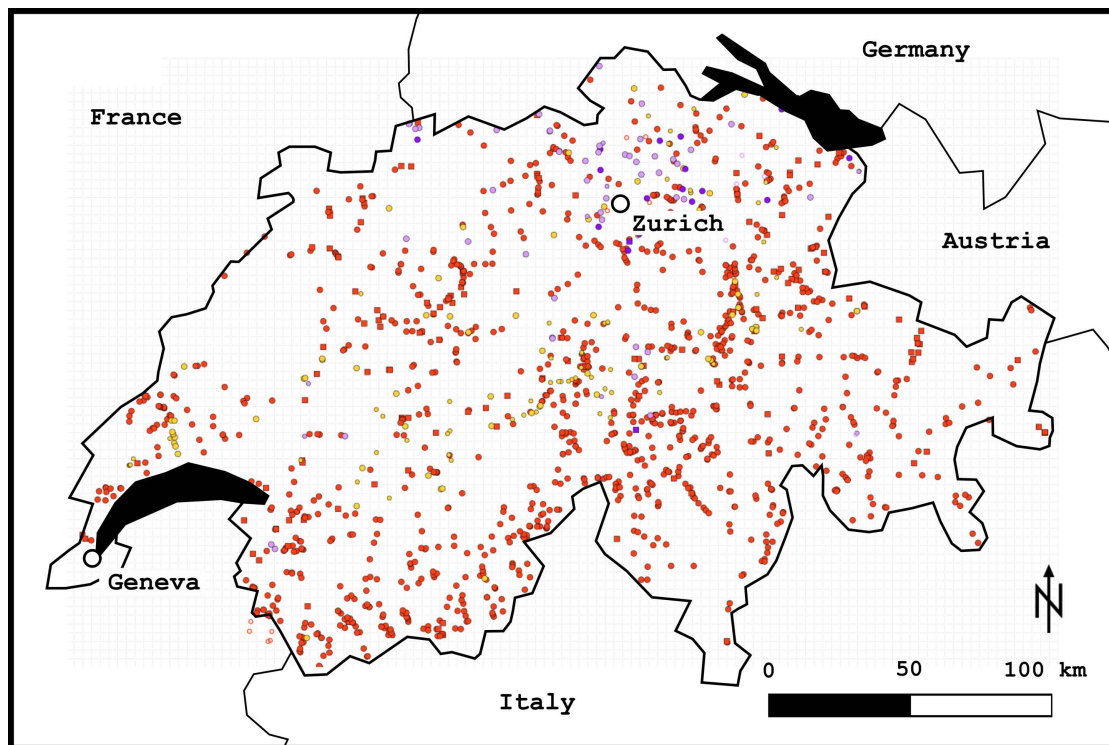
Figure A.1 – Locations of water intakes. Orange and yellow data points are for hydropower use, purple data points are for other uses. Orange and dark purple data points: water abstraction > 0.5*Q_{347}, yellow and light purple data points: water abstraction < 0.5*Q_{347}. Data from FOEN, status of 01 January 2004.
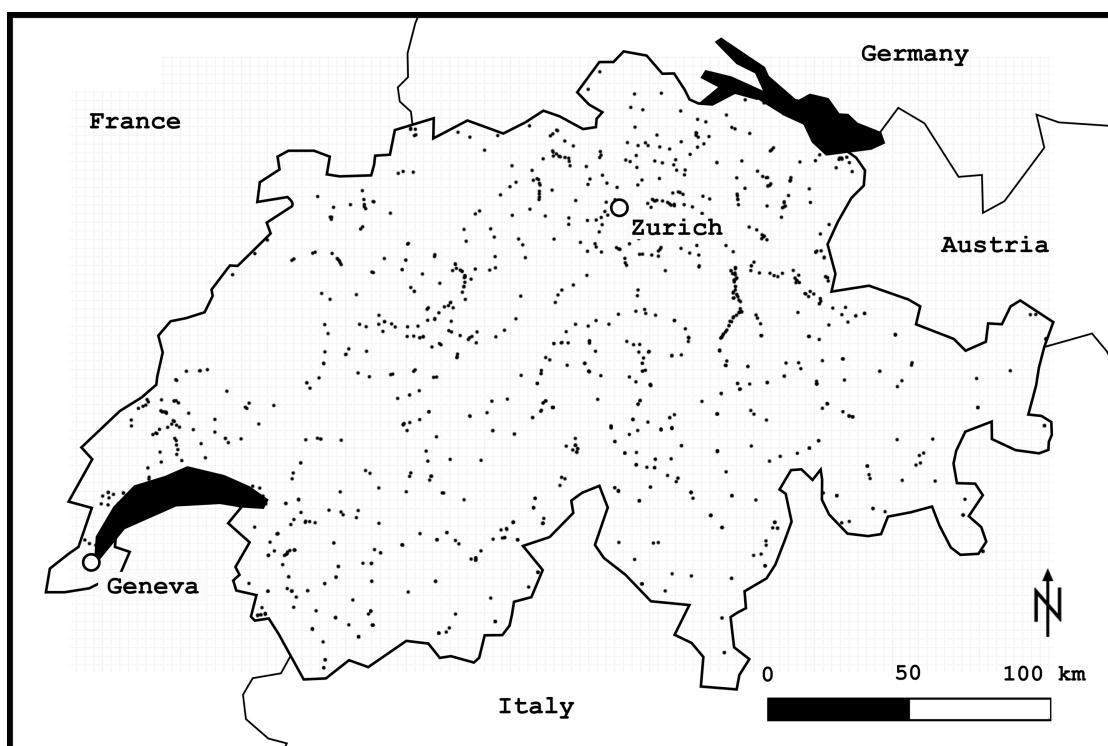
Figure A.2 – Locations of water releases. Data from FOEN and cantons, status of 01 January 2004.

B Appendix: Site information

B.1 Sarine river

Images from the Sarine sorted from upstream (Rossens, figure B.1) to downstream (Pont de Pérolle in the city of Fribourg, figure B.8).

Figure B.1 – Bottom outlets of Rossens Dam with residual flow turbine producing 13.6 GWh per year. Image taken on 13 September 2016. Image courtesy Research unit Ecohydrology, ZHAW

Figure B.2 – Stilling basin of the Rossens Dam and the begin of the residual flow segment in a narrow valley (wetted width 20-30 m). Image taken on 13 September 2016, courtesy Research unit Ecohydrology, ZHAW

Figure B.3 – Typical situation in the incised residual flow segment of the Sarine. small gravel banks with grass, willows and then hardwood. Image taken on 29 October 2015, courtesy Pierre Bourqui

Figure B.4 – One the only easy access to the residual flow segment via the bridge at Hauterive Abbaye. This large river segment reserves as recreation area, where people swim and do barbecue in summer. Image taken on 13 September 2016, courtesy Research unit Ecohydrology, ZHAW

Figure B.5 – Turbine house in Hauterive, Fribourg, is located in a sharp left bend of the Sarine. Up to 75 m^3s^{-1} are released by the four Francis turbines. The four restitution tunnels can be seen right of the turbine house, the restitution channel enters the Sarine below the pedestrian bridge in the center of the image. Image taken on 11 April 2016, courtesy Severin Stähly

Figure B.6 – Junction of the Sarine and the Gérine downstream of the turbine house in Hauterive. The Gérine (entering from the right side) supplies the Sarine with a significant amount of sediment. Image taken on 24 November 2015, courtesy Elena Battisacco

Figure B.7 – View from the Pont de Pérolle upstream into the Creux-du-Loup when no electricity is produced in Hauterive, discharge 7 m^3s^{-1}. Image taken on 2 April 2016, courtesy Severin Stähly

Figure B.8 – Looking upstream in a dry channel during low flow in the Creux-du-Loup when no electricity is produced in Hauterive, discharge 7 m^3s^{-1}. The dry channel can be seen in figure B.7 in the top center of the image, on the right of the large island. Image taken on 2 April 2016, courtesy Severin Stähly

Figure B.9 – Typical observation the dry channel (figure B.8), due to the absence of flood events: algae population of sediment. This is also observed in the residual flow river segment of the Sarine. Image taken during low flow in the Creux-du-Loup when no electricity is produced in Hauterive, discharge 7 m^3s^{-1}, on 2 April 2016, courtesy Severin Stähly
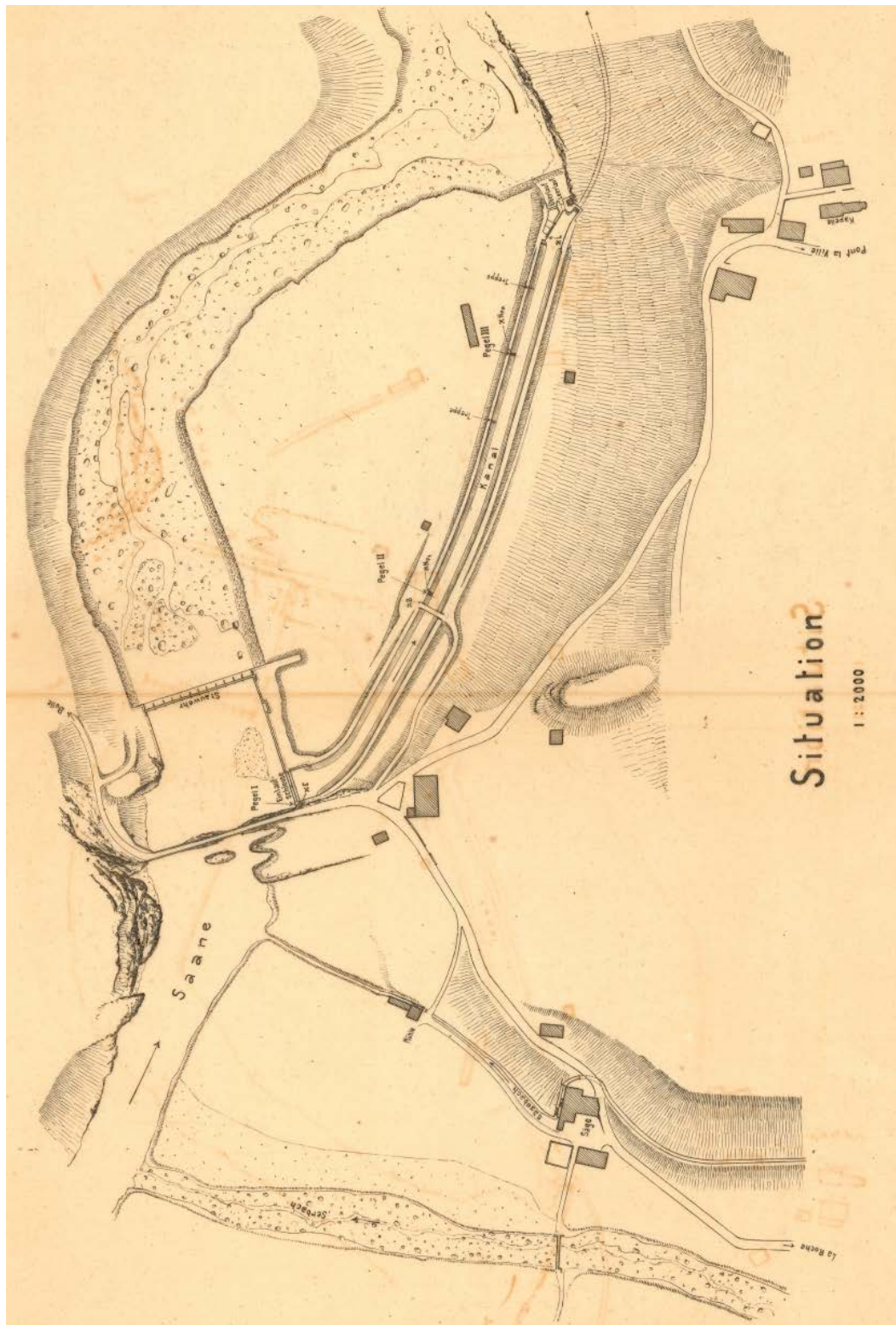
Figure B.10 – Top-view 1:2000 scale plan of the hydropower intake Thusy Fribourg, prior to the construction of the Rossens Dam. The intake was constructed in 1902 and in operation until the construction of the Rossens Dam finished in 1948. Image courtesy FOEN

Two analyzed segments in the residual flow segment of the Sarine River
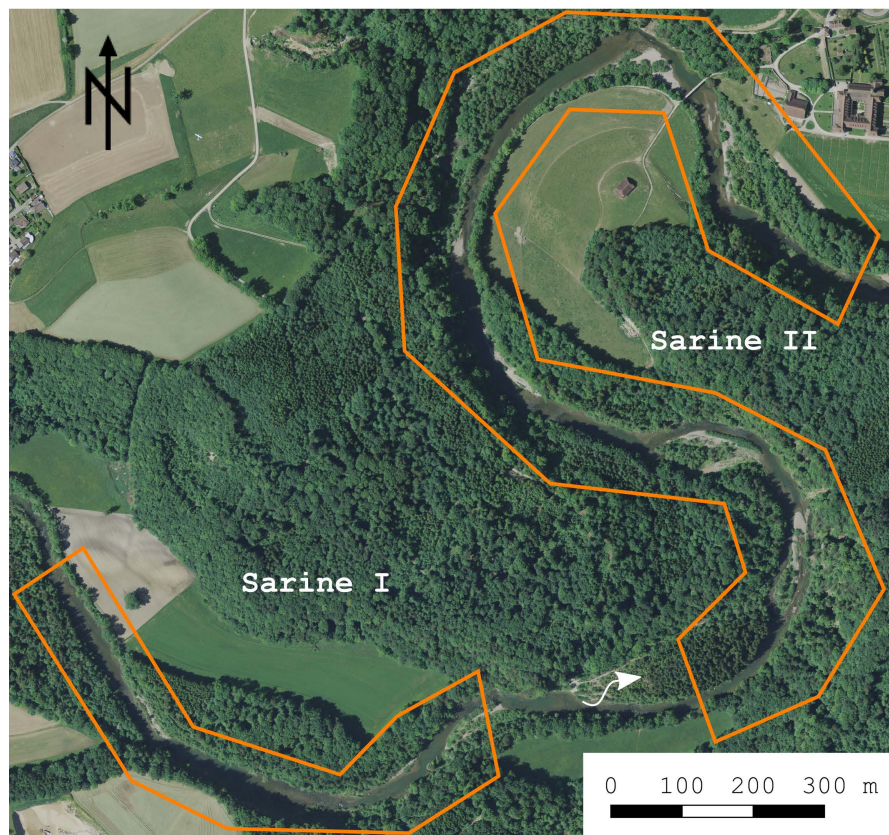
Figure B.11 – Perimeter of the two segments Sarine I and Sarine II in the residual flow segment downstream of Rossens Dam. Geodata courtesy Swisstopo

Figure B.12 – Impressions of the two segments Sarine I and Sarine II in the residual flow segment downstream of Rossens Dam. Images taken on 6 July 2016 (left) and 1 March 2016 (right), courtesy Severin Stähly

B.2   Spöl River and Ova di Cluozza

Figure B.13 – Gorge of the Spöl River between the Ova Spin Dam and the junction with the Ova da Cluozza, looking upstream. One of numerous hunting shelters on the left. The wetted-width is 10-15 m, the discharge 0.9 m^{3}s^{-1}. Image taken on 19 July 2018, courtesy Severin Stähly

Figure B.14 – River mouth of the Ova da Cluozza and the gauging station at its end. It supplies the Spöl with sediment. At this point, the gorge opens and a up. This braided river segment has a wetted-width of 25-35 m, the discharge is 0.9 m^{3}s^{-1} in the Spöl and 0.55 m^{3}s^{-1} in the Ova da Cluozza. Image taken on 17 September 2018, courtesy Severin Stähly
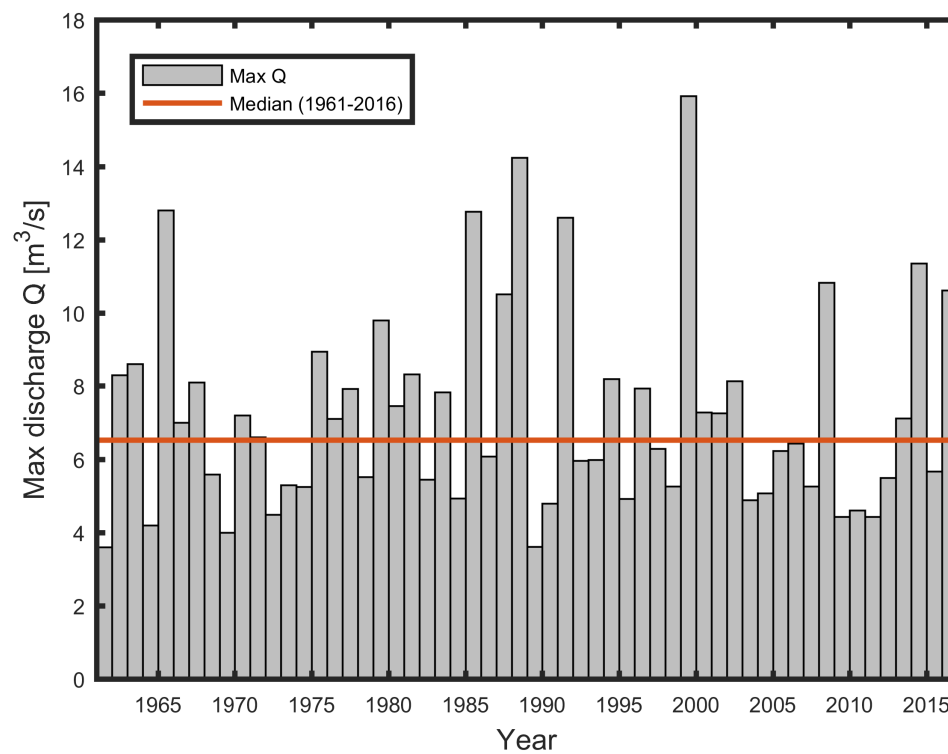
Figure B.15 – Maximum discharge measured in the Ova da Cluozza at the gauging station 2319 in Zernez between 1961 and 2016. Data source FOEN

Figure B.16 – Upstream-view in the braided segment of the Spöl in Zernez, with *Spölbrücke* in the back. Channel width 30 m, the discharge is 1.4 m^3s^{-1}. Image taken on 19 July 2018, courtesy Severin Stähly

B.3   Sense River

Figure B.17 – The 200 m wide floodplain of the Sense in Plaffeien. Discharge about $12\,\mathrm{m^3s^{-1}}$ (discharge data from gauging station 2179 in Thörishaus, corrected with factor 0.44). Image taken on 2 April 2015 on the decreasing limb of a one-year-flood, courtesy Severin Stähly
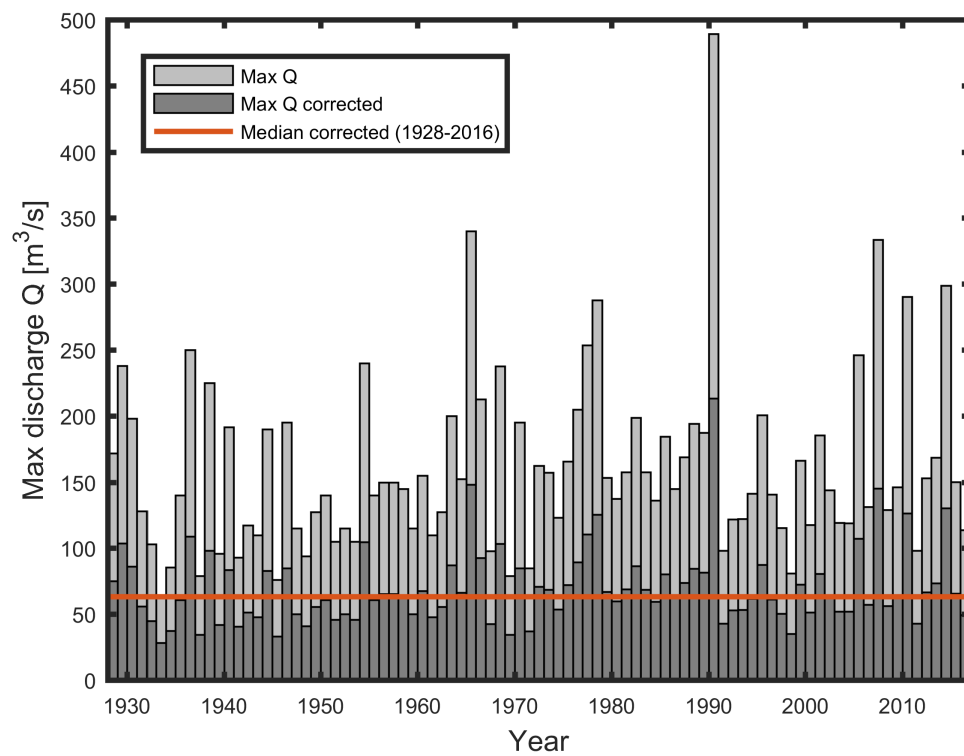
Figure B.18 – Maximum discharge measured in the Sense at the gauging station 2179 in Thörishaus between 1928 and 2016. The corrected dataset (factor 0.44) represent the flood statistics at the braided river segment at Plaffeien (see Figure B.17). Data source FOEN

Five analyzed segments in the Sense River
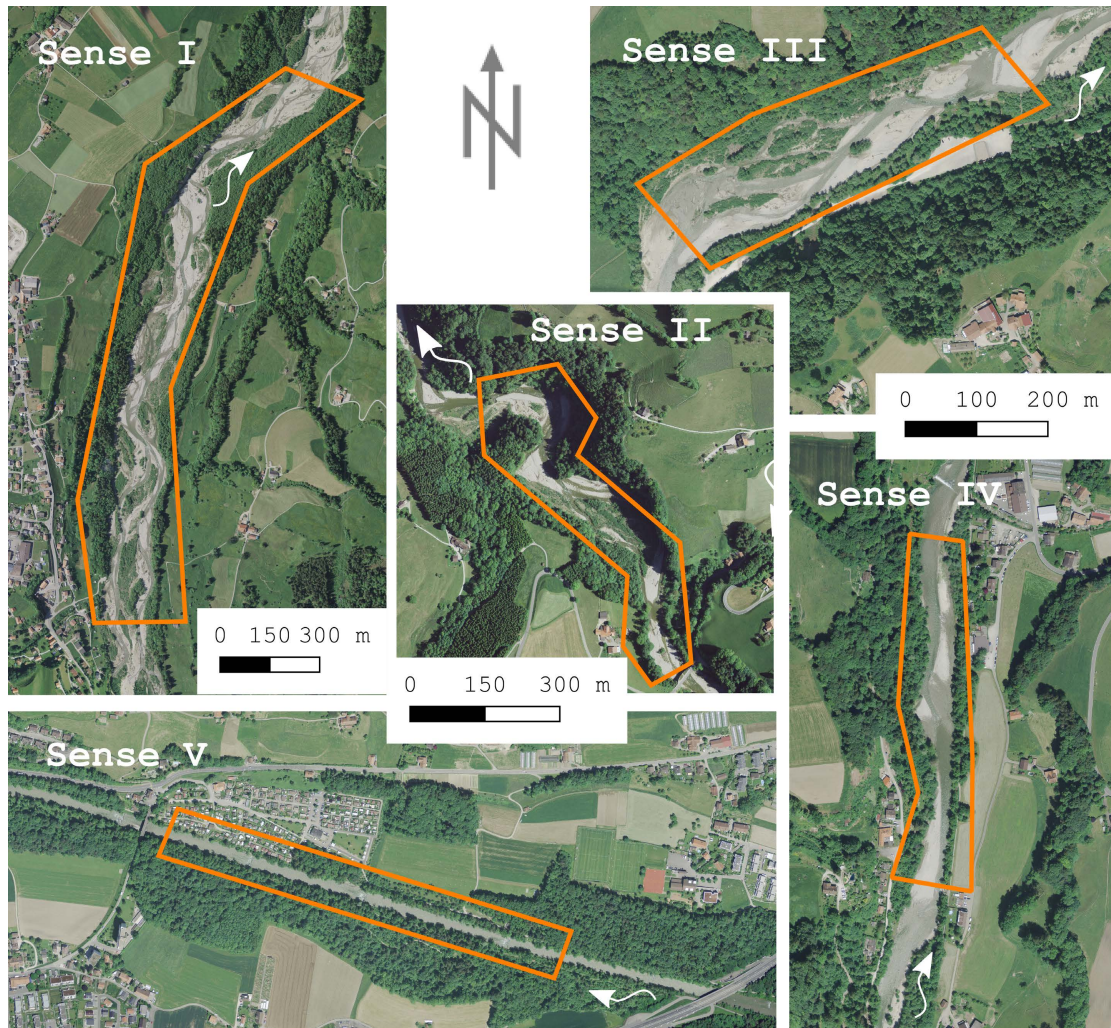
Figure B.19 – Perimeter of the five segments Sense I-V. Geodata courtesy Swisstopo

Figure B.20 – Impressions of the five segments Sense I-V. Images courtesy Walter Gostner

B.4 Buenz River

Four analyzed segments in the Buenz River
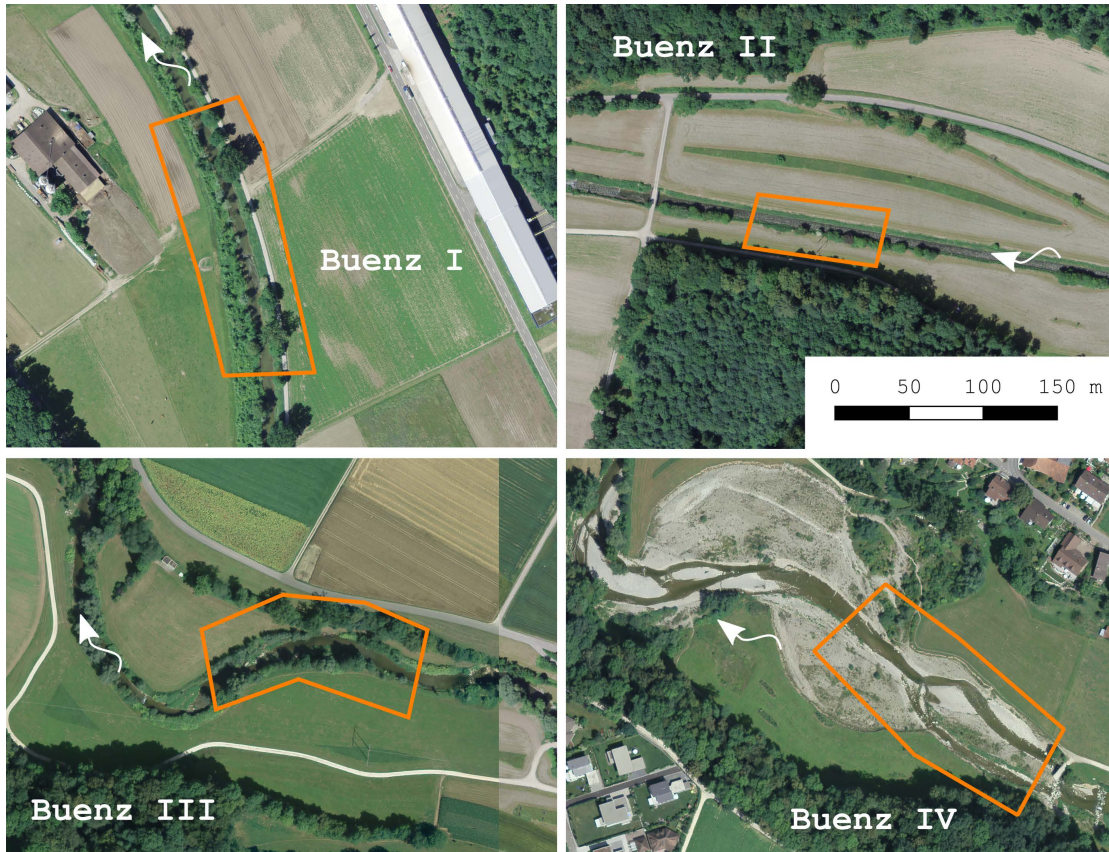
Figure B.21 – Perimeter of the four segments Buenz I-IV. Geodata courtesy Swisstopo

Figure B.22 – Impressions of the four segments Buenz I-IV. Image courtesy Walter Gostner

B.5 Passer River

Four analyzed segments in the Passer River
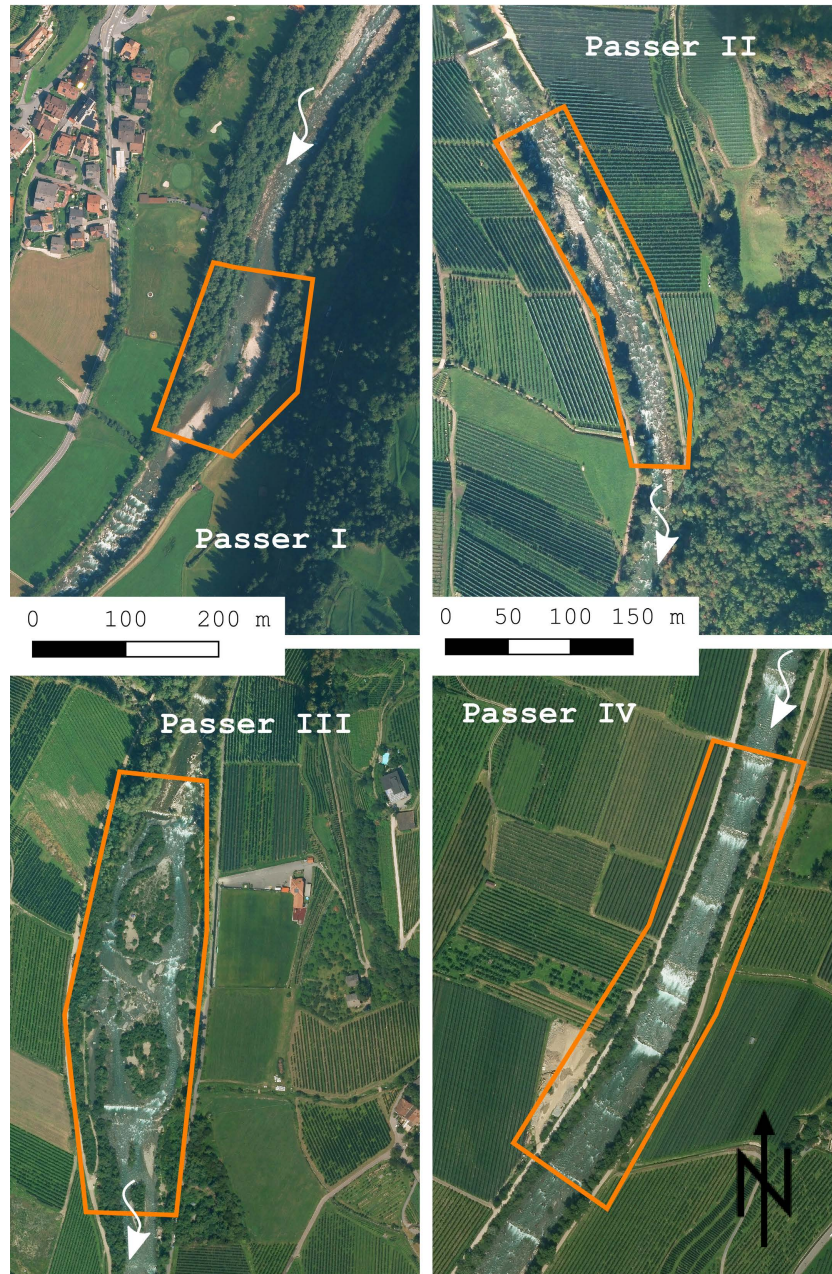
Figure B.23 – Perimeter of the four segments Passer I-IV. Geodata CCO from Autonome Provinz Bozen

Figure B.24 – Impressions of the four segments Passer I-IV. Image courtesy Walter Gostner

B.6   Venoge River

Four analyzed segments in the Venoge River
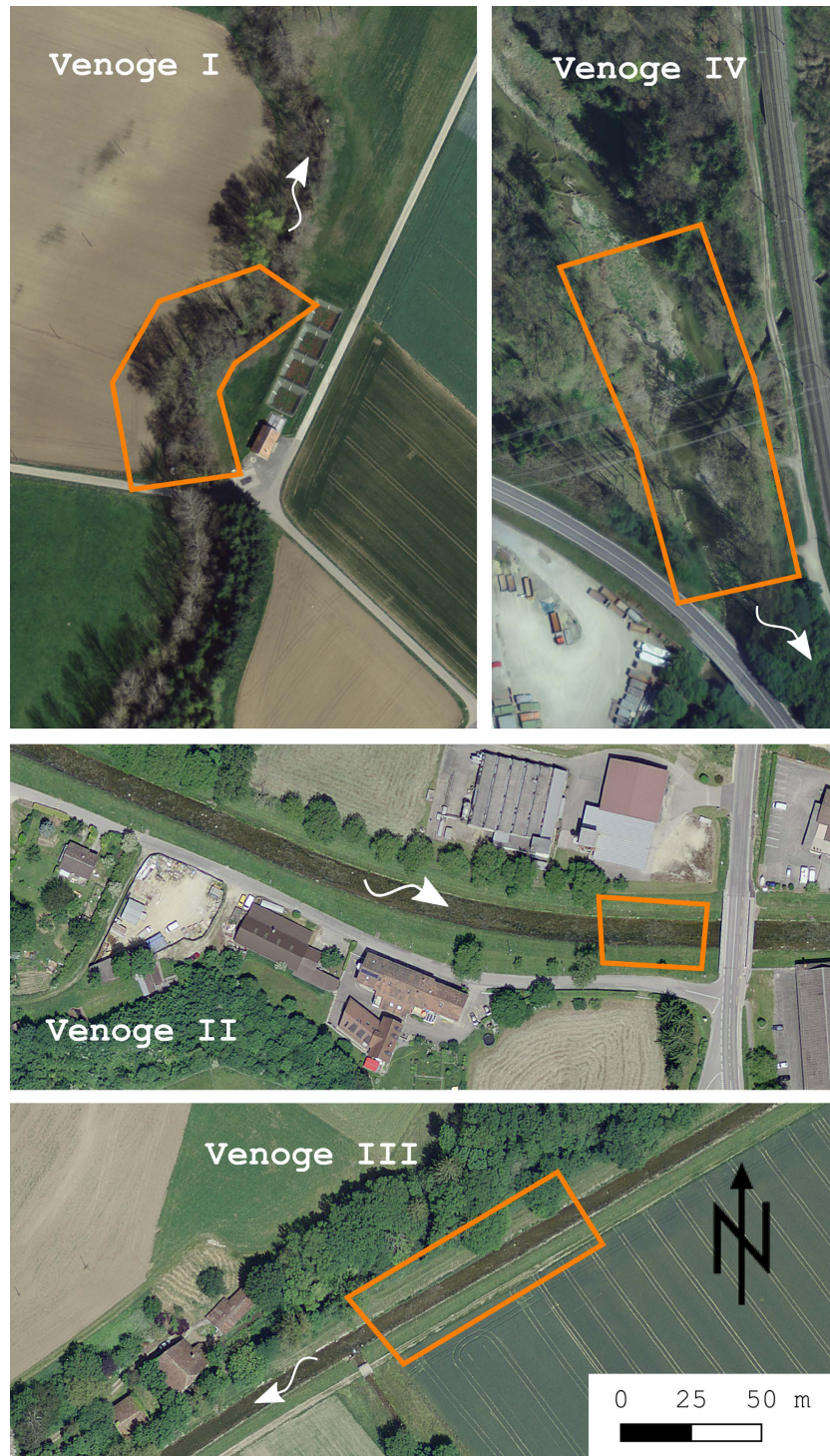
Figure B.25 – Perimeter of the four segments Venoge I-IV. Geodata courtesy Swisstopo
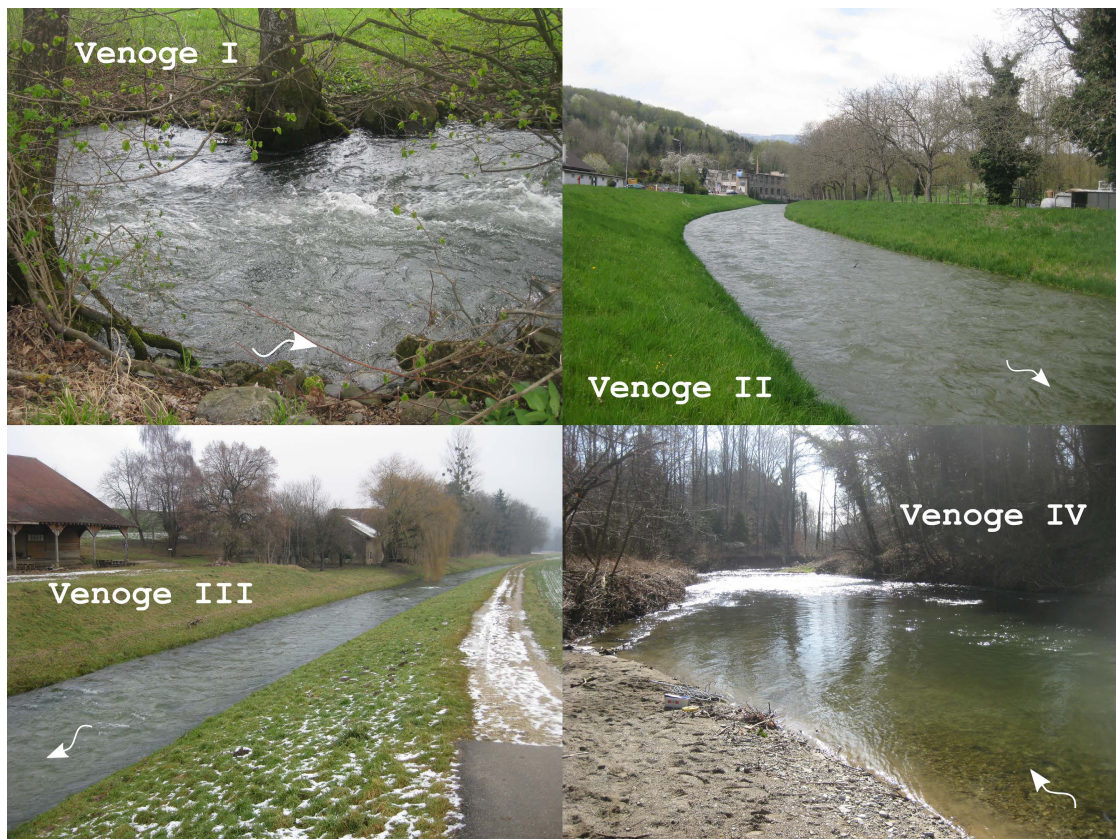
Figure B.26 – Impressions of the four segments Venoge I-IV. Image courtesy Laura Vigne

C **Appendix: Sampling sufficiency**

C.1 Evolution of flow depth and velocity in the 19 river segments
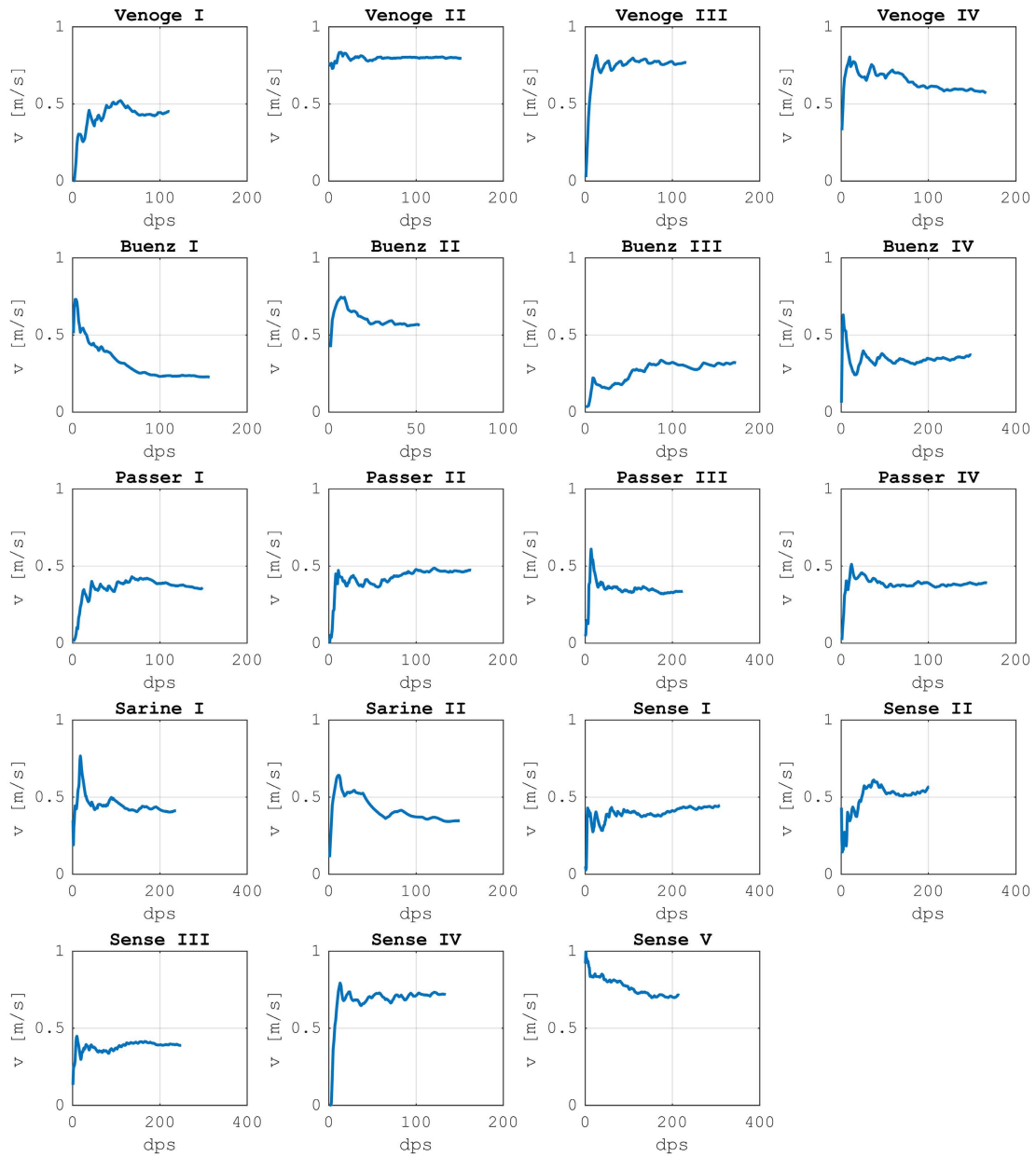
Figure C.1 – Evolution of the flow velocity v with increasing number of measurement points for the 19 segments of the five study rivers, *dps* = data points
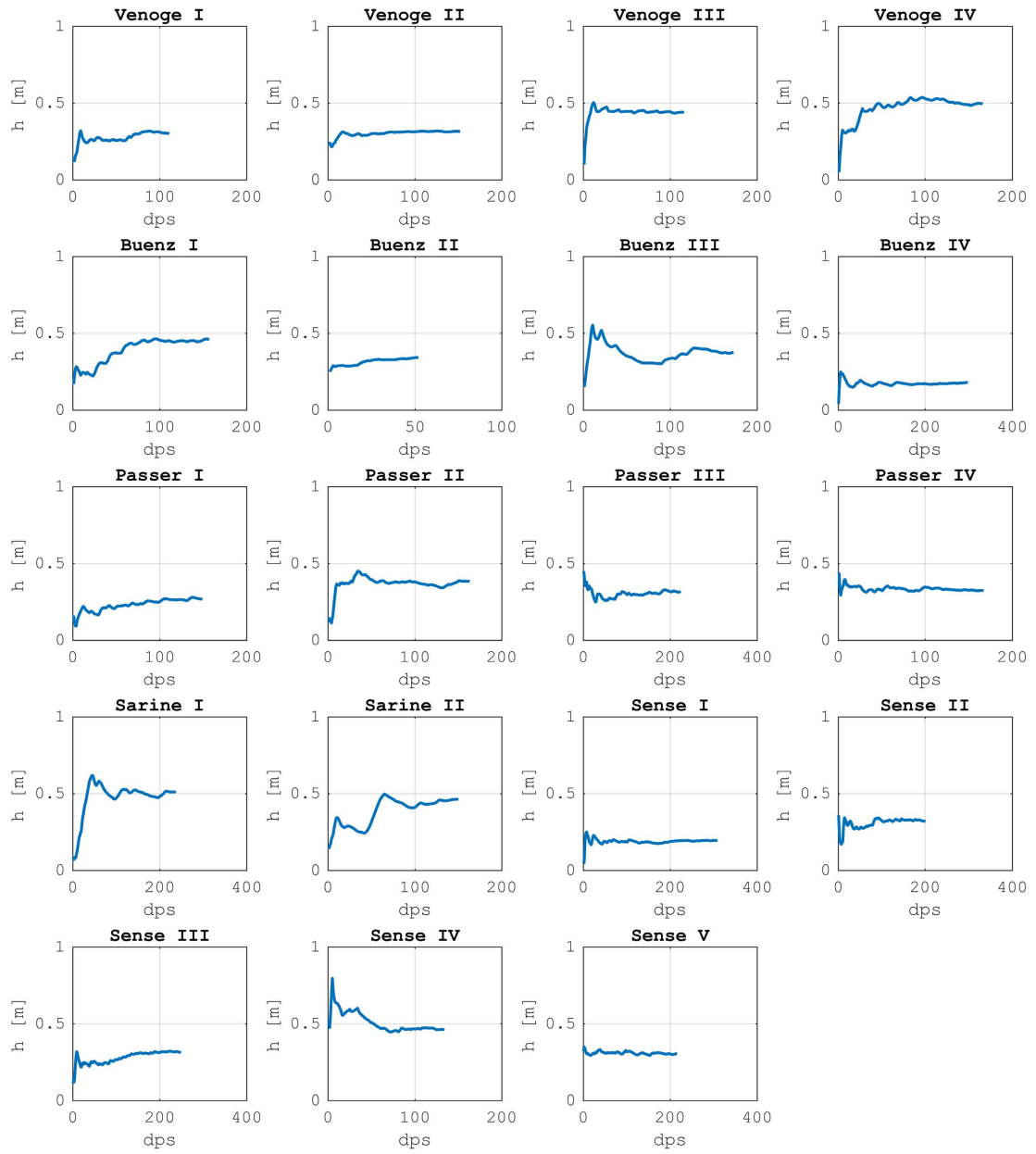
Figure C.2 – Evolution of the flow depth h with increasing number of measurement points for the 19 segments of the five study rivers, *dps* = data points

C.2   HMID results longitudinal sub-sampling sorted by segment geomorphology
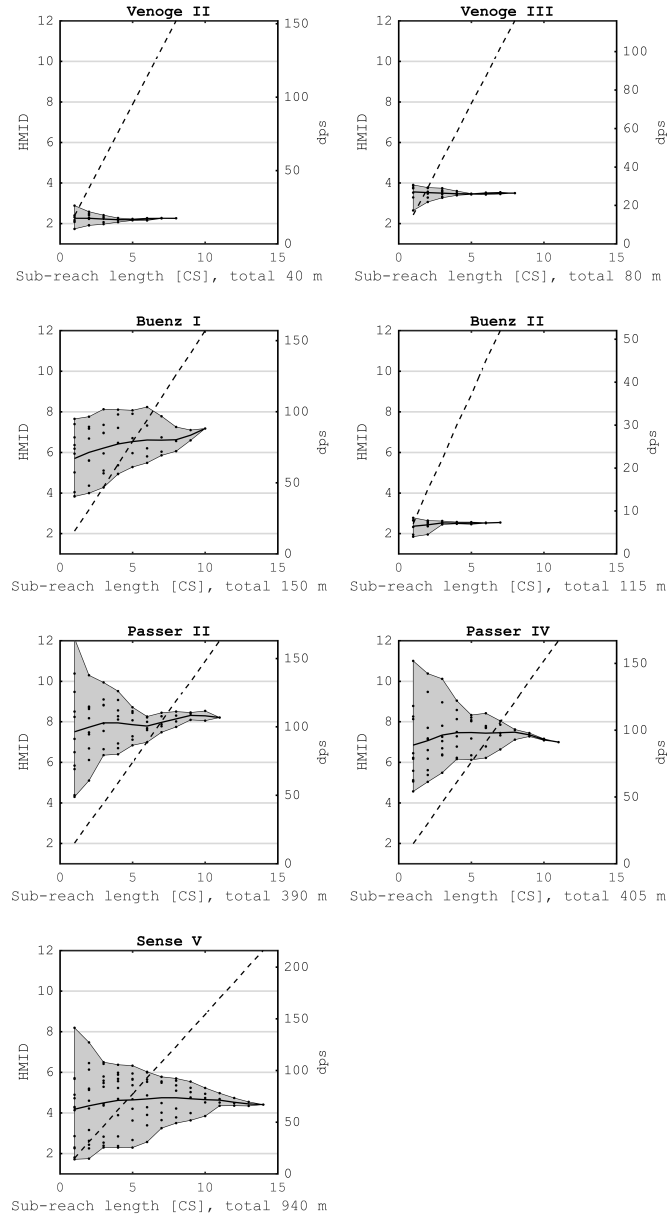
Figure C.3 – HMID values for the seven analyzed straight segments with increasing sub-segment length characterized by the number of consecutive cross-sections (CS). Each dot corresponds to the HMID value computed from the data of a sub-segment. The distribution of these HMID values is accentuated with the shaded area. The solid line in the middle indicates the mean HMID and is independent of the starting point in the initial segment. The last HMID value comprised the entire sampled data representing the segment-scale HMID value. The dashed line belongs to the second y-axis and demonstrates the average number of data points used for the computation of an HMID value for each sub-segment size.

Figure C.4 – HMID values for the four analyzed meandering segments with increasing sub-segment length characterized by the number of consecutive cross-sections (CS). Each dot corresponds to the HMID value computed from the data of a sub-segment. The distribution of these HMID values is accentuated with the shaded area. The solid line in the middle indicates the mean HMID and is independent of the starting point in the initial segment. The last HMID value comprised the entire sampled data representing the segment-scale HMID value. The dashed line belongs to the second y-axis and demonstrates the average number of data points used for the computation of an HMID value for each sub-segment size.
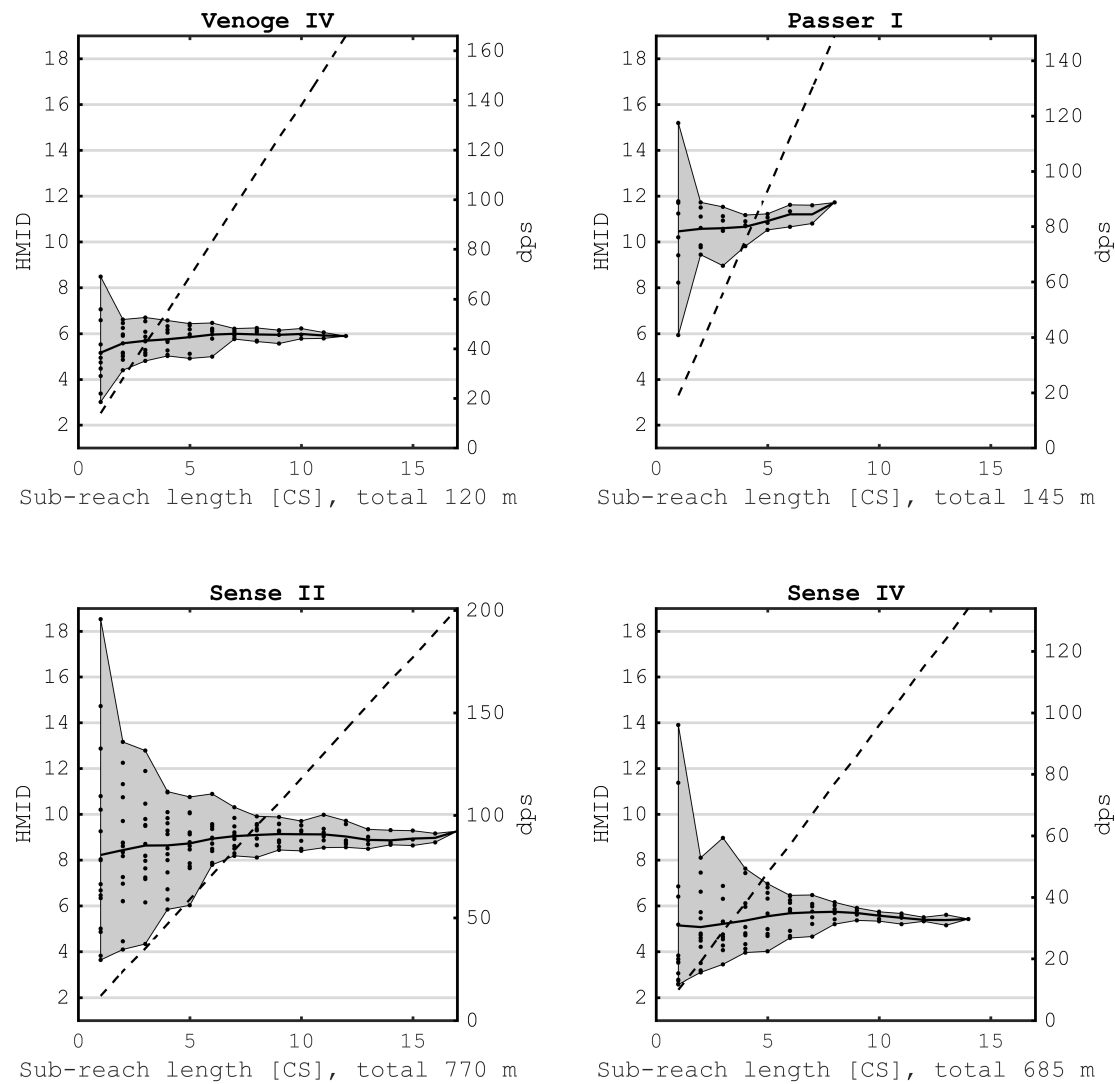
Figure C.5 – HMID values for the four analyzed and segments with alternate bars with increasing sub-segment length characterized by the number of consecutive cross-sections (CS). Each dot corresponds to the HMID value computed from the data of a sub-segment. The distribution of these HMID values is accentuated with the shaded area. The solid line in the middle indicates the mean HMID and is independent of the starting point in the initial segment. The last HMID value comprised the entire sampled data representing the segment-scale HMID value. The dashed line belongs to the second y-axis and demonstrates the average number of data points used for the computation of an HMID value for each sub-segment size.

Figure C.6 – HMID values for the four analyzed braided segments with increasing sub-segment length characterized by the number of consecutive cross-sections (CS). Each dot corresponds to the HMID value computed from the data of a sub-segment. The distribution of these HMID values is accentuated with the shaded area. The solid line in the middle indicates the mean HMID and is independent of the starting point in the initial segment. The last HMID value comprised the entire sampled data representing the segment-scale HMID value. The dashed line belongs to the second y-axis and demonstrates the average number of data points used for the computation of an HMID value for each sub-segment size.

C.3 HMID results combined sub-sampling sorted by segment geomorphology
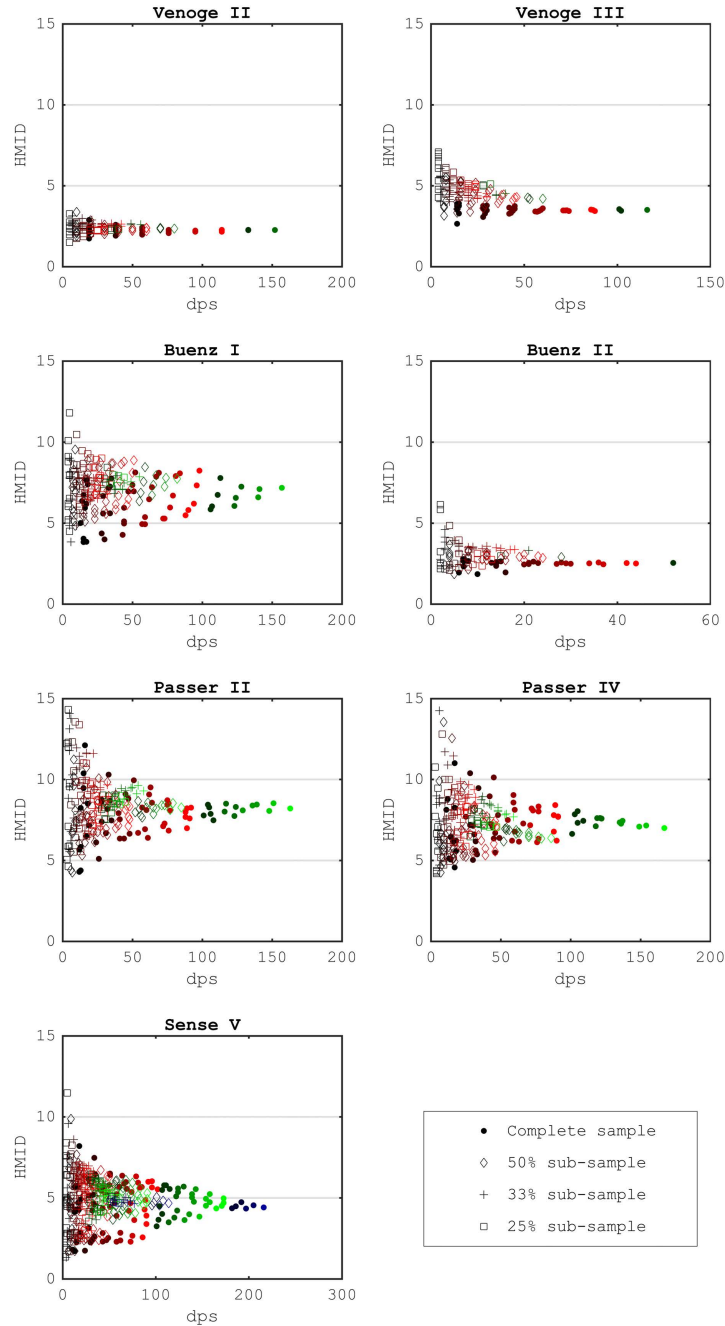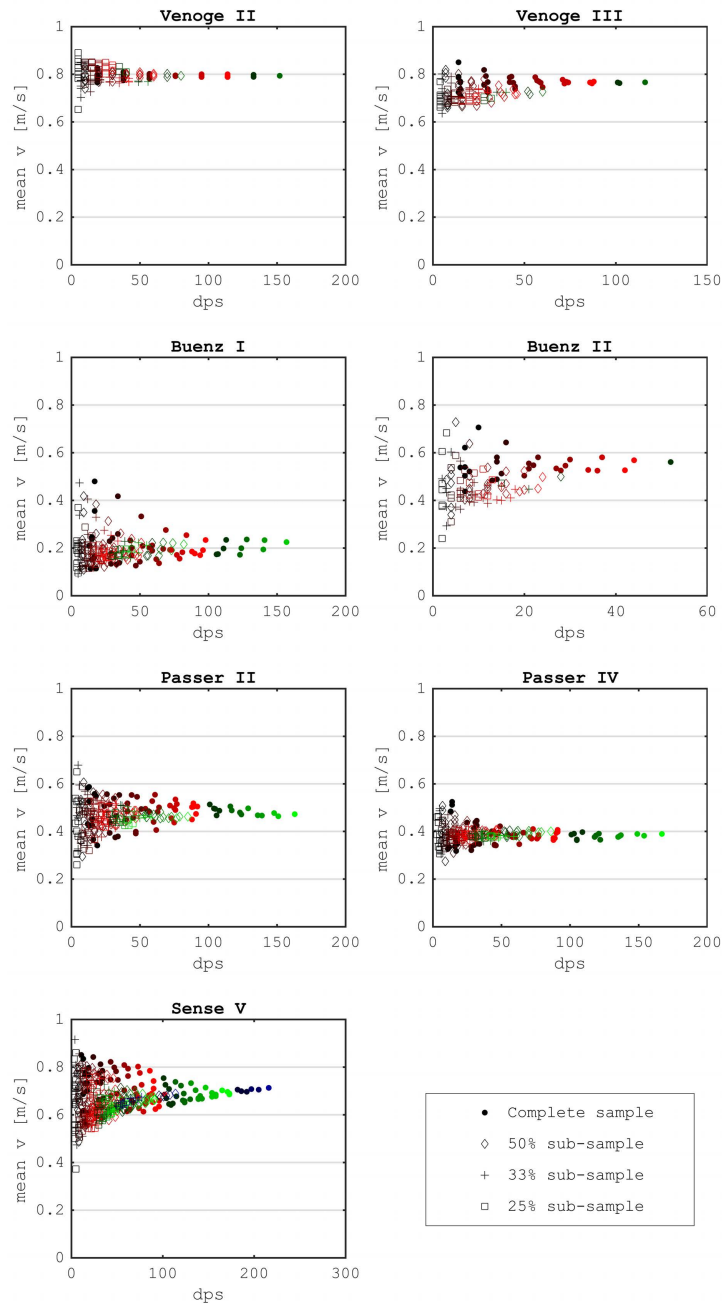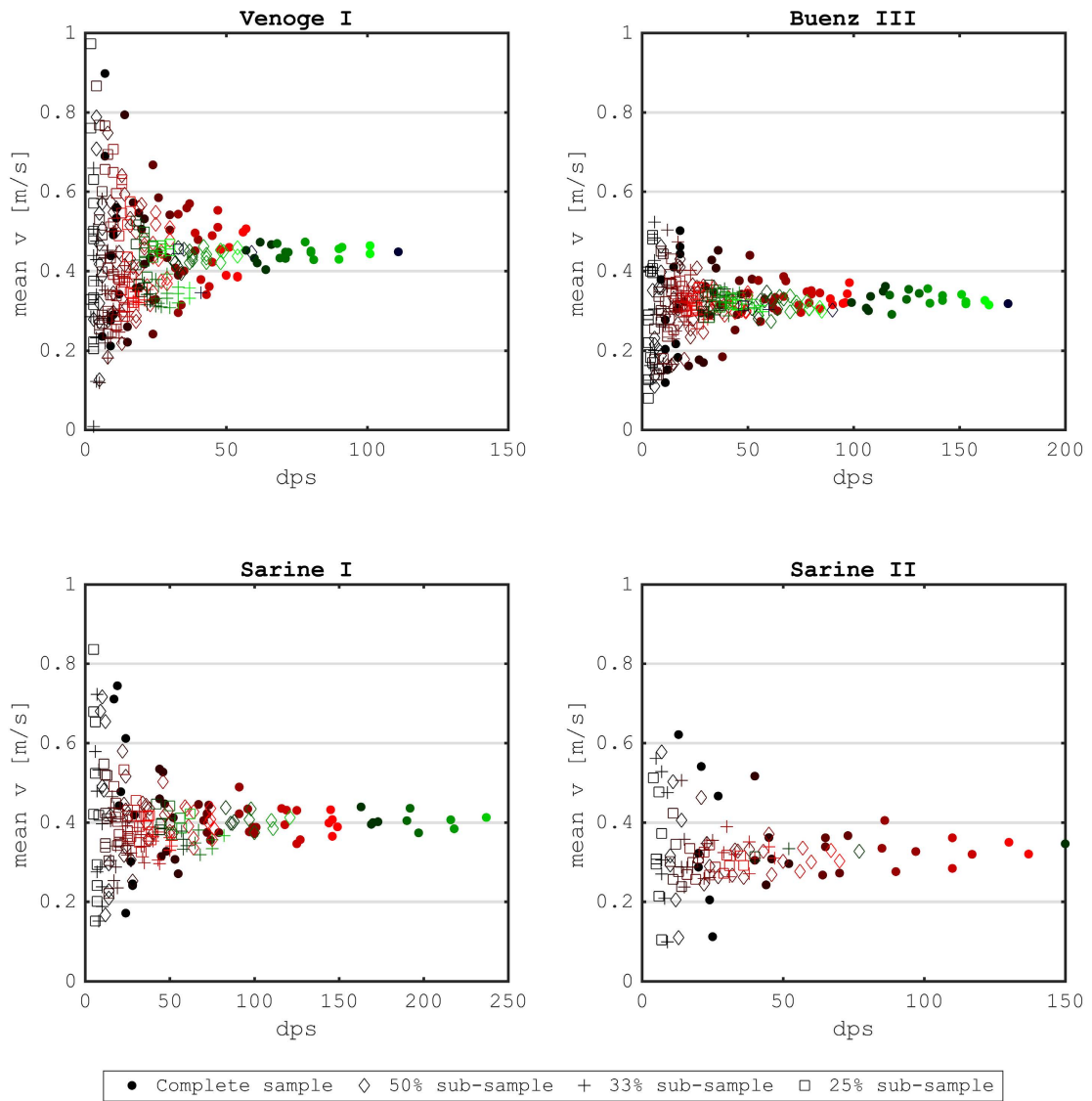

Figure C.7 – HMID values for the seven analyzed straight segments with increasing number of measurement points. The colors indicate the number of cross-sections. The red markers finish at a sub-segment length of six cross-sections, green starts at seven cross-sections and purple starts at a sub-segment length of twelve cross-sections.
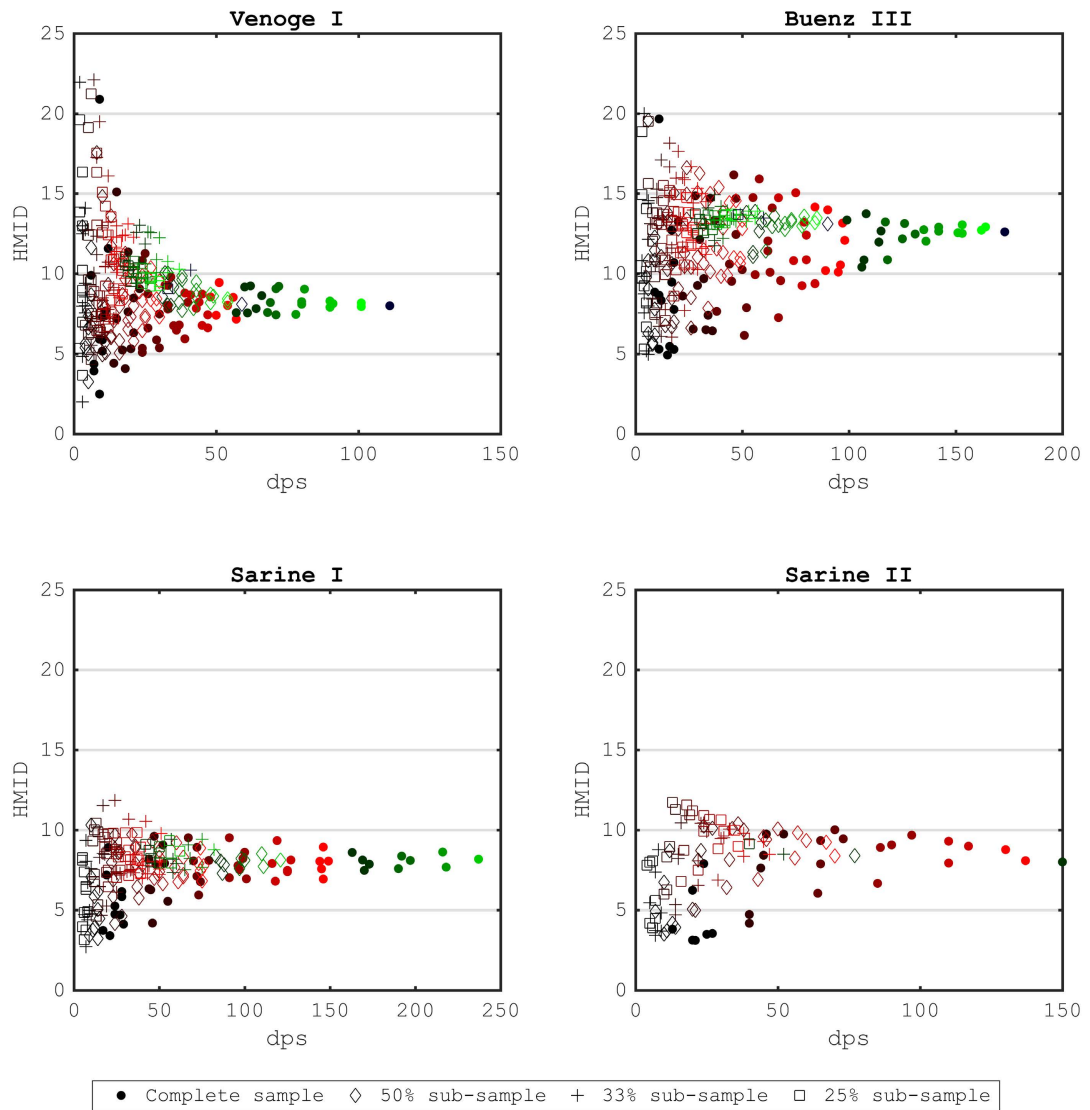
Figure C.8 – HMID values for the four analyzed meandering segments with increasing number of measurement points. The colors indicate the number of cross-sections. The red markers finish at a sub-segment length of six cross-sections, green starts at seven cross-sections and purple starts at a sub-segment length of twelve cross-sections.
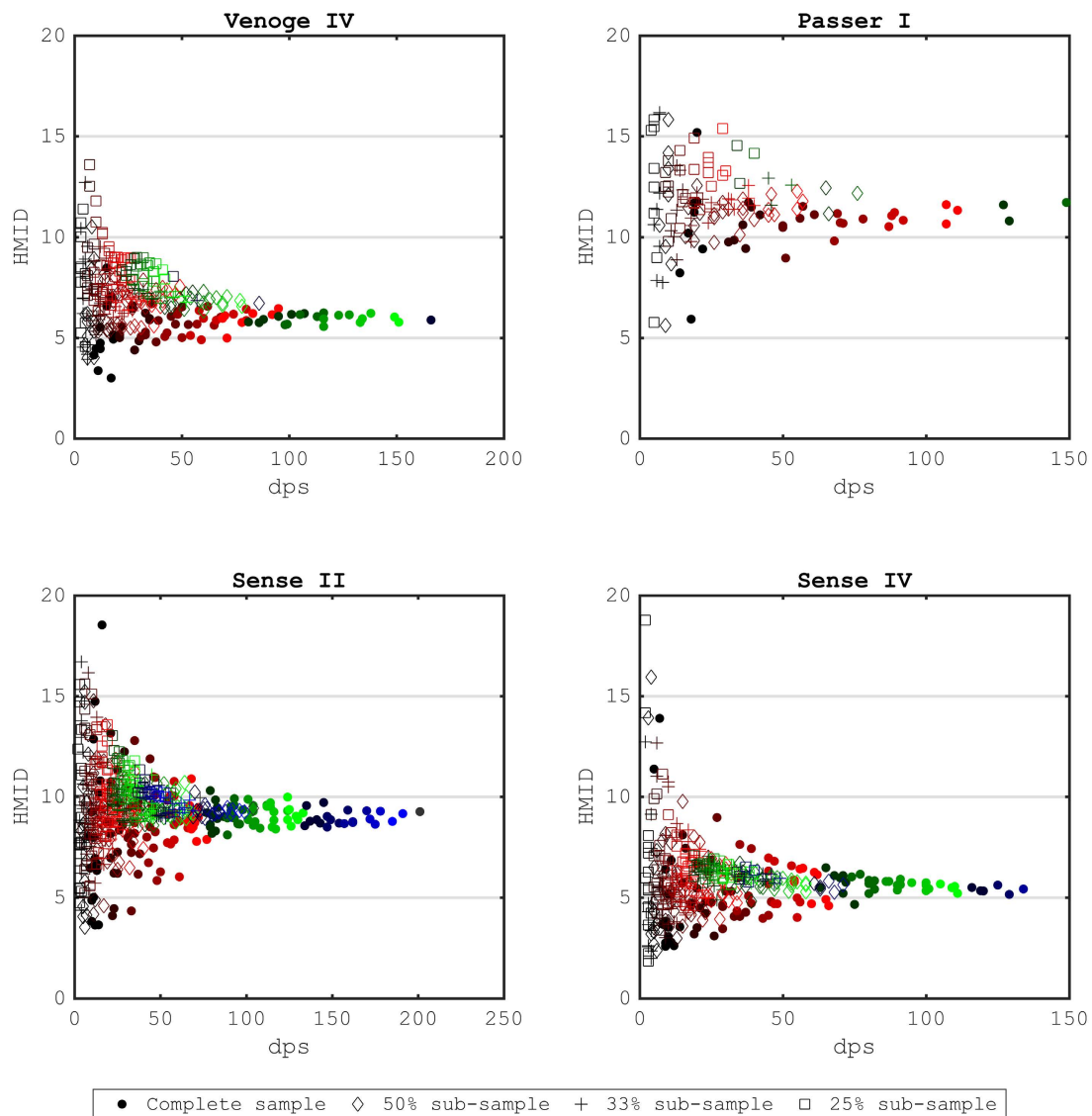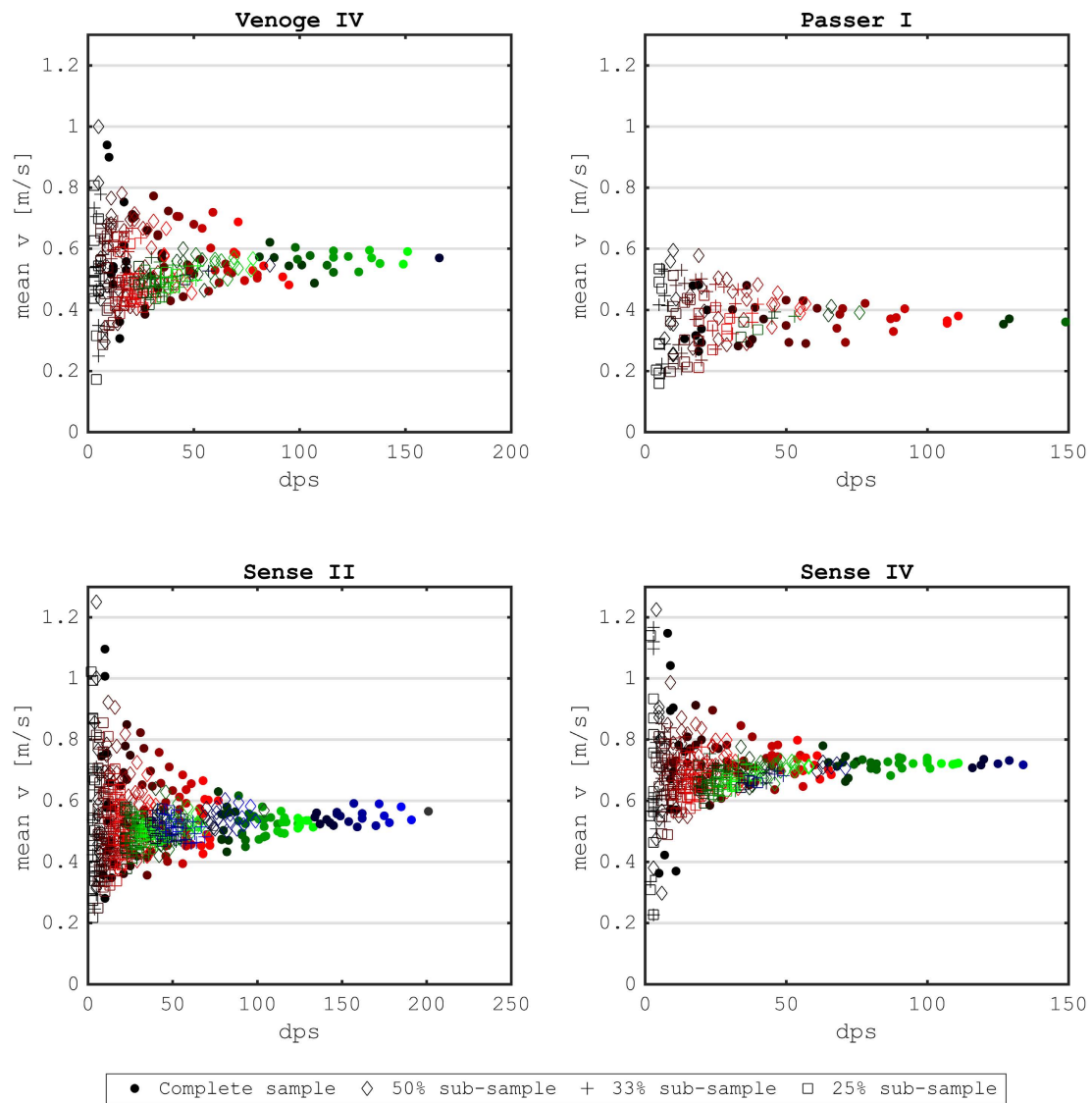
Figure C.9 – HMID values for the four analyzed segments with alternate bars with increasing number of measurement points. The colors indicate the number of cross-sections. The red markers finish at a sub-segment length of six cross-sections, green starts at seven cross-sections and purple starts at a sub-segment length of twelve cross-sections.

Figure C.10 – HMID values for the four analyzed braided segments with increasing number of measurement points. The colors indicate the number of cross-sections. The red markers finish at a sub-segment length of six cross-sections, green starts at seven cross-sections and purple starts at a sub-segment length of twelve cross-sections.

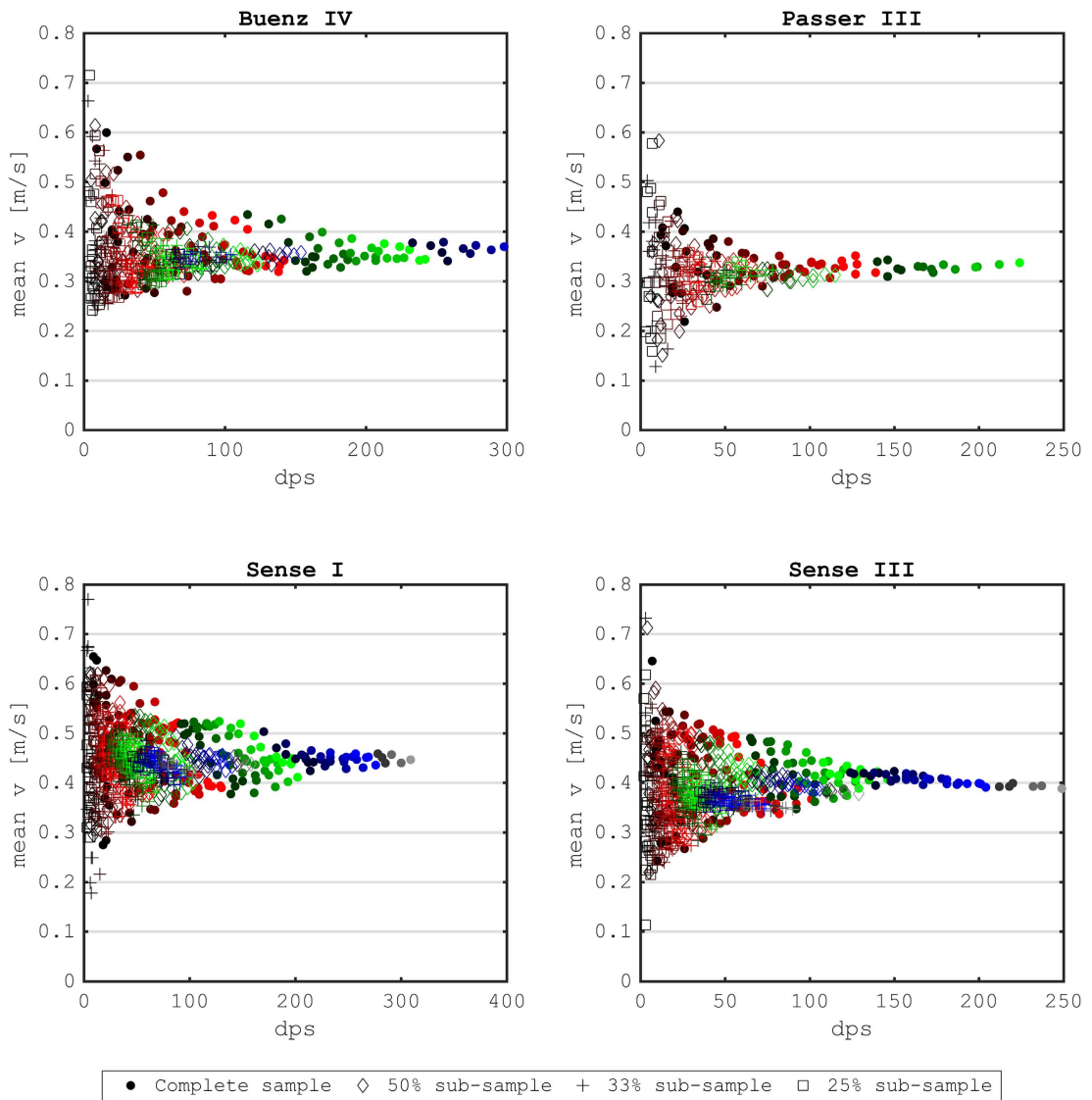## C.4   Flow depth *h* results combined sub-sampling sorted by segment geomorphology
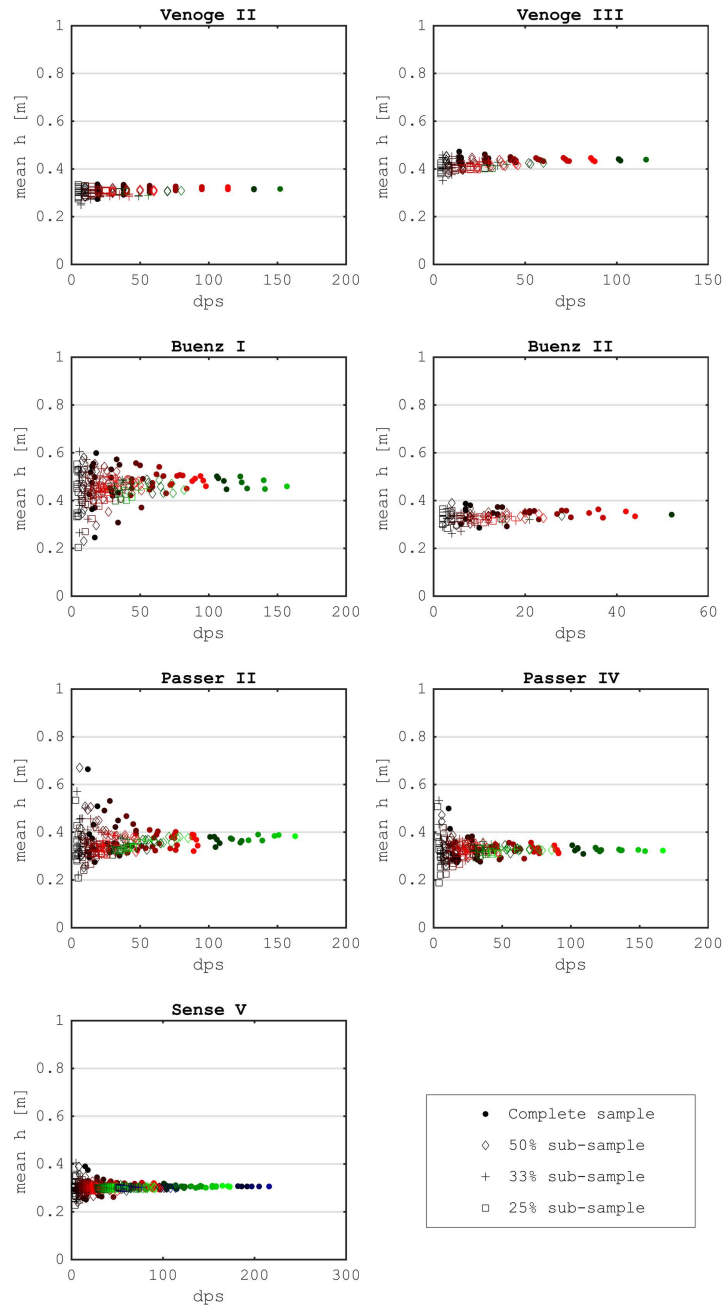
Figure C.11 – Mean flow depth values for the seven analyzed straight segments with increasing number of measurement points. The colors indicate the number of cross-sections. The red markers finish at a sub-segment length of six cross-sections, green starts at seven cross-sections and purple starts at a sub-segment length of twelve cross-sections.
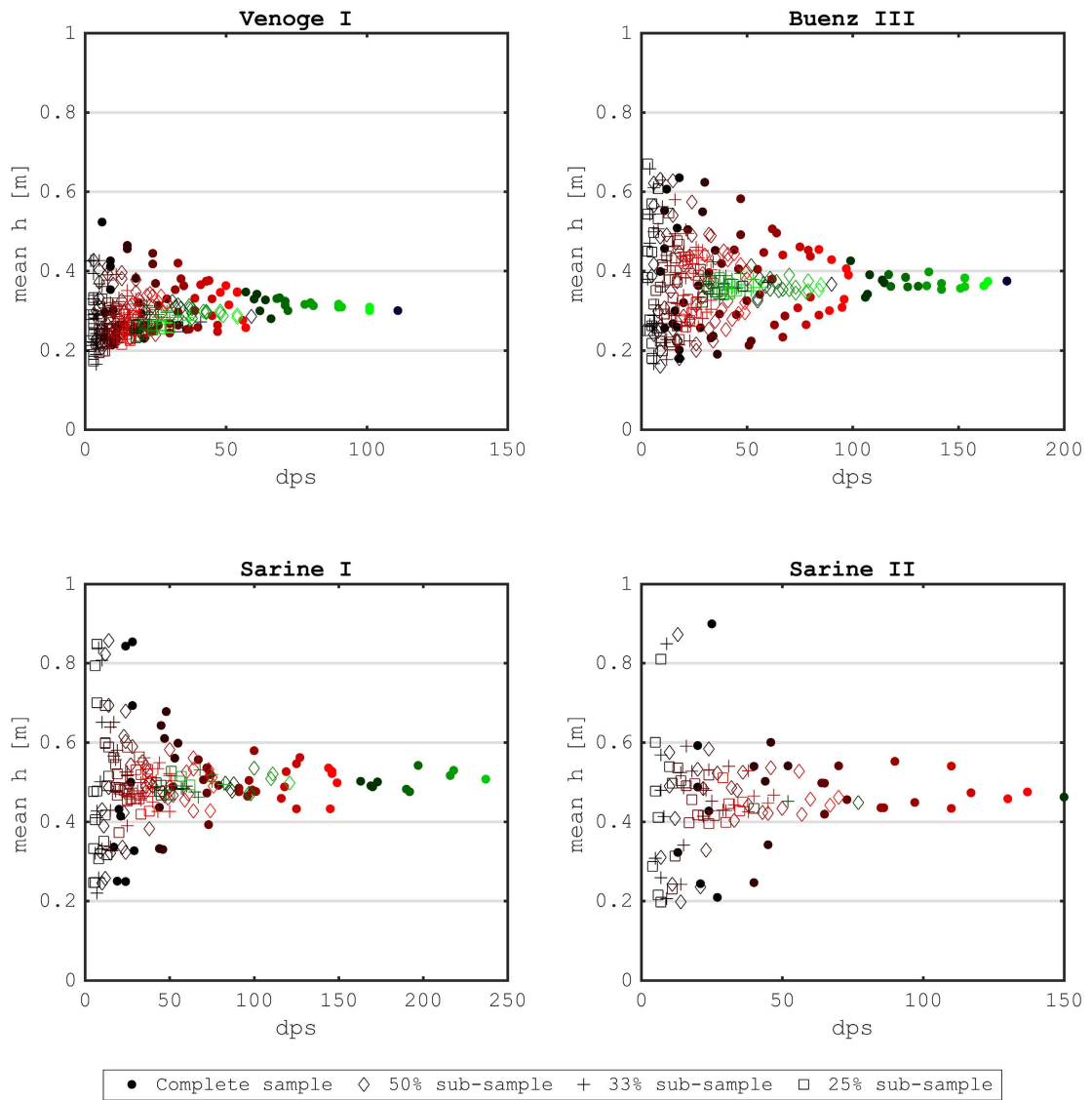
Figure C.12 – Mean flow depth values for the four analyzed meandering segments with increasing number of measurement points. The colors indicate the number of cross-sections. The red markers finish at a sub-segment length of six cross-sections, green starts at seven cross-sections and purple starts at a sub-segment length of twelve cross-sections.
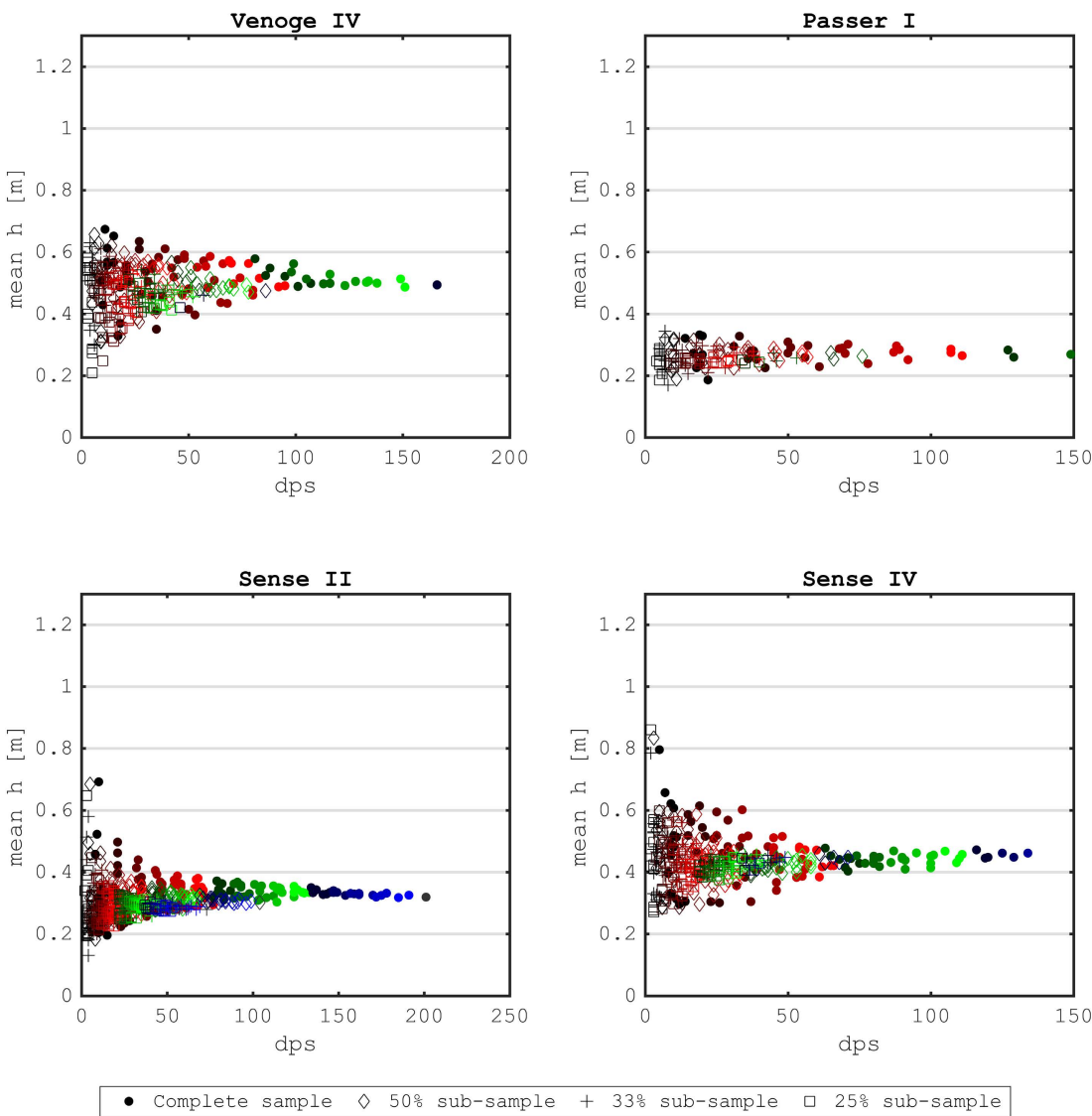
Figure C.13 – Mean flow depth values for the four analyzed segments with alternate bars with increasing number of measurement points. The colors indicate the number of cross-sections. The red markers finish at a sub-segment length of six cross-sections, green starts at seven cross-sections and purple starts at a sub-segment length of twelve cross-sections.

Figure C.14 – Mean flow depth values for the four analyzed braided segments increasing number of measurement points. The colors indicate the number of cross-sections. The red markers finish at a sub-segment length of six cross-sections, green starts at seven cross-sections and purple starts at a sub-segment length of twelve cross-sections.

C.5 Flow velocity *v* results combined sub-sampling sorted by segment geomorphology

Figure C.15 – Mean flow velocity values for the seven analyzed straight segments with increasing number of measurement points. The colors indicate the number of cross-sections. The red markers finish at a sub-segment length of six cross-sections, green starts at seven cross-sections and purple starts at a sub-segment length of twelve cross-sections.

Figure C.16 – Mean flow velocity values for the four analyzed meandering segments with increasing number of measurement points. The colors indicate the number of cross-sections. The red markers finish at a sub-segment length of six cross-sections, green starts at seven cross-sections and purple starts at a sub-segment length of twelve cross-sections.

Figure C.17 – Mean flow velocity values for the four analyzed segments with alternate bars with increasing number of measurement points. The colors indicate the number of cross-sections. The red markers finish at a sub-segment length of six cross-sections, green starts at seven cross-sections and purple starts at a sub-segment length of twelve cross-sections.

Figure C.18 – Mean flow velocity values for the four analyzed braided segments with increasing number of measurement points. The colors indicate the number of cross-sections. The red markers finish at a sub-segment length of six cross-sections, green starts at seven cross-sections and purple starts at a sub-segment length of twelve cross-sections.

D Appendix: Sediment replenishment

Figure D.1 – Excavation resulting from the sediment replenishment in the adjacent alluvial forest. Groundwater infiltration created a pond which serves as new created habitat in the floodplain and only meters away from the river channel. Image courtesy Elena Battisacco
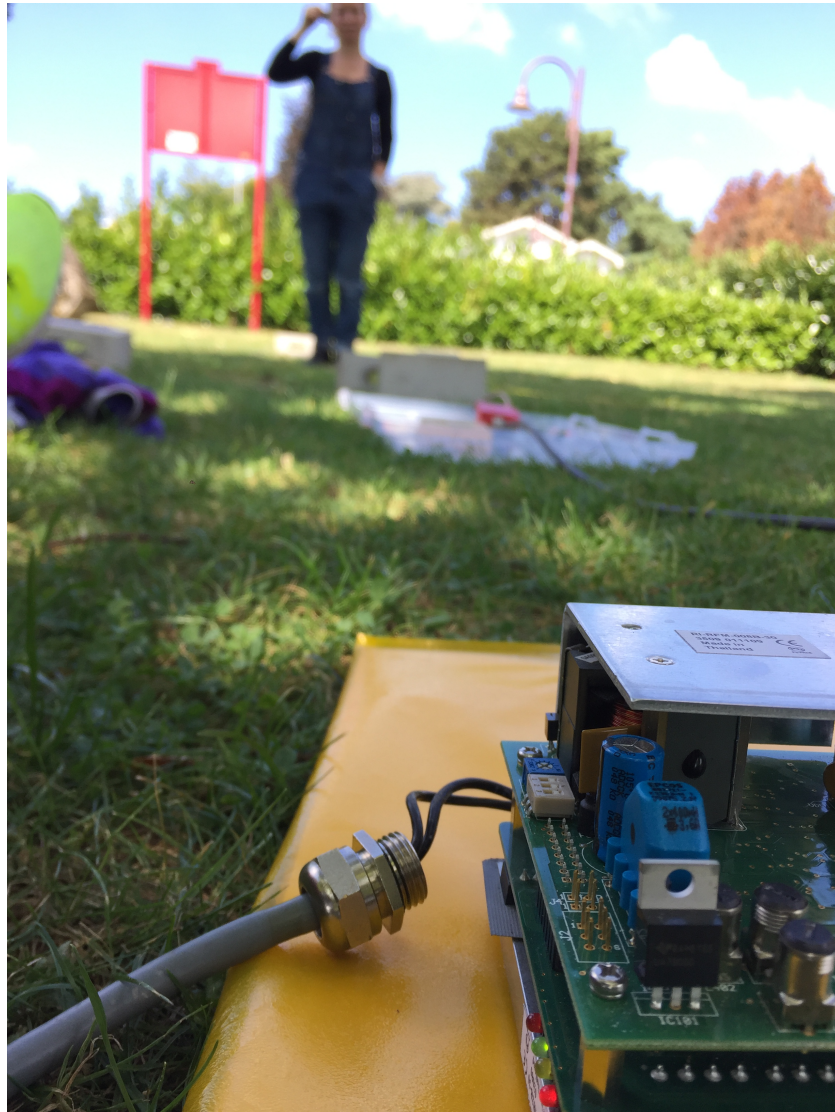
Figure D.2 – Optimization of the pass-over loop fix-antenna under dry conditions. Image courtesy Severin Stähly

Figure D.3 – Installation of the pass-over loop fix-antenna. Image courtesy Elena Battisacco
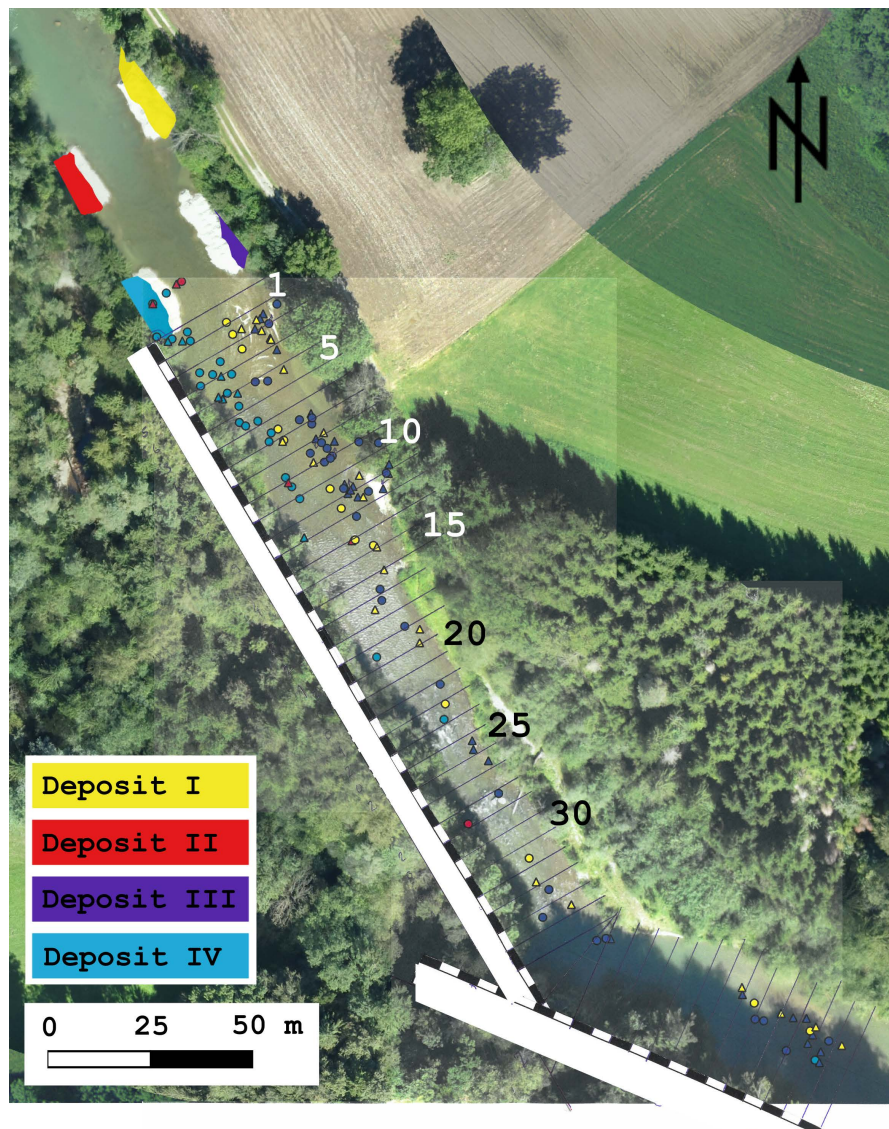
Figure D.4 – The exposed dry surface of the four deposits before (air-image background) and after (colored areas) the artificial flood event. The residual flow discharge was $3.5\,\text{m}^3\text{s}^{-1}$ when the air-image was taken before the flood event and $2.5\,\text{m}^3\text{s}^{-1}$ when the dry surface was measured after the flood event. The 5-m-intervals with RFID PIT tag equipped sediments recovered after the flood event are noted. Based on this count, the OCR was calculated.

0 min - start

30 min

60 min

120 min
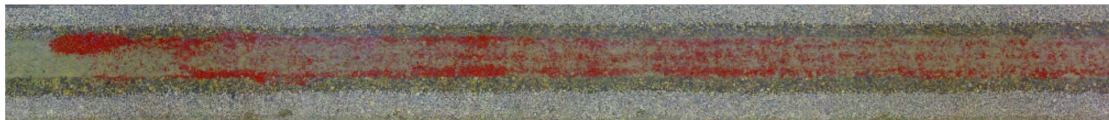
180 min - end
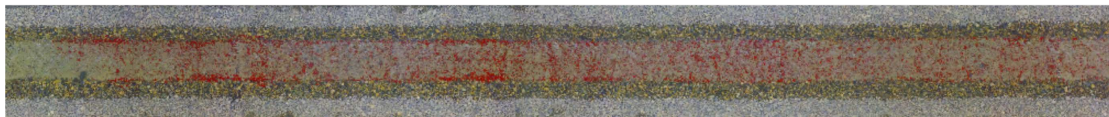
Figure D.5 – Results from the laboratory results with a left-skewed hydrograph. Images assembled from Battisacco (2016), figures 8.4 and 8.5, hydrograph H_4

Figure D.6 – Water level in the Sarine 50 m downstream of deposit III after the peak discharge passed. The wetted boundary is marked with a white line and serves as a reference of the maximum water level. The elevation difference between the wetted area and the floodplain from where the photo was taken is more than 1 m. Flow direction from right to left. Image courtesy Elena Battisacco

Figure D.7 – River bed of the Sarine river, after the flood passed. Algae was removed. The residual part of deposit IV is at the top ofthe image. Image taken on 15 September 2016, courtesy Severin Stähly

E Appendix: Artificial flood Sarine

Figure E.1 – Bottom outlet of the Rossens Dam during the artificial flood in the Sarine River on 14 September 2016. Image courtesy Research unit Ecohydrology, ZHAW

Figure E.2 – Front view on the Rossens Dam during the artificial flood in the Sarine River on 14 September 2016. Image courtesy Research unit Ecohydrology, ZHAW

Figure E.3 – Inundated floodplain during the artificial flood in the Sarine River on 14 September 2016. Image courtesy Severin Stähly

Bibliography

Allan, J. and Castillo, M. (2007). *Stream ecology: Structure and function of running waters: Second edition.* Springer, Dordrecht, The Netherlands.

Alp, M., Keller, I., Westram, A. M., and Robinson, C. T. (2012). How river structure and biological traits influence gene flow: A population genetic study of two stream invertebrates with differing dispersal abilities. *Freshwater Biology*, 57(5):969–981.

Arnaud, F., Piégay, H., Béal, D., Collery, P., Vaudor, L., and Rollet, A. J. (2017). Monitoring gravel augmentation in a large regulated river and implications for process-based restoration. *Earth Surface Processes and Landforms*, 42(13):2147–2166.

Arnaud, F., Piégay, H., Vaudor, L., Bultingaire, L., and Fantino, G. (2015). Technical specifications of low-frequency radio identification bedload tracking from field experiments: Differences in antennas, tags and operators. *Geomorphology*, 238:37–46.

BAFU (1998). Ökomorphologie Stufe F. *Mitteilungen zum Gewässerschutz*, (27):1–49.

Barbour, M. T., Gerritsen, J., Snyder, B. D., and Stribling, J. B. (1999). *Rapid Bioassessment Protocols for Use in Streams and Wadeable Rivers: Periphyton, Benthic Macroinvertebrates, and Fish - Second Edition.* EPA- 841-B-99-002. U. S. Environmental Protection Agency. Office of Water. Waschinton, D.C.

Bathurst, J. C., Thorne, C. R., and Hey, R. D. (1977). Erratum: Direct measurements of secondary currents in river bends (Nature 269 (504)). *Nature*, 270(5633):191.

Battisacco, E. (2016). *Replenishment of sediment downstream of dams: erosion and transport processes.* EPFL Ph.D Thesis No. 7293 and Communication 67 of Laboratory of Hydraulic Constructions (Ed. A. Schleiss), Ecole polytechnique fédérale de Lausanne (EPFL). Lausanne.

Battisacco, E., Franca, M. J., and Schleiss, A. J. (2016). Sediment replenishment: Influence of the geometrical configuration on the morphological evolution of channel-bed. *Water Resources Research*, 52(11):8879–8894.

Benn, D. I. and Ballantyne, C. K. (1993). The description and representation of particle shape. *Earth Surface Processes and Landforms*, 18(7):665–672.

Bernhardt, E. S., Palmer, M. A., Allan, J. D., Alexander, G., Barnas, K., Brooks, S., Carr, J., Clayton, S., Dahm, C., Follstad-Shah, J., Galat, D., Gloss, S., Goodwin, P., Hart, D., Hassett, B., Jenkinson, R., Katz, S., Kondolf, G. M., Lake, P. S., Lave, R., Meyer, J. L., O'Donnell, T. K., Pagano, L., Powell, B., and Sudduth, O. (2005). Synthesizing U.S. river restoration efforts. *Science*, 308(5722):636–637.

BFE (2012). Wasserkraftpotenzial der Schweiz - Abschätzung des Ausbaupotenzials der Wasserkraftnutzung im Rahmen der Energiestrategie 2050. Technical report, Swiss Federal Institute for Energy, Ittingen, Switzerland.

BFE (2018a). *Statistik der Wasserkraftanlagen der Schweiz.* Bern, Switzerland.

BFE (2018b). *Wasserkraftanlagen der Schweiz Entwicklung der Leistung und der mittleren Produktionserwartung.* Bern, Switzerland.

Bisson, P. A., Montgomery, D. R., and Buffington, J. M. (2017). Valley Segments, Stream Reaches, and Channel Units. In Hauer, F. R. and Lamberti, G. A., editors, *Methods in Stream Ecology: Third Edition*, volume 1, pages 21–47. Elsevier.

Brandt, S. A. (2000). Classification of geomorphological effects downstream of dams. *Catena*, 40(4):375–401.

Brenna, A., Surian, N., and Mao, L. (2019). Virtual Velocity Approach for Estimating Bed Material Transport in Gravel-Bed Rivers: Key Factors and Significance. *Water Resources Research*, 55.

Buffington, J. and Montgomery, D. (2013). Geomorphic Classification of Rivers. In Shroder, J. and Wohl, E., editors, *Treatise on Geomorphology, Vol. 9*, pages 730–767. Academic Press, San Diego, CA.

Bunn, S. E. and Arthington, A. H. (2002). Basic principles and ecological consequences of altered flow regimes for aquatic biodiversity. *Environmental Management*, 30(4):492–507.

Bunte, K. and Abt, S. R. (2001). *Sampling Surface and Subsurface Particle-Size Distributions in Wadable Gravel- and Cobble-Bed Streams for Analyses in Sediment Transport , Hydraulics , and Streambed Monitoring.*

Cameron, A. C., Gelbach, J. B., and Miller, D. L. (2008). Bootstrap-Based Improvements for Inference with Clustered Errors. *Review of Economics and Statistics*, 90(3):414–427.

Carter, G., Duncan, M., and Biggs, B. (1998). Numerical hydrodynamic modelling of mountain streams for assessing instream habitat. In *IAHS Publication no. 248*, volume 248, pages 217–223.

Cassel, M., Dépret, T., and Piégay, H. (2017a). Assessment of a new solution for tracking pebbles in rivers based on active RFID. *Earth Surface Processes and Landforms*, 42(13):1938–1951.

Cassel, M., Piégay, H., and Lavé, J. (2017b). Effects of transport and insertion of radio frequency identification (RFID) transponders on resistance and shape of natural and synthetic pebbles: applications for riverine and coastal bedload tracking. *Earth Surface Processes and Landforms*, 42(3):399–413.

Chapuis, M., Bright, C. J., Hufnagel, J., and Macvicar, B. (2014). Detection ranges and uncertainty of passive Radio Frequency Identification (RFID) transponders for sediment tracking in gravel rivers and coastal environments. *Earth Surface Processes and Landforms*, 39(15):2109–2120.

Chapuis, M., Dufour, S., Provansal, M., Couvert, B., and de Linares, M. (2015). Coupling channel evolution monitoring and RFID tracking in a large, wandering, gravel-bed river: Insights into sediment routing on geomorphic continuity through a riffle-pool sequence. *Geomorphology*, 231:258–269.

Coopersmith, E., Yaeger, M. A., Ye, S., Cheng, L., and Sivapalan, M. (2012). Exploring the physical controls of regional patterns of flow duration curves - Part 3: A catchment classification system based on regime curve indicators. *Hydrology and Earth System Sciences*, 16(11):4467–4482.

Da Silva, A. M. F. (1991). *Alternate Bars and Related Allubial Processes*. Thesis of master of science, Queen's University, Kingston Ontario, Canada.

DAEC (2014). *Planification de l'assainissement du charriage - Rapport final*. Fribourg.

Davis, W. M. (1899). The Geographical Cycle. *The Geographical Journal*, 14(5):481–504.

Davison, A. C. and Hinkley, D. V. (1997). *Bootstrap Methods and their Application*. Cambridge University Press, New York, USA.

Döring, M., Tonolla, D., Robinson, C. T., Schleiss, A. J., Stähly, S., Gufler, C., Geilhausen, M., and Di Cugno, N. (2018). Künstliches Hochwasser an der Saane – Eine Massnahme zum nachhaltigen Auenmanagement [in german]. *Wasser Energie Luft*, 2:119–127.

Fehr, R. (1987). *Geschiebeanalysen in Gebirgsflüssen*. PhD thesis, Mitteilungen der Versuchsanstalt für Wasserbau, Hydrologie und Glaziologie Nr. 92 (Ed. D. Vischer). Swiss Federal Institute of Technology (ETH) Zurich, Switzerland.

Feio, M. J., Calapez, A. R., Elias, C. L., Cortes, R. M., Graça, M. A., Pinto, P., and Almeida, S. F. (2016). The paradox of expert judgment in rivers ecological monitoring. *Journal of Environmental Management*, 184:609–616.

Friedl, F., Weitbrecht, V., and Boes, R. M. (2018). Erosion pattern of artificial gravel deposits. *International Journal of Sediment Research*, 33(1):57–67.

Frissell, C. A., Liss, W. J., Warren, C. E., and Hurley, M. D. (1986). A hierarchical framework for stream habitat classification: Viewing streams in a watershed context. *Environmental Management*, 10(2):199–214.

Gaeuman, D. (2012). Mitigating Downstream Effects of Dams. In Church, M., Biron, P. M., and Roy, A. G., editors, *Gravel-Bed Rivers: Processes, Tools, Environments*, pages 182–189. John Wiley & Sons Ltd.

Gaeuman, D., Stewart, R., Schmandt, B., and Pryor, C. (2017). Geomorphic response to gravel augmentation and high-flow dam release in the Trinity River, California. *Earth Surface Processes and Landforms*, 42(15):2523–2540.

Genevois, R. and Ghirotti, M. (2005). The 1963 Vaiont Landslide. *Giornale di Geologia Applicata*, 1:41–52.

Gilvear, D. J., Spray, C. J., and Casas-Mulet, R. (2013). River rehabilitation for the delivery of multiple ecosystem services at the river network scale. *Journal of Environmental Management*, 126:30–43.

Gómez, C. M., Pérez-Blanco, C. D., and Batalla, R. J. (2013). Tradeoffs in river restoration: Flushing flows vs. hydropower generation in the Lower Ebro River, Spain. *Journal of Hydrology*, 518(PA):130–139.

Gostner, W. (2012). *The Hydro-Morphological Index of Diversity : a planning tool for river restoration projects*. EPFL Ph.D Thesis No. 5408 and Communication 51 of Laboratory of Hydraulic Constructions (Ed. A. Schleiss), Ecole polytechnique fédérale de Lausanne (EPFL). Lausanne.

Gostner, W., Alp, M., Schleiss, A. J., and Robinson, C. T. (2013a). The hydro-morphological index of diversity: A tool for describing habitat heterogeneity in river engineering projects. *Hydrobiologia*, 712(1):43–60.

Gostner, W., Parasiewicz, P., and Schleiss, A. J. (2013b). A case study on spatial and temporal hydraulic variability in an alpine gravel-bed stream based on the hydromorphological index of diversity. *Ecohydrology*, 6(4):652–667.

Haeberli, W., Bütler, M., Huggel, C., Müller, H., and Schleiss, A. (2013). *Neue Seen als Folge des Gletscherschwundes im Hochgebirge – Chancen und Risiken. Formation des nouveux lacs suite au recul des glaciers en haute montagne – chances et risques. Forschungsbericht NFP 61*. vdf Hochschulverlag AG an der ETH Zürich, Zürich.

Hassan, M. A., Church, M., and Schick, A. P. (1991). Distance of movement of coarse particles in gravel bed streams. *Water Resources Research*, 27(4):503–511.

Heckmann, T., Haas, F., Abel, J., Rimböck, A., and Becht, M. (2017). Feeding the hungry river: Fluvial morphodynamics and the entrainment of artificially inserted sediment at the dammed river Isar, Eastern Alps, Germany. *Geomorphology*, 291:128–142.

Heggenes, J. (1996). Habitat selection by brown trout (Salmo trutta) and young Atlantic salmon (S-salar) in streams: Static and dynamic hydraulic modelling. *Regulated Rivers-Research & Management*, 12(July 1994):155–169.

Hilsenhoff, W. L. (1982). *Using a biotic index to evaluate water quality in streams. Technical Bulletin No. 132*. Madison, Wisconsin.

HLS (2002). *Historisches Lexikon der Schweiz*, volume 3. Stiftung Historisches Lexikon der Schweiz.

Hodge, R. A., Hoey, T. B., and Sklar, L. S. (2011). Bed load transport in bedrock rivers: The role of sediment cover in grain entrainment, translation, and deposition. *Journal of Geophysical Research: Earth Surface*, 116(4).

IHA (2018). Hydropower status report. Technical report, International Hydropower Association, London, United Kingdom.

Jäggi, M. (1983). *Alternierende Kiesbanke*. PhD thesis, Mitteilungen der Versuchsanstalt für Wasserbau, Hydrologie und Glaziologie Nr. 62 (Ed. D. Vischer). Swiss Federal Institute of Technology (ETH) Zurich, Switzerland.

Jäggi, M. and Hunziker, R. (2002). Petite-Sarine - Etude sur l'incidence du barrage de Rossens sur la morphologie fluviale, le charriage et l'évolution future de cette zone alluviale. Technical report, Direction des travaux publics du Canton de Fribourg, Fribourg.

Jowett, I. G. (1993). A method for objectively identifying pool, run, and riffle habitats from physical measurements. *New Zealand Journal of Marine and Freshwater Research*, 27(2):241–248.

Jowett, I. G. (1998). Hydraulic geometry of New Zealand rivers and its use as a preliminary method of habitat assessment. *Regulated Rivers: Research & Management*, 14(5):451–466.

Juez, C., Battisacco, E., Schleiss, A. J., and Franca, M. J. (2016). Assessment of the performance of numerical modeling in reproducing a replenishment of sediments in a water-worked channel. *Advances in Water Resources*, 92:10–22.

Kantoush, S. A. and Schleiss, A. J. (2009). Channel formation during flushing of large shallow reservoirs with different geometries. *Environmental Technology*, 30(8):855–863.

Kantoush, S. A. and Sumi, T. (2010). River morphology and sediment management strategies for sustainable reservoir in Japan and European Alps. *Ann Disas Prev Res Inst Kyoto Univ*, 53(B):821–839.

Kondolf, G. M. (1994). Geomorphic and environmental effects of instream gravel mining. *Landscape and Urban Planning*, 28(2-3):225–243.

Kondolf, G. M. (1997). HungryWater: Effects of Dams and Gravel Mining on River Channels. *Environmental Management*, 21(4):533–551.

Kondolf, G. M. (1998). Lessons learned from river restoration projects in California. *Aquatic Conservation: Marine and Freshwater Ecosystems*, 8(1):39–52.

Kondolf, G. M., Anderson, S., Lave, R., Pagano, L., Merenlender, A., and Bernhardt, E. S. (2007). Two decades of river restoration in California: What can we learn? *Restoration Ecology*, 15(3):516–523.

Kondolf, G. M., Montgomery, D. R., Piégay, H., and Schmitt, L. (2005). Geomorphic Classification of Rivers and Streams. In Kondolf, G. M. and Piégay, H., editors, *Tools in Fluvial Geomorphology*, pages 171–204. John Wiley & Sons Ltd., Chichester, UK.

Kondolf, G. M. and Piégay, H. (2003). Tools in Fluvial Geomorphology : Problem Statement and Recent Practice. In Kondolf, G. M. and Piégay, H., editors, *Tools in Fluvial Geomorphology*, pages 1–22. John Wiley & Sons Ltd.

Kondolf, G. M. and Wilcock, P. R. (1996). The flushing flow problem: Defining and evaluating objectives. *Water Resources Research*, 32(8):2589–2599.

Kondolf, G. M. and Wolman, M. G. (1993). The sizes of salmonid spawning gravels. *Water Resources Research*, 29(7):2275–2285.

Konrad, C. P., Olden, J. D., Lytle, D. A., Melis, T. S., Schmidt, J. C., Bray, E. N., Freeman, M. C., Gido, K. B., Hemphill, N. P., Kennard, M. J., McMullen, L. E., Mims, M. C., Pyron, M., Robinson, C. T., and Williams, J. G. (2011). Large-scale Flow Experiments for Managing River Systems. *BioScience*, 61(12):948–959.

Krumbein, W. C. (1941). The Effects of Abrasion on the Size, Shape and Roundness of Rock Fragments. *The Journal of Geology*, 49(5):482–520.

Kuenen, P. (1956). Experimental Abrasion of Pebbles : 2 . Rolling by Current. *The Journal of Geology*, 64(4):336–368.

Lamouroux, N. (1998). Depth probability distributions in stream reaches. *Journal of Hydraulic Engineering*, 124(2):224–227.

Lamouroux, N. (2007). 25 Hydraulic geometry of stream reaches and ecological implications. *Developments in Earth Surface Processes*, 11:661–675.

Lamouroux, N., Capra, H., and Pouilly, M. (1998). Predicting habitat suitability for lotic fish: linking statistical hydraulic models with multivariate habitat use models. *Regulated Rivers: Research and Management*, 14(1):1–11.

Lamouroux, N. and Jowett, I. G. (2005). Generalized instream habitat models. *Canadian Journal of Fisheries and Aquatic Sciences*, 62(1):7–14.

Lamouroux, N., Souchon, Y., and Herouin, E. (1995). Predicting Velocity Frequency Distributions in Stream Reaches. *Water Resources Research*, 31(9):2367–2375.

Lane, B. A., Pasternack, G. B., Dahlke, H. E., and Sandoval-Solis, S. (2017). The role of topographic variability in river channel classification. *Progress in Physical Geography*, 41(5):570–600.

Lave, R. (2012). Bridging political ecology and STS: A field analysis of the Rosgen Wars. *Annals of the Association of American Geographers*, 102(2):366–382.

Lave, R. (2016). Stream restoration and the surprisingly social dynamics of science. *Wiley Interdisciplinary Reviews: Water*, 3(1):75–81.

Leopold, L. B. (1973). River Channel Change with Time: An Example. *GSA Bulletin*, 84(6):1845–1860.

Leopold, L. B. and Maddock, T. J. (1953). The Hydraulic Geometry of Stream Channels and Some Physiographic Implications. *Geological Survey Professional Paper 252*, 252:57.

Leopold, L. B. and Wolman, M. G. (1957). River channel patterns: braided, meandering, and straight. *Geological Survey Professional Paper 282-B*, 282-B:51.

Leopold, L. B., Wolman, M. G., and Miller, J. P. (1965). Fluvial processes in geomorphology. *Journal of Hydrology*, 3:342.

Liébault, F., Bellot, H., Chapuis, M., Klotz, S., and Deschâtres, M. (2012). Bedload tracing in a high-sediment-load mountain stream. *Earth Surface Processes and Landforms*, 37(4):385–399.

Liébault, F., Piégay, H., Frey, P., and Landon, N. (2008). Tributaries and the Management of Main-Stem Geomorphology. In Rice, S., Roy, A., and Rhoads, B., editors, *River Confluences, Tributaries and the Fluvial Network*, pages 243–270. John Wiley & Sons Ltd.

Magilligan, F. J. and Nislow, K. H. (2005). Changes in hydrologic regime by dams. *Geomorphology*, 71(1-2):61–78.

Maurer, B. and McGill, B. (2011). Measurement of species diversity. *Biological Diversity: Frontiers in measurement and assessment. Oxford University Press.*, pages 55–65.

McNeill, J. R. (2000). Something New Under the Sun: An Environmental History of the Twentieth-Century World (Global Century Series). *Nature*, 407(6805):674–675.

Meile, T., Boillat, J. L., and Schleiss, A. J. (2011). Hydropeaking indicators for characterization of the Upper-Rhone River in Switzerland. *Aquatic Sciences*, 73(1):171–182.

Meyer-Peter, E. and Müller, R. (1948). Formulas for Bed-Load Transport. *Proceedings of the 2nd Meeting of the International Association of Hydraulic Research*, pages 39–64.

Montgomery, D. R. and Buffington, J. M. (1997). Channel-reach morphology in mountain drainage basins. *Bulletin of the Geological Society of America*, 109(5):596–611.

Moyle, P. B. and Mount, J. F. (2007). Homogenous rivers, homogenous faunas. *Proceedings of the National Academy of Sciences*, 104(14):5711–5712.

Nathan Bradley, D. and Tucker, G. E. (2012). Measuring gravel transport and dispersion in a mountain river using passive radio tracers. *Earth Surface Processes and Landforms*, 37(10):1034–1045.

Ock, G., Kondolf, G. M., Takemon, Y., and Sumi, T. (2013a). Missing link of coarse sediment augmentation to ecological functions in regulated rivers below dams: Comparative approach in Nunome River, Japan and Trinity River, California, US. *Advances in River Sediment Research*, pages 1531–1538.

Ock, G., Sumi, T., and Takemon, Y. (2013b). Sediment replenishment to downstream reaches below dams: implementation perspectives. *Hydrological Research Letters*, 7(3):54–59.

Parasiewicz, P. (2001). MesoHABSIM: A concept for application of instream flow models in river restoration planning. *Fisheries*, 26(9):6–13.

Parker, G. (1976). On the cause and characteristic scales of meandering and braiding in rivers. *Journal of Fluid Mechanics*, 76(3):457–480.

Parker, G. (1990). Surface-based bedload transport relation for gravel rivers. *Journal of Hydraulic Research*, 28(4):417–436.

Parker, G. and Sutherland, A. J. (1990). Fluvial armor. *Journal of Hydraulic Research*, 28(5):529–544.

Pasquale, N., Perona, P., Schneider, P., Shrestha, J., Wombacher, A., and Burlando, P. (2011). Modern comprehensive approach to monitor the morphodynamic evolution of a restored river corridor. *Hydrology and Earth System Sciences*, 15:1197–1212.

Pennisi, E. (2004). The Grand (Canyon) experiment. *Science*, 306(5703):1884–1886.

Petts, G. E. and Gurnell, A. M. (2005). Dams and geomorphology: Research progress and future directions. *Geomorphology*, 71(1-2):27–47.

Pfammatter, R. and Piot, M. (2014). Situation und Perspektiven der Schweizer Wasserkraft. *Wasser Energie Luft*, 106(1):1–11.

Pfammatter, R. and Wicki, N. S. (2018). Energieeinbussen aus Restwasser-bestimmungen – Stand und Ausblick. *Wasser Energie Luft*, 110(4):233–245.

Pont, D., Piégay, H., Farinetti, A., Allain, S., Landon, N., Liébault, F., Dumont, B., and Richard-Mazet, A. (2009). Conceptual framework and interdisciplinary approach for the sustainable management of gravel-bed rivers: The case of the Drôme River basin (S.E. France). *Aquatic Sciences*, 71(3):356–370.

Prognos (2012). Die Energieperspektiven für die Schweiz bis 2050. Technical report, Swiss Federal Office of Energy, Ittigen, Switzerland.

Rinaldi, M., Belletti, B., Bussettini, M., Comiti, F., Golfieri, B., Lastoria, B., Marchese, E., Nardi, L., and Surian, N. (2017). New tools for the hydromorphological assessment and monitoring of European streams. *Journal of Environmental Management*, 202:363–378.

Rinaldi, M., Surian, N., Comiti, F., and Bussettini, M. (2013). A method for the assessment and analysis of the hydromorphological condition of Italian streams: The Morphological Quality Index (MQI). *Geomorphology*, 180-181:96–108.

Robinson, C. T. (2012). Long-term changes in community assembly, resistance, and resilience following experimental floods. *Ecological applications : a publication of the Ecological Society of America*, 22(7):1949–1961.

Robinson, C. T., Siebers, A. R., and Ortlepp, J. (2018). Long-term ecological responses of the River Spöl to experimental floods. *Freshwater Science*, pages 433–447.

Robinson, C. T. and Uehlinger, U. (2008). Experimental floods cause ecosystem regime shift in a regulated river. *Ecological Applications*, 18(2):511–526.

Rosgen, D. L. (1994). A classification of natural rivers. *Catena*, 22(3):169–199.

Salo, J., Kalliola, R., Häkkinen, I., Mäkinen, Y., Niemelä, P., Puhakka, M., and Coley, P. D. (1986). River dynamics and the diversity of Amazon lowland forest. *Nature*, 322(6076):254–258.

SCCER (2018). Roadmap for Hydropower R&D in Switzerland.

Schaefli, B., Manso, P., Fischer, M., Huss, M., and Farinotti, D. (2019). The role of glacier retreat for Swiss hydropower production. *Renewable Energy*, 132:615–627.

Schirmer, M., Luster, J., Linde, N., Perona, P., Mitchell, E. A. D., Barry, D. A., Hollender, J., Cirpka, O. A., Schneider, P., Vogt, T., Radny, D., and Durisch-Kaiser, E. (2014). Morphological , hydrological , biogeochemical and ecological changes and challenges in river restoration – the Thur River case study. *Hydrology and Earth System Sciences*, 18:2449–2462.

Schleiss, A. (2016). Talsperren und Speicher als lebenswichtige Infrastrukturanlagen für den weltweiten Wohlstand. *WasserWirtschaft*, 106(6):12–15.

Schleiss, A. J. (2000). Importance of hydraulic schemes for sustainable development in the 21st century. *International Journal on Hydropower and Dams*, 7(1):19–24.

Schleiss, A. J. (2005). Flussbauliche Hochwasserschutzmassrnahmen und Verbesserung der Gewässerökologie-Vorschlag eines hydraulisch morphologischen Vielfältigkeitsindexes. *Wasser Energie Luft*, 7(8):195–200.

Schleiss, A. J., Franca, M. J., Juez, C., and De Cesare, G. (2016). Reservoir sedimentation. *Journal of Hydraulic Research*, 54(6):595–614.

Schmidt, J. C., Parnell, R. A., Grams, P. E., Hazel, J. E., Kaplinski, M. A., Stevens, L. E., and Hoffnagle, T. L. (2001). The 1996 controlled flood in grand canyon: Flow, sediment transport, and geomorphic change. *Ecological Applications*, 11(3):657–671.

Schneider, J., Hegglin, R., Meier, S., Turowski, J. M., Nitsche, M., and Rickenmann, D. (2010). Studying sediment transport in mountain rivers by mobile and stationary RFID antennas. *River Flow*, pages 1723–1730.

Schnitter, N. (1971). Staumauer und Maschinenhaus Ova Spin der Engadiner Kraftwerke AG. *Schweizerische Bauzeitung*, 89(33):811–816.

Schumm, S. A. (1977). *The fluvial system.* John Wiley & Sons Ltd., New York, USA.

Schweizer, S., Borsuk, M. E., Jowett, I., and Reichert, P. (2007). Predicting joint frequency distributions of depth and velocity for instream habitat assessment. *River Research and Applications*, 23(3):287–302.

Schwindt, S., Pasternack, G., Bratovich, P., Rabone, G., and Simodynes, D. (2019). Hydromorphological parameters generate lifespan maps for stream restoration management. *Journal of Environmental Management*, 232(June 2018):475–489.

Semenza, E. and Ghirotti, M. (2000). History of the 1963 Vaiont slide: The importance of geological factors. *Bulletin of Engineering Geology and the Environment*, 59(2):87–97.

Shannon, C. E. and Weaver, W. (1949). Theory - Mathematical Theory of Communication. *The mathematical theory of communication*, 27(4):117.

Simon, A., Castro, J., and Rinaldi, M. (2016). Channel form and adjustment: characterization, measurement, interpretation and analysis. In Kondolf, G. M. and Piégay, H., editors, *Tools in Fluvial Geomorphology*, pages 233–259. John Wiley & Sons Ltd.

Simpson, E. H. (1949). Measurement of diversity [16]. *Nature*, 163(4148):688.

Sklar, L. S., Fadde, J., Venditti, J. G., Nelson, P., Aleksandra Wydzga, M., Cui, Y., and Dietrich, W. E. (2009). Translation and dispersion of sediment pulses in flume experiments simulating gravel augmentation below dams. *Water Resources Research*, 45(8).

Spellerberg, I. F. and Fedor, P. J. (2003). A tribute to Claude-Shannon (1916-2001) and a plea for more rigorous use of species richness, species diversity and the 'Shannon-Wiener' Index. *Global Ecology and Biogeography*, 12(3):177–179.

Staentzel, C., Arnaud, F., Combroux, I., Schmitt, L., Trémolières, M., Grac, C., Piégay, H., Barillier, A., Chardon, V., and Beisel, J. N. (2018). How do instream flow increase and gravel augmentation impact biological communities in large rivers: A case study on the Upper Rhine River. *River Research and Applications*, 34(2):153–164.

Stähly, S., Friedrich, H., and Detert, M. (2017). Size Ratio of Fluvial Grains' Intermediate Axes Assessed by Image Processing and Square-Hole Sieving. *Journal of Hydraulic Engineering*, 143(6):06017005.

Statzner, B., Gore, J. A., and Resh, V. H. (1988). Hydraulic Stream Ecology: Observed Patterns and Potential Applications. *Journal of the North American Benthological Society*, 7(4):307–360.

Stewardson, M. (2005). Hydraulic geometry of stream reaches. *Journal of Hydrology*, 306(1-4):97–111.

Stoica, P., Moses, R. L., and Hall, P. (2005). Introduction to Spectral Analysis. *Technometrics*, 47(1):104–105.

Sumi, T. and Kantoush, S. A. (2010). Integrated Management of Reservoir Sediment Routing by Flushing, Replenishing, and Bypassing Sediments in Japanese River Basins Dam. In *Proceedings of the 8th International Symposium on Ecohydraulics, Seoul, Korea*, pages 831–838.

Surian, N., Mao, L., Giacomin, M., and Ziliani, L. (2009). Morphological effects of different channel-forming discharges in a gravel-bed river. *Earth Surface Processes and Landforms*, 34(8):1093–1107.

Tamagni, S., Weitbrecht, V., and Boes, R. M. (2014). Experimental study on the flow characteristics of unstructured block ramps. *Journal of Hydraulic Research*, 52(5):600–613.

Termini, D. (2004). Flow in meandering bends. In Greco, Carravetta, and Della Morte, editors, *River Flow 2004: Proceedings of the Second International Conference on Fluvial Hydraulics*, pages 109–117. Taylor & Francis Group, London.

UN FCCC (2015). Paris Agreement. In *Conference of the Parties on its twenty-first session*, number December, page 32, Paris, France. United Nations, Framework Convention on Climate Change, Paris, France.

United Nations (2018). *Climate Change 2013: The Physical Science Basis. Contribution of Working Group I to the Fifth Assessment Report of the Intergovernmental Panel on Climate Change*. Cambridge University Press, Cambridge, United Kingdom and New York, NY, USA.

Valentin, S., Wasson, J. G., and Philippe, M. (1995). Effects of hydropower peaking on epilithon and invertebrate community trophic structure. *Regulated Rivers: Research & Management*, 10(2-4):105–119.

Varnes, D. J. (1958). Landslide types and processes. *Landslides and engineering practice*, 29(3):20–47.

Warner, R. F. (2012). Environmental impacts of hydroelectric power and other anthropogenic developments on the hydromorphology and ecology of the Durance channel and the Etang de Berre, southeast France. *Journal of Environmental Management*, 104:35–50.

Weber, C., Schager, E., and Peter, A. (2009). Habitat diversity and fish assemblage structure in local river widenings : a case study on a Swiss river. *River Research and Applications*, 25:687–701.

Weingartner, R. and Aschwanden, H. (1992). Discharge Regime - the Basis for the Estimation of Average Flows. In *Hydrological Atlas of Switzerland*.

Wilcock, P. R., Kondolf, G. M., Matthews, W. V., and Barta, A. F. (1996). Specification of sediment maintenance flows for a large gravel-bed river. *Water Resources Research*, 32(9):2911–2921.

Williams, G. P. and Wolman, M. G. (1984). Downstream effects of dams on alluvial rivers. *U.S. Geol. Surv., Prof. Pap.; (United States); Journal Volume: 1286*, page 83.

Wohl, E., Bledsoe, B. P., Jacobson, R. B., Poff, N. L., Rathburn, S. L., Walters, D. M., and Wilcox, A. C. (2015). The natural sediment regime in rivers: Broadening the foundation for ecosystem management.

Yalin, M. S. (1992). *River Mechanics*. Pergamon Press Ltd., Oxford, UK.

Zemp, M., Haeberli, W., Hoelzle, M., and Paul, F. (2006). Alpine glaciers to disappear within decades? *Geophysical Research Letters*, 33(13).

Zingg, T. (1935). Beitrag zur Schotteranalyse. *Schweizerische Mineralogisch-Petrographische Mitteilungen*, 15:39–140.

Acknowledgements

SEVERIN STÄHLY

Rinderweidstrasse 10, CH-8910 Affoltern am Albis, Switzerland

(0041)·77·400·77·47   –   sev.staehly@gmail.com

CURRENT POSITION

École Polytechnique Fédérale de Lausanne (EPFL)   Since March 2015
PhD student at the Laboratoire de Constructions Hydrauliques (LCH)   *Lausanne, Switzerland*

Thesis title: *Hydraulic-morphological habitat assessment in rivers considering residual flow, sediment replenishment and artificial flood events*
Keywords: eflows, hydropower, river restoration, sediment replenishment, ecohydraulics

EDUCATION

Master of Science (M.Sc.) ETH in Environmental Engineering   *Sep 2012 - Jan 2015*
Swiss Federal Institute of Technology (ETH) Zurich
Majors: Hydraulic Engineering and Urban Water Management
Master thesis at the University of Auckland (NZ)

Bachelor of Science (B.Sc.) ETH in Environmental Engineering   *Sep 2009 - Aug 2012*
Swiss Federal Institute of Technology (ETH) Zurich
Major: Energy technology
Bachelor thesis at the Norwegian University of Science and Technology, NTNU (NO)

EXPERIENCE

École Polytechnique Fédérale de Lausanne (EPFL)   March 2015 - Mai 2019
PhD-researcher   *Lausanne, Switzerland*

· Assistant-teacher in the master classes for: Hydraulic structures I & II, Dam Engineering and Fluvial Ecomorphology.
· Supervision of six Master projects in the field of hydropower and river restoration
· Collaboration in applied research projects
· Co-responsible for social events of the doctoral school, EDCE

UNESCO-IHE Delft Institute for Water Education   October - December 2018
Visiting PhD student (3 months)   *Delft, The Netherlands*

· Collaboration for the ecohydraulic index development and eflows.

University of Auckland   Jul 2014 – Oct 2014
Master thesis in the Water Engineering Laboratory (4 months)   *Auckland, New Zealand*

· Writing the thesis proposal: *Comparison of Fluvial Grains' Body Axes*
· Planning, conduction and analysis of flume and field experiments.
· Master thesis report and publication in the *Journal of Hydraulic Engineering*

Basler & Hofmann   Nov 2013 – Apr 2014
Internship at the Water Department (6 months)   *Esslingen, Switzerland*

· Contributing in projects in the domain of river restoration, hydrometry, mudflows and urban water management

Danish Hydraulic Institute, DHI Jan 2012 – Apr 2012
Student intern during the bachelor thesis (3 months) *Trondheim, Norway*

· Creation and simulations with a numerical model of the sewer system of Trondheim, using MIKE

LANGUAGES

German: natal tongue
French: C1 level
English: C1 level

COMPUTER PROGRAMS

Matlab, QGIS, BASEMENT

HONORS AND AWARDS

Grant from the Zeno Karl Schindler (ZKS) and the Erich Degen Foundation of the master thesis, 2014

JOURNAL PUBLICATIONS

· **Stähly S**, Franca MJ, Robinson CT, Schleiss AJ (2019). Erosion, transport and deposition of a sediment replenishment under flood conditions. *Earth Surface Processes and Landforms* [under review].

· **Stähly S**, Gostner W, Franca MJ, Robinson CT, Schleiss AJ (2019). Sampling sufficiency for determining hydraulic habitat diversity. *Journal of Ecohydraulics.* DOI : 10.1080/24705357.2019.1576021

· **Stähly S**, Franca MJ, Robinson CT, Schleiss AJ (2019). Sediment replenishment combined with an artificial flood improves river habitats downstream of a dam. *Scientific Reports 9*(1), 5176 . DOI : 10.1038/s41598-019-41575-6

· Döring M, Tonolla D, Robinson CT, Schleiss AJ, **Stähly S**, Gufler C, Geilhausen M, Di Cugno N (2018). Künstliches Hochwasser an der Saane - Eine Massnahme zum nachhaltigen Auenmanagement. *Wasser Energie Luft*, 110(2): 119-127.

· Juez C, Franca MJ, Fink S, Scheidegger Ch, Siviglia A, **Stähly S**, Trautwein C, Weber Ch, Schleiss AJ (2017). Bedeutung und Einflussfaktoren der Feindsedimentdynamik. In: *Geschiebe- und Habitatdynamik*, Bundesamt für Umwelt BAFU, Bern, Merkblatt 3.

· **Stähly S**, Friedrich H, Detert M (2017). Size ratio of fluvial grains' intermediate axes assessed by image processing and square-hole sieving. *Journal of Hydraulic Engineering*, 143(6): 06017005.

CONFERENCE PAPERS

· **Stähly S**, Franca MJ, Robinson CT, Schleiss AJ (2019). Erosion processes of a novel configuration of sediment replenishment during an artificial flood. *38th IAHR World Congress*, 1.-6. September 2019, Panama City, Panama.

· **Stähly S** (2019). Artificial floods in residual flow reaches - how do they affect hydraulic habitats? *38th IAHR World Congress*, 1.-6. September 2019, Panama City, Panama.

· **Stähly S**, Franca MJ, Robinson CT, Schleiss AJ (2019). Sediment replenishment as a measure to enhance river habitats in a residual flow reach downstream of a dam. *27th International Congress on Large Dams, ICOLD*, 9.-14. June 2019, Ottawa, Canada.

· **Stähly S**, Franca MJ, Tonolla D, Döring M, Robinson CT, Schleiss AJ (2019). Increase of hydraulic habitat diversity downstream of dams with sediment replenishment and artificial flooding. *Africa 2019*, 2.-4. April 2019, Windhoek, Namibia.

· **Stähly S**, Franca MJ, Robinson CT, Schleiss AJ (2018). Aufwertung der Habitatvielfalt in einer Restwasserstrecke mittels eines künstlichen Hochwassers und Geschiebebeigaben - Vergleich von Feldversuchen mit Laborexperimenten. *19. Wasserbausymposium*, 18.-20. September 2018, Graz, Austria, pages 289-296.

· **Stähly S**, Maître A, Franca MJ, Robinson CT, Schleiss AJ (2018). Experiments with sediment replenishment in a residual flow reach: Comparison of field data with laboratory experiments. *9th International conference on fluvial hydraulics River Flow 2018*, 5.-8. September 2018, Lyon, France, pages 02022.

· **Stähly S**, Gostner W, Franca MJ, Robinson CT, Schleiss AJ (2018). Analysis of the sensitivity of the hydromorphological index of diversity, HMID. *8th International Symposium on Environmental Hydraulics (ISEH 2018)*, 4.-8. June 2018, Notre Dame, Indiana, United States, pages 95-98.

· **Stähly S**, Bourqui P, Robinson CT, Schleiss AJ (2017). Sensitivity analysis of the hydromorphological index of diversity using numerical generated data. *37th IAHR World Congress*, 13.-18. August 2017, Kuala Lumpur, Malaysia, pages 99-104 (ISSN 1562-6865).

· **Stähly S**, Bourqui P, Robinson CT, Schleiss AJ (2016). Numerische Modellierungen zur Bestimmung der Habitatvielfalt an einem mäandrierenden wasserkraftbeeinträchtigten Fliessgewässer. *18. Wasserbausymposium*, 29. June -1. July 2016, Wallgau, Germany, pages 720-728.

All publications: https://www.researchgate.net/profile/Severin_Staehly